Methods to Reduce the Starting Current of an Induction Motor

Mathew Habyarimana

213573647

A dissertation submitted to
the University of KwaZulu-Natal,
College of Agriculture, Engineering and Science,
in partial fulfillment of the requirements for the degree of

Doctor of Philosophy

Supervisor: Dr R. Pillay Carpanen

Co-Supervisor: Prof David Dorrell

School of Engineering, Electrical Engineering

University of KwaZulu-Natal

January 2022

Copyright © 2022 Mathew Habyarimana

All Rights Reserved

I, Mathew Habyarimana , declare that:

(i) The research reported in this dissertation, except where otherwise indicated, is my original research.

(ii) This dissertation has not been submitted for any degree or examination at any other university.

(iii) This dissertation does not contain other persons' data, pictures, graphs or other information, unless specifically acknowledged as being sourced from other persons.

(iv) This dissertation does not contain other persons' writing, unless specifically acknowledged as being sourced from other researchers. Where other written sources have been quoted, then:

a) their words have been re-written but the general information attributed to them has been referenced:

b) where their exact words have been used, their writing has been placed inside quotation marks, and referenced.

(v) This dissertation does not contain text, graphics or tables copied and pasted from the Internet, unless specifically acknowledged, and the source being detailed in the dissertation/thesis and in the References sections.

Candidate: Mathew Habyarimana

Signature: _____

As the candidate's supervisor I agree to the submission of this dissertation for examination.

Supervisor: Dr R. Pillay Carpanen

Signature: _____

CoSupervisor: Prof David Dorrell

Signature: _____

ABSTRACT

Methods to Reduce the Starting Current of an Induction Motor

Mathew Habyarimana
School of Engineering
Doctor of Philosophy

Power system loads that have high starting currents are a serious source of concern in smaller grids or remote locations on the main grid. This problem is envisaged to be exacerbated by the roll-out of smart microgrids. When a high power induction motor is turned on in such a power system, its inrush current can be up to about ten times the full-load current. This transient current can cause problems when attached to weak grids. The increased current is due to the power required to start the load and the increased reactive power demand during the starting process. To protect the grid connection as well as the load, energy storage units can be used to compensate for the increased power requirement. A more pragmatic approach is to reduce the reactive power requirement using tuned compensation capacitors in order to reduce the inrush current. The aim of this research is to address the selection, calculation and switching of the capacitor bank for reactive power compensation. The capacitors are calculated and switched on to compensate the starting transient and disconnected when the machine has run up to speed using a point-on switching approach that reduces the switching transient.

Keywords: Motor starting, Inrush current, Capacitor switching, Algorithm.

PUBLICATION ARISING

M. Habyarimana and D. G. Dorrell. Methods to reduce the starting current of an induction motor. IEEE International Conference on Power, Control, Signals and Instrumentation Engineering (ICPCSI), pages 34–38, 2017.

M. Habyarimana, R. Musumpuka and D. G. Dorrell. Mitigating In-rush Currents for Induction Motor Loads. IEEE Southern Power Electronics Conference (SPEC), 2021.

M. Habyarimana, D. G. Dorrell and R. Musumpuka. Reduction of Starting Current in Large Induction Motors. Submitted to *Energies* journal for consideration.

ACKNOWLEDGMENTS

I would like to thank my esteemed supervisors, Prof. David Dorrell for his invaluable supervision, support, funding opportunity and tutelage during the course of my PhD degree, and to Dr. Pillay Carpanen for his mentorship. My gratitude extends to Dr. Remmy Musumpuka for his kind advice and technical support. Additionally, I would like to express gratitude to the Smart Grid Research Centre and the school of Engineering, University of KwaZulu-Natal for the opportunity to undertake my studies.

Contents

List of Figures

List of Tables

Chapter 1

Introduction

1.1 Background

In power systems, the inrush current, also called the input surge current or switch-on surge, of a large load can cause problems related to excessive current drawn. It has the potential to damage system apparatus as well as destabilizing the system network in weak grids. It can trip protection relays unnecessarily thereby causing voltage drops that impair the function of other equipment connected to the same system.

Inrush current can be defined as the maximum instantaneous input current drawn by an electrical device when first turned on [2, 3]. Induction motors (IMs), switched-mode power supplies, transformers and incandescent lamps are devices that exhibit high inrush current. When there are large electro-magnetic devices then there will be a surge during switch-on to establish the magnetic field. Induction motors have the transient start-up period as well as magnetization if it is direct on-

line connected. During the run-up to steady-state the machine can draw between five and ten times the rated current.

If the inrush current is left unaddressed for a large load, it can cause voltage busbars to fall out of regulation. In more serious cases this results in the system exceeding the current carrying capability of the system and possibly leading to overloading and system tripping.

Three-phase IMs are the main industrial workhorse and they consume both active and reactive power [4, 5]. They can produce power quality problems due to high inductive loading. In industry, capacitor banks are often used to correct poor power factor in plants.

When starting a line-connected IM, the induced voltage in the rotor is maximum because slip is maximum ($s = 1$). At this stage the rotor impedance is low, therefore the rotor current becomes large and the high current in the rotor reflects into the stator due to transformer action. This results in a large starting current in the stator at low power factor. Depending on the motor size and design, the starting torque may be low. This is particularly true for large high-efficiency machines. This may negate the use of a high resistance or star-delta starter to restrict the starting current. These reduce the starting current but also the starting torque.

The use of capacitors in conjunction with induction motors is not new. They have been used for many decades in single-phase induction motors for both starting and running where they are in series with the auxiliary winding [6], as well as steady-state power factor improvement, as already mentioned. There have been studies of induction motors where they have been controlled electronically when in series [7, 8] and in parallel to give a leading power factor correction and boost the output voltage during starting [9]. This could however have implications on the system with potential over-voltage as highlighted by [10]. None of these studies addressed the reactive power requirements of an IM. Power factor correction requirements were discussed by [11] though

this was for steady-state operation.

This work focuses on reducing the inrush current in induction motors by way of capacitor compensation during the starting cycle and switching the machine on at a precise position of the voltage cycle. In smaller IMs it is possible to use an inverter to reduce the starting current since it becomes a variable speed drive. However in larger IMs this will not be cost effective. If they are driving pumps and fans then variable speed may not be required. During the starting cycle in large IMs, most current is for reactive power absorption and thus it is possible to compensate for this by generating reactive power using capacitors. This work will illustrate this. A model is developed that reduces inrush current with the target of large induction motors in islanded microgrids and those remotely located from the main grid.

During the starting of an induction motor there are also pulsating torques and unbalanced currents. Such performance is undesirable for electrical supply, mechanical gearing systems and the electrical protection unit of the machine. If the motor is connected to a weak power system, the sudden high current can cause a temporary voltage drop, not only at the motor terminals, but the entire power bus feeding the starting motor [12]. The work outlines the use of point-on switching to reduce this transient.

The induction motor is analogous to the transformer - it is formed from electrical circuits linked by a magnetic circuit. According to [13] the induction motor behaves as a transformer but with the secondary windings shorted until the rotor begins to move when an electro-mechanical energy conversion component in the rotor circuit (represented by $(1-s)/s \times R_2^{/}$) comes into play as stated in Table 1.1. The length of the starting transient is less if the mechanical load on the motor is reduced but mechanical systems have a degree of inertia. For low- to medium-power motors, the winding arrangement might be changed during start-up to reduce the inrush current - this is called

start-delta starting.

There are different methods for solving the problem of inrush current in induction motors as explained in the literature. These are:

- Star-delta starter
- Autotransformer (reduced voltage)
- High resistance starter
- Part Winding
- Adjustable Frequency Drives (AFD)
- Rotor resistance (wound rotor machine)

In practice, apart from slip ring motors (which can be started by adding rotor resistance) and the AFD, the other methods reduce the starting torque as well as the inrush current

Table 1.1 Transformer and induction motor comparison.

No.	Transformer	Induction motor
1.	Static device	Dynamic machine with moving parts.
2.	Transfers electrical power from one circuit to another without changing the supply frequency, i.e., it only steps-up or steps-down the level of voltage and current.	Converts electrical power into mechanical power; wound rotor machines can be used as a frequency converter.
3.	The frequency of induced EMF and current in the secondary is same as supply frequency, i.e., primary and secondary frequency is constant.	The frequency of current and EMF on stator remains same. The frequency of the rotor is variable which depends on slip and slip is further depends on motor load. The frequency of induced EMF on the rotor is equal to slip times the stator frequency.
4.	Both the input and output energy (primary and secondary) is in the form of electrical energy.	The energy transferred to the rotor is either electrical losses or converted to the mechanical energy; wound rotor machines can have energy transfer through the slip rings.
5.	A transformer is an alternating flux machine.	Induction motor is a rotating flux machine.
6.	Mostly a ferromagnetic iron core is used as a medium for the passage of flux from primary to secondary	An air gap is used between the rotor and stator.
7.	Operated at any kind of power factor depending on load	Operates at lagging power factor because it draws lagging current to magnetize the machine at starting and at steady-state operation due to the air gap.
8.	Efficiency is always higher than the induction motor efficiency because there is no moving parts and no air gap.	Mechanical losses occur as it is not static machine.

1.2 Objectives of the Thesis

In this work, a model is developed that reduces inrush current in large IMs using parallel capacitors. The switching of the machine and capacitors is also investigated.

The requirement of the inrush current compensation system to meet current capacity in the network during the current surge due to loads, as well as high inductive nature of the motor, is the motivation for this research. The compensating system to be used acts as an alternate source to supply for the reactive power required for starting. Thus the general objectives of the thesis are:

(a) Design the capacitor bank for the reactive power which reduces the inrush current of a squirrel cage induction motor.

(b) To investigate the switching of the induction motor using point-on switching to minimise the magnetizing inrush current (rather than the starting transient current).

(c) To investigate and design a point-on switching system to switch the capacitor bank in the network with a set preconditions using microcontrollers and relays.

(d) To present findings by comparing the results obtained from the designed compensation system with the existing starting methods and simulations.

The design is an automatic system; where at start and during the starting current surge in the induction motor, the capacitor bank is switched into the network while at the other running times of the induction load only runs from the mains supply with the capacitor bank switched out.

As mentioned in the objectives, the design includes a point-on switching system controlled by a microcontroller. The switching point will be investigated to provide the minimum switching. To fulfil the general objectives, the following specific objectives are required to be fulfilled:

(a) Design of capacitor bank size for the required induction motor.

(b) Design of the AC zero cross detector that works with the switches to switch the capacitors

bank in and out of the network

(c) Design of the threshold current detector circuit that operates the capacitor bank to give a signal to make a full switch.

(d) Design of the switching algorithm using the microcontroller; the circuit which works as interface between capacitor bank and the zero cross detector circuits for the entire compensation circuit to be in or out of the network.

1.3 Originality and Contribution of the Thesis

The main contributions of the thesis are:

(a) The detailed examination of the induction motor and the reactive power requirements is fundamental to the needs of the starter. The author can find no details on this. This allows the correct capacitor to be selected.

(b) The understanding of point-on switching of the motor and capacitor bank to allow soft starting is novel.

(c) The inrush current compensation system during the current surge due to induction motor starting, or any high inductive load, is new. This method of starting is not reported in the literature.

(d) The sizing of capacitor bank that supply the reactive power to the load for the inrush current reduction is demonstrated and found to be a compromise - this is new theory.

(e) The practical design of the point-on-switching system that switches in and out the capacitor bank into the network is of industrial interest.

1.4 Outline of the Thesis

The thesis is organized as follows:

Chapter one introduces the subject matter and objectives of this project. The major problems caused by the inrush current are addressed, different techniques used to handle it.

Chapter two reviews the literature about inrush current; earlier challenges and alternative solutions are investigated through different works.

Chapter three discusses the theory of operation of the induction motor and focuses on the starting behaviour.

Chapter four give simulations for different starting scenarios for different machines and includes different simulation techniques.

Chapter five describes the development of the experimental rig. This includes the design and implementation of the inrush current compensation system is discussed. The microcontroller programming and connection circuits and switching modelling is put forward in.

Chapter six gives the experimental results and compares them with the simulations.

Chapter seven concludes and recommends the future studies.

Chapter 2

Literature Review

2.1 Introduction

The observation of inrush current phenomenon dates from 1892 and pioneered by Fleming [14, 15]; although other observations were made by Ferranti in 1890 [16, 14]. Up to 1944 there were few reported studies regarding which parameters may affect inrush current in the design of high power loads [17].

Inrush current is associated with other significant effects on the supply and neighboring connections. These include:

- Supply voltage dips, where customers connected to the system experience the disturbance. This disturbance can contribute to malfunction of sensitive electronics and can interrupt the supply to other equipment.
- The inrush current waveform is different from the normal AC sinusoidal and contains low

and high frequency components. Such harmonics can interact with filters installed in the system.

- The longer-period transient current offset components of the inrush current can lead to oscillatory torque in motors resulting to increase motor vibration.

Devices such as AC electric motors, switched-mode power supplies (SMPS), incandescent lamps, power converters and transformers can draw several times their normal full-load current when first energized for a few cycles of the input waveform. The selection of over-current-protection devices such as fuses and circuit breakers is made more complicated when high inrush currents must be tolerated.

For inrush current, according to [18], the time of the transient matters. It also depends at the point on the ac line voltage sine wave at which the power switch closes. Depending on the load switched, the inrush spike can be high, but at another point, it can be of lower and shorter duration. Point-on switching of the induction motor and capacitors in the network can reduce the inrush current using voltage and current zero and point-on crossing detection.

2.2 Induction Motor Characteristics

The induction or asynchronous machine is the most commonly used AC machine. As with all electrical machines, the IM can be used as a motor or a generator. The induction machine has two parts: the stator, which is the mechanical stationary part and the rotor, which is the rotating cylindrical part. The stator and rotor magnetic cores are composed of laminations of fractional millimetre in thickness cut from iron sheets. This reduces the iron losses. The stator laminations are slotted on the inner surface to accommodate a three-phase winding. This winding is distributed, these dictate the specified number of poles and the speed for a given supply frequency. For a 2-pole

motor connected to a 50 Hz supply, the synchronous speed 3000 rpm, for a 4-pole machine, the synchronous speed is 1500 rpm. The ends of every coil are connected to form a winding which is connected to the terminal box in either in star (Y) or in delta (Δ) to form the 3-phase load [19, 20, 21]. The start point is not earthed. At full load the machine will run at a fraction below the synchronous. Usually less than 5 % with this decreasing with increasing machine size.

2.2.1 The Difference Between a 3-phase Induction Motor and a 3-phase Synchronous Motor

There are two common forms of 3-phase machine - the induction (also know as an asynchronous) machine and synchronous machine. It is worth comparing them.

The induction machine creates a rotating magnetic field in the airgap through a 3-phase current set in the stator windings which links the rotor and induces voltages in the rotor conductors which generates current in the rotor windings. This is synchronized with the stator magnetic field rotation. Induction motors are called so because of this EMF induction in the rotor coils [22, 23]. The interaction of the stator and rotor magnetic fields produces torque.

The IM rotor does not rotate at the same speed as the stator rotating magnetic field. The rotor speed always slips behind and thus the concept of 'slip speed' [24]. If the rotor rotates at the synchronous speed then the rotor does not see a varying magnetic field which means no EMFs are induced into it and so no torque is developed. The slip is given by

$$s = \frac{\omega_s - \omega_r}{\omega_s} \times 100\ [\%] \tag{2.1}$$

where ω_s is the synchronous speed and ω_r is the rotor speed, both in in rad/s. The synchronous

speed is given by

$$\omega_s = \frac{2\pi f_s}{p_m} \tag{2.2}$$

where f_s is the supply frequency and p_m is the machine pole-pair number.

The synchronous machine has the same distributed 3-phase winding but there is a fundamental difference with the rotor. The rotor rotates in synchronizm with the stator magnetic field. Since there will be no induction into the rotor then there is as external supply is provided to the rotor coils. This supplies a DC current to produce a rotor field [25, 26]. Steady torque will only be produced when the rotor rotates at synchronous speed and no other speed.

3-phase induction motors may have six or three terminals for the stator windings depending upon whether there is an internal star point. If it is squirrel cage type of rotor then the rotor conductors are shorted. If it is wound rotor, with a 3-phase winding embedded in the rotor slots, it will have three slip rings to bring the phase winding connections out and there will be an internal star point on the rotor.

The synchronous motor will again have six or three stator terminals depending on if there is an internal star point. Since they are often used as generators. There is usually a need bring out a star point to be connected as a neutral. The rotor winding is DC and will have two slip rings or a brushless exciter and rotor-mounted rectifier for rotor excitation [27].

Table 2.1 lists the differences between synchronous and induction machines. The two main differences are that the synchronous machine will not self-start because it runs at synchronous speed (though there are self-starting synchronous motors that starts as induction machines using the damper bars as a cage for starting) but they can be used for power factor control, whereas there is not control of a squirrel cage machine reactive power but they will self start when connected

to a grid. Hence the synchronous machine is primarily a generator and the induction machine is primarily a motor.

Table 2.1 Three Phase induction motor and synchronous motor differences.

Difference	**Synchronous motor**	**Induction motor**
Type of Excitation	A synchronous motor is a doubly excited machine.	An induction motor is a single excited machine.
Supply System	Its armature winding is energized from an AC source and its field winding from a DC source.	Its stator winding is energized from an AC source.
Speed	It always runs at synchronous speed. The speed is independent of load.	If the load increases the speed decreases. It is always less than the synchronous speed.
Starting	It is not self starting. It has to be run up to synchronous speed by another means before it can be synchronized to the AC supply.	Induction motor has self starting torque.
Operation	A synchronous motor can be operated with lagging or leading power by changing its excitation.	An induction motor operates only at a lagging power factor.
Usage	It can be used for power factor correction in addition to generating or driving mechanical loads.	An induction motor is used for driving mechanical loads, it can generate above synchronous speed.
Efficiency	It is more efficient than an induction motor of the same output and voltage rating.	Its efficiency is less than that of the synchronous machine.
Cost	A synchronous motor is more expensive than an induction motor of the same output and voltage rating	An induction motor is cheaper than the synchronous machine.

Table 2.1 takes a traditional view of these machines which has recently become less confined. There are now synchronous machines that are brushless with permanent magnets so the excitation cannot be controlled. They tend to operate as inverter-fed torque-dense variable-speed drive motors and usually in an under-excited state (absorbing reactive power). The wound-field induction

motor was traditionally used in soft-start motoring situations where additional resistance is added to the rotor circuit to limit the inrush current and improve the starting torque - these external rotor resistors are switched out after the start cycle. At full load they are not as efficient as a squirrel-cage induction motor and have largely been replaced by variable-speed inverter-fed squirrel cage drives. However, they have now found a niche as variable-speed generators in wind turbines using an improved slip-energy recovery system attached though the rotor circuit. They can generate both below and above the synchronous speed and offer a system with an inverter that is only a fractional rating of the total output power of the generator, probably about 25 % rated.

2.3 Induction Motor Starting Techniques

As recently as 1988 the only common methods for reducing inrush current in cage induction motors was the installation of starting resistors or star-delta starting. For starting resistors, they are connected in series and slowly reduced to reduce the net load impedance during switch-on; this is however not the best solution because resistors must be included in the circuit breaker design which will require maintenance with switch arcing leading to wear. For start-delta starting, the IM is started with the windings in star, then reconnected in delta close to full load. Both of these methods give reduced starting torque as well as current. There can also be a problem with false or unnecessary tripping of protection relays which can affect power quality. These are the motivations for further study of the inrush and starting current phenomena [28, 29, 30, 31]. The inrush currents in a transfomer and induction motor are compared below before detailing induction motor starting methods.

2.3.1 Inrush Current in Transformers and Starting Techniques

For the transformer, it was stated in [32] that:

"When a transformer is first energized, a transient current up to 10 to 15 times larger than the rated transformer current can flow for several cycles. For the toroidal transformers which use less copper; with the same power handling can have up to 60 times inrush to running current. Inrush current is actually as high as the short circuit current".

The inrush current is drawn when the secondary side is unloaded or in the open-circuit condition. This can cause unwanted tripping of the transformer circuit breaker. The worst-case is when the primary winding is connected at an instant around the zero crossing of the primary voltage (which for a pure inductance would be the maximum current point in the AC cycle) and the polarity of the voltage half-cycle has the same polarity as the remanence in the iron core (the magnetic remanence being left high from a preceding half cycle).

The transient can create huge forces in the transformer windings so repeated turn-on transients can reduce the life-cycle of power transformers, which are one of the most expensive components in electric power systems [33].

2.3.2 Inrush Current in Induction Motors and Starting Techniques

In an IM, the air gap between the rotor and the stator causes a higher magnetic reluctance. Therefore, this requires a higher magnetizing current to produce the rotating magnetic field when starting. At starting, the current can be very high and damage the electrical system. The initial high torque ripple can affect the mechanical system of the motor. A literature survey shows that attempt-

ing to overcome this by reducing the initial voltage value by 50 % can result in 75 % reduction of the motor torque since the torque is a function of the square of the voltage. So many studies have attempted to address the reduction in torque due to limitation of the starting current.

There are several methods of starting induction motors [34, 35, 36] which are review below.

2.3.2.1 Direct-on-line starting- DOL

DOL starting is the traditional way of starting a machine without reducing the supply voltage to the motor. The starting current in a DOL start is usually in the range of five to ten times the motor full load current rating [35], but can be higher. The transient starting torque oscillation can produce torque peaks that are up to three times higher than the rated torque. The inrush current is a phenomenon that can adversely affect an electrical power system. Fig. 2.1 shows the inrush current for an initial simulation of a 200 HP, 3-phase induction motor in PSCAD [37]. It may be the worst case where the inrush current is sixteen times the steady current for the larger machines generally. This generates mechanical stress on the machine which can affect service life [38].

DOL starting is often used in applications below 25 kW and when the starting load is relatively light [39]. The machine can be either delta or star connected as shown in Fig. 2.2 which gives flexibility in the voltage range.

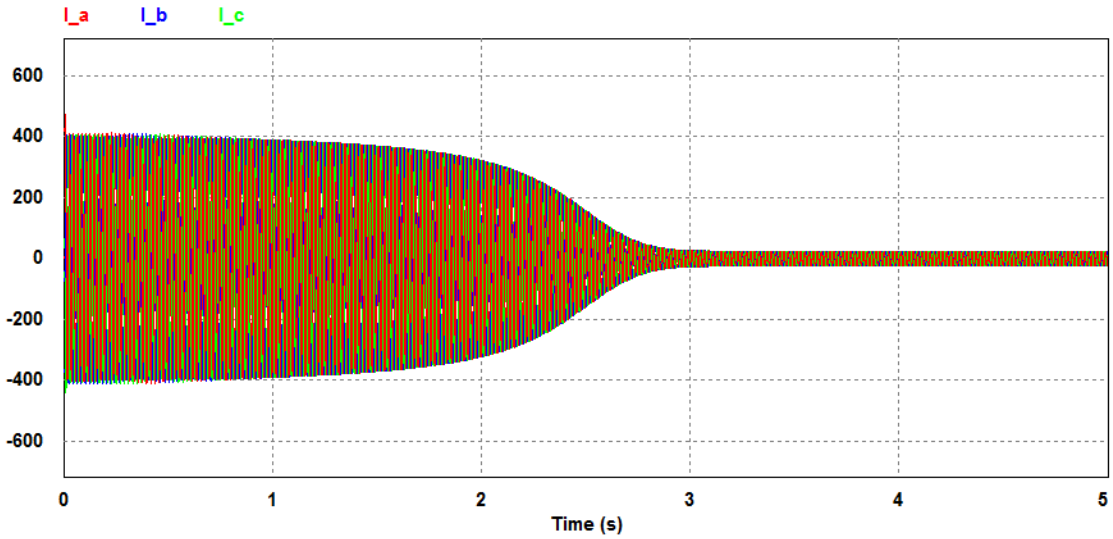

Figure 2.1 Phase *a*, *b* and *c* currents. 200 HP 6000 V motor. Steady current is 25A peak (17.5 A rms).

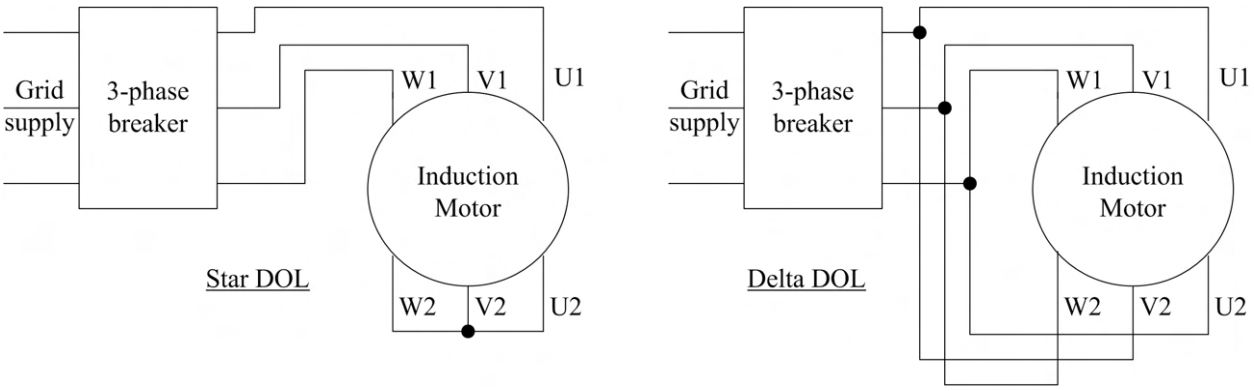

Figure 2.2 Star-delta starter connections.

2.3.2.2 Star-delta starter

Except for the DOL starting method, the main objective of other alternative starting methods is to reduce the supply voltage to the motor, with the express purpose of reducing inrush currents that occur during the starting operation. Star-delta starting is an effective way of reducing inrush

currents because the starting currents are directly proportional to the supply voltage.

The voltage per phase supplied to each winding is reduced by $1/\sqrt{3}$ when the windings are connected in star. Fig. 2.3 shows the connection. First the star contactors are closed, for a period of time, then the delta contactors are closed. For a delta-connected machine, if the phase current in each stator winding is V_s/Z_s, where the voltage across a phase winding is the line voltage V_s and input impedance of a phase winding is Z_s at standstill, the line current to the motor is $I_{st(delta)} = \sqrt{3} \times V_s/Z_s$. If the machine is star connected then the applied winding voltage is reduced by $\sqrt{3}$ while the line current is now equal to the phase current so that $I_{st(star)} = (1/\sqrt{3}) \times Vs/Zs$. Hence, the starting current using a star-delta starter is 1/3 of the starting current during a DOL. This also reduces the starting torque by 3. However, the star-delta starter has some disadvantages [34, 40]:

- Low starting torque;
- Six terminal motor required;
- It requires two sets of cables from starter to motor;
- The transients produced when switching from star to delta connections during run-up stress the equipment;
- Star-delta starter will not be able to start a load with a high starting torque; and
- Large machines tend to be star connected.

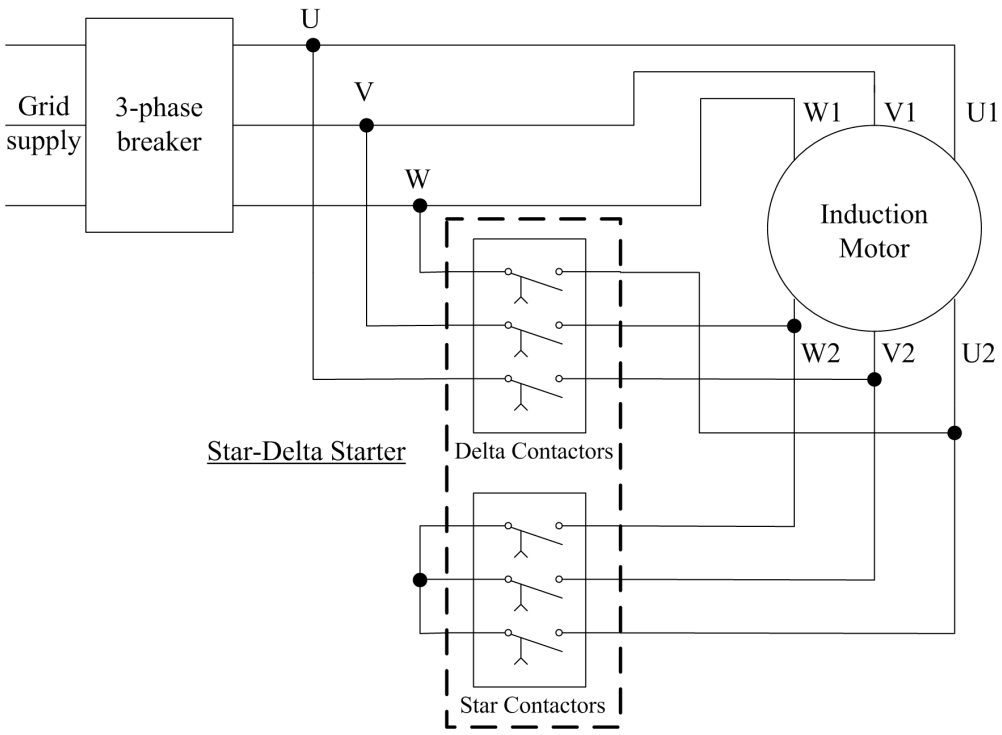

Figure 2.3 Star-delta starter connections.

2.3.2.3 Autotransformer

For the autotransformer starting method, taps on the autotransformer allow for a variable selection of starting voltage which can control the starting current and torque and gives more flexibility than the star-delta starter [35]. Fig. 2.4 shows a three-tap autotransformer allowing 100 %, 75 % and 50 % voltage. The torque is reduced as the square of the applied voltage. If the machine is left connected at the lower tap setting then the machine will operate at a higher slip and slightly lower speed at steady state which will increase the machine current and reduce the efficiency [41]. The method of starting is popular in laboratories and test facilities.

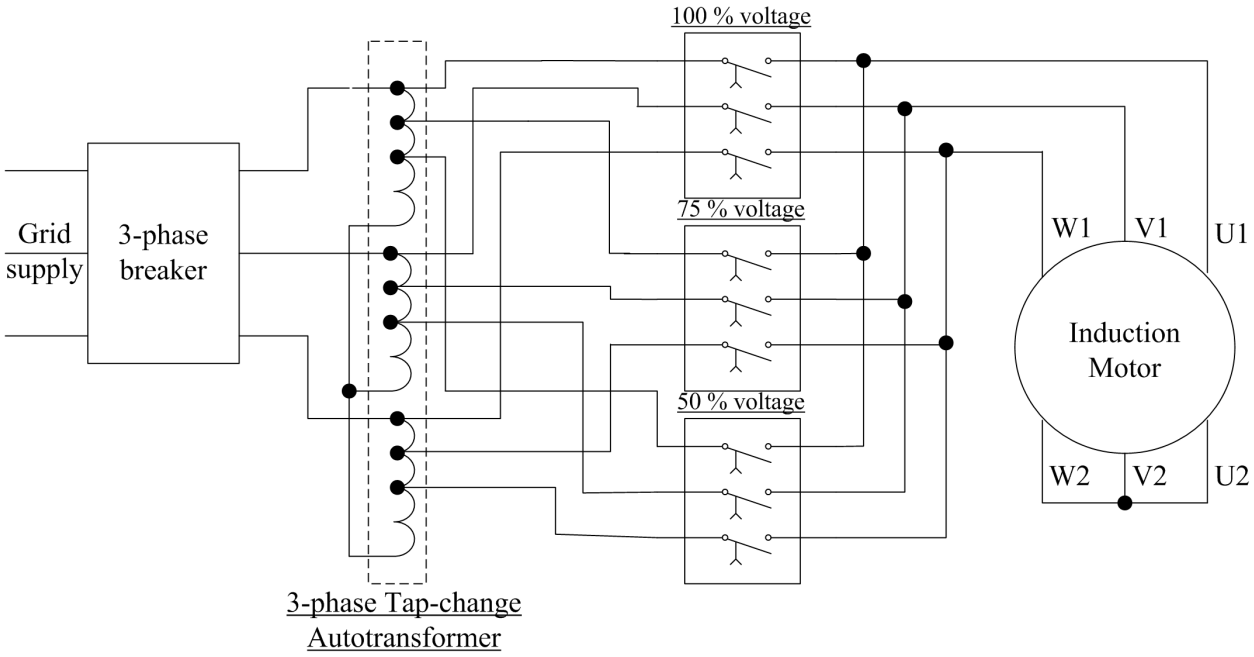

Figure 2.4 3-phase tap-change autotransformer.

2.3.2.4 High resistor or reactor starting

This method uses fixed or variable resistors or reactors that are in line with the motor and switched out of the circuit as the speed increases. Fig. 2.5 shows variable forms of the these starters rather than fixed values of resistance or reactance. This additional impedance to the circuit which will draw additional power or reactive power during starting [42, 43]. These are old-fashioned types of starter. In-line resistance and reactance can be used together for starting [44].

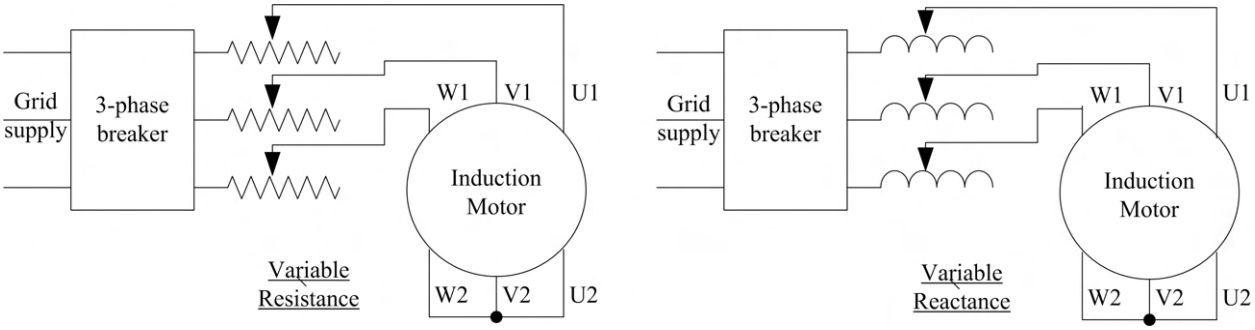

Figure 2.5 Variable high resistance and reactance starter.

2.3.2.5 Alternative starting techniques

In addition to the basic starting methods (DOL, star-delta and Autotransformer, resistor and reactor soft starting), according to [41] two more starting methods are also used and other starting techniques have been reported.

2.3.2.5.1 Series thyristor/triac or floating capacitor H-bridge. Rather than have series resistors or reactors, other forms of in-line soft starters have been suggested such as in-line anti-parallel thyristors (or triacs in smaller starters) using phase angle control to restrict the voltage [34] or in-line floating capacitor H-bridges [8]. These are shown in Fig. 2.6. These have different effects; the phase angle control will essentially restrict the voltage to the induction motor hence reducing the starting current. It causes a delay to the current conduction thus it acts like a reactor and will absorb VArs. However, the floating capacitor H-bridge will add capacitance to the circuit. To restrict the starting current then the capacitors have to be large since they will produce a leading power factor correction. If the capacitor reactance is less to the motor reactance then they can actually increase the starting torque. Both of these allow variable in-line control.

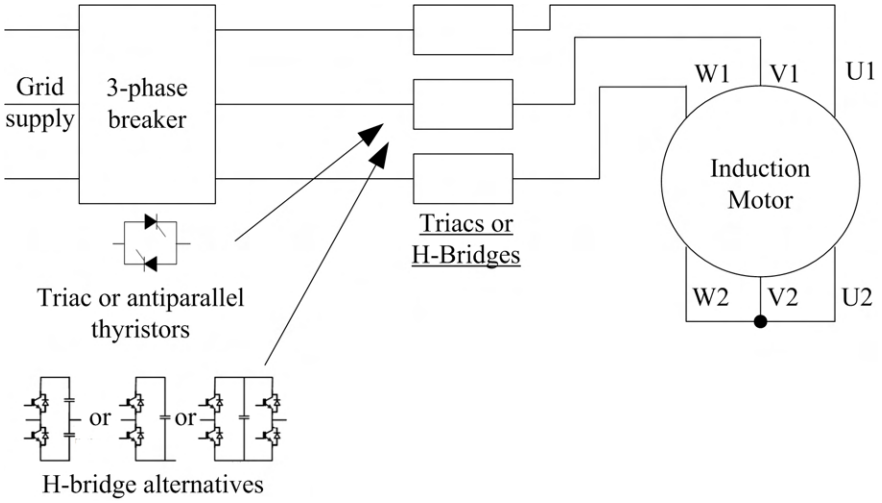

Figure 2.6 Series thyristor or H-bridge floating capacitors.

2.3.2.5.2 Adjustable speed drives (AFD). This type of starting gives the greatest overall control and flexibility in starting induction motors. It gives the most torque for a given current. The greatest drawback of the AFD is in the cost; variable speed drives are expensive and the cost for high power inverters rises sharply when they go into the 100 kW and above range [45]. A typical arrangement is given in Fig. 2.7. This is not studied here since fixed-frequency line-connected induction motors are being studied.

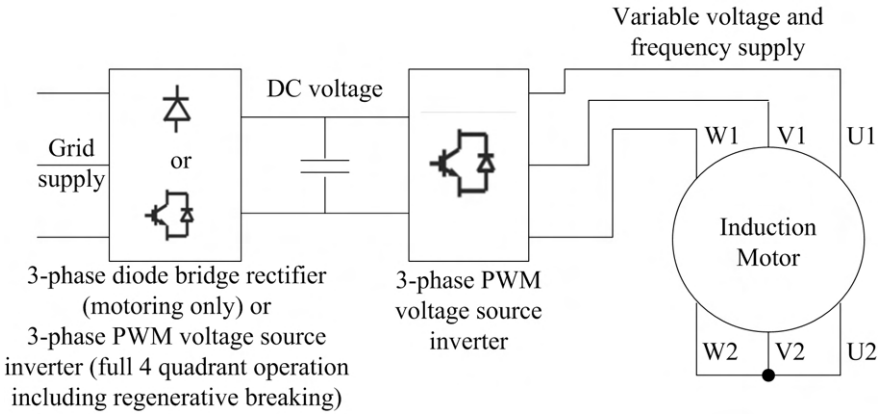

Figure 2.7 Variable speed operation.

2.3.2.5.3 Part winding. With this method the stator winding is formed from two separate 3-phase windings. They are connected in parallel and the motor is starting using only one winding before the second is switched in as shown in Fig. 2.8. This method reduces the starting current and the starting torque by 50 to 60 %. However, this method causes the motor to heat up on starting. Furthermore, this method increases the magnetic noise of the motor [42, 46]. It is rarely used.

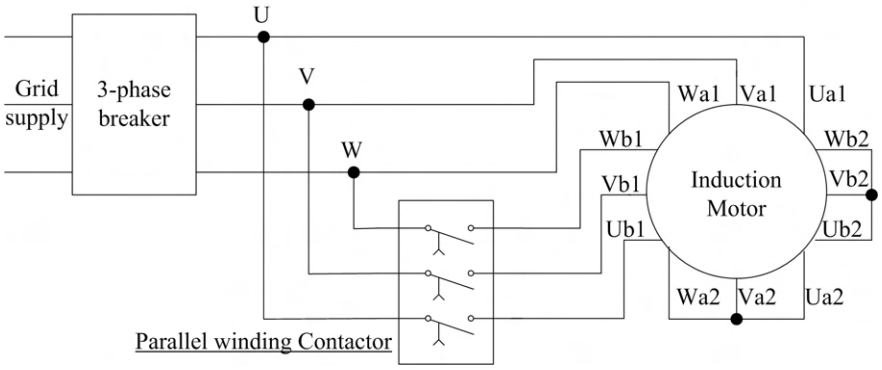

Figure 2.8 Part winding connection - two windings in parallel.

2.3.2.5.4 Wound rotor induction motor - external rotor resistance. In this method additional resistors are connected to the rotor windings through the slip rings and slowly switched out as the motor approaches full load. The connection is shown in Fig. 2.9. This increases the starting torque while reducing the starting current. They were widely used but wound rotor motors are now rarely used and have been replaced by VSDs. They are more expensive than cage motors and will run at a higher slip at full load, hence they are less efficient.

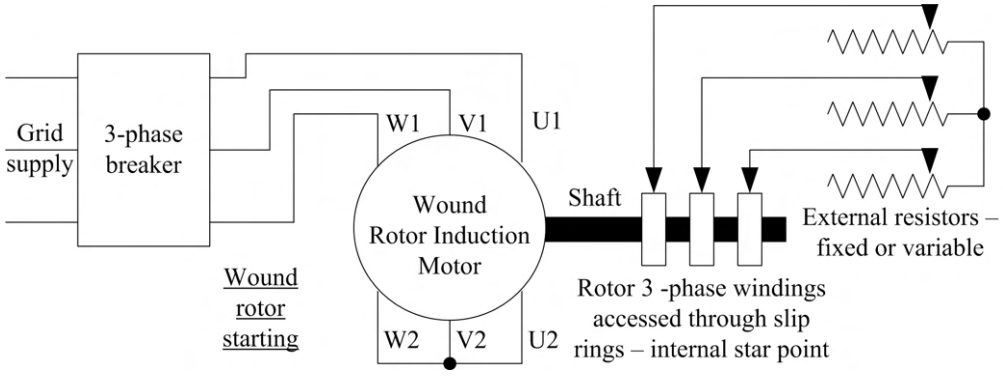

Figure 2.9 Wound rotor induction motor starting.

2.3.2.5.5 Parallel capacitor. This is similar to the method studied in this work but the capacitors are rated much higher to inject much more reactive power to give leading power factor operation and increased grid voltage [9]. This is a similar concept to the series floating capacitor H-bridge in [8, 47] although the motor voltage is not reduced in the same way and the parallel capacitors will supply reactive power to the motor and the grid. The arrangement is shown in Fig. 2.10.

At this point it is worth looking at what typical line impedances are to be expected in a line. In [48], the impedance is stated as being either an impedance or a percentage (typically 10 %) of the load. Unless the induction motor is a single load at the end of a line, the line should be rated much higher than the induction motor. However, with a starting current of five to ten times the rated current then during this period the grid voltage could be pulled out of maximum regulation. In [1] tables for All-Aluminum-Conductors (AAC) are given. As the cable become larger then the line impedance becomes more inductive. Choosing two which could represent low voltage (LV) and medium voltage (MV cables), These are given in Table 2.2. It can be seen that the LV cable is mostly resistive while the MV cable is more inductive. Under these short lengths the capacitor effect is minimal. The effects of the line inductance can be reduced using a leading power factor

load as [9] and [8] did but the line resistance cannot be tuned out.

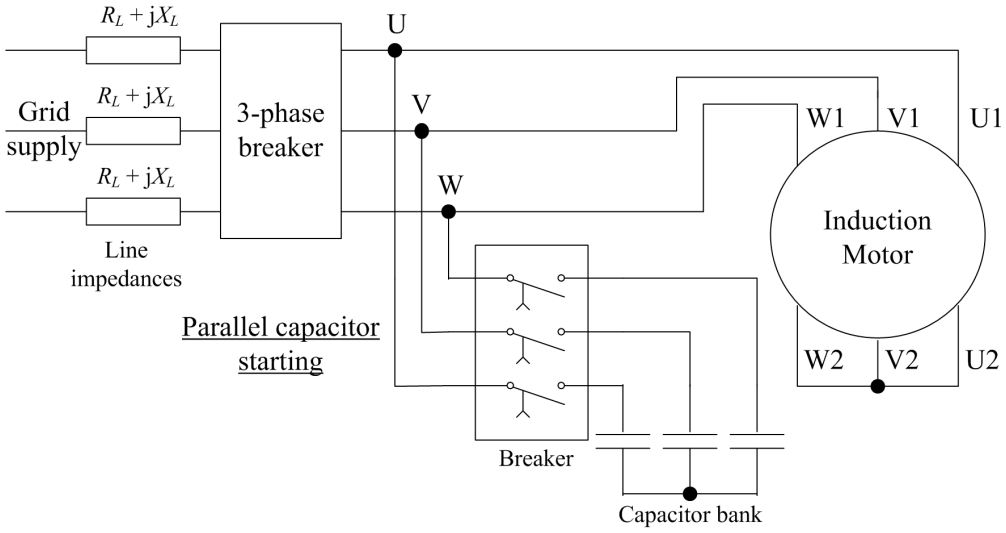

Figure 2.10 Parallel capacitor compensation.

Table 2.2 Typical LV and MV cables for All-Aluminum-Conductors (AAC) [1].

Parameter	**LV cable**	**MV cable**
Diameter [mm]	4.67	36.93
Layers	1	4
Aluminum area [mm^2]	13.3	806.2
Suggested max. current [A]	140	1380
R_L [Ω/km]	2.2	0.042
X_L [Ω/km]	0.481	0.32
X_c [MΩ/km]	0.289	0.19
V_{drop} max [V]	315.3	445.4
Suggested and calculated cables		
Suggested max length [m]	100	1000
Suggested voltage [V]	420	6000
Calculated max. voltage drop	13 %	12.8 %

2.3.2.5.6 DSTATCOM compensation. Capacitor compensation will only address the reactive power demand and studies have been done in the use of distribution static compensators (DSTAT-

COMs) in parallel with the motor during starting [49]. The system is shown in Fig. 2.11. The disadvantages with this system are that it is expensive and the DC capacitor on the DC side of the STATCOM needs to store most of the energy needed to start the machine to compensate for the motor power demand if it is controlled to compensate for energy drawn by the motor during starting and the reactive power.

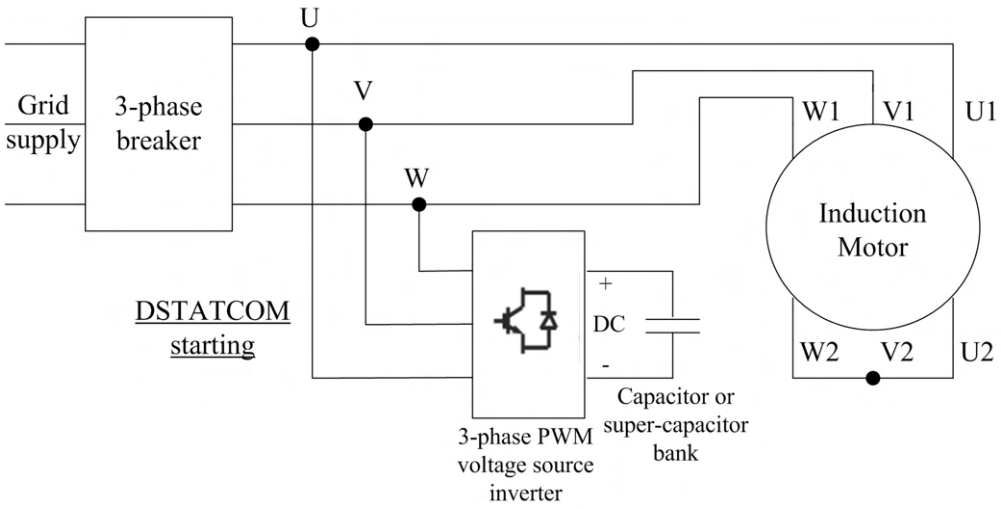

Figure 2.11 DSTATCOM induction motor starting.

2.3.3 Comparison of Starting Methods

The authors of [35] conducted an experimental study in order to compare DOL, star-delta and autotransformer starting methods for small motors of less than 3 HP. The results are shown in Table 2.3. These are applicable to large machines although there will be differences in supply requirements in terms of p.u. current, power and reactive power demands, and the p.u. torque performance.

Table 2.3 DOL, star-delta and autotransformer starting methods comparison.

Criteria	**Direct-On-Line**	**Star-Delta**	**Autotransformer**
Inrush Current	High	Moderate	Low
Voltage Sags	Severe > 0.5 p.u.	Less Severe < 0.2 p.u.	Less Sever < 0.2 p.u.
Harmonics	(THD < 1 %)	Less (THD < 1%)	Severe during starting (THD = 18.9 %)
Transients	Severe	Less Severe	Severe

In Section 4.3, a comparitave set of simulations is carried out using different motor models. However, it can be stated here that grid-connected squirrel cage induction motor starters lie in three different groups: starters that reduce the motor voltage and current using transformation or winding re-connection; starters that put impedances in series with the motor to restrict the motor current which can be resistive, reactive or capacitive; and parallel circuits that try to compensate for the motor reactive power or power demand.

2.4 Point-on Switching in Power Systems

In addition to the transient run-up period when there is high current there is the transient turn-on current when the motor is magnetized and switching of the capacitors. Turn-on has been improved in large devices by controlling the point of turn-on during a voltage cycle.

Point-on switching has been looked at in transformers [50, 51, 52] and there have been studies of thyristor switching of capacitors [53] and IGBT switching [54].

There now exist larger solid-state relays that can do point-on switching though they use Triac technology and they can take as long as 10 ms to complete their turn-on or turn off [55, 56].

However, [57] studied this and the switching can be faster. These devices switch on when there is a zero voltage across them [58].

In power systems, there are specialists in point-on switching to avoid incorrect switching leading to overvoltage [59]. In some instances, if the switching time is known then the point-on switch can be triggered some time before the switching occurs [60].

In this work the use of point-on switching is simulated to assess how it affects the system inrush currents and an experimental system is developed using solid-state relays.

2.5 Conclusions

The standard starting techniques commonly used to reduce the inrush current were reviewed in [61] and these have been further detailed in this chapter. The reviewed methods show that the starting current can be reduced by the different methods (by about three times in the case of star-delta starting) but with a similar reduction in starting torque. Some novel methods that were assessed used series or parallel capacitors which can reduce starting current though they did not assess the starting torque. With series capacitors, with a reduction in current comes a reduction in torque since the motor current is the same as the line current. With parallel capacitors, the line current can be reduced without reduction in starting torque. This is shown through simulation in Chapter 4.

The aim of this work is the reduction of starting current, with no further motor design and at a relatively low cost.

Induction motors typically have very low power factor during starting, as a result they have very large reactive power draw. There are mainly three types of equipment used to compensate the

reactive power:

- Synchronous condensers;
- Static capacitors or capacitor banks; and
- Power electronic converters such as STATCOMs.

Synchronous condensers are synchronous generators that operate with reactive power generation only, i.e., overexcited. They are often the mode that older generating stations work in until they are required to deliver power at peak periods. They can produce reactive power and the production of reactive power can be regulated. Due to this regulating advantage, the synchronous condensers are very suitable for correcting the power factor of the system, but this equipment is quite expensive compared to static capacitors. That is why synchronous condensers are only used for voltage regulation of a high voltage transmission systems rather than used at distribution level.

Early methods of mitigating inrush currents (Table 2.4), mostly involved the calculation for the first peak of inrush current [62, 63, 64]. The proposed method in this work can be implemented using a microcontroller where the program algorithm is written in such way that the switching of capacitors in the network is done any time the current arises above a given value indicating inrush current as well as the starting period. The method is governed by the load power factor at start

$$\cos\theta = \frac{P}{VI\sqrt{3}} \tag{2.3}$$

where $\cos\theta$ is the power factor; P is the real power; I is the input line current; and V is the line voltage.

Table 2.4 The various starting methods and characteristics.

	DOL	**Auto Transformer**	**Solid State Starters**	**Adjustable Frequency Drives**	**Primary Resistor or Reactor**	**Part Winding**	**Star-Delta**
Initial System Cost	Low	Moderate	Higher	Highest	Moderate	Low	Low
Starting Current	Highest	Low	Moderate	Lowest	Moderate	Moderate	Low
Starting Torque	Highest	Low	Low	Highest	Low	Low	Low

With the added capacitors connected in parallel with the motor then the inrush current is reduced. The large reactive currents required by the motor can lag close to 90° elec.. As an alternative to an independent motor-starter system, if the system is a Smart Grid that is islanded the reactive power in the system can be balanced using a central control system [65]. However, these systems are still not common.

In a stand-alone starting system that compensates for the motor reactive power, the capacitors act to supply a current that leads the applied voltage by 90° elec.. The leading currents supplied by the capacitors cancel the lagging current demanded by the motor, reducing the amount of reactive power required to be drawn from the power system [66]. As discussed earlier, some systems will further compensate to have a net generation of reactive power that can boost the line voltage.

One problem reported by [41] is that if the motor loses power when connected to a high inertia load, and with the capacitor compensation still connected then, there can be resonance with the capacitors and machine reactance that can result in severe over-voltage. They report 45% over-voltage in their example and this would be sufficient to possibly cause damage.

Chapter 3

Theory

3.1 Introduction

In this chapter, the theory and analysis used in the development of the system is put forward. This can be split into steady-state analysis and transient analysis. Considering the relatively long staring period, an equivalent circuit analysis can be carried out. To address the turn-on and run-up transients a four-coil model of an induction motor can be used.

3.2 Steady-State Analysis

In this section, analysis is done which assumes the starting transient is long compared to electrical transients so that so the analysis can be done using reactances and steady-state variables. This includes the consideration of power and reactive power measurement, equivalent circuit analysis

and capacitor compensation.

3.2.1 Steady-State Power and Reactive Power

The total power P and total reactive power Q in a 3-phase AC system can be given by

$$P = \sum_{ph=1}^{3} \Re \left\{ \overline{E}_{ph} \overline{I}_{ph}^{*} \right\} \tag{3.1}$$

and

$$Q = \sum_{ph=1}^{3} \Im \left\{ \overline{E}_{ph} \overline{I}_{ph}^{*} \right\} \tag{3.2}$$

where ph is the phase number, $\overline{E}_{ph}$ is the phase voltage phasor and $\overline{I}_{ph}$ is the phase current phasor. These are rms values.

The induction motor is a three wire system so that the fourth neutral line is not available for obtaining the the phase voltages. The "two wattmeter" method can be used to measure the total power where

$$P = \sum_{ph=1}^{3} \Re \left\{ \left(\overline{E}_1 - \overline{E}_2 \right) \overline{I}_2^{*} + \left(\overline{E}_3 - \overline{E}_2 \right) \overline{I}_2^{*} \right\} \tag{3.3}$$

this is a well know relationship and will work for an unbalanced 3-phase system.

Less well known is that two wattmeters can be used to measure the reactive power too. However this is for a balanced system. For this it is assumed that

$$\overline{I}_1 = \frac{j}{\sqrt{3}} \left(\overline{I}_2 - \overline{I}_3 \right) \tag{3.4}$$

The total reactive power is obtained by considering the reactive power in Phase a and multiplying

by three

$$\begin{aligned} Q =& 3 \times \Im \left\{ \overline{E}_1 \overline{I}_1^* \right\} = 3 \times \Im \left\{ \frac{j}{\sqrt{3}} \overline{E}_1 \left(\overline{I}_2^* - \overline{I}_3^* \right) \right\} \\ =& \Re \left\{ \frac{1}{\sqrt{3}} \overline{E}_1 \left(\overline{I}_2^* - \overline{I}_3^* \right) \right\} = \sqrt{3} \Re \left\{ \overline{E}_1 \overline{I}_2^* - \overline{E}_1 \overline{I}_3^* \right\} \end{aligned} \tag{3.5}$$

In a modern 3-phase power analyser the power factor and reactive power is electronically calculated but the connections often require the two wattmeter connection.

3.2.2 Steady-State Equivalent Circuit Analysis

The standard per-phase equivalent circuit for a 3-phase induction motor is given in Fig. 3.1(a). In this:

R_1 is the stator winding resistance.

$R_2^{/}$ is the rotor resistance referred to the stator.

X_1 is the stator winding leakage reactance.

$X_2^{/}$ is the rotor leakage reactance referred to the stator.

X_m is the magnetising reactance.

R_c is the core loss resistance for the stator and rotor.

E_{ph} is the per-phase terminal voltage.

This is a per-phase model so the assumption is that if the motor was a three terminal black-box, the internal connection is star, no matter if it was connected internally as star or delta. If it was star, then reconnecting in delta internally would reduce all the impedances in the per-phase equivalent circuit by three and the rated voltage would go down by $\sqrt{3}$ while the rated current would go up by $\sqrt{3}$. These parameters can be obtained using the simple running-light and locked-rotor tests as

illustrated in Appendix A.2.

As stated above, X_m and R_c are the magnetizing reactance and core loss resistance and these are, for a well designed machine, much greater then at stator resistance R_1, the stator leakage reactance X_1, the referred rotor leakage reactance $X_2^{/}$ and the referred rotor resistance $R_2^{/}$. The slip s is given by

$$s = \frac{\omega_s - \omega_r}{\omega_s} \tag{3.6}$$

where ω_s is the synchronous speed and ω_r is the motor speed, both in rad/s. The effective rotor resistance $\frac{R_2^{/}}{s}$ is the sum of the rotor resistance and the electro-mechanical energy conversion component in the circuit so that

$$\frac{R_2^{/}}{s} = R_2^{/} + \frac{(1-s)R_2^{/}}{s} \tag{3.7}$$

The rotor loss is then $3|I_r|^2 R_2^{/}$ and the mechanical power is

$$\frac{3(1-s)|I_r|^2 R_2^{/}}{s}. \tag{3.8}$$

Using (3.8) and (3.6), the torque can be written as

$$\begin{aligned} T_{mech} =& \frac{P_{mech}}{\omega_r} = \frac{3(1-s)|I_r|^2 R_2^{/}}{s} \times \frac{1}{\omega_r} \\ =& \frac{3(1-s)|I_r|^2 R_2^{/}}{s} \times \frac{1}{(1-s)\omega_s} = \frac{3|I_r|^2 R_2^{/}}{s\omega_s} \end{aligned} \tag{3.9}$$

and

$$I_r = I_{in} \times \frac{Z_m \left(\frac{R_2^{/}}{s} + jX_2^{/} \right)}{Z_m + \left(\frac{R_2^{/}}{s} + jX_2^{/} \right)} \tag{3.10}$$

where

$$Z_m = \frac{jX_m R_c}{R_c + jX_m} \tag{3.11}$$

With a knowledge of the equivalent circuit parameters, the torque/speed and current/speed steady-state curves can be easily obtained. The steady-state power and reactive power can also be obtained.

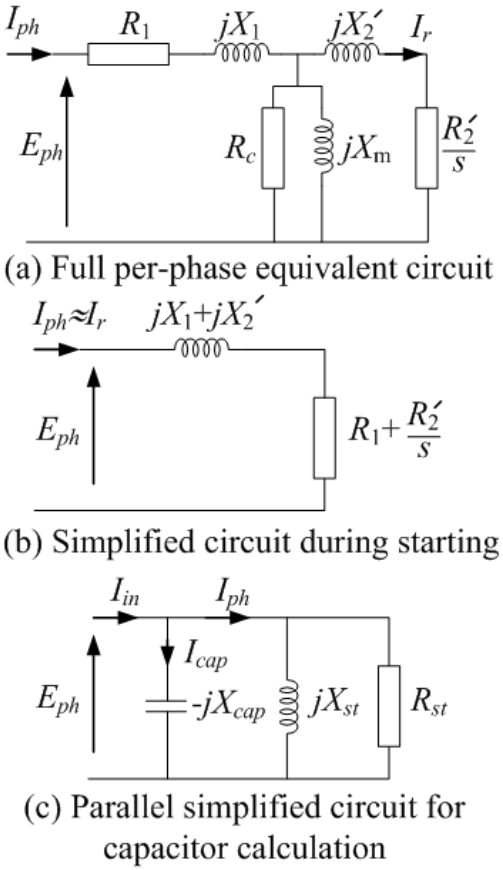

Figure 3.1 Equivalent circuits.

3.2.3 Compensation During Starting

As stated earlier, the magnetizing components of the equivalent circuit which form Z_m are much higher than the other components of the equivalent so that they can be ignored when s is close to 1 in Fig. 3.1(a) which gives the approximate circuit in Fig. 3.1(b). At what point this ceases to be valid depends on the ratio of X/R of the circuit. If it is high, i.e., very inductive, the speed will have increased to close to the synchronous speed before the resistive part begins to have an affect. This means that the starting current will be almost constant through the run-up of the motor. This is very much a function of the motor though they generally become more inductive as the size increases. This will be addressed in the simulations. The simplified circuit in Fig. 3.1(b) can be put into parallel in order to calculate the capacitance of the compensating capacitors. For the circuit in Fig. 3.1(c) with $s = 1$:

$$R_1 + R_2^{/} + j\left(X_1 + X_2^{/}\right) = \frac{jR_{st}X_{st}}{R_{st} + jX_{st}} \tag{3.12}$$

giving

$$R_{st} = \frac{1}{\left(R_1 + R_2^{/}\right)}\left(\left(R_1 + R_2^{/}\right)^2 + \left(X_1 + X_2^{/}\right)^2\right) \tag{3.13}$$

$$X_{st} = \frac{1}{\left(X_1 + X_2^{/}\right)}\left(\left(R_1 + R_2^{/}\right)^2 + \left(X_1 + X_2^{/}\right)^2\right) \tag{3.14}$$

To get resonance, when I_{in} will be wholly real, then in Fig. 3.1(c)

$$X_{cap} = Xst \tag{3.15}$$

These are easily calculated.

3.2.3.1 Effects of saturation

The induction motor can be substantially effected by magnetic saturation, particularly during starting, and for smaller motors with skewing on the rotor or stator that will cause axial saturation [67, 68]. The models developed here are linear and do not account for saturation since they use equivalent circuit analysis and motor tests. The locked rotor test is done at reduced level if done manually so may not include saturation effects. For the industrial machines used in the Chapter 4 the locked rotor test may be automated and done at a level where the saturation is incorporated into the equivalent circuit parameters.

Saturation will tend to reduce the motor impedance and increase the starting current and torque, generating "pull-up" torque where the torque increases from about $s = 0.5$ down to standstill where $s = 1$. Papers which address this are [69, 70].

Analytical methods [71, 72] and electromagnetic finite element analysis [73] can be used to assess saturation in machines. Here equivalent circuit and 4-coil models (in Simulink) are used for machine performance assessment over a variety of machines.

3.2.3.2 Star or delta connection

The capacitors can be connected as either

- Shunt capacitors, or
- Series capacitor

In this work the capacitors are be connected in shunt. There are some specific advantages of using shunt capacitors, as previously discussed:

- They reduce the line current of the system;

- They can improve the voltage level of the load;
- They can reduce system losses;
- They can improve the power factor of the source current; and
- Can reduce capital investment of the load because the supply may not need to be upgraded.

Obviously these benefits come from the fact that the effects of the capacitor are to reduce the reactive current flowing through the whole system.

Series-connected capacitors for motors are not an appropriate application because they have to be very large and carry the full load current while their voltage is lower than for shunt-connected capacitors. This can potentially cause a catastrophic failure. For the series connection, capacitor failure can cause motor failure because it makes the load unbalanced therefore the motor may be damaged due to the unbalanced voltage and possible 2-phase operation, causing overheating [74, 75].

Series connected capacitors are more vulnerable to failure due to harmonics [76, 77] since they have to carry the full motor current.

Delta connection is chosen in this work. They provide capacitance to each phase and do not provide voltage unbalance harmonics. However, they can be susceptible to low frequency harmonics and filters may be necessary [78]. These are shown in Fig. 3.2. A low pass filter should be suitable in this application to suppress the 5th, 7th, 11th, 13th, etc harmonics. In the case of a failure of one capacitor for one phase for any reason, it moves from a closed delta to an open delta configuration [53, 79] as illustrated in Fig. 3.3. In this case the voltage remains unchanged. When in delta, if a capacitor is lost, the other two will continue to deliver reactive power, whereas they will produce less reactive power if they were connected in star. In Fig. 3.3, if they normally produce 10 kVAr at 600 V, when a delta-connected capacitor is lost then two will continue to produce

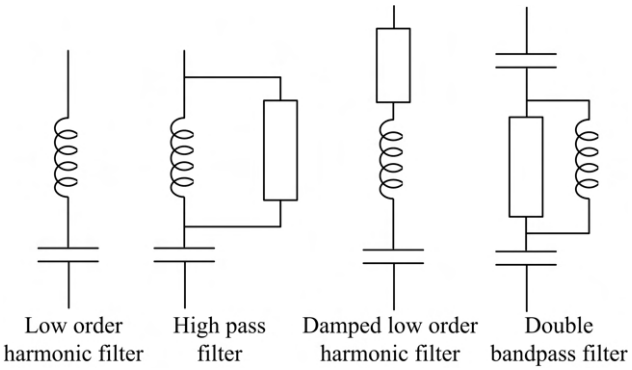

Figure 3.2 Possible filter arrangements - low pass filter most suitable in this application.

20 kVAr in total. However, in star, they are now series connected across two phases so that the capacitor voltage goes down from $\frac{600}{\sqrt{3}}$ to $\frac{600}{2}$. The reactive power in a capacitor is $Q = I^2 X_c = \frac{V^2}{X_c}$. Taking voltage-squared ratios then $Q_{tot} = 2 \times 10 \times \left(\frac{\sqrt{3}}{2}\right)^2 = 15$ kVAr.

In delta connection, capacitors are capable of circulating harmonic currents within the circuit, therefore reducing the harmonics on the electrical system. Also, when there is a capacitor open-circuit, the other two will supply reactive power to the system than a star-connected network as shown in Fig. 3.3.

Fig. 3.23 later illustrates the full system with the capacitor connection in a delta together with the 3-phase induction motor.

3.2.3.3 Variation with voltage

The voltage has an effect on an induction motor. From (3.9) it can be seen that the torque is a function of the rotor current squared and in (3.10) the rotor current is proportional to the input current. Assuming no saturation, then the input current is proportional to the applied voltage. Hence, the torque is a function of the voltage-squared. The required reactive power will also be

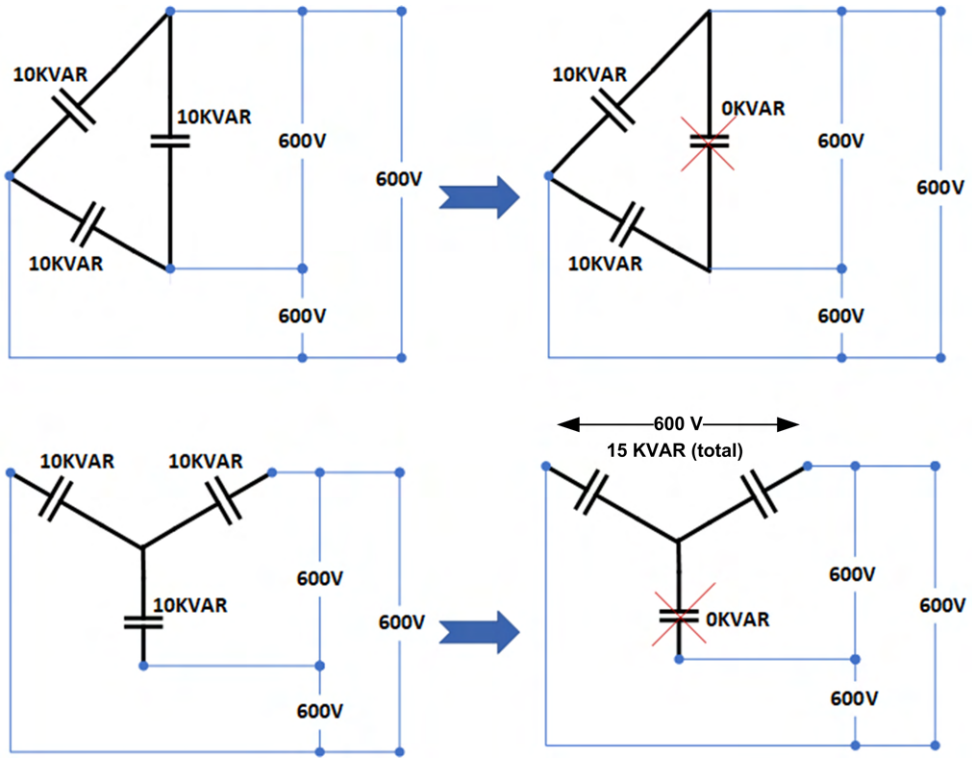

Figure 3.3 Failure of a capacitor in a star or delta connected bank.

a function of the voltage-squared. However, as described in Section 3.2.3.1, higher voltages may saturate the iron and cause a disproportionately higher torque and current.

Neglecting saturation effects then for a 10 % increase in voltage, there will be a 21 % increase in torque and current. For a 10 % decrease in voltage there will be a 19 % decrease in torque and current. This is addressed in [80].

In terms of capacitor compensation, since the reactive power absorbed by the induction motor is a function of the voltage-squared, and the reactive power generated by the capacitor bank is a function of the voltage-squared, then the capacitors remain matched with the motor even with voltage variation unless there is substantial saturation effects.

3.2.4 Steady-State Run-up Time

Using equivalent circuit analysis the speed or slip can be stepped through to obtain current, torque, power, reactive power, etc, against speed or slip. It is useful for the motor torque to be matched against a load to get results against time as the motor runs up to speed. This can be done by considering the electro-mechanical system. To estimate the run-up time then the torque equation can be used. This is

$$T_{mech} = T_{load} + T_{FW} + J\frac{d\omega_m}{dt} \tag{3.16}$$

where J is the inertia and ω_m is the motor speed in rad/s. The load torque T_{load} and friction and windage torque T_{FW} may take the general form

$$T = K_1 + K_2\omega_m + K_3\omega_m^2 \tag{3.17}$$

The coefficients will vary greatly. For instance, a positive displacement pump requires a constant torque given constant output pressure so K_1 will be dominant (and the power proportional to the speed [81]), whereas a large fan has a torque that is a mostly a function of the square of the speed (with the power a cubic function) so that that K_3 is dominant [82].

If the motor is started with no load, for instance with no fluid flowing in the pump, then the system inertia can be used to find the approximate run-up time. This means

$$T_m = J\frac{d\omega_m}{dt} \tag{3.18}$$

when stepping through the slip and calculating the torque, the time step can also be calculated from

$$\Delta t \approx J\frac{\Delta\omega_m}{T_{mech}} \tag{3.19}$$

For a set step in speed $\Delta\omega_m$ then

$$\Delta t(n) \approx \frac{2J\Delta\omega_m}{(T_{mech}(n) + T_{mech}(n-1))} \tag{3.20}$$

This uses the mean torque between steps $n-1$ and n. If there is a load then this can be included:

$$\Delta t(n) \approx \frac{2J\Delta\omega_m}{(T_{mech}(n) - T_{load}(n) + T_{mech}(n-1) - T_{load}(n-1))} \tag{3.21}$$

The time at each step can then be obtained by numerical summation of the time steps:

$$t(n) = \sum_{1}^{n} \Delta t(n) \tag{3.22}$$

3.3 Transient Analysis

3.3.1 Instantaneous Power and Reactive Power During Starting

Real and reactive power flow are associated with averaged values over a cycle in a sinusoidal AC system. However, during the transient starting sequence is it convenient to give instantaneous power and reactive power. Since reactive power is associated with the cycling of energy in an AC system then for instantaneous reactive power to have meaning then the transient starting cycle is assumed to be much longer than the supply period.

3.3.1.1 Park's transformation

A 3-phase system can be converted to a 2-phase system using Park's Transformation (abc-to-dq0). This allows the forwards, backwards and zero order components to be accounted for. However, there will be no zero order currents going into an induction motor because the machine is either delta-connected or star-connected with now earth on the start point. The 2-axis reference frame is either static or rotating. In this work it is assumed to be static $\alpha - \beta$ axes where α corresponds with the a-axis of the 3-phase system. This is illustrated in Fig. 3.4.

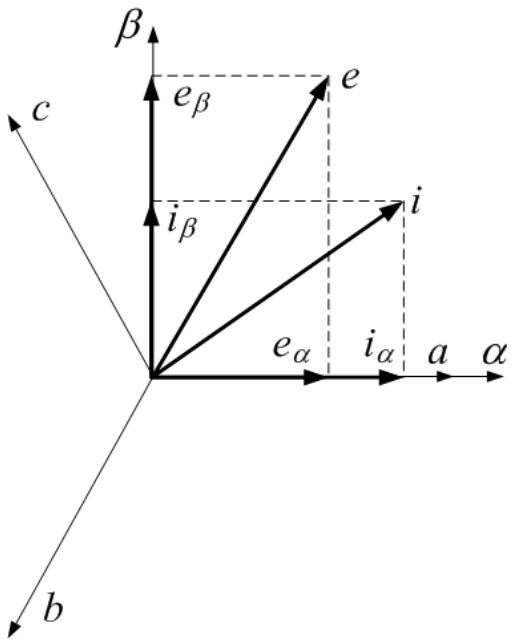

Figure 3.4 $\alpha - \beta$ transformation.

The transformations from 3-phases to 2-phases for the voltages and currents are

$$\begin{bmatrix} e_\alpha \\ e_\beta \end{bmatrix} = \sqrt{\frac{2}{3}} \begin{bmatrix} 1 & -\frac{1}{2} & -\frac{1}{2} \\ 0 & \frac{\sqrt{3}}{2} & -\frac{\sqrt{3}}{2} \end{bmatrix} \begin{bmatrix} e_a \\ e_b \\ e_c \end{bmatrix} \tag{3.23}$$

and

$$\begin{bmatrix} i_\alpha \\ i_\beta \end{bmatrix} = \sqrt{\frac{2}{3}} \begin{bmatrix} 1 & -\frac{1}{2} & -\frac{1}{2} \\ 0 & \frac{\sqrt{3}}{2} & -\frac{\sqrt{3}}{2} \end{bmatrix} \begin{bmatrix} i_a \\ i_b \\ i_c \end{bmatrix} \tag{3.24}$$

With voltages e_α, e_β and currents i_α, i_β which are instantaneous values. These can be vectorized so that

$$\bar{e} = e_\alpha + j e_\beta \tag{3.25}$$

and

$$\bar{i} = i_\alpha + j i_\beta \tag{3.26}$$

3.3.1.2 Instantaneous power

The instantaneous power p of a 3-phase circuit is represented generally by

$$p = e_a i_a + e_b i_b + e_c i_c \tag{3.27}$$

In $\alpha - \beta$ coordinates, p is expressed as:

$$p = e_\alpha i_\alpha + e_\beta i_\beta \tag{3.28}$$

Moving from 3-phase to a 2-phase system means that the power in one phase of the two phase system is 3/2 times that in one phase of the 3-phase system. Using (3.23) and (3.24) then for the α phase

$$e_\alpha = \sqrt{\frac{2}{3}} \left(e_a - \frac{1}{2} e_b - \frac{1}{2} e_c \right) \tag{3.29}$$

and

$$i_\alpha = \sqrt{\frac{2}{3}} \left(i_a - \frac{1}{2} i_b - \frac{1}{2} i_c \right) \tag{3.30}$$

To verify this balances then assume the Phase a voltage is peaking and the power factor is unity. If the system is a balanced 3-phase system then:

$$e_b = e_c = -0.5\hat{e}_a \text{ and } i_b = i_c = -0.5\hat{i}_a$$

so that working through from (3.29) gives

$$\hat{e}_\alpha = \sqrt{\frac{2}{3}}\left(\hat{e}_a + \frac{1}{4}\hat{e}_a + \frac{1}{4}\hat{e}_a\right) = \sqrt{\frac{3}{2}}\hat{e}_a \tag{3.31}$$

and

$$\hat{i}_\alpha = \sqrt{\frac{2}{3}}\left(\hat{i}_a + \frac{1}{4}\hat{i}_a + \frac{1}{4}\hat{i}_a\right) = \sqrt{\frac{3}{2}}\hat{i}_a \tag{3.32}$$

So the peak instantaneous power in the α phase is

$$\hat{e}_\alpha \hat{i}_\alpha = \frac{3}{2}\hat{e}_a \hat{i}_a \tag{3.33}$$

which validates the Park's Transform and gives the correct ratio between the peak power in the Phase a and α-phase.

It is worth looking at how the power varies instantaneously. Assuming that the 3-phase set is sinusoidal with unity power factor and balanced then (3.27) can be rewritten as

$$\begin{aligned} p =& \hat{e}\hat{i}\sin^2(\omega t) + \hat{e}\hat{i}\sin^2(\omega t - 120°) + \hat{e}\hat{i}\sin^2(\omega t + 120°) \\ =& \frac{3\hat{e}\hat{i}}{2}\left((1 + \cos(2\omega t)) + \cos(2\omega t + 120°) + \cos(2\omega t - 120°)\right) \\ =& \frac{3\hat{e}\hat{i}}{2} \end{aligned} \tag{3.34}$$

This illustrates that the power is constant.

3.3.1.3 Instantaneous reactive power

Reactive power is related to circulating cycling energy so instantaneous reactive power is difficult to assess. However, in $\alpha - \beta$ coordinates the reactive power can be assessed using

$$q = e_\alpha i_\beta - e_\beta i_\alpha \tag{3.35}$$

which can be rewritten as

$$q = \begin{bmatrix} e_\alpha & -e_\beta \end{bmatrix} \begin{bmatrix} i_\beta \\ i_\alpha \end{bmatrix} \tag{3.36}$$

From (3.23)

$$\begin{aligned} &\begin{bmatrix} e_\alpha & -e_\beta \end{bmatrix} \\ =&\sqrt{\frac{2}{3}} \begin{bmatrix} e_a - 0.5\,(e_b + e_c) & 0.866\,(e_b - e_c) \end{bmatrix} \\ =&\sqrt{\frac{2}{3}} \begin{bmatrix} 0.5\,(e_{ab} - e_{ca}) & -0.866 e_{bc}) \end{bmatrix} \end{aligned} \tag{3.37}$$

where e_{ab}, e_{bc} and e_{ca} are the instantaneous line voltages.

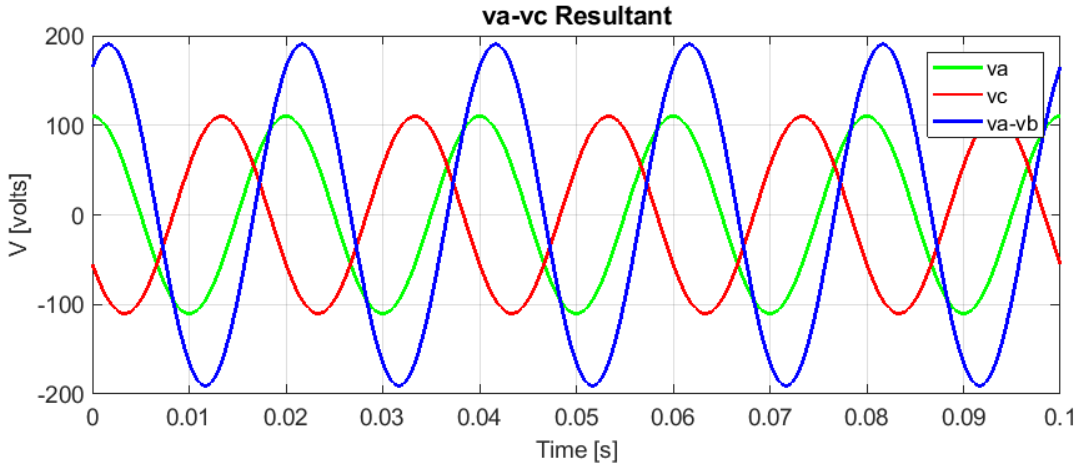

Figure 3.5 Voltages e_a, e_b and e_a-e_b waveforms.

It can be seen in Fig. 3.5 that the line voltage e_{ab} leads phase voltage e_a by 30°.

From (3.24)

$$\begin{aligned}\begin{bmatrix} i_\beta \\ i_\alpha \end{bmatrix} &= \sqrt{\frac{2}{3}} \begin{bmatrix} 0.866\,(i_b - i_c) \\ i_a - 0.5\,(i_b + i_c) \end{bmatrix} \\ &= \sqrt{\frac{2}{3}} \begin{bmatrix} 0.866\,(i_b - i_c) \\ -1.5\,(i_b + i_c) \end{bmatrix}\end{aligned} \tag{3.38}$$

What can be seen from (3.37) and (3.38) is that the instantaneous reactive power can be obtained from the measurement of the line voltages and currents in Phases b and c. By measurements of the voltages and currents instantaneously it is possible to compensate for reactive power. A block diagram is shown in Fig. 3.6 as put forward in [83]. The realisation of this constitutes the focus of this study.

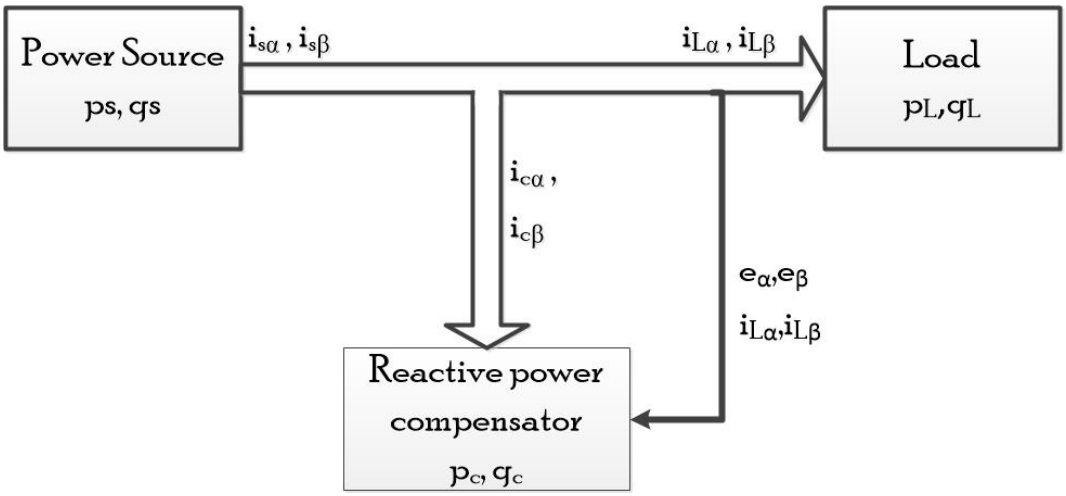

Figure 3.6 The reactive power compensator.

Further detailing of instantaneous reactive power flow is given by [83] in terms of instantaneous power. This is further backed up by [84].

3.3.2 Transient Run-Up

The machine can be analysed using the 4-coil model and Park's transforms in Section 3.3.1.1. The system in shown in Fig. 3.7. This has static $\alpha-\beta$ coordinates and rotating $d-q$ coordinates which rotate at synchronous speed. The rotor coils are short circuited so that $e_{2d}=e_{2q}=0$ and the $d-q$ axes rotate with respect to the $\alpha-\beta$ axes where

$$\theta_d = \theta_\alpha + \omega_r t \tag{3.39}$$

and

$$\theta_q = \theta_\beta + \omega_r t \tag{3.40}$$

The α and β axes do not link each other since they are orthogonal, and similarly for the d and q axes. However, because the $d-q$ axes are rotating then they do link the $\alpha-\beta$ and this can be accounted for using

$$e = \frac{\mathrm{d}(Li)}{\mathrm{d}t} = L\frac{\mathrm{d}(i)}{\mathrm{d}t} + i\frac{\mathrm{d}(L)}{\mathrm{d}t} \tag{3.41}$$

since the rotation will generate variation in mutual linkage - these are the second term in (3.41) and often called the speed terms. Fig. 3.8 shows the α and β equivalent circuits and the speed terms are represented by the voltage sources. These circuits look similar to the steady-state equivalent circuit although the core loss resistance is neglected. This is a common approximation.

From Fig. 3.8 we can write the voltage equations for system. For the α axis stator loop

$$e_{1\alpha} = R_1 i_{1\alpha} + \frac{\mathrm{d}\phi_{1\alpha}}{\mathrm{d}t} + \omega\phi_{1\beta} \tag{3.42}$$

where

$$\phi_{1\alpha} = (L_1 + L_m)\, i_{1\alpha} + L_m i'_{2\alpha} \tag{3.43}$$

and

$$e_{1\beta} = R_1 i_{1\beta} + \frac{\mathrm{d}\phi_{1\beta}}{\mathrm{d}t} + \omega\phi_{1\alpha} \tag{3.44}$$

For the β axis stator

$$\phi_{1\beta} = (L_1 + L_m)\, i_{1\beta} + L_m i'_{2\beta} \tag{3.45}$$

The rotor values are referred to the stator. The rotor voltage equations can also be defined by

$$e'_{2\alpha} = 0 = R_1 i_{2\alpha} + \frac{\mathrm{d}\phi'_{2\alpha}}{\mathrm{d}t} - (\omega - \omega_r)\, \phi_{2\beta} \tag{3.46}$$

and

$$e'_{2\beta} = 0 = R_1 i_{2\beta} + \frac{\mathrm{d}\phi'_{2\beta}}{\mathrm{d}t} + (\omega - \omega_r)\, \phi_{2\alpha} \tag{3.47}$$

where

$$\phi'_{2\alpha} = \left(L'_2 + L_m\right) i_{2\alpha} + L_m i_{1\alpha} \tag{3.48}$$

and

$$\phi'_{2\beta} = \left(L'_2 + L_m\right) i'_{2\beta} + L_m i_{1\beta} \tag{3.49}$$

These equations can be combined with the Park's equations in Section 3.3.1.1 to develop a transient system. Various methods can be used to do this though in this instance the induction motor model in Matlab/Simulink [85] is used as given in Fig. 3.9. This model will allow investigation of the transient turn-on and run-up. The parameters will be the per-phase equivalent circuit parameters with the reactances converted to inductances. They are therefore obtained from the running-light and locked rotor tests making implementation straightforward.

The torque can be obtained using

$$T_m = 1.5\left(\phi_{1\alpha} i_{1\beta} - \phi_{1\beta} i_{1\alpha}\right) \tag{3.50}$$

To test this then assume one phase is disconnected. There should be no torque produced at standstill if only two phases are excited. If Phase a is lost then $i_b = -i_c$. When this happens, if Phase a and the α-phase axes are the same. This will lead to no flux or current on the β axis so that no torque will be generated according to (3.50). The field is pulsing rather than rotating.

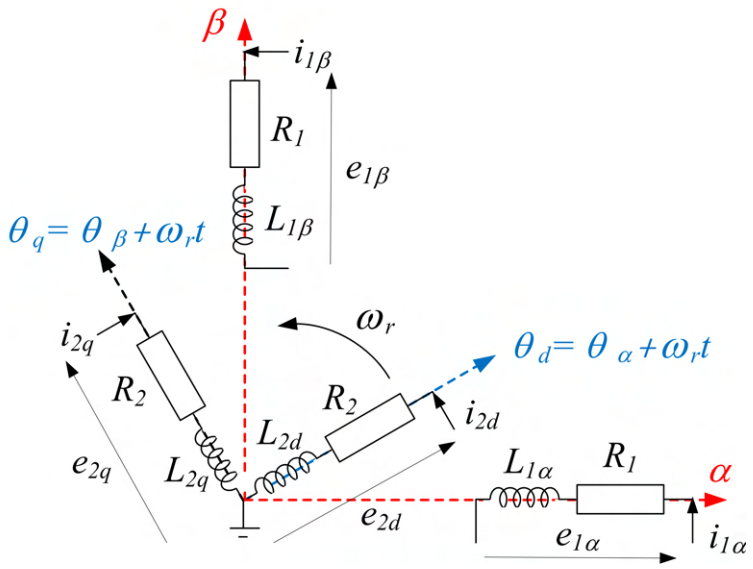

Figure 3.7 Four coil model of induction motor.

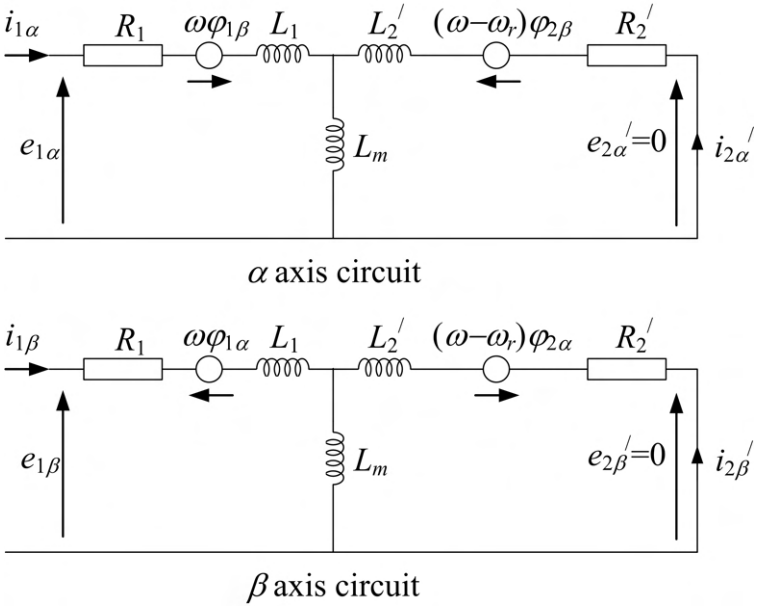

Figure 3.8 $\alpha - \beta$ equivalent circuits.

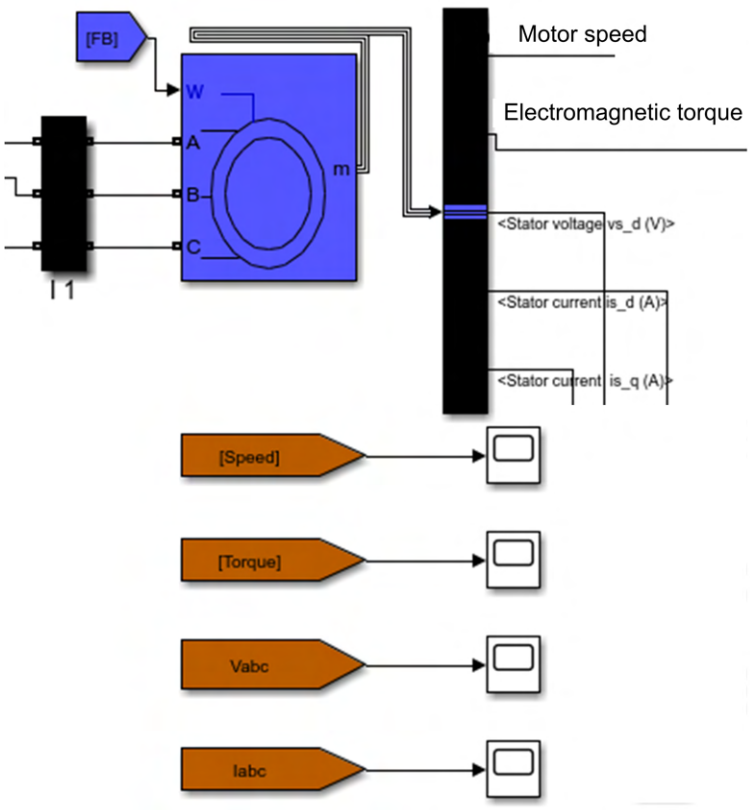

Figure 3.9 Simulink motor using 4-coil model.

3.3.3 Soft Turn-On of Induction Motor and Capacitor Bank

Point-on switching was reviewed in Section 2.4 and it is now possible to switch at a particular point on a waveform. In this project soft turn-on can be divided into the soft turn-on of the induction motor and the capacitor bank.

For a resistive load then soft starting is unnecessary since the current will follow the voltage $v = Ri$. However, switching an inductive 3-phase load onto the grid and a capacitor can give transient current peaks and spikes.

3.3.3.1 Soft Turn-On of an induction motor

For a pure inductor, since $v = L\dfrac{\mathrm{d}i}{\mathrm{d}t}$ then the current cannot change instantaneously. This equation can obviously be solved using mathematical derivations or using time-stepped methods such as the Runge-Kutta method. For such a simple equation a simple time-stepped solution is

$$v(t_n) = L\frac{i(t_n) - i(t_{n-1})}{t_n - t_{n-1}} = L\frac{i(t_n) - i(t_{n-1})}{\Delta t} \tag{3.51}$$

where Δt is the time step and $t(n)$ is the n^{th} time step. This can be re-arranged so that

$$i(t_n) = \frac{v(t_n)\Delta t + Li(t_{n-1})}{L} \tag{3.52}$$

For an R-L circuit:

$$v(t_n) = Ri(t_n) + L\frac{i(t_n) - i(t_{n-1})}{\Delta t} \tag{3.53}$$

Again, this can be rearranged

$$i(t_n) = \frac{v(t_n)\Delta t + Li(t_{n-1})}{L + R\Delta t} \tag{3.54}$$

The solution to this gives the transient decay together with the steady-state solution as illustrated in Fig. 3.10(a) where the voltage is alternating sinusoidally and the R-L circuit is switched in at $t = 0$. To remove the transient decay, which will reduce the overall starting current peak, then the circuit should be switched in at an angle of $\arctan(\omega L/R)$ as shown in Fig. 3.10(b). These simulations were carried out with a peak voltage of 100 V, an inductance of 5 mH and a resistance of 0.05 Ω. The time step is 0.5 ms and the simulation is for 200 ms. This gave a reactance of 1.57 Ω. This gives a switching point of 88.17° past the zero voltage point. This represents a large machine that is very inductive when starting. The peak of the steady state current is 63.6 A and the peak is 120 A when switching at the zero crossing point.

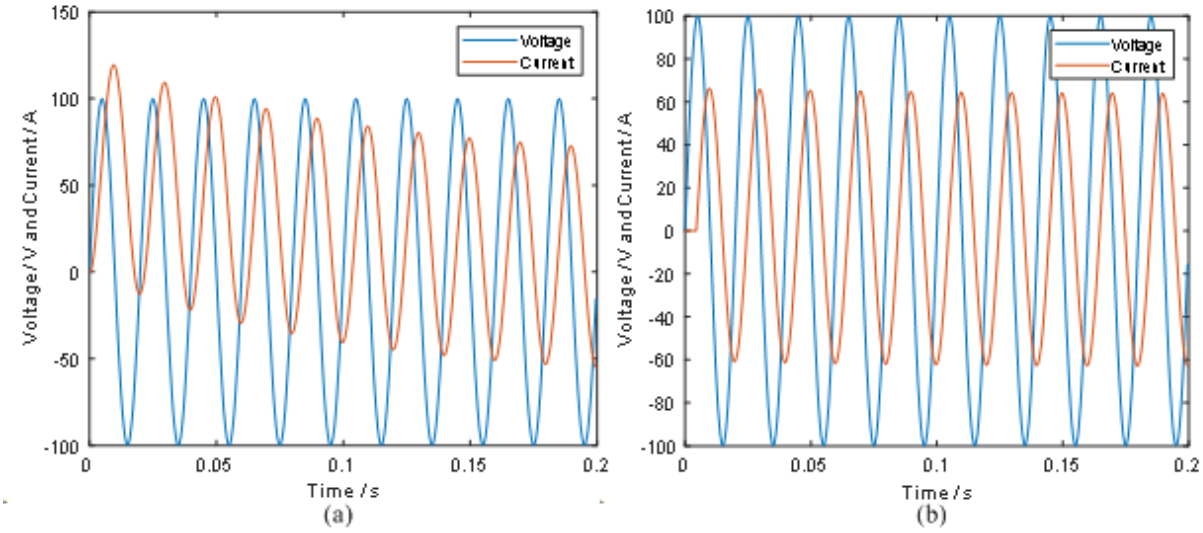

Figure 3.10 R-L circuit switching on at (a) $v = 0$ and (b) when the angle is $\arctan(\omega L/R)$. $X = 1.57\ \Omega$ and $R = 0.05\ \Omega$ representing a large machine.

To represent a smaller machine, the inductance was changed to 2.5 mH and the resistance increased to 0.5 Ω. This gave an $X = 0.785\ \Omega$ and a switching point of 57.52°. The steady state peak current is 107.4 A. Fig. 3.11(a) shows the switching at zero voltage with a peak current of 122 A. This illustrates that the transient turn-on current in smaller machines is not as significant. Fig. 3.11(b) shows the current turn-on at about 60°.

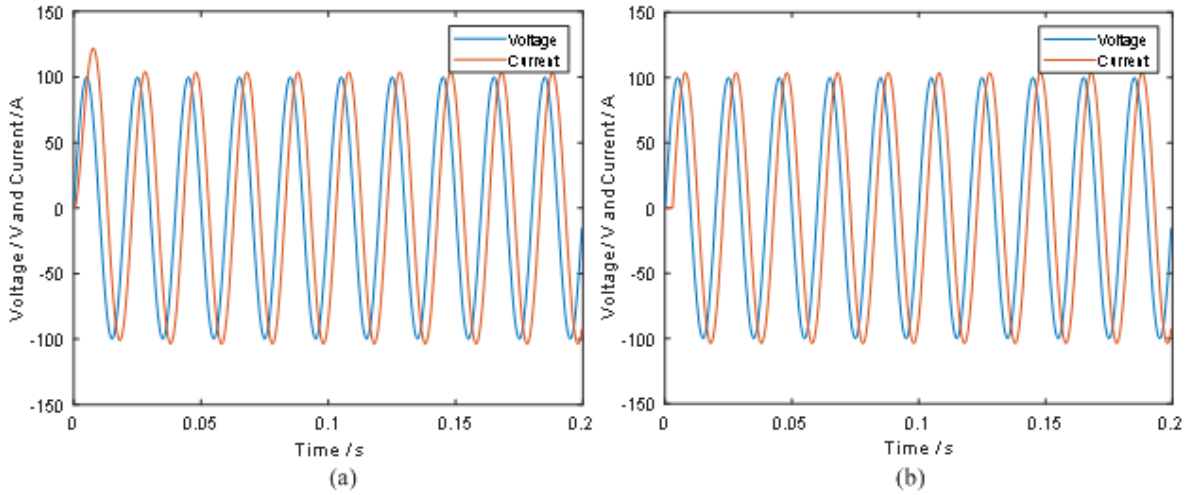

Figure 3.11 R-L circuit switching on at (a) $v = 0$ and (b) when the angle is $\arctan(\omega L/R)$. $X = 0.785\ \Omega$ and $R = 0.5\ \Omega$ representing a smaller machine.

While soft-switching can be used to reduced transient starting current by removing the transient decay as shown in Fig. 3.10(b), many smaller point-on switches are designed to switch when the voltage across it is zero which is the scenario in Figs. 3.10(a) and 3.11(a).

The sequence of turn-on for the 3-phase turn-on can now be addressed. The circuit can be considered as a 3-phase network with two voltage sources as shown in Fig. 3.12. There will be linkage between the phases through the inductance. The linkage is from the combination of leakage and magnetizing inductance. The phases are 120° with respect with each other so that the mutual linkage is often taken as $M = L_s \cos(120) = -L_s \cos(60) = -0.5L_s$. For Phase a

$$v_a = R_a i_a + L_a \dot{i}_a + M_{ab} \dot{i}_b + M_{ca} \dot{i}_c \tag{3.55}$$

If a balanced 3-phase system is assumed and a balance machine so that $L_s = L_a = L_b + L_c$ then

$$v_a = R_a i_a + L_a \dot{i}_a - 0.5L_s \dot{i}_b - 0.5L_s \dot{i}_c \tag{3.56}$$

which gives

$$v_a = \left(R_1 + R_2^{/}\right) i_a + L_s \dot{i}_a - 0.5 L_s \dot{i}_b - 0.5 L_s \dot{i}_c = \left(R_1 + R_2^{/}\right) i_a + \frac{3L_s}{2} \frac{\mathrm{d}i_a}{\mathrm{d}t} \tag{3.57}$$

since $-i_b - i_c = i_a$.

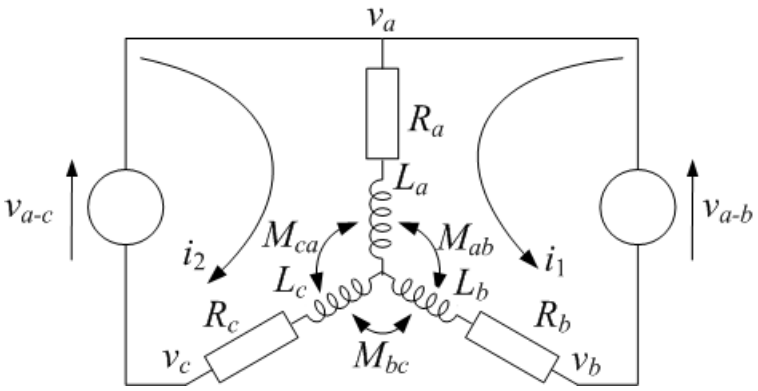

Figure 3.12 Equivalent circuit for turn-on.

Now consider the loops in Fig. 3.12. A matrix can be formed:

$$\begin{bmatrix} v_{a-b} \\ v_{a-c} \end{bmatrix} = \begin{bmatrix} 2R & R \\ R & 2R \end{bmatrix} \begin{bmatrix} i_1 \\ i_2 \end{bmatrix} + \begin{bmatrix} 2L_s + 2M & L_s + M \\ L_s + M & 2L_s + 2M \end{bmatrix} \begin{bmatrix} \dot{i}_1 \\ \dot{i}_2 \end{bmatrix} \tag{3.58}$$

where $R = \left(R_1 + R_2^{/}\right)$. Using the same time step approach:

$$\begin{bmatrix} v_{a-b}(t_n) \\ v_{a-c}(t_n) \end{bmatrix} = \begin{bmatrix} 2(R + L_s + M) & R + L_s + M \\ R + L_s + M & 2(R + L_s + M) \end{bmatrix} \begin{bmatrix} i_1(t_n) \\ i_2(t_n) \end{bmatrix} - \begin{bmatrix} 2(L_s + M) & L_s + M \\ L_s + M & 2(L_s + M) \end{bmatrix} \begin{bmatrix} i_1(t_{n-1}) \\ i_2(t_{n-1}) \end{bmatrix} \tag{3.59}$$

Rearranging:

$$\begin{bmatrix} i_1(t_n) \\ i_2(t_n) \end{bmatrix} = \frac{\begin{bmatrix} v_{a-b}(t_n) \\ v_{a-c}(t_n) \end{bmatrix} + \begin{bmatrix} 2(L_s+M) & L_s+M \\ L_s+M & 2(L_s+M) \end{bmatrix} \begin{bmatrix} i_1(t_{n-1}) \\ i_2(t_{n-1}) \end{bmatrix}}{\begin{bmatrix} 2(R+L_s+M) & R+L_s+M \\ R+L_s+M & 2(R+L_s+M) \end{bmatrix}} \tag{3.60}$$

Which can be solved in Matlab. If the sources are switched on at different times, so that i_2 is zero for a period then

$$i_1(t_n) = \frac{v_{a-b}(t_n) + 2(L_s+M) i_1(t_{n-1})}{2(R+L_s+M)} \tag{3.61}$$

3.3.3.1.1 Simulations of turn-on current in 3-phase machines. Chapter 4 carries out simulations of actual machines parameters both in steady-state and transient run-up. However, the simulations of the turn-on current are placed here to help understand this process.

The first few cycles of the turn-on sequence can be examined under different conditions using the machine impedances in Figs. 3.10 and 3.11. The first is more inductive representing a large machine and the second a smaller machine where the reactance and resistance are of a similar size. The scenarios that are addressed are:

1. Turn on all when $v_a = 0$ - this is more of a random switching point with no particular alignment of measurable line voltages;

2. Turn on all when $v_a - v_b = 0$; For point-on switching, then this is when many breakers would close. For Phase c then v_c is peaking, i.e., at the 90° point. For the large machine the switching point is 88.17° so this may be the correct point of switching for this phase;

3. Turn on Phases a and b when $v_a - v_b = 0$ and turn Phase c on when $v_c - v_{star} = 0$ - this would be the switching sequence for zero-crossing switching;

4. Turn on delay for $v_a - v_b$ of $\arctan(\omega L/R)$, i.e., 88.17° for the large machine and 57.52° for the smaller machine. This is a full soft-start turn-on simulation.

The simulations in Matlab are for only the first four cycles (8 ms) and the time step is again 0.5 ms; after this the machine is likely to be rotating where equivalent circuit parameters will change. For these simulations, example parameters for effectively large and small machines are used rather than the seven actual machine examples used later - the main interest here is the effect of X/R rather than their magnitude in order to directly compare the results using the same voltage (100 V peak) and similar current values.

Large machine - $X = 1.57\ \Omega$ and $R = 0.05\ \Omega$. The large machine has a peak steady-state current of 63.7 A. Scenario 1 is shown in Fig. 3.13 and it can be seen that there are transient offsets for all three phases with a peak current of 125 A which is double the steady-state starting current. Scenario 2 is given in Fig. 3.14. It can be seen that Phase a still has a high peak current of 120 A and Phase b has a peak of 100 A. However, Phase c is reduces to 86 A which is only 35% above the steady-state peak.

Fig. 3.15 shows soft switching when the phases are switched in when there is zero voltage across the breakers. For Phases a and b this is when the line voltage between them is zero, i.e., with reference to v_a, with 30° advance, and for connection of Phase c, a further 90° after that, i.e., 60° lagging with reference to Phase a. This is the point where $(v_a - v_b)/2 = v_{star} = 0$ and $v_c = 0$, i.e., the voltage across the breaker is zero. This switching point is also used for switching in the line-to-line connected capacitors. The current in Phase a has the highest current at 127 A which

Phase b is is 90 A and Phase c is 106 A. This switching strategy is good for protecting switchgear it does not offer a reduced turn-on transient.

Fig. 3.16 shows all phases going straight to steady-state. for the large machine this is at 88.17° delay with reference to the zero line voltage between Phases a and b. This is therefore a lag of 58.17° with reference to Phase a. Phase c is switched in at 88.17° after the zero point across the Phase c breaker, this is at 0.0049 s in the figure which is at 88.2°past the point where Phases a and b are connected. this is a lag of 146.4° from Phase a. This illustrates that it is possible to use careful point-on switching in very large machines to restrict the transient turn-on current of the machine and go straight to steady-state operation. This may also help limit torque oscillation.

Smaller machine - $X = 0.785\ \Omega$ **and** $R = 0.5\ \Omega$**.** The smaller machine has a peak steady-state current of 107.4 A. Scenario 1 is shown in Fig. 3.17 and it can be seen that there are transient offsets for all three phases with a peak current of 120 A which is only about 10% more than the steady-state current. Therefore Scenarios 2 and 3 are not needed here.

Scenario 4 is given in Fig. 3.18 and this illustrates again that correct switching will allow for straight to steady state current. This time the switching lags are 58.17° since the circuit is not as inductive.

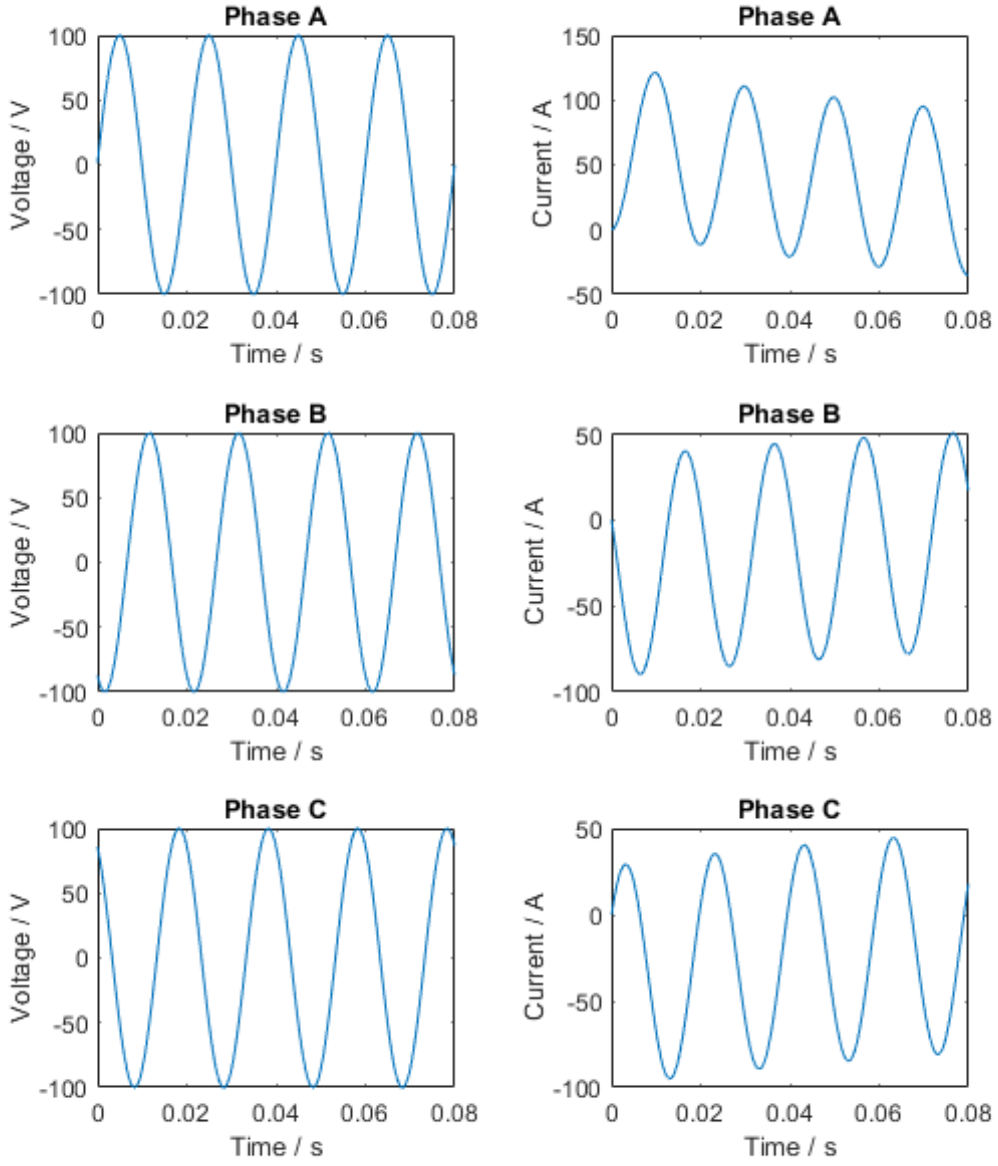

Figure 3.13 Scenario 1 - Large machine.

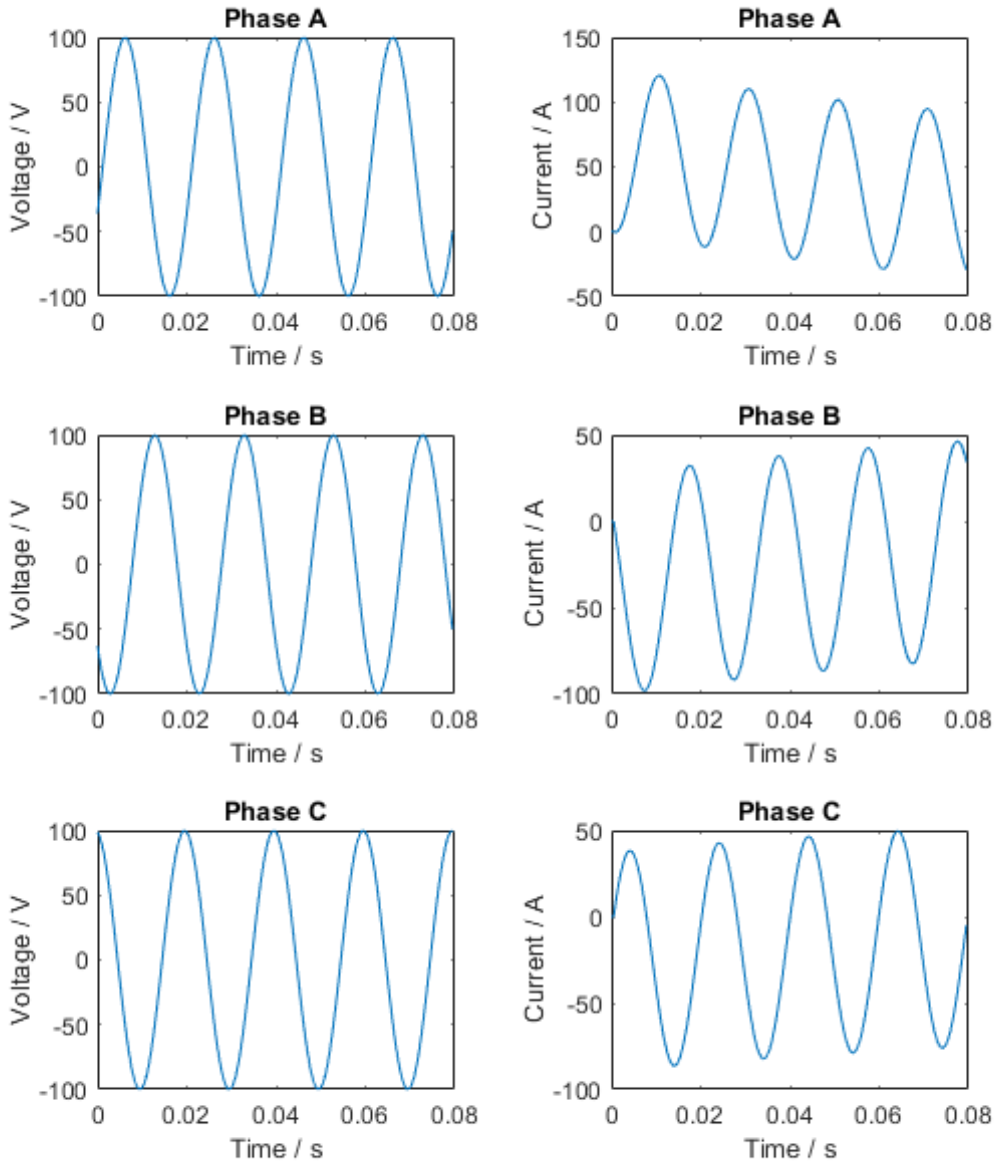

Figure 3.14 Scenario 2 - Large machine.

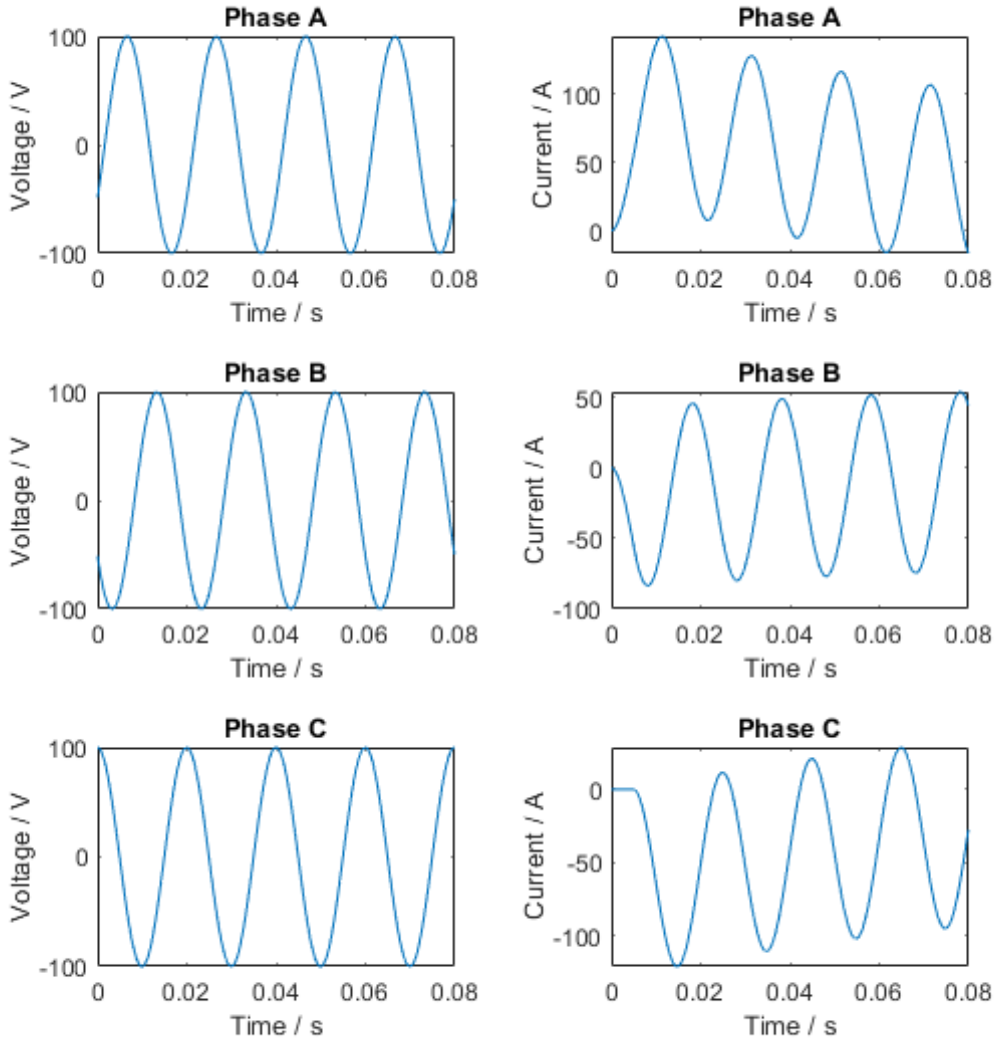

Figure 3.15 Scenario 3 - Large machine.

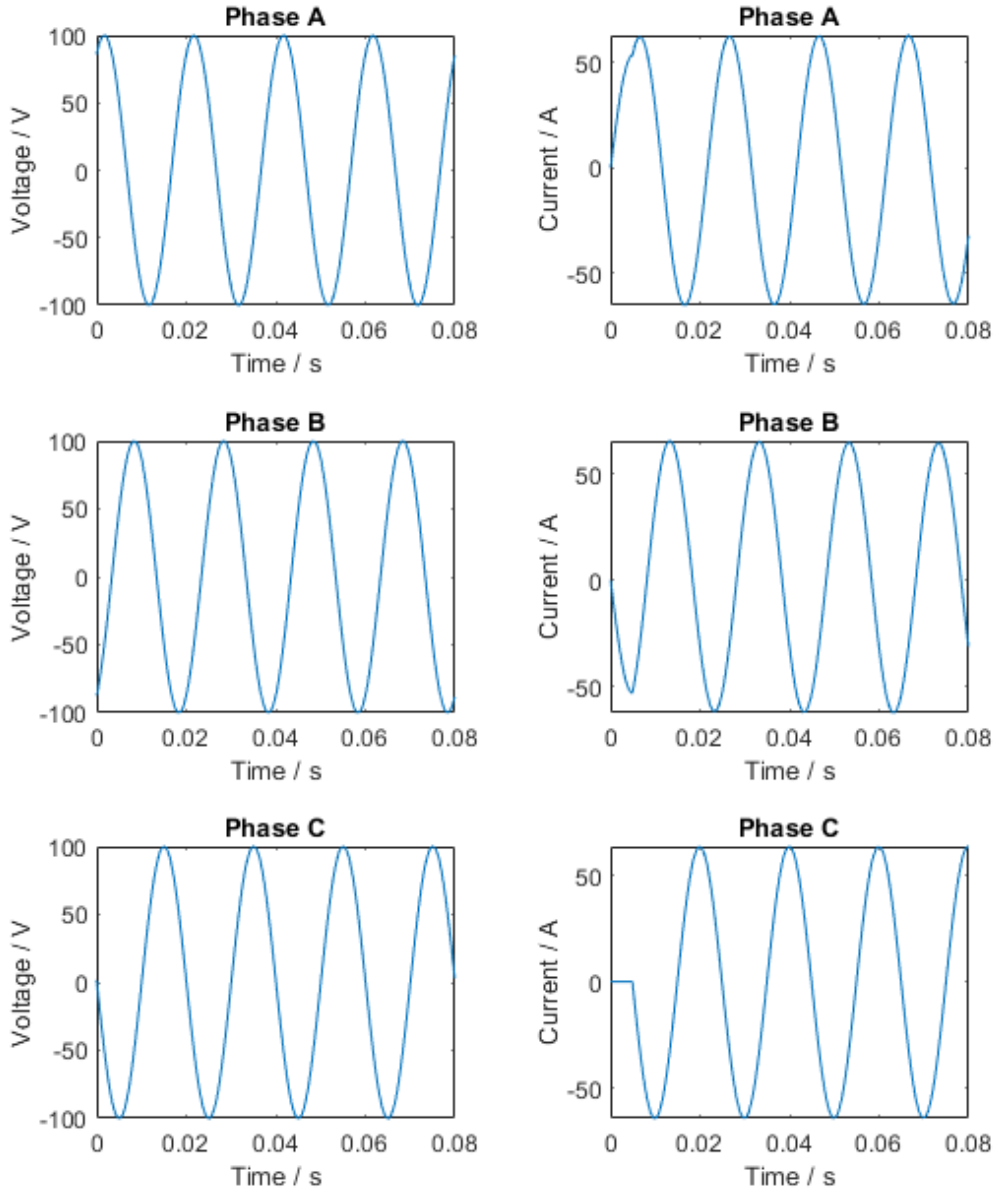

Figure 3.16 Scenario 4 - Large machine.

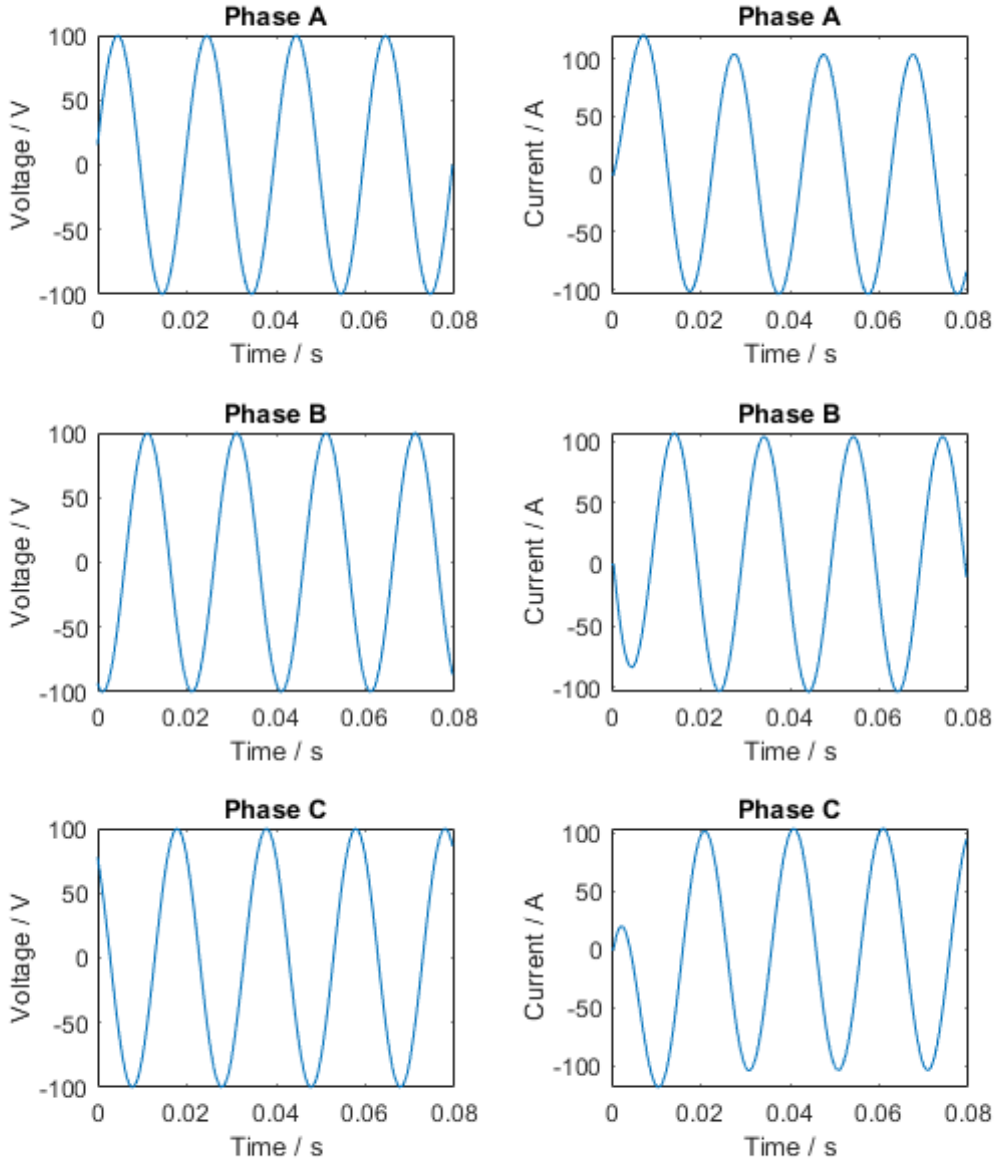

Figure 3.17 Scenario 1 - Smaller machine.

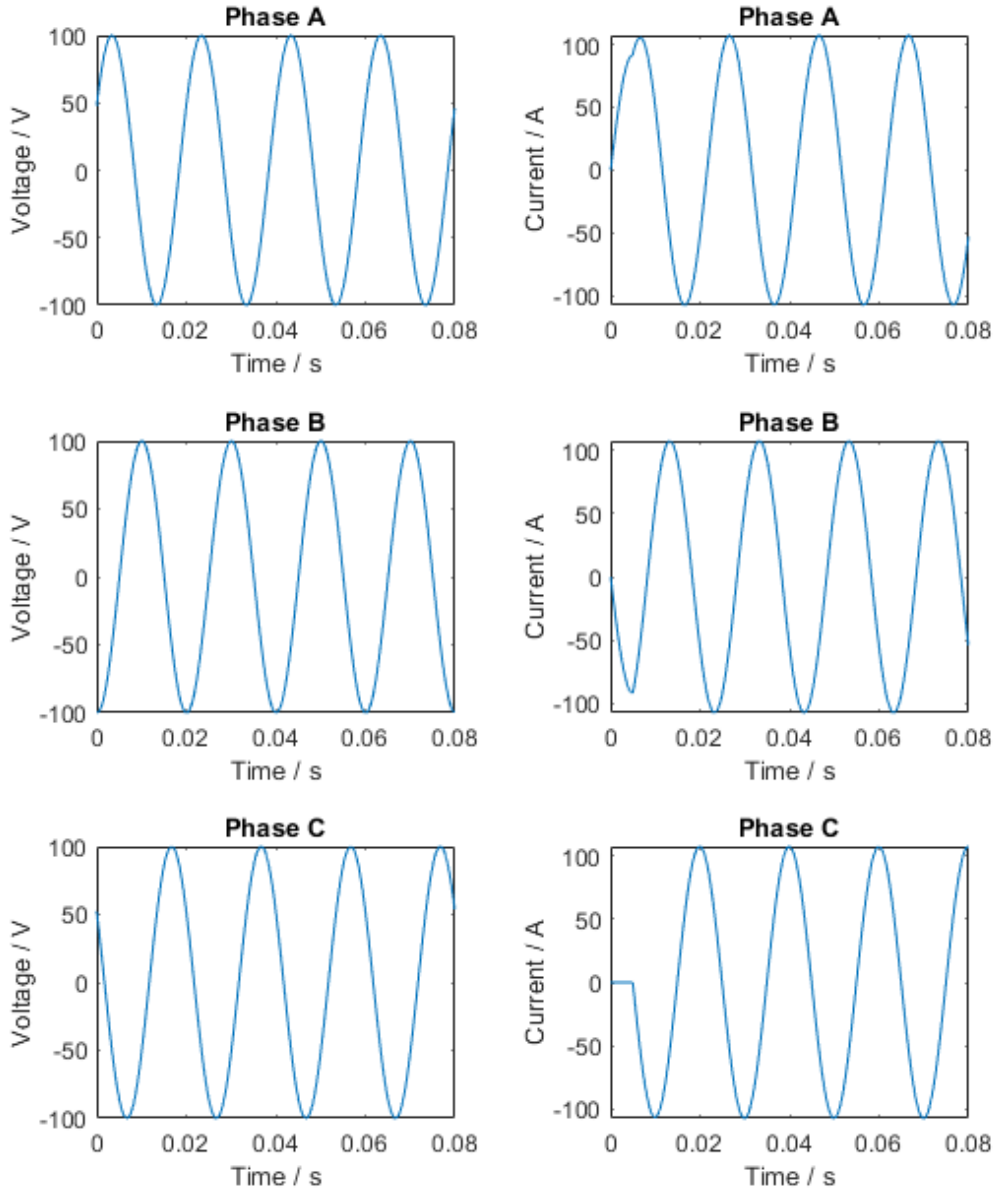

Figure 3.18 Scenario 4 - Smaller machine.

3.3.3.2 Soft turn-on of capacitors

For a capacitor

$$i = C\frac{\mathrm{d}v}{\mathrm{d}t} \tag{3.62}$$

For a delta connected capacitor bank, assuming the three capacitors are equal size, $C_1 = C_2 = C_3 = C$, the current through each capacitor are:

$$\begin{bmatrix} i_{C1} \\ i_{C2} \\ i_{C3} \end{bmatrix} = \frac{d}{dt} \begin{bmatrix} V_a - V_b \\ V_b - V_c \\ V_c - V_a \end{bmatrix} \begin{bmatrix} C \end{bmatrix} \tag{3.63}$$

The capacitance can be calculated as discussed in Section 3.2.3.

The point to be made here is that to avoid voltages spikes the the voltage being applied during turn-on should equal the voltage that the capacitor is charged to. The voltage cannot be changed instantaneously across a capacitor because the energy is stored in the electric field so that any voltage difference will cause a current that is only blocked by the capacitor internal resistance and any supply impedance.

For the capacitor current to go straight to steady state then the current should be going through the zero point and at this point the capacitor voltage would be maximum since in an alternating system the voltage lags the current by 90°. This means ..... if the capacitor is switched in when the current would be crossing from negative to positive, then the capacitor needs to be charged to $-V_{peak}$. This is not practical. However, if the capacitors are not charged (they can be automatically discharged when disconnected) then for a pure capacitor when switched in at the zero crossing point for the voltage, it will have a current that alternated between 0 and $|2V_{peak}|$ with a transient

decay only if there is other impedance in the circuit. Section 3.2.3.2 discusses the use of series inductances with the capacitors to reduce the effects of harmonics. For instance, for the 7^{th} harmonic voltage, without a filter a 5 % harmonic will give a 35 % harmonic current since the capacitive reactance reduces by seven times at a frequency of $7f_s$. With 10 % inductive reactance added, then this will give about 8 % harmonic current which is a substantial reduction. More inductance can still further reduce this.

In terms of starting, the series inductance will prevent high current spikes and damp the transient turn-on. This is simulated here in combination with the motor to address the total transient turn-on current.

3.3.3.2.1 Simulation of transient turn-on with capacitor bank. In this section the motor Scenario 4 from Section 3.3.3.1.1 is used to provide the induction motor currents. Scenario 4 gives induction motor currents that go straight to steady state. For the large machine the delta-connected capacitive reactance is 4.7 Ω which gives capacitors of 225 μF. The series reactance is 0.47 Ω which is 1.5 mH. For the smaller machine the delta-connected capacitive reactance is 3.31 Ω which gives capacitors of 961 μF. The series reactance is 0.33 Ω which is 1.1 mH.

The switching points for the induction motor and capacitors are different. When Phases *a* and *b* are switched on then with a delta connection all the capacitors can be switched in when the voltage across them is zero. Alternatively the capacitor across Phases *a* and *b* can be switched in and the other capacitors switched in when the Phase *c* is switched in.

Large machine - $X = 1.57\ \Omega$ and $R = 0.05\ \Omega$. Figs. 3.19 and 3.20 show the simulations with the different switch-in points for the second and third capacitors. Both show the turn-on current to

be less than the steady-state start-up current. Switching the capacitors in when Phases a and b are connected gives marginally better results with Phase b having a lower turn-on spike. Note that the capacitor currents are currents contributing to the line current, not the actual currents through the capacitors.

Smaller machine - $X = 0.785\ \Omega$ and $R = 0.5\ \Omega$. Figs. 3.21 and 3.22 show the simulations with the different switch-in points for the second and third capacitors. Again the result are similar although there are turn-on spikes for the first cycle that are higher than the steady-state starting current. However, when the first cycle is done, the total current is reduces from 100 A peak for the motor current to 70 A drawn from the supply.

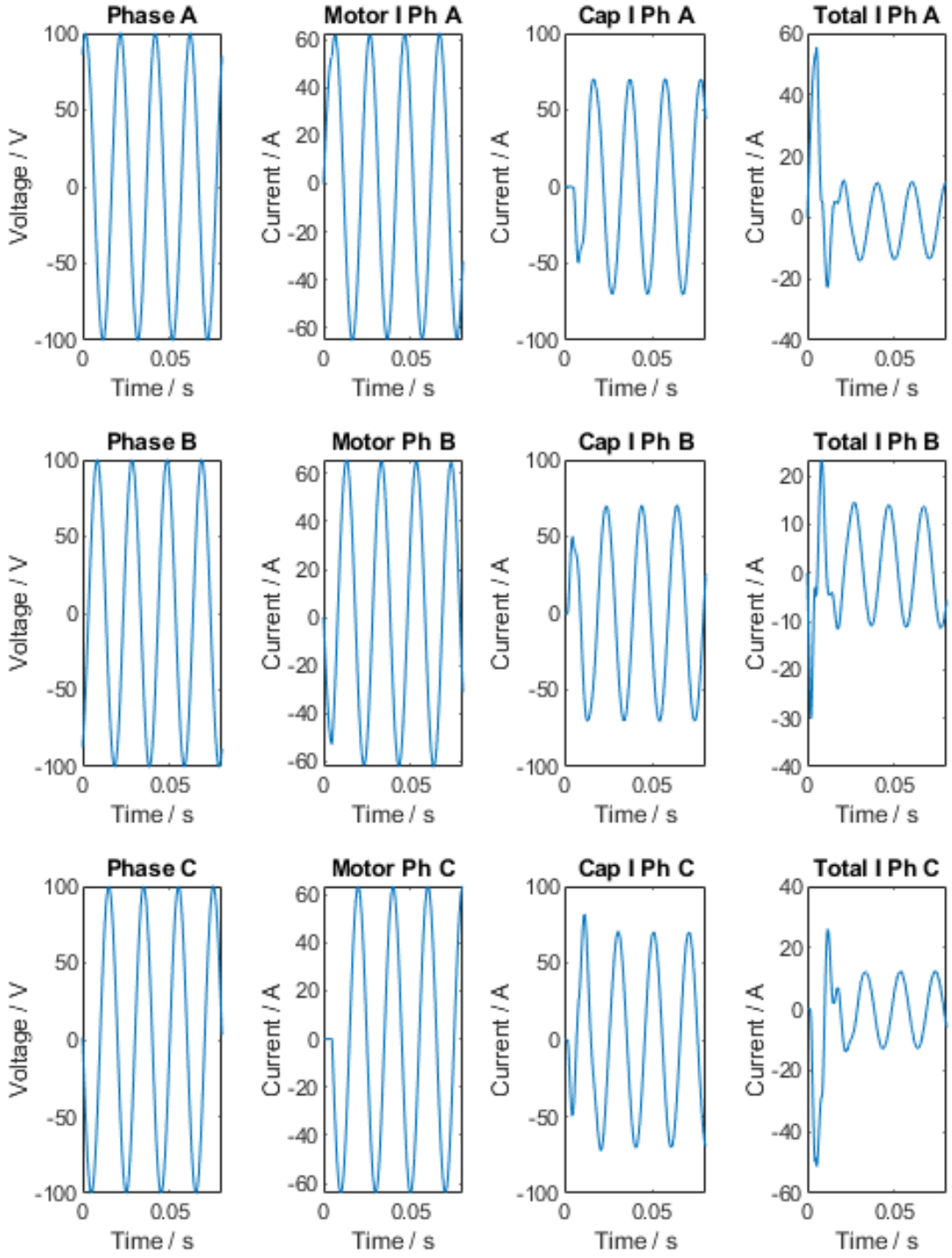

Figure 3.19 Scenario 4 with capacitors - Large machine, capacitors switched in when Phase *a* and *b* switched in.

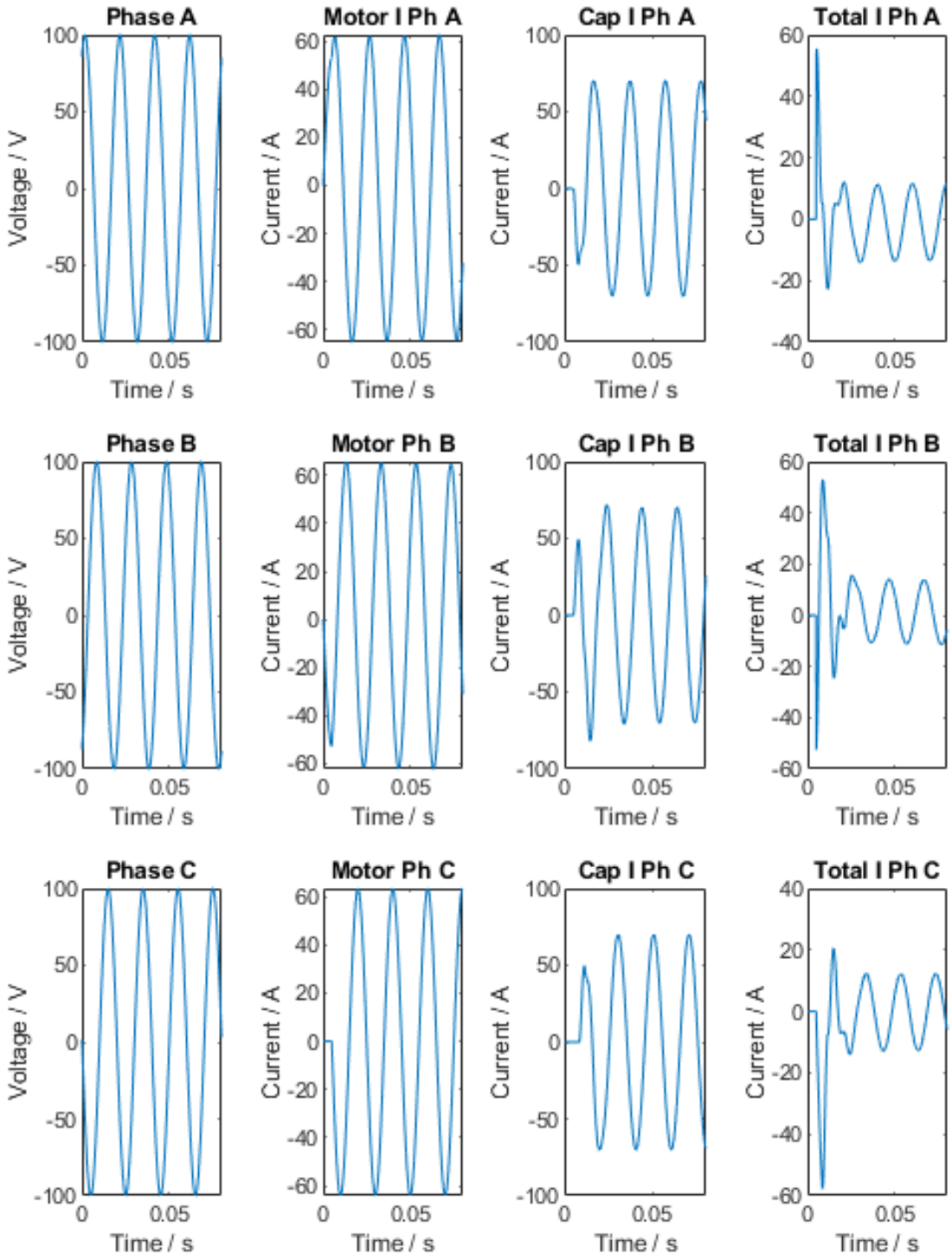

Figure 3.20 Scenario 4 with capacitors - Large machine, 2nd and 3rd capacitors switched in when Phase *c* switched in.

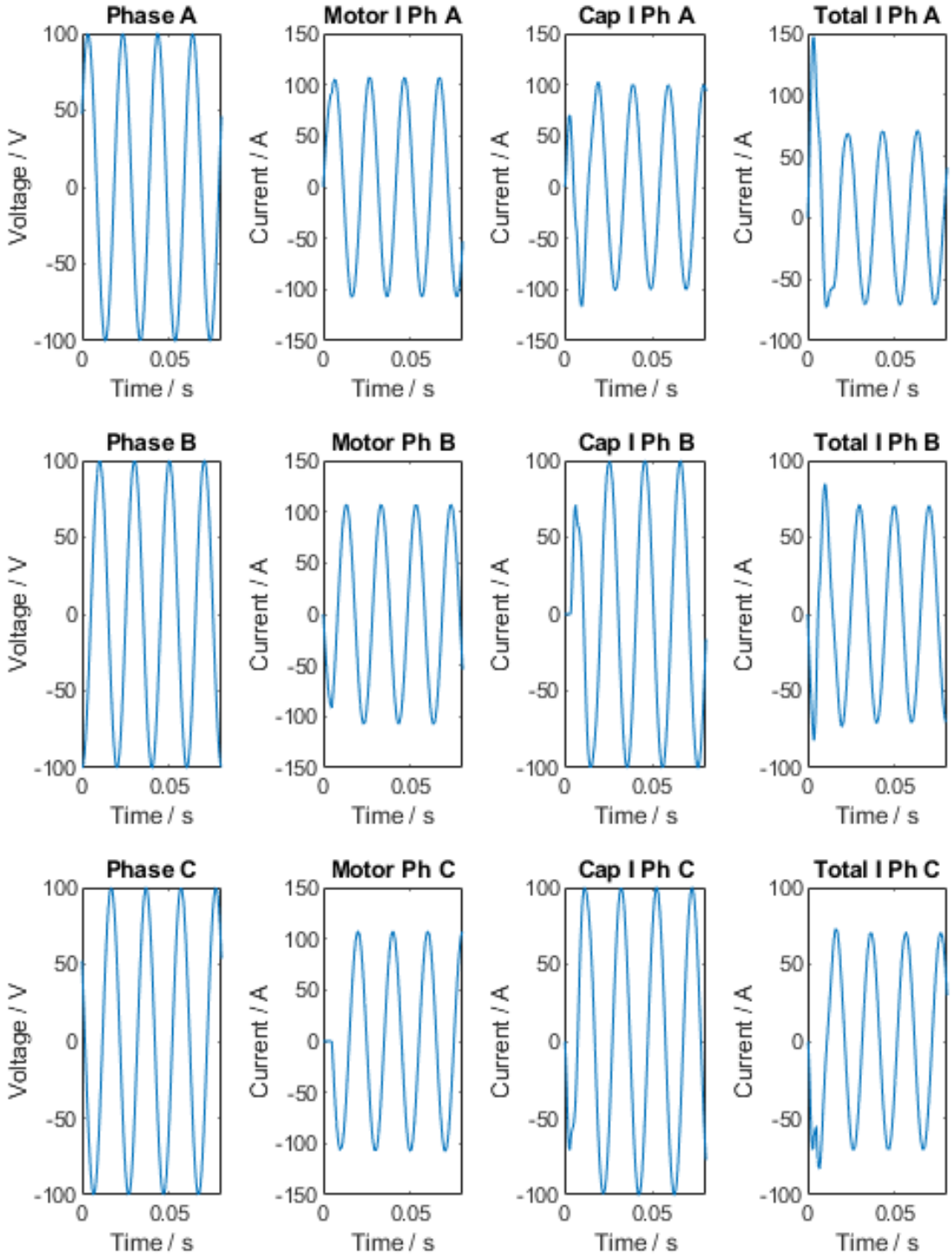

Figure 3.21 Scenario 4 with capacitors - Smaller machine, capacitors switched in when Phase *a* and *b* switched in.

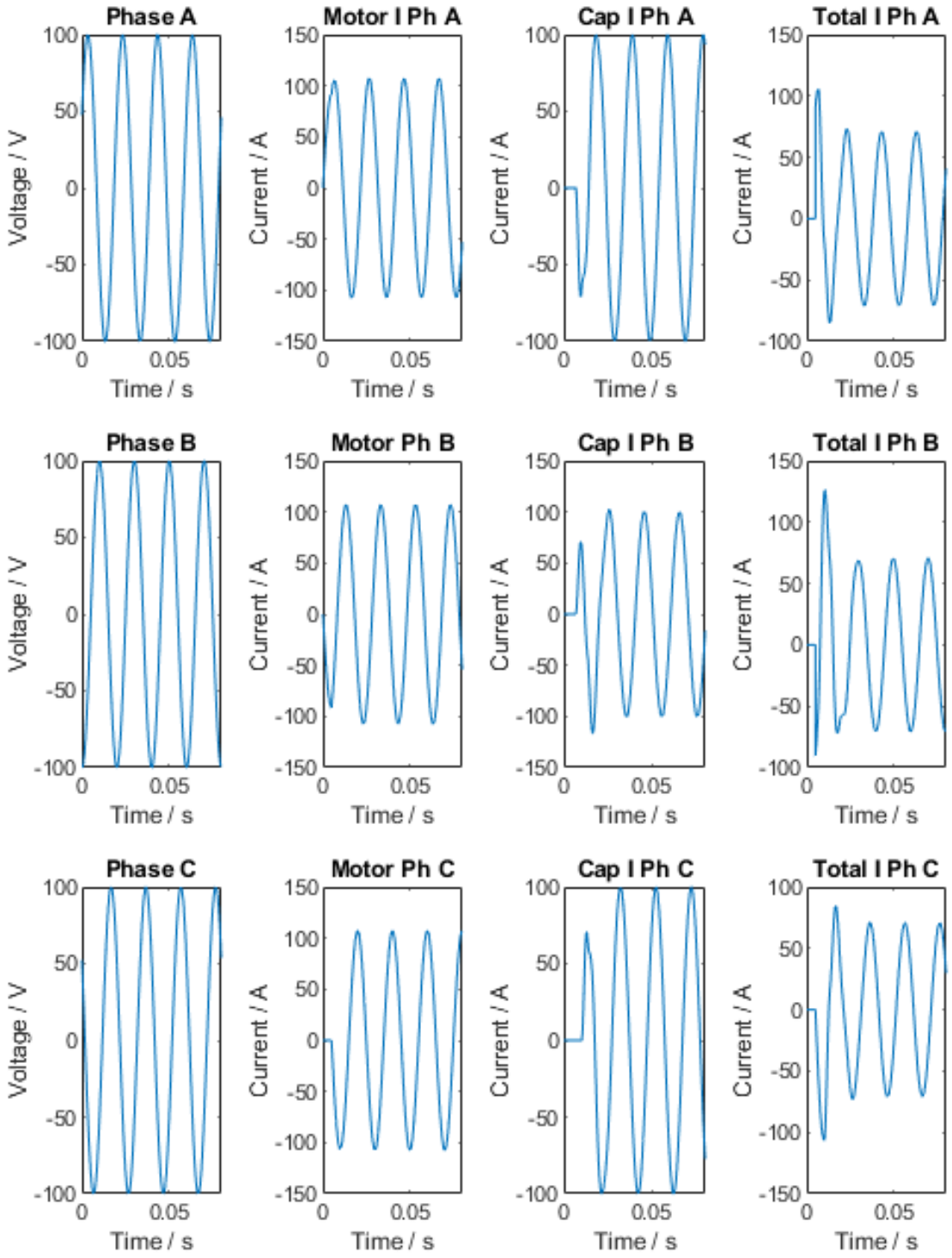

Figure 3.22 Scenario 4 with capacitors - Smaller machine, 2nd and 3rd capacitors switched in when Phase *c* switched in.

3.4 Induction Motor Starting System

The different starting techniques were reviewed in Chapter 2. In this work soft starting is investigated. There are two aspects to this: capacitor compensation and point-on switching. The aim is to investigate the system shown in Fig. 3.23. The single-phase point-on switch on the motor may or may not be required - in the experimental work here it is not used. The capacitors are a combination of a capacitor and the filtering reactance.

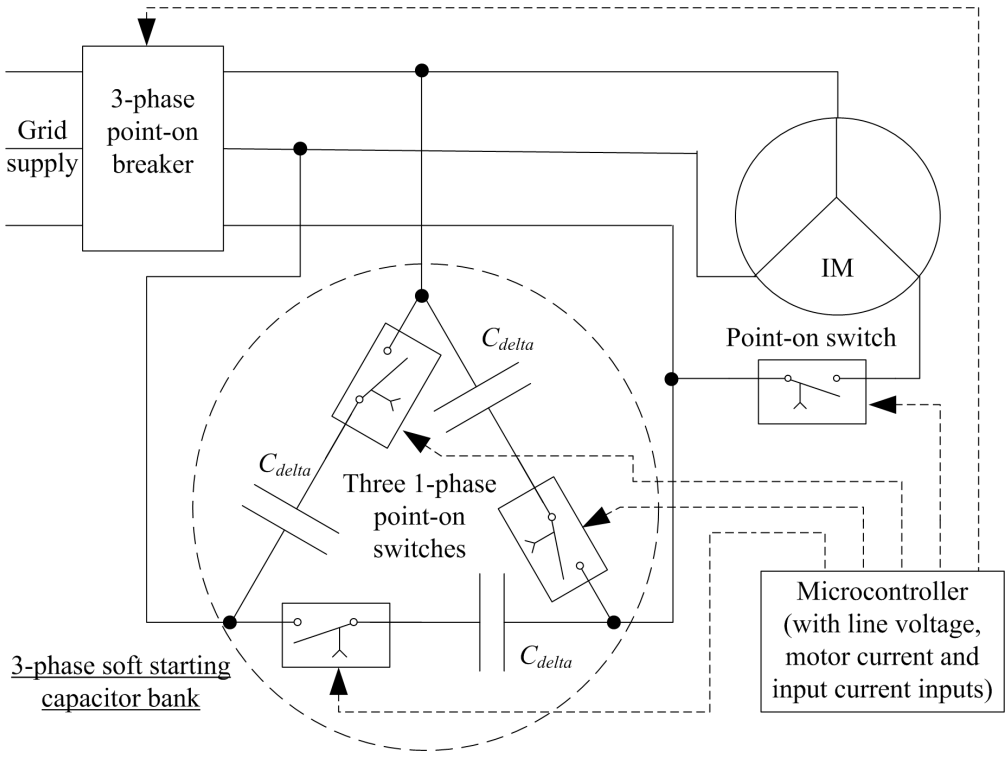

Figure 3.23 Complete system power circuit.

3.5 Conclusions

This Chapter has developed theory to analyse the starting currents in a 3-phase induction motor. This covers both the steady-state and transient analysis. Starting current reduction was considered in terms of the reactive power mitigation using capacitor compensation which are connected in parallel with the motor. The transient starting current can be split up into the turn-on current and the run-up current. While the capacitors compensate for the run-up current, the transient turn-on current is is also examined to assess whether using point on-switching can reduce turn-on current. It is found that in large machines that are more inductive when starting, this can be done.

In the next chapter simulations of several actual machines are carried out using their equivalent circuit parameters to assess the use of capacitor compensation during starting for a variety of motors.

Chapter 4

Simulations of Run-Up

4.1 Introduction

This chapter presents simulations based on the theory put forward in Chapter 3. It has several sections. The first section puts forward seven machines that represent a broad spectrum of induction motors and includes the experimental machine described in Appendix A and tested in Chapter 6. They are put forward in terms of their ratings and per-phase equivalent circuit parameters.

The first two sets of simulations use steady-state equivalent circuit analysis. A set of simulations that compare different starting parameters are put forward in Section 4.3. These are a prelude to the simulations in Section 4.4 which compare the starting characteristics of the motors and assesses the effect of capacitor compensation.

To check if these match the transient d-q analysis then a machine is tested with the Simulink model given in Section 3.3.2 and compared to the steady state results.

The results in this section address the transient run-up. The transient turn-on was assessed in Section 3.3.3.1.1 and will be investigated experimentally in Chapter 6.

4.2 Parameters for different machines

Seven machines are studied here to address various characteristics of induction machine over a wide range of power, voltage and pole number.

The first is a small 4 pole 1.5 kW 346 V laboratory machine and the description and testing of this, through running-light and locked-rotor tests, are given in Appendix A. This machine was de-rated to 220 V in the experimental work.

There are four commercial machines from Valiadas. There is a 1.5 kW, 400V, 4-pole, 50 Hz machine for comparison with the laboratory machine, a 45 kW, 400 V, 4-pole, 50 Hz machine as an example of a larger LV machine, a larger 2-pole, 200 kW, 3300 V machine as an example of a higher-speed MV machine, and then a 1 MW 6-pole 6000 V as an example of a larger MV low speed motor. The data was obtained from data sheets and test reports, including running-light and locked-rotor tests, obtained through the company website [86].

To further add machines to the mix, then two example machines that were analysed by Sen [87] and these are 60 Hz examples to give variation. There is a small 3.75 kW, 440 V, 4-pole, 60 Hz machine and a very large 3.75 MW, 6900 V, 12-pole, 60 Hz machine as an example of a very large MV machine.

These machines present a wide range of machines and their parameters are given in Table 4.1. They will be tested using the various techniques. The parameters were either obtained from man-

ufacturer data sheets or calculated with running-light and locked rotor test data.

Table 4.1 Motor parameters.

No.	**Machine**	**kW**	V_{Line} [V]	I_{Line} [A]	**Poles**	f_s **[Hz]**	**rpm**	J **[kg.m^2]**
1	Lab machine	1.5	220	5.8	4	50	1425	0.012
2	Valiadas K90L-4	1.5	400	3.3	4	50	1440	—
3	Sen 5 HP	3.75	440	3.73	4	60	1753	0.05
4	Valiadis K200L-4	45	400	81.1	4	50	1480	0.246
5	Valiadas KHV355-2	200	3300	44.4	2	50	—	2.6
6	Valiadas TMKHV560-6	1000	6000	110	6	50	990	79
7	Sen 5000 HP	3730	6900	358	12	60	596	145.47

The per-phase equivalent circuit parameters as obtained from the sources or measured through testing are given in Table 4.2. The ratio X/R is the reactance/resistance at start and it can be seen that the larger machines, generally, are far more inductive at start than the smaller machines. The starting power factors are shown in Fig. 4.1 and these confirm the general trend of the power factor at start decreasing with increasing size. Obviously this is very much a function of the motor design but the power range of the machines studied probably cover the whole range of available 3-phase induction motors. Note that the power is on a logarithmic scale.

Table 4.2 Motor equivalent circuit parameters (values in Ω).

No.	Machine	X_m	R_c	R_1	$R_2^{/}$	$X_1+X_2^{/}$	X/R
1	Lab machine	58	81	2.13	1.34	2.99	0.86
2	Valiadas K90L-4	115.2	1568.2	1.325	3.87	8.44	1.62
3	Sen 5 HP	110	900	1.2	1.5	6.0	2.22
4	Valiadis K200L-4	5.13	178.1	0.059	0.013	0.48	6.67
5	Valiadas KHV355-2	118	1333	0.79	0.57	5.75	4.2
6	Valiadas TMKHV560-6	102.5	900.0	0.97	0.24	4.78	3.97
7	Sen 5000 HP	46.0	600.0	0.083	0.080	2.60	15.95

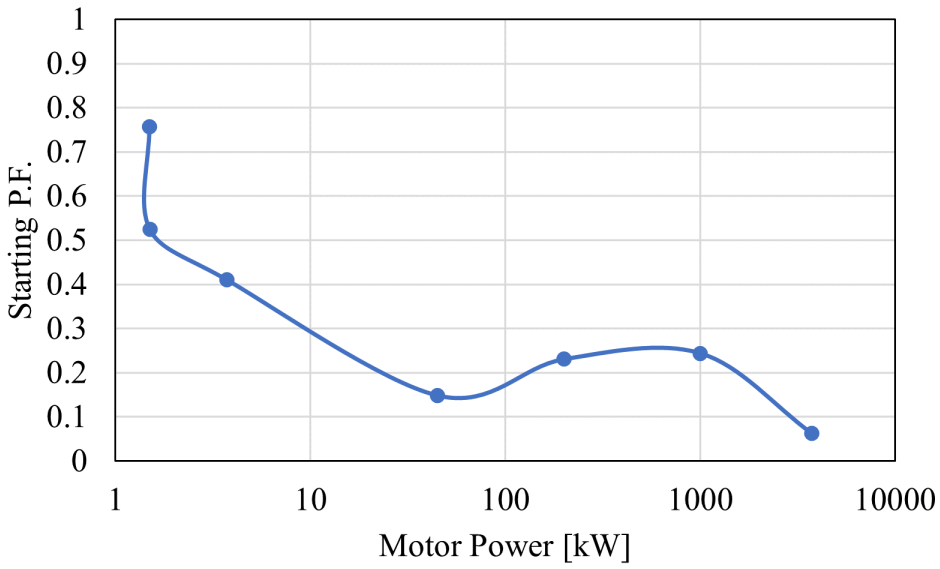

Figure 4.1 Power factor start for different motors.

The actual parameters in Table 4.2 can be used for the simulations; however, for direct comparison, then the parameters can be converted into P.U. as shown in Table 4.3. The normalization

is done using

$$Z_{in}(1 \text{ p.u.}) = \frac{V_{Line}(\text{rated})}{\sqrt{3} I_{Line}(\text{rated})} \tag{4.1}$$

The P.U. values for $R_1 + R_2^{/}$ and $X_1 + X_2^{/}$ are plotted against motor power in Fig. 4.2. Note that both axes are logarithmic scale. It can be seen that $X_1 + X_2^{/}$ is generally constant across the logarithmic with the 1.5 kW lab machine being an outlier whereas $R_1 + R_2^{/}$ varies with a general trend downwards with increasing motor power.

In Fig. 4.3, X_m and R_c are plotted. Again both axes are logerithmic. The magnetizing reactance X_m stays almost steady with a slight upward trend with increasing power. The core loss resistance is much larger with the same upward trend; however, the lab machine is again an outlier with the core loss resistance being much lower.

Table 4.3 Motor equivalent circuit parameters (values in p.u.).

No.	**Machine**	Z_{in} **1 p.u.[Ω]**	X_m	R_c	R_1	$R_2^{/}$	$X_1 + X_2^{/}$
1	Lab machine	37.478	1.54	2.17	0.0568	0.0357	0.080
2	Valiadas K90L-4	69.98	1.65	22.41	0.189	0.0554	0.121
3	Sen 5 HP	36.29	3.03	24.8	0.0331	0.0413	0.165
4	Valiadis K200L-4	2.85	1.80	62.56	0.0207	0.0046	0.169
5	Valiadas KHV355-2	42.91	2.75	31.08	0.0184	0.0314	0.134
6	Valiadas TMKHV560-6	29.11	3.5	40.00	0.0332	0.0082	0.164
7	Sen 5000 HP	11.13	4.13	53.92	0.0075	0.0072	0.234

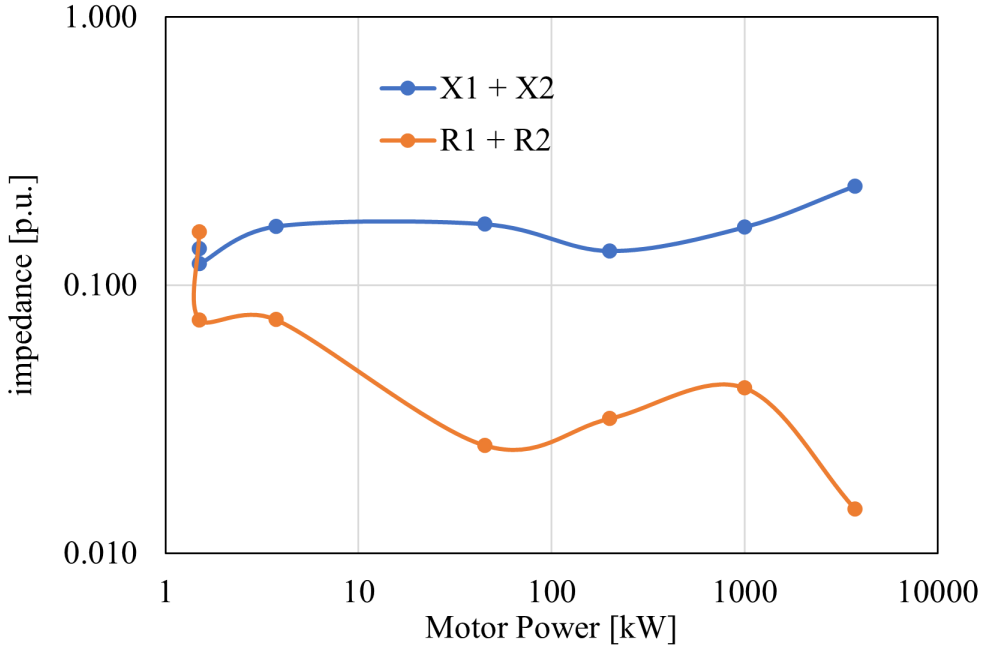

Figure 4.2 P.U. input resistances and reactances at start for different motors.

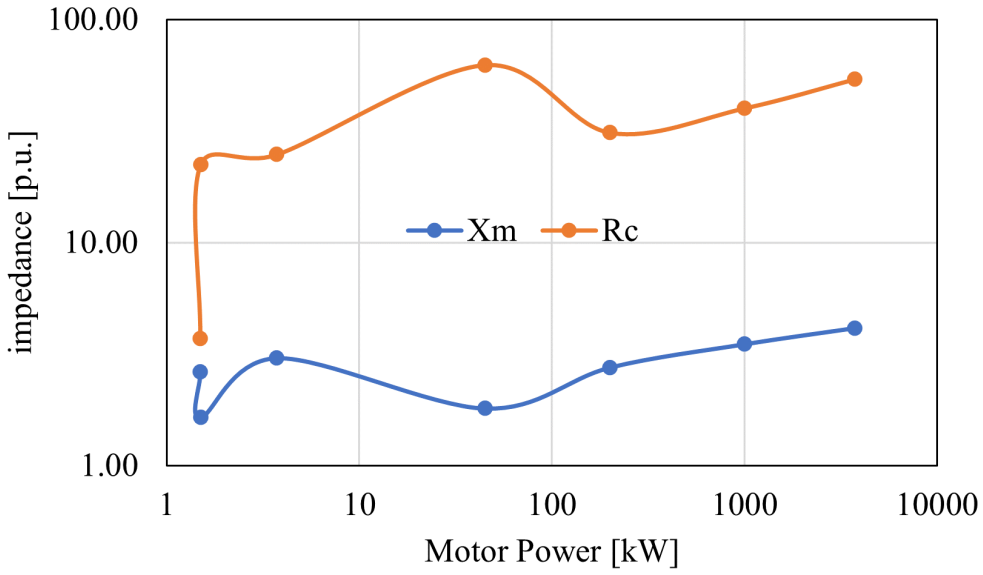

Figure 4.3 Variation of P.U. X_m and R_c for different motors.

4.3 Comparison of Conventional Starting Methods

In this section the efficacy of the different starting methods are assessed for the seven different machines. A DOL start is used for comparison and then four different starting methods are used.

First the star-delta starter is used and this assumes that the motors are delta connected and can be reconnected in star for starting purposes. In reality, this will not be the case but it allows comparison. Small machines (sub 1 kW) are often duel frequency and voltage so that they can be run in star on a European 400 V 50 Hz system and run in delta on a north American 220 V 60 Hz system. Larger LV machines are often designed to run in delta to facilitate star-delta starting. Larger MV and HV machines run in star. This will allow for the periodic reversal of the winding connections (so that the star-connected ends become the phase-connected ends) to spread out voltage stressing of the insulation across the winding with time. For all simulations the switch point is set at $s = 0.33$ so that it has run up to two-thirds full speed. This may not be the correct place to switch, especially for the higher power motors, but it is done for comparison purposes.

The second starter system tested is the auto-transformer starting and this has two switching points. The machine starts at 60 % voltage and runs up to $s = 0.6$ at this voltage, then switches to 75 % voltage, which it runs up to $s = 0.25$, then switches to full voltage up to full load speed.

The third starting system uses high resistance starting. This is a continuously varying resistance from zero speed up to $s = 0.1$. The resistance is calculated using

$$R_{ex} = \left(\sqrt{(3)} - 1\right) \times |\overline{Z}_{in}| \times K_{res} \tag{4.2}$$

where $\overline{Z}_{in}$ is the per-phase input impedance of the machine and

$$K_{res} = \frac{(s-0.1)}{0.9} \tag{4.3}$$

This is added in-line with the machine so the total input impedance to the machine is $\overline{Z}_{in} + R_{ex}$.

The fourth starting technique uses phase angle control of a triac type device which is effectively an inductance. The simulation uses an inductance so that

$$X_{ex} = \left(\sqrt{(3)} - 1\right) \times |\overline{Z}_{in}| \times K_{res} \tag{4.4}$$

with K_{res} defined as in (4.3) and the input impedance given by $\overline{Z}_{in} + jX_{ex}$. A load torque is also added as defined in (3.17) [34].

4.3.1 Loading

First the full load point is obtained using the torque speed curve by moving back from the no load point until $P_m(\text{rated}) = T_m\omega_r$. At this point the rated slip is s_{fl}. From this, the load torque is

$$\begin{aligned} T_l(s) =& T_m(\text{rated})\left(K_1 + K_2(1-s+s_{fl}) + K_3(1-s+s_{fl})^2\right) \\ T_l(s) =& T_m(\text{rated})\left(0.05 + 0.1(1-s+s_{fl}) + 0.85(1-s+s_{fl})^2\right) \end{aligned} \tag{4.5}$$

This means that the speed-squared coefficient K_3 is 85 % of the the total torque at rated speed, the speed coefficient K_2 is 10 % and constant coefficient K_1 is 5 %. This may reasonable for a smaller machine attached to a pump or a fan but for a large machine, often the dominant term is K_3 which approaches 100 % or the machine is started with no load where it only has to overcome the inertia and friction and windage terms (for instance, for a pump, the fluid supply-side valve is kept closed until it runs up to speed, then it is opened).

4.3.2 Motor No. 1: 1.5 kW 220 V Lab Machine

This machine was available in the laboratory and described in Appendix A. As seen in Fig. 4.2 and Table 4.2 it has a low X/R when starting. The machine works for all the starting methods in Fig. 4.4. It an be seen to draw more power than reactive power in starting.

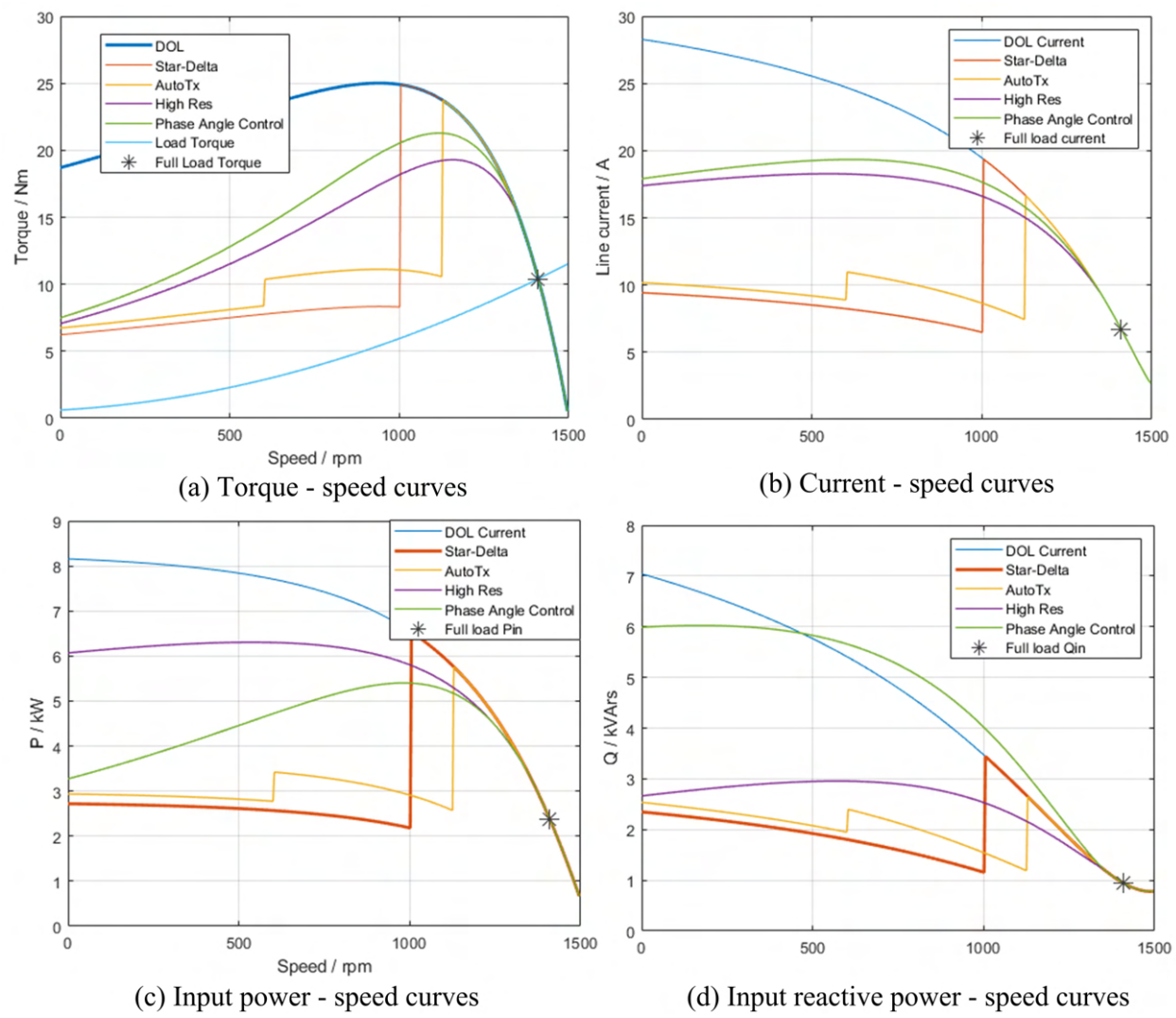

(a) Torque - speed curves

(b) Current - speed curves

(c) Input power - speed curves

(d) Input reactive power - speed curves

Figure 4.4 Comparison of 1.5 kW 220 V lab machine starting methods.

4.3.3 Motor No. 2: 1.5 kW 400 V Valiadas K90L-4

This machine represents a more commercial 1.5 kW machine and it can be seen in Fig. 4.5 that the full load torque is quite low compared to the peak torque. The parameters are taken from the manufacturers website [86]. This machine could work with a constant torque load with all the starting methods. The starting current is reduced for all methods. For star-delta starting the reconnection is at 1000 rpm - this speed could be increased to further reduce the run-up current. This machine is more reactive than resistive as illustrated by the power and reactive power demands during run-up.

4.3.4 Motor No. 3: 3.75 kW 440 V Sen 5 HP Machine

This equivalent circuit was taken from the a textbook by Sen [87] and it is another relatively small machine. The steady-state simulations are shown in Fig. 4.6 and it can be seen the starting methods work well. High resistance starting draws more power during starting than the DOL start. Again, the reconnection of the start-delta starter is at a speed that is too low. It should probably be between 1500 an 1650 rpm. If it was controlled on a timer the machine would run up to a steady-state speed for the star connection, then when reconnected, it would increase speed to the steady-state speed for the delta connection.

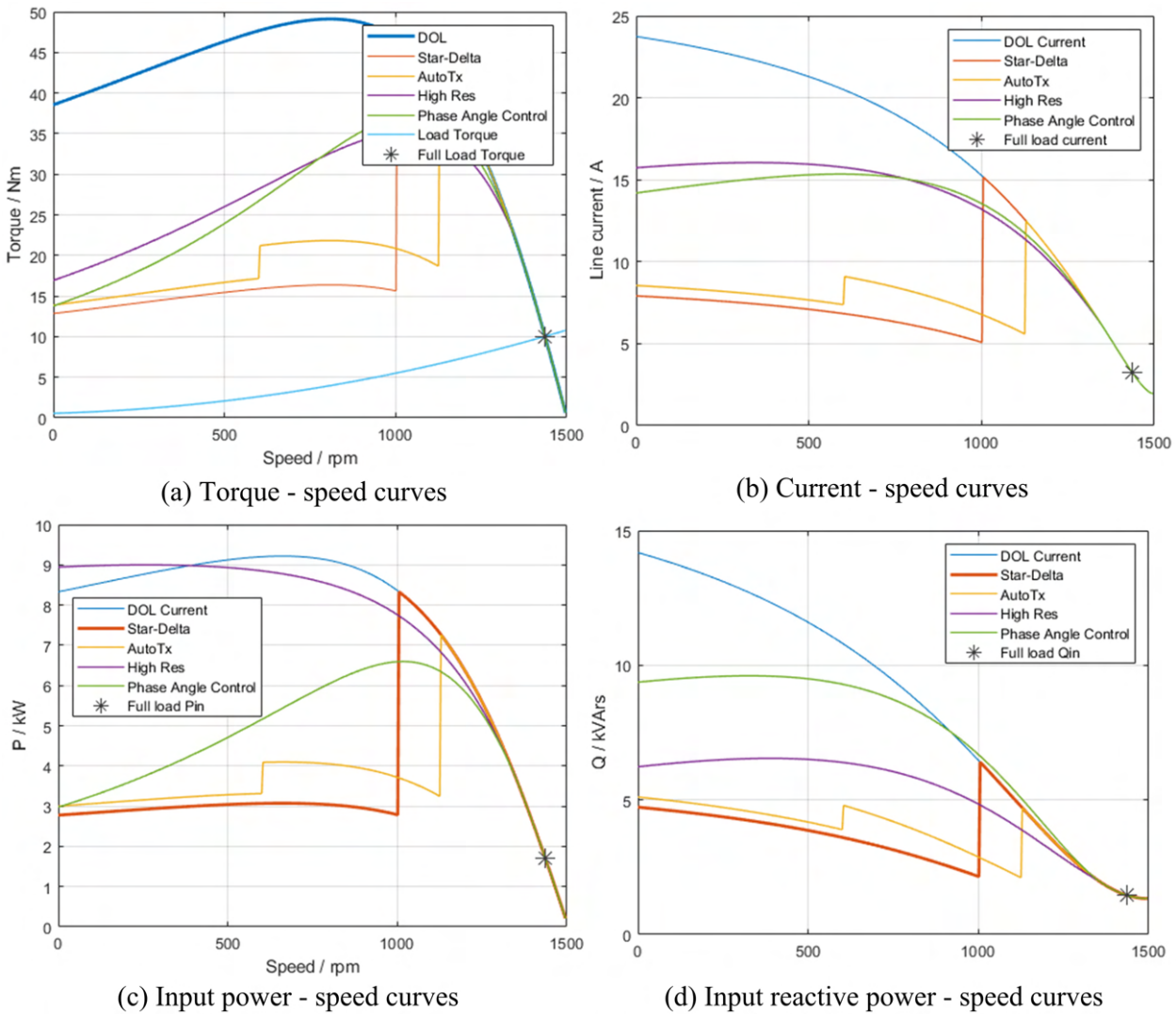

(a) Torque - speed curves

(b) Current - speed curves

(c) Input power - speed curves

(d) Input reactive power - speed curves

Figure 4.5 Comparison of 1.5 kW 400 V Valiadas K90L-4 machine starting methods.

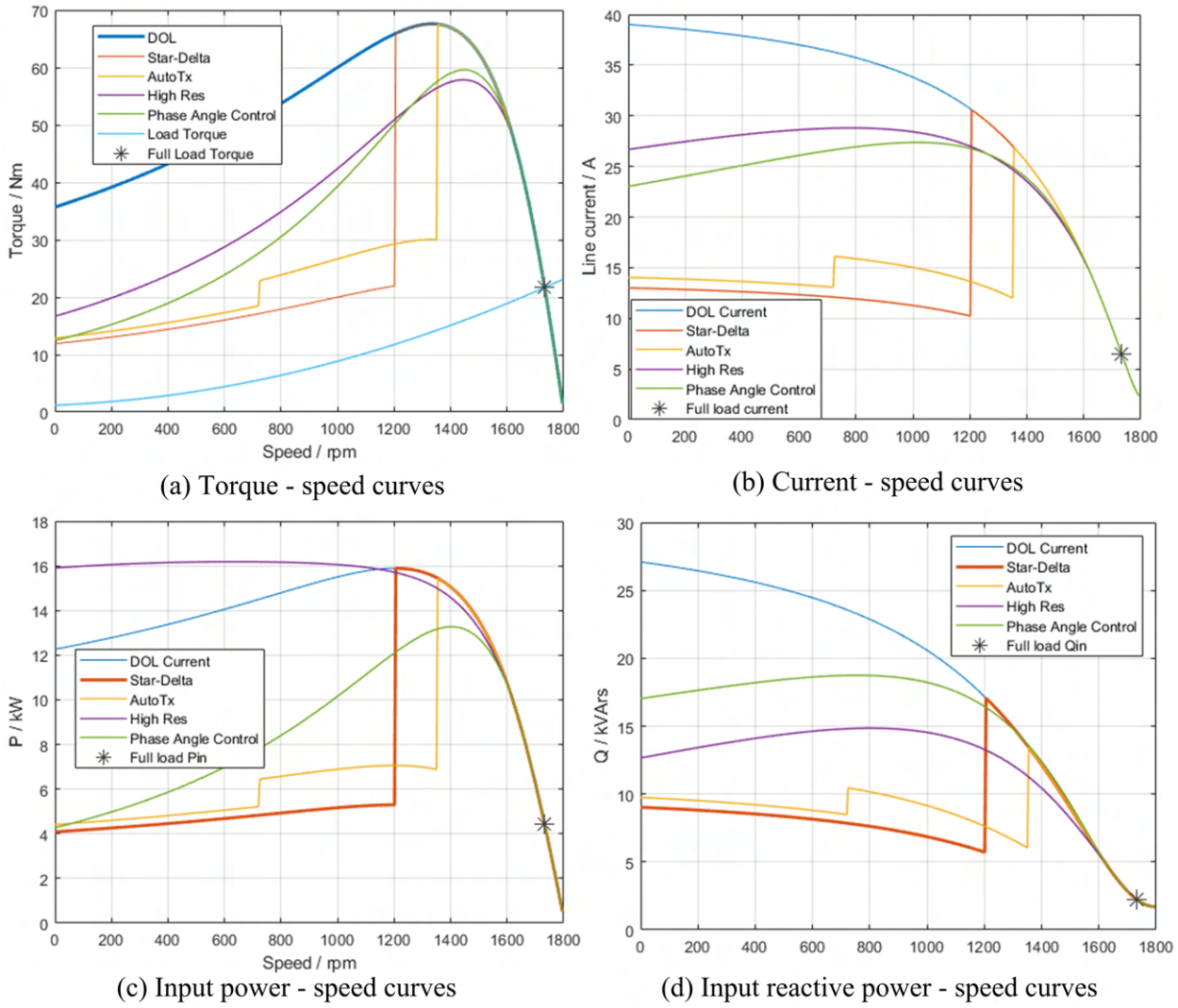

(a) Torque - speed curves

(b) Current - speed curves

(c) Input power - speed curves

(d) Input reactive power - speed curves

Figure 4.6 Comparison of 3.75 kW 440 V Sen 5 HP machine starting methods.

4.3.5 Motor No. 4: 45 kW 400 V Valiadis K200L-4

This machine is 45 kW but only 400 V. The equivlant circuit parameters were taken from the manufacturers website [86]. This means it is a relatively large machine for the voltage rating. This gives it the second highest X/R ratio of 6.67 in Table 4.2. Fig. 4.7 shows that torque is

very "peaky" and this machine would struggle to start even for a DOL start. It would therefore need to start without a load or using an inverter. This machine would be very efficient given this characteristic. Again, for a start-delta starter, the speed for reconnection should be higher. It can be stated when referring to the terms "small" and "large" machines it should be within the context of the voltage rating.

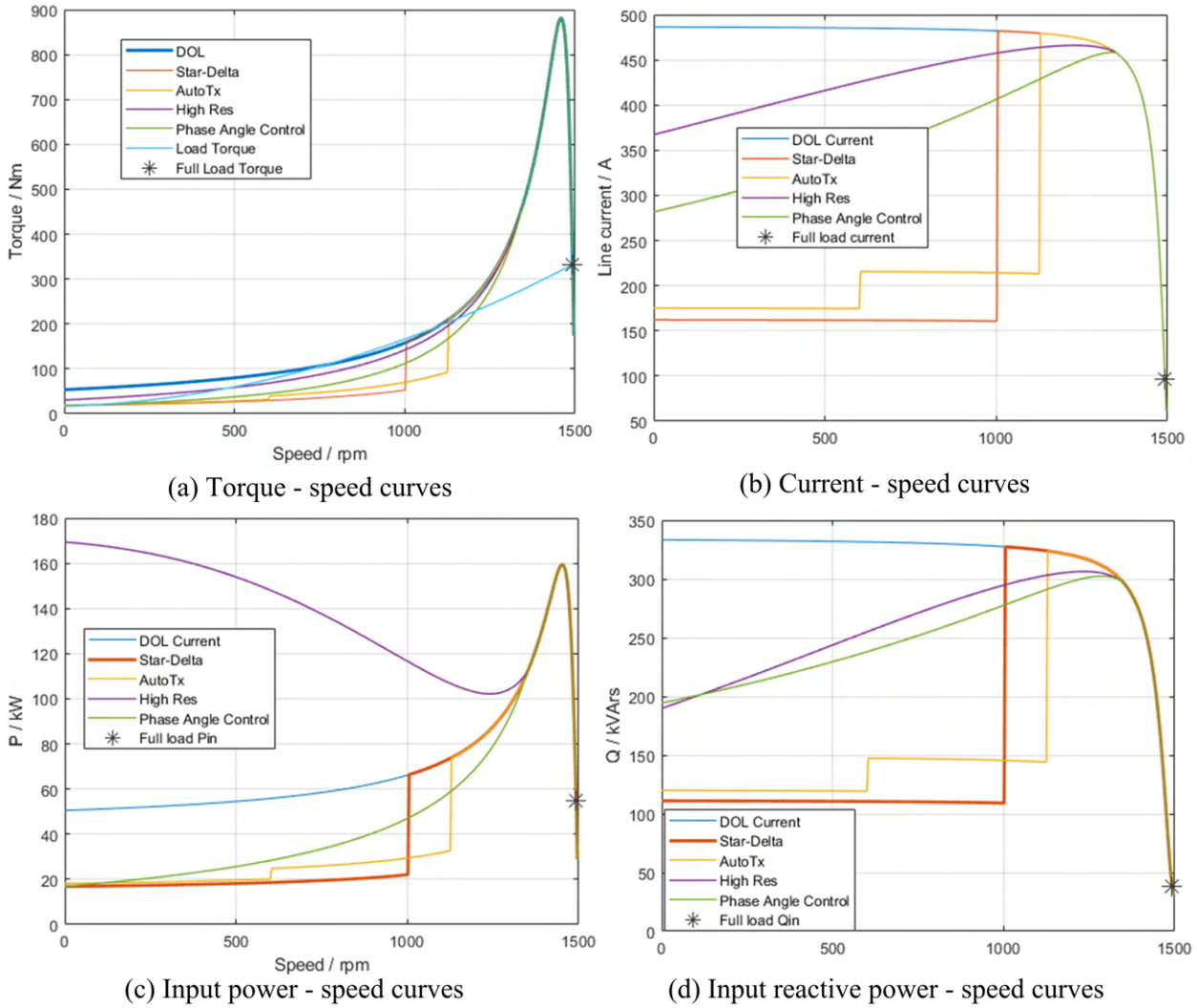

(a) Torque - speed curves

(b) Current - speed curves

(c) Input power - speed curves

(d) Input reactive power - speed curves

Figure 4.7 Comparison of 45 kW 400 V Valiadis K200L-4 machine starting methods.

4.3.6 Motor No. 5: 200 kW 3300 V Valiadas KHV355-2

This machine is 200 kW 2-pole machine but the voltage rating is 3300 V so it is a relatively small machine for its voltage rating. All the starting methods would work but it can be seen that the star-delta starting method needs to reconnect at a higher speed, probably at above 2800 rpm. It is very reactive during starting which is illustrated by comparison of the reactive power requirement to the power requirement. The reactive power is much higher.

4.3.7 Motor No. 6: 1 MW 6000 V Valiadas TMKHV560-6

This is a 1 MW 6-pole machine rated at 6000 V which is probably a medium to large sized machine. Many of the starting methods become ineffective at this rating if the machine is started on-line. It can be seen that the star-delta and auto-transformer methods are not effective mid-speed. The starting torque is low compared to the peak torque. This machine is probably too big to use an inverter just for starting reasons so it would probably be started with no load or reduced load. The reactive power demand is virtually double the power demand during starting.

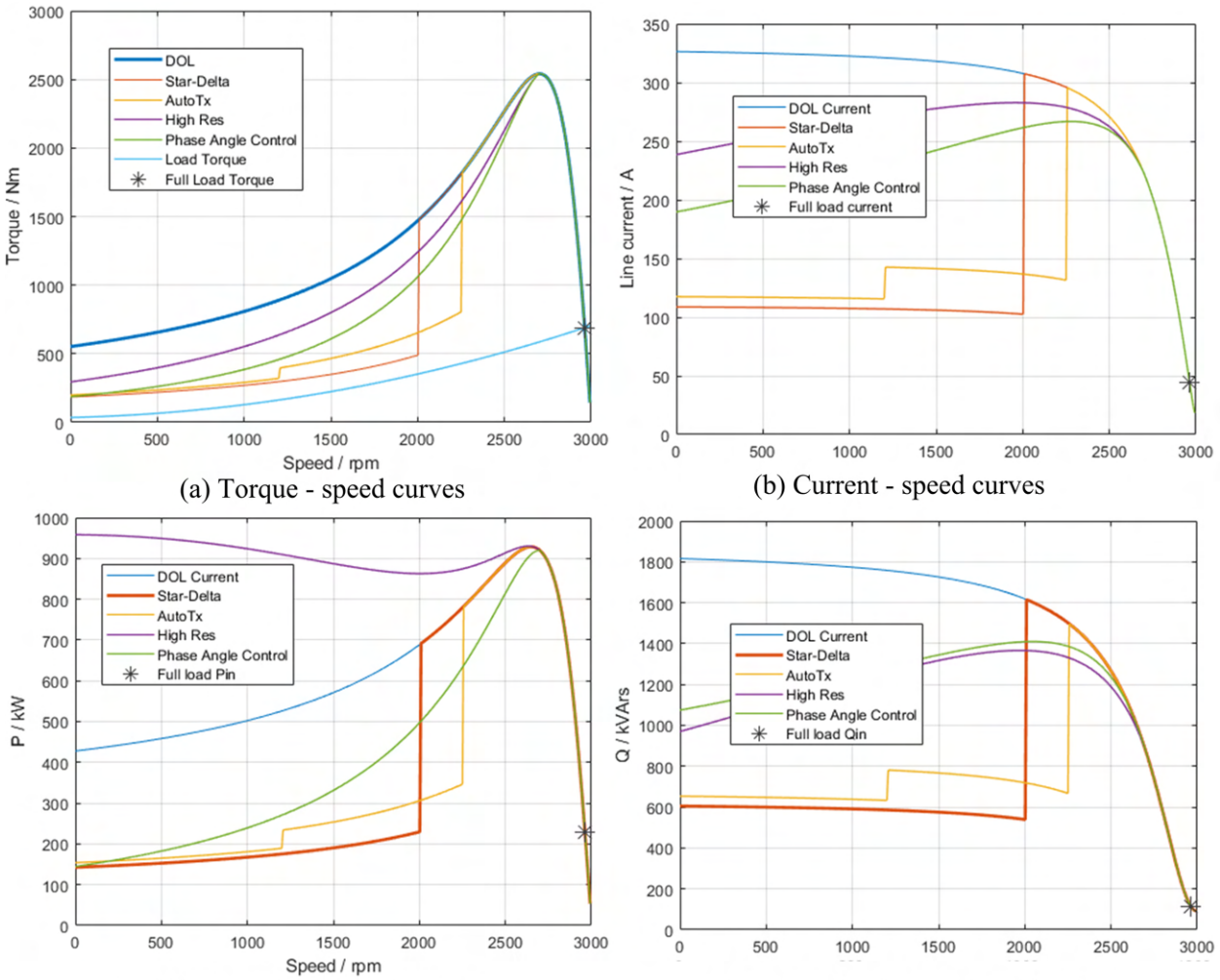

(a) Torque - speed curves

(b) Current - speed curves

(c) Input power - speed curves

(d) Input reactive power - speed curves

Figure 4.8 Comparison of 200 kW 3300 V Valiadas KHV355-2 machine starting methods.

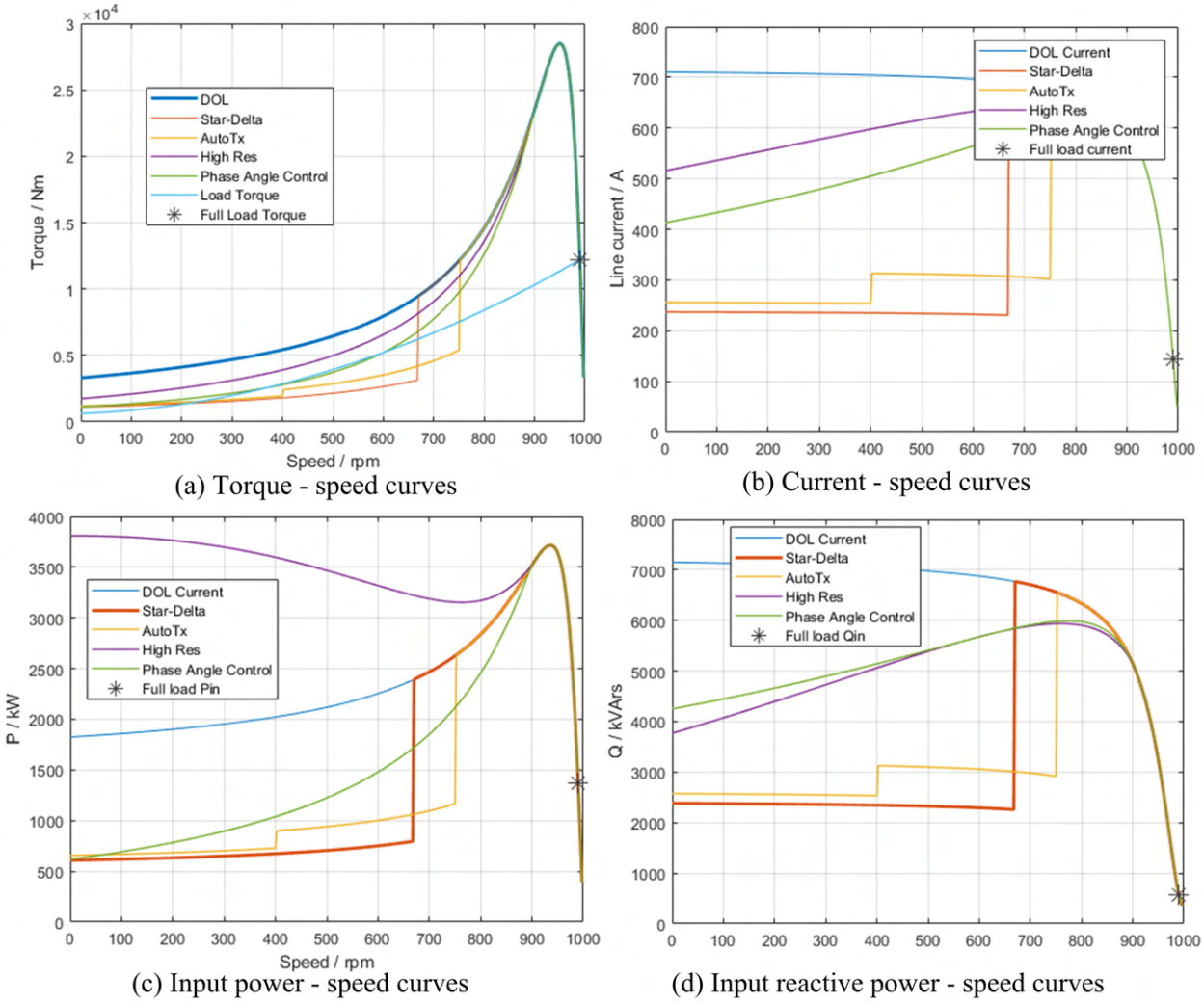

(a) Torque - speed curves

(b) Current - speed curves

(c) Input power - speed curves

(d) Input reactive power - speed curves

Figure 4.9 Comparison of 1 MW 6000 V Valiadas TMKHV560-6 machine starting methods.

4.3.8 Motor No. 7: 3.75 MW 6900 V Sen 5000 HP Machine

This is very large 3.75 MW 12 pole machine running at 6900 V which was again taken from Sen's book [87] and used for comparison to Motor No. 2. It can be seen to have a "peaky" torque and the full load slip is very small. Just as with Motor No. 4, this machine would struggle to start

with the load shown. The starting torque is very low. It would either have a pump load that is virtually a squared function with speed with little friction, or with no load. At this size these starting techniques are not appropriate. However, as with motor No. 6, the reactive power demand is over double the power demand during starting.

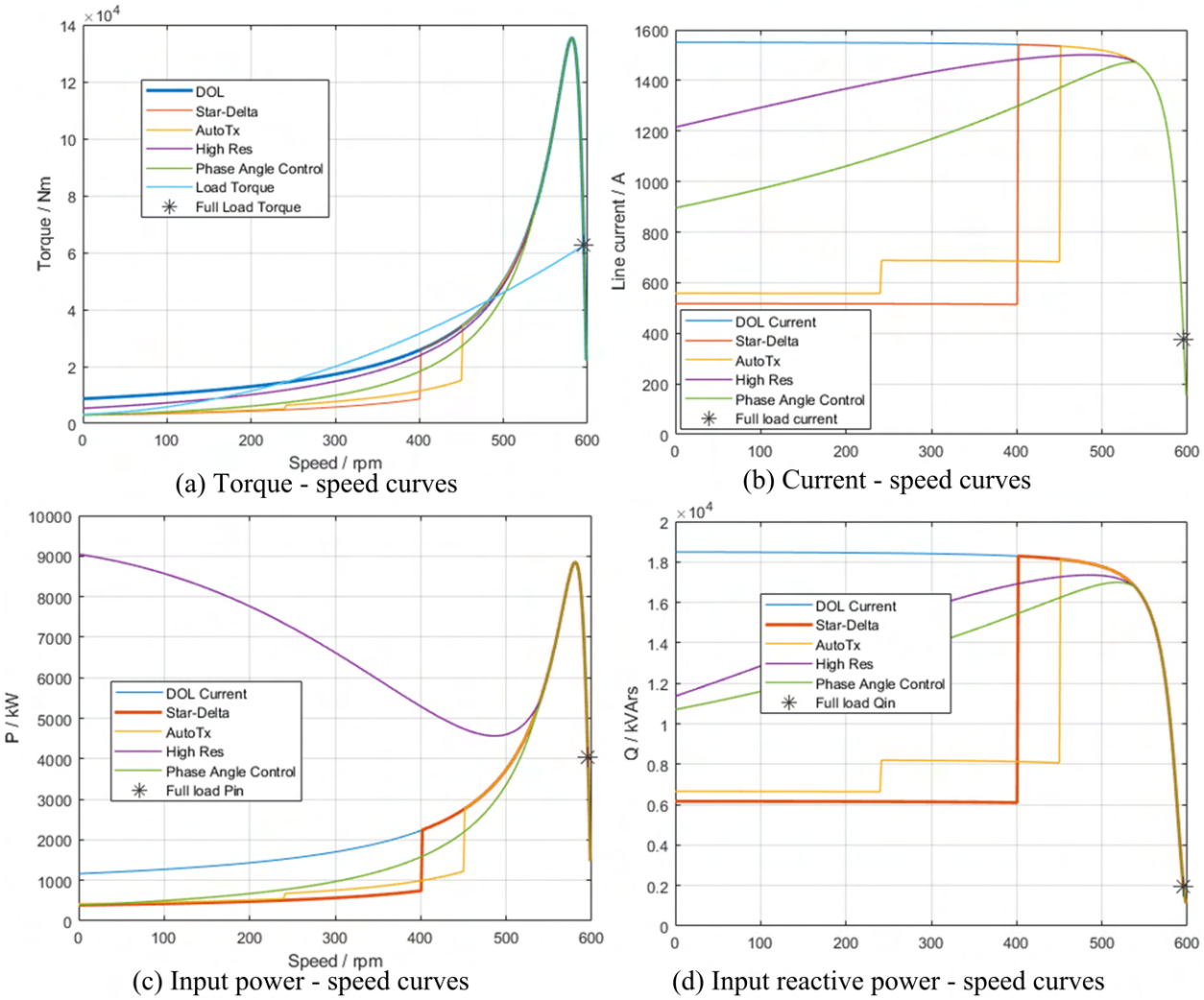

(a) Torque - speed curves

(b) Current - speed curves

(c) Input power - speed curves

(d) Input reactive power - speed curves

Figure 4.10 Comparison of 3.75 MW 6900 V Sen 5000 HP machine starting methods.

4.4 Steady-State Equivalent Circuit Analysis Method for Assessing Capacitor Compensation

In this section the machines are simulated with capacitor starting to assess the efficacy of the method using steady-state equivalent circuits to step though the speed range. For the figures for each machine, the run-up current and torque are first put into graph (a). Power and reactive power is in (b) in order to see how inductive the machine is across the speed range. The delta-connected parallel compensation capacitance required to correct the power factor during starting to unity is given in (c). The total input current to the motor and compensation capacitors is shown in (d) and this is done for three capacitances - the values calculated at start, then with half this capacitance and then third capacitance. This is because the required capacitance decreases with speed so that the selection of the capacitors is, to some extent, a compromise. Each machine was simulated.

4.4.1 Motor No. 1: 1.5 kW 220 V Lab Machine

This experimental machine is not very inductive as can be seen in Fig. 4.11(b) where the power is greater than the reactive power. Consequently in (c), it can be seen that only a reduction of about 25 % is possible. The machine was tested at reduced voltage and, to increase its inductance, additional reactances added to make it behave more like a large machine.

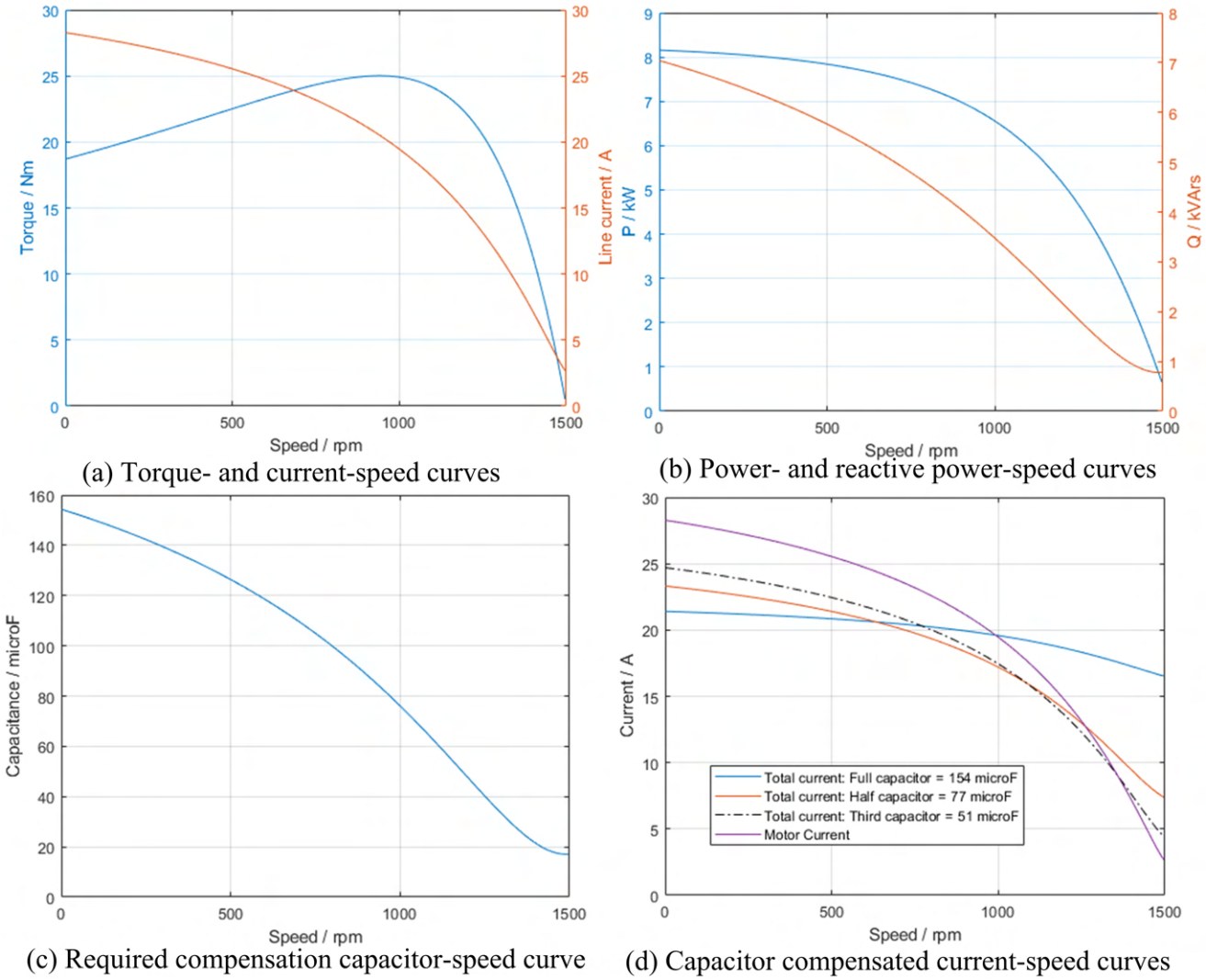

(a) Torque- and current-speed curves

(b) Power- and reactive power-speed curves

(c) Required compensation capacitor-speed curve

(d) Capacitor compensated current-speed curves

Figure 4.11 Comparison of 1.5 kW 220 V lab machine capacitor compensation starting.

4.4.1.1 Run-up time at 100 V no-load for experiments

The experiments are conducted at 100 V to reduce stressing on the system. A further calculation can be done using (3.20) and setting the inertia to 0.012 kgm^2 as given in Table 4.1. The run-up time is shown in Fig. 4.12 to be about 0.55 s. Also shown are the PEAK currents when 50 µF and 90 µF delta-connected capacitors are used to correct the current. It can be seen that the capacitors

should be switched out after 0.35 s if a timer is used and it starts on no load. However, this time would be extended if there is load. A centripetal switch can be used and Fig. 4.4 shows that this should be about 1250 rpm in this instance.

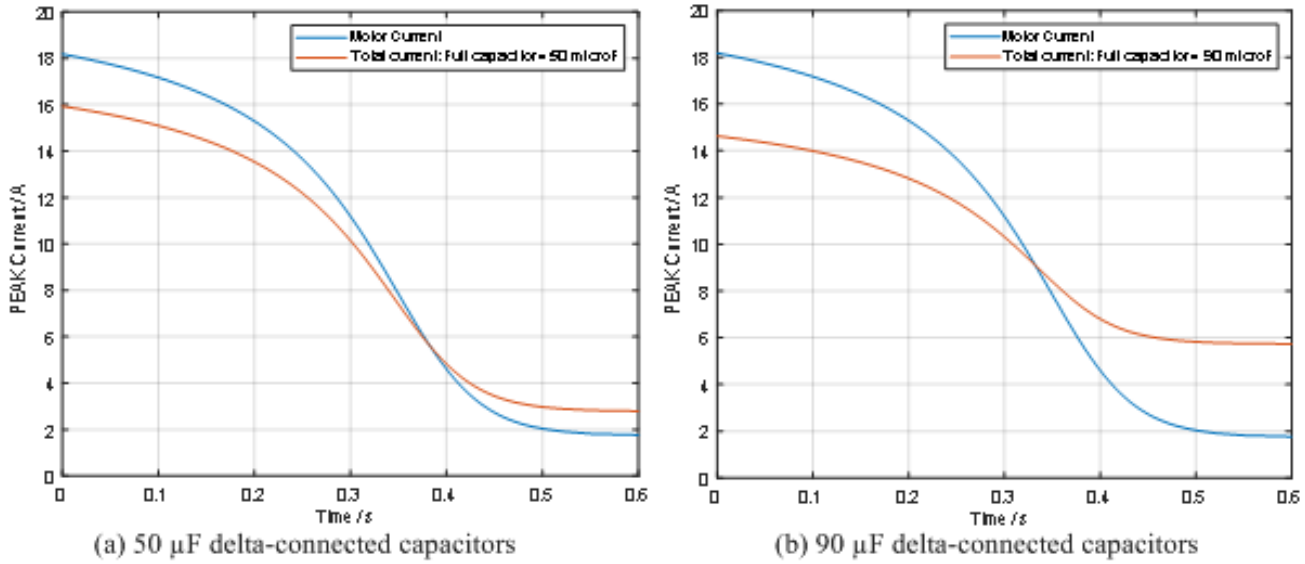

(a) 50 µF delta-connected capacitors (b) 90 µF delta-connected capacitors

Figure 4.12 Run-up time prediction for experimental machine at 100 V - currents with 50 µF and 90 µF.

4.4.2 Motor No. 2: 1.5 kW 400 V Valiadas K90L-4

As previously stated, this is a commercial machine and it is more reactive when starting compared to Motor No. 1. It can be seen in Fig. 4.13(c) that the required capacitance varies considerably over the speed range. In (d) it can be seen that using 94 µF capacitors offers a 50 % reduction in starting current but need to be switched out below 1000 rpm. Better operation across the whole range is possible using 47 µF which would be switched out at 1200 rpm.

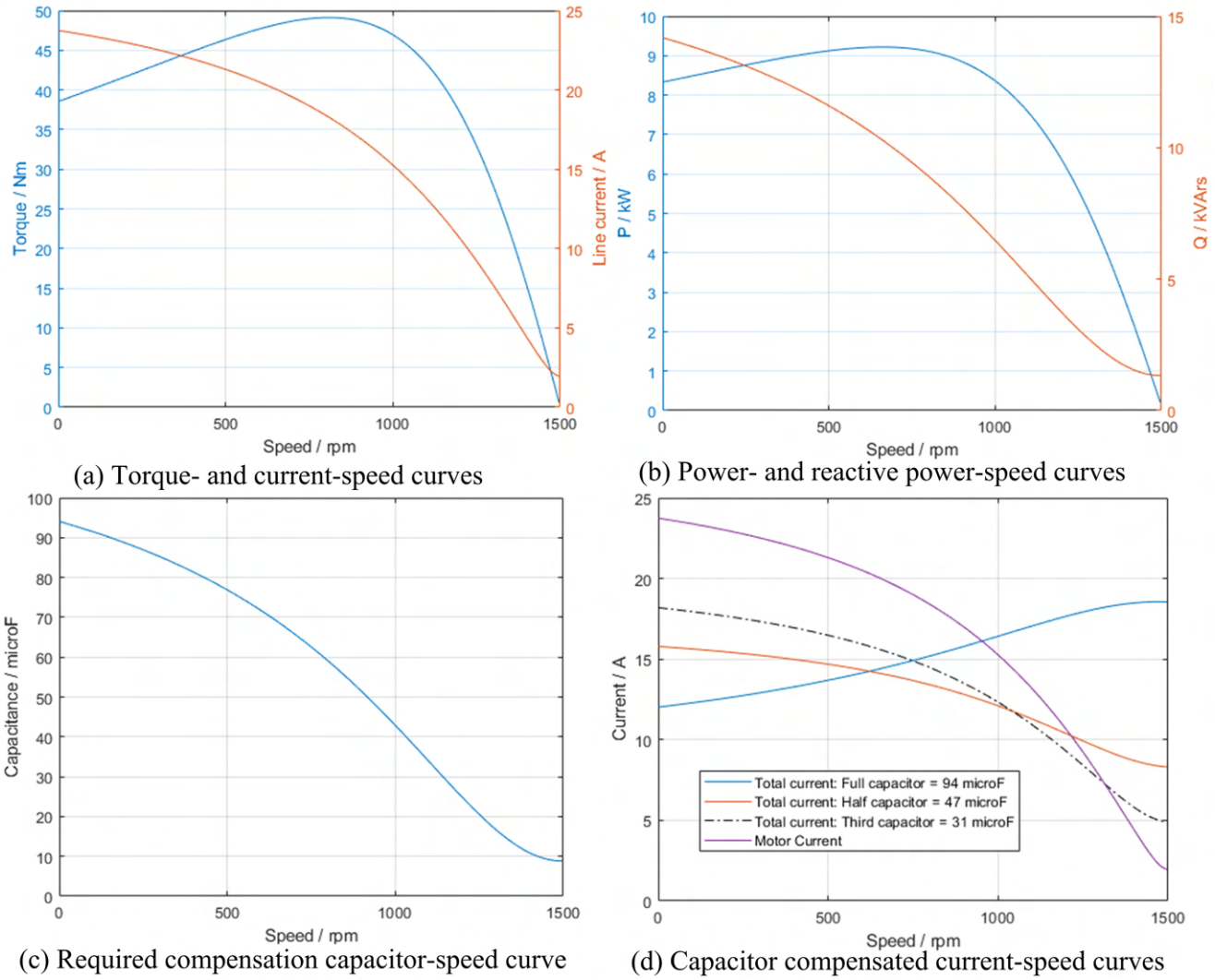

(a) Torque- and current-speed curves

(b) Power- and reactive power-speed curves

(c) Required compensation capacitor-speed curve

(d) Capacitor compensated current-speed curves

Figure 4.13 Comparison of 1.5 kW 400 V Valiadas K90L-4 machine capacitor compensation starting.

4.4.3 Motor No. 3: 3.75 kW 440 V Sen 5 HP Machine

This is a small 4-pole machine operating at 440 V and the capacitance requirement in Fig. 4.14(c) still varies considerably across the speed range. In (b), it can be seen that the reactive power is higher that the power at start but the reactive power decreases until the power is higher at about

1300 rpm (note the different scales on the left and right axes and that it is a 60 Hz machine so that the synchronous speed is 1800 rpm). If 62 μF capacitors are used then the starting current is reduced by 38 % which should be switched out at 1600 rpm. Again, using the capacitance calculated at start leads to a value that is too high because the current increases and the power factor will begin to lead.

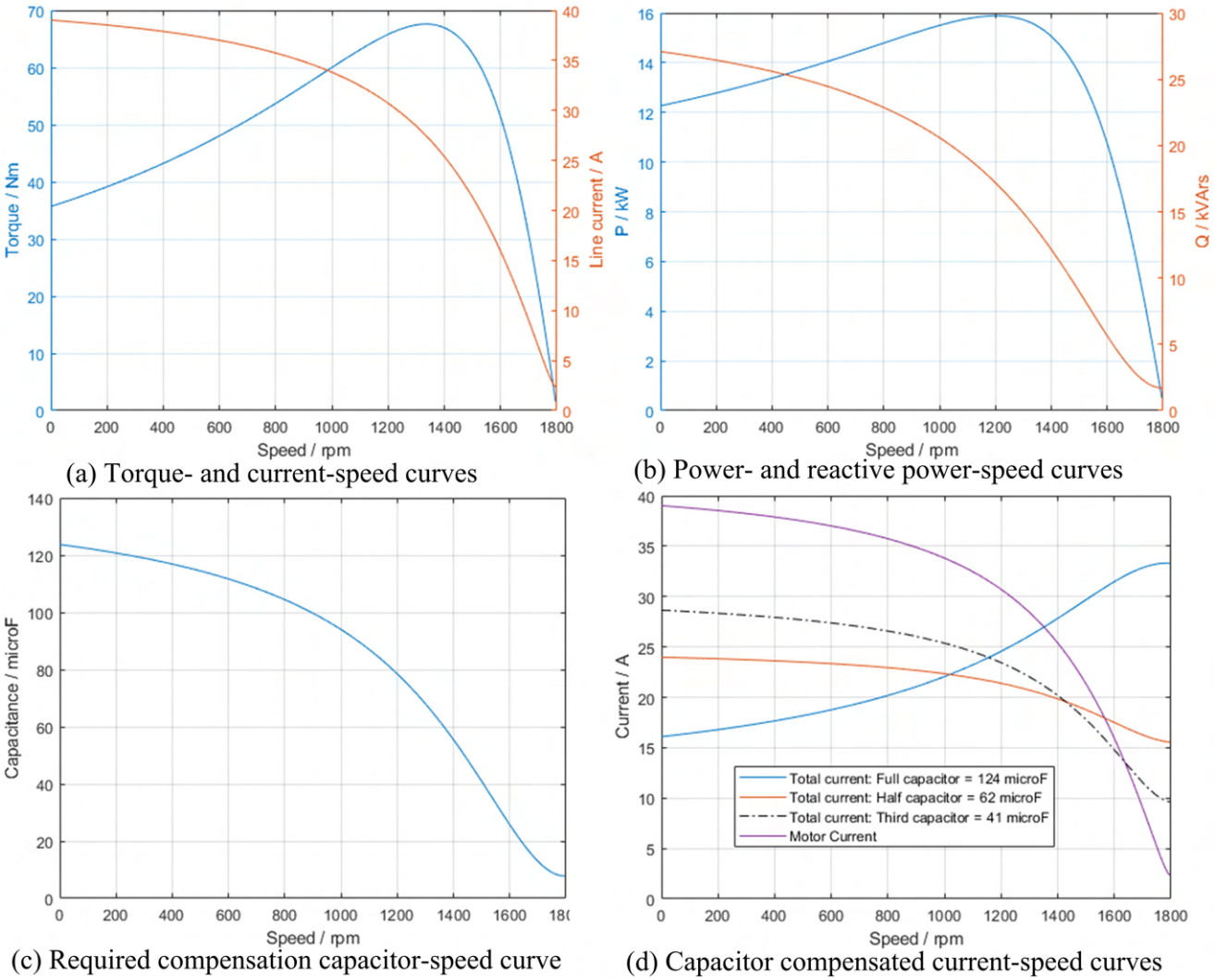

(a) Torque- and current-speed curves

(b) Power- and reactive power-speed curves

(c) Required compensation capacitor-speed curve

(d) Capacitor compensated current-speed curves

Figure 4.14 Comparison of 3.75 kW 440 V Sen 5 HP machine capacitor compensation starting.

4.4.4 Motor No. 4: 45 kW 400 V Valiadis K200L-4

As previously mentioned, this machine can be considered as a large machine for the 400 V rating. This means a high current rating. The required capacitance in Fig. 4.15(c) is shown to be nearly constant across the speed range. This illustrates that this method is more suitable for large machines. However, because it is a low-voltage, high-current machine, the required capacitance is high at 2.21 mF at the starting point. This does reduce the starting current by 85 % though there will be a peak of 325 A close to the steady-state operating point, when the capacitors should be switched out to avoid the current increasing still further and the system operating with a leading power factor. If 1.15 mF capacitors are used for the capacitance then these give nearly a 50 % reduction without the peak being close to the synchronous speed. This may be a better compromise since it does not need accurate control of the capacitor switch-out.

4.4.4.1 Run-up time at rated voltage and no load

This is a repeat of timed run-up for the 1 MW machine in Section 4.4.6.1; however, as can be seen in Fig. 4.7 the machine does not produce sufficient torque to overcome the load specified in (4.5). If this is changed to $K_1 = K_2 = 0$ and $K_3 = 1$ the motor can start. This is illustrated in Fig. 4.16. It can be seen, though, that the motor torque is only just greater than the load torque at about 1000 rpm. Therefore it would be recommended that this motor be started with no load.

The run up has to be conducted with some sort of load which could simply be the inertia and the squared speed term. It is given as 0.246 kgm^2 but the machine will possibly be attached to a pump or fan. To accommodate this then the inertia is doubled so that $J = 0.246 \times 2 = 0.492$ kgm^2. The run-up is shown in Fig. 4.17 and takes approximately 2.8 s. But in Fig. 4.16 if is marginal as

to whether this machine would start with a load, then a simulation can be carried out with no load as shown in Fig. 4.18. The run up time is now much faster at 0.75 s.

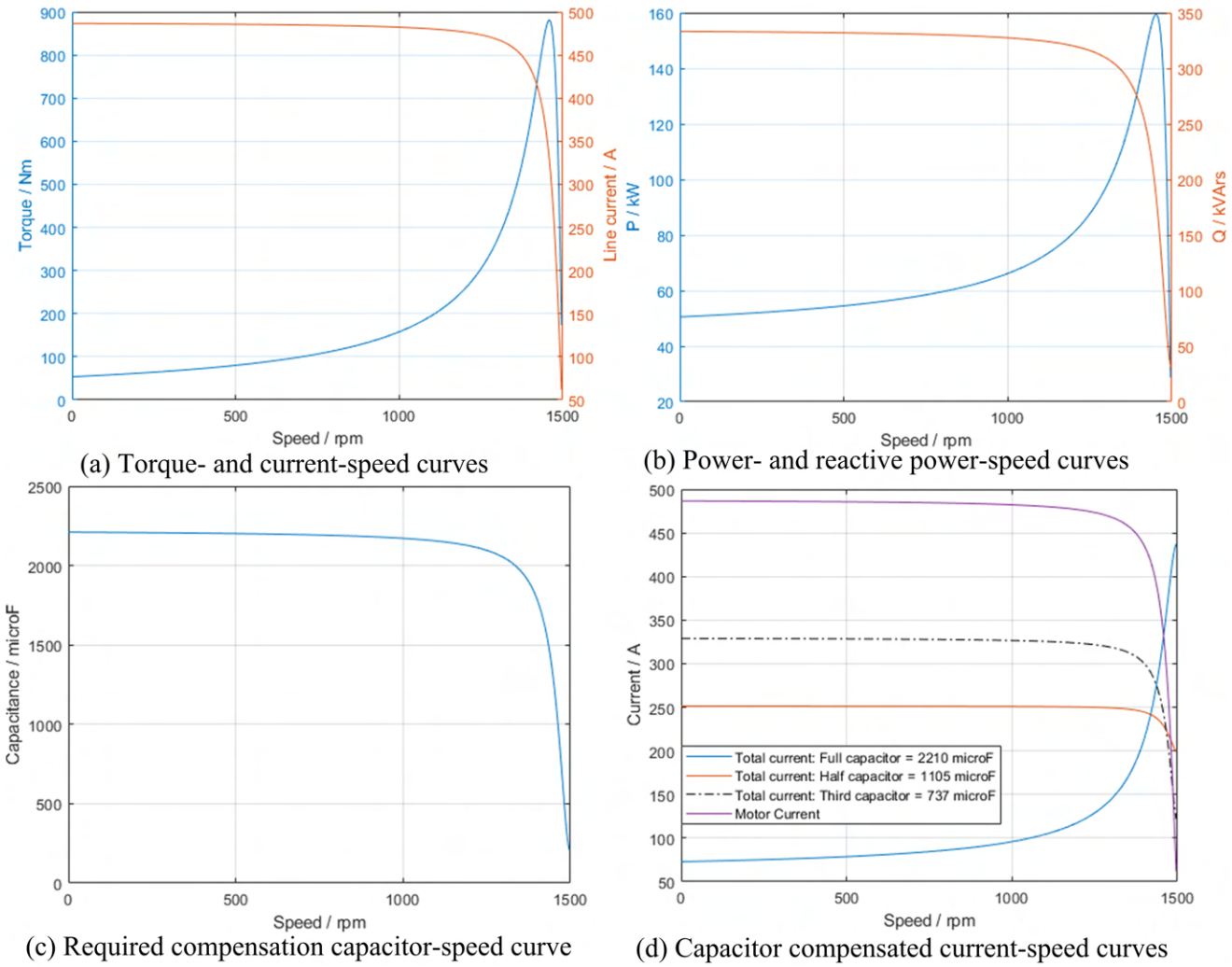

(a) Torque- and current-speed curves

(b) Power- and reactive power-speed curves

(c) Required compensation capacitor-speed curve

(d) Capacitor compensated current-speed curves

Figure 4.15 Comparison of 45 kW 400 V Valiadis K200L-4 machine capacitor compensation starting.

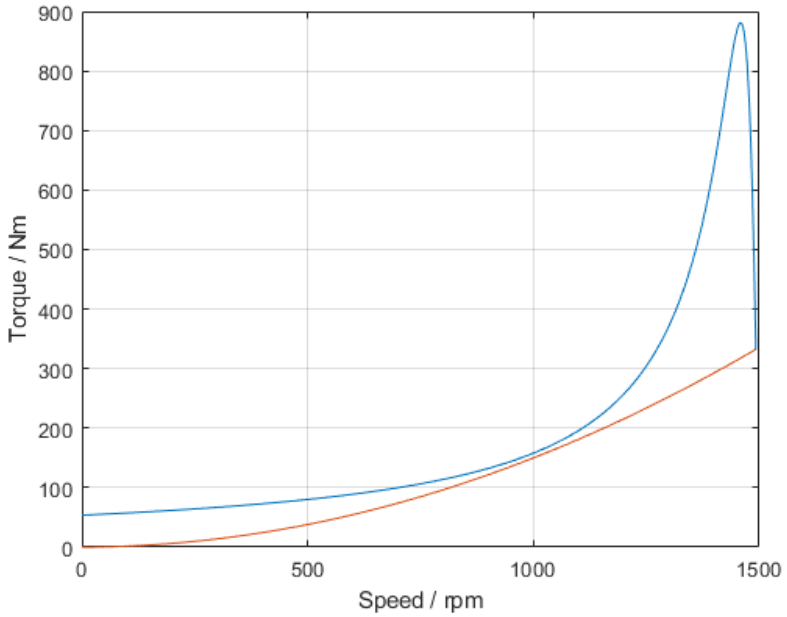

Figure 4.16 Speed-torque curve of 45 kW 400 V Valiadis K200L-4 machine and load torque with $K_3 = 1$.

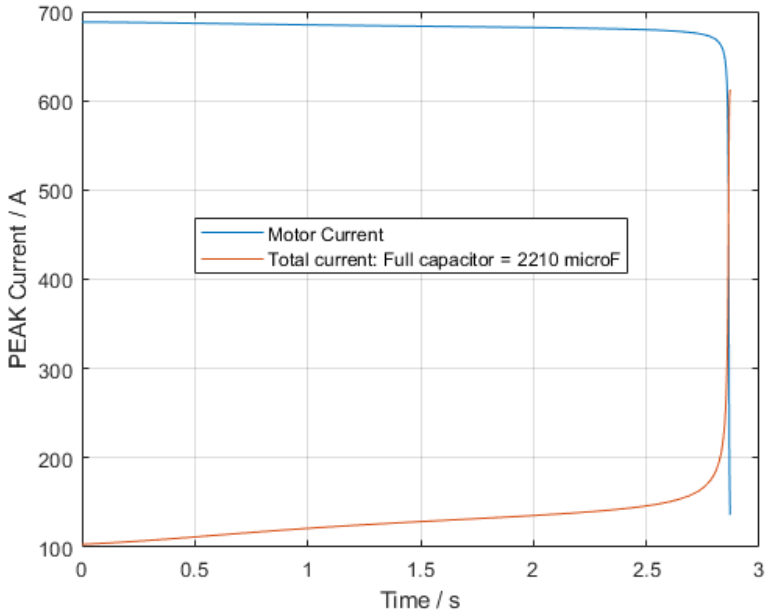

Figure 4.17 Speed-time curve of 45 kW 400 V Valiadis K200L-4 machine with inertia of 0.492 kgm^2 and speed-squared load torque function $K_3 = 1$.

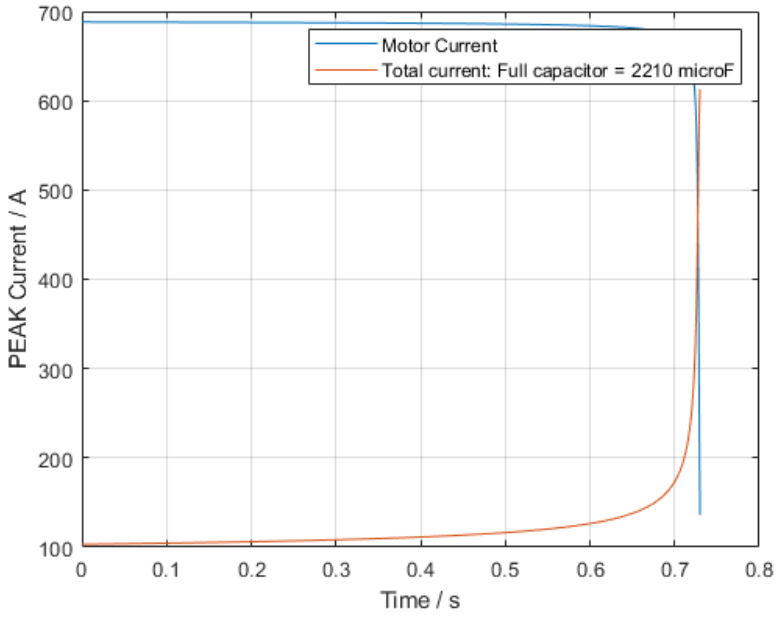

Figure 4.18 Speed-time curve of 45 kW 400 V Valiadis K200L-4 machine with inertia of 0.492 kgm^2 and no load.

4.4.5 Motor No. 5: 200 kW 3300 V Valiadas KHV355-2

This is a small- to medium-sized machine for the voltage rating. As shown in Fig. 4.19, the starting current can be reduced by 77 % using 177 µF capacitors though this will increase to a peak of 225 A at 2750 rpm where the capacitors should be switched out to avoid the grid current increasing still further. If 88 µF capacitors are used then the starting current is halved to 175 A and there is no peak current. Again, this may be a better compromise solution not requiring accurate capacitor turn-off.

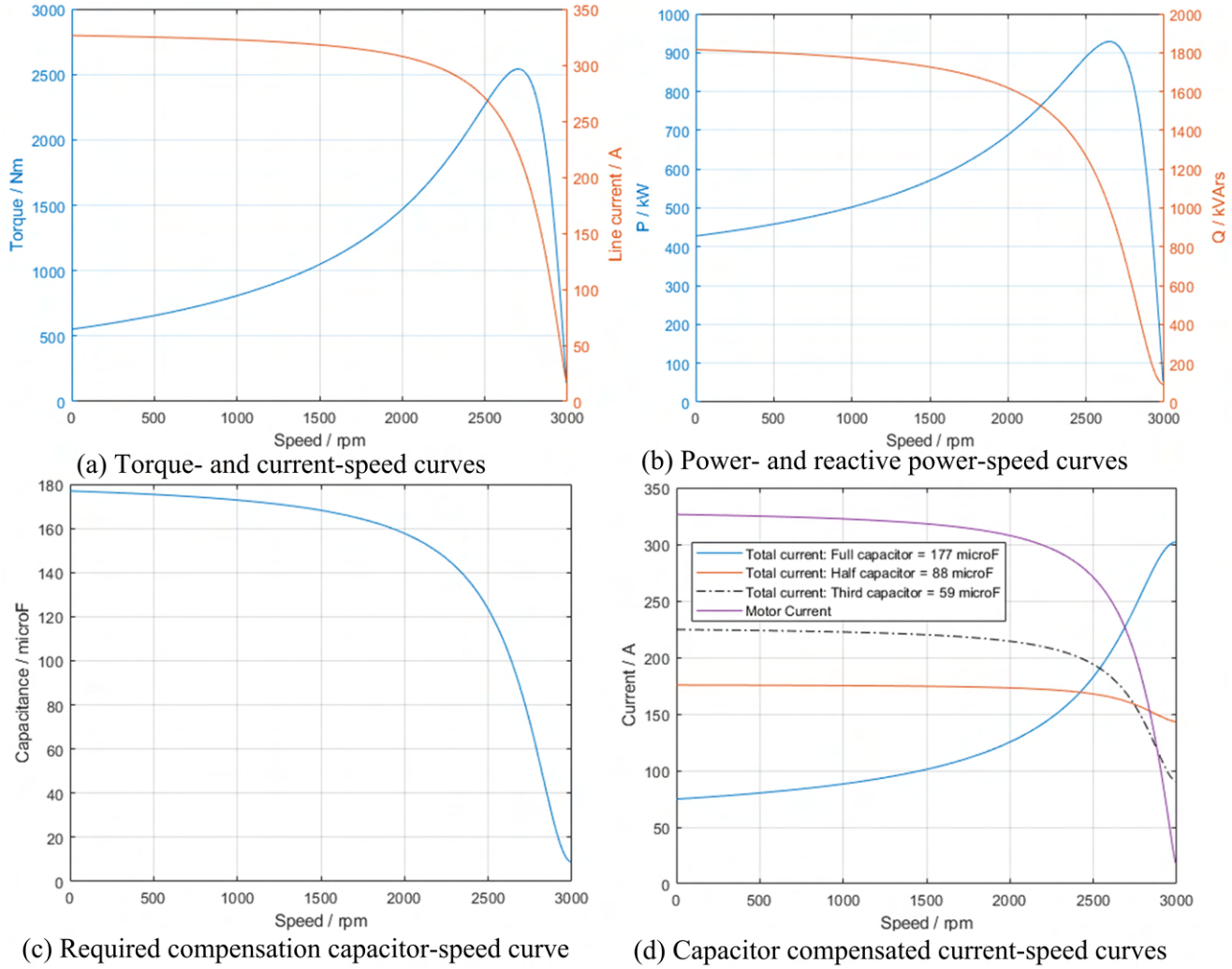

(a) Torque- and current-speed curves

(b) Power- and reactive power-speed curves

(c) Required compensation capacitor-speed curve

(d) Capacitor compensated current-speed curves

Figure 4.19 Comparison of 200 kW 3300 V Valiadas KHV355-2 machine capacitor compensation starting.

4.4.6 Motor No. 6: 1 MW 6000 V Valiadas TMKHV560-6

This is a large machine for the voltage rating. As with Motor No. 4 the required capacitance is almost constant across much of the speed range. Using 211 µF capacitors can reduce the current by 73 % at start but the current will rise to 2/3rds of the starting motor current at about 950 rpm

when the capacitors should be switched out to prevent further increase in current. If 105 µF is used then a 45 % reduction is possible with no peak current before capacitor turn-off.

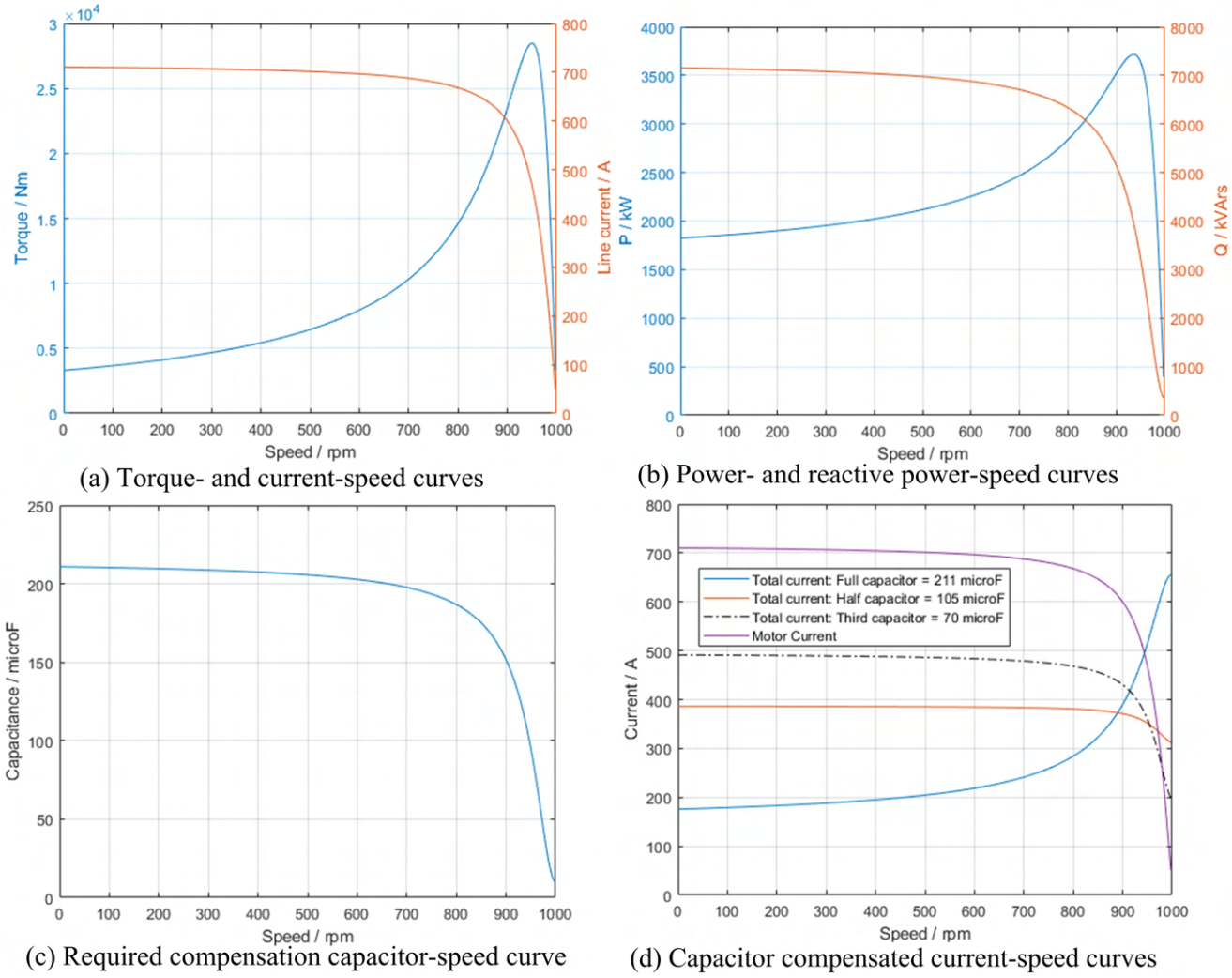

(a) Torque- and current-speed curves

(b) Power- and reactive power-speed curves

(c) Required compensation capacitor-speed curve

(d) Capacitor compensated current-speed curves

Figure 4.20 Comparison of 1 MW 6000 V Valiadas TMKHV560-6 machine capacitor compensation starting.

4.4.6.1 Run-up time at rated voltage and load

To show the speed of a large machine running up to speed then a simulation was carried out at the rated voltage of 6000 V and the load torque as given in Fig. 4.9(a). A further calculation can be done using (3.21) and setting the inertia to 79 kgm^2 as given in Table 4.1. The load torque coefficients are given in (4.5). The run-up time is shown in Fig. 4.21 to be about 2.5 s showing that large machines can take time to run up to speed. Also shown is the current when 221 μF delta-connected capacitors are used to correct the current. It can be seen that they can be disconnected very close to the full load speed. With the load removed, the run-up time reduces as shown in Fig. 4.22.

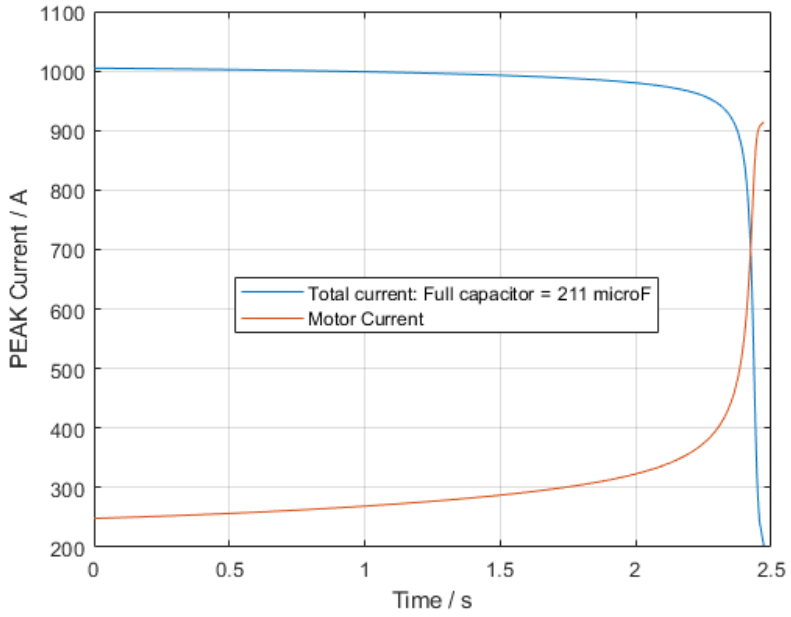

Figure 4.21 Run-up time prediction for 200 kW machine at rated voltage and with load.

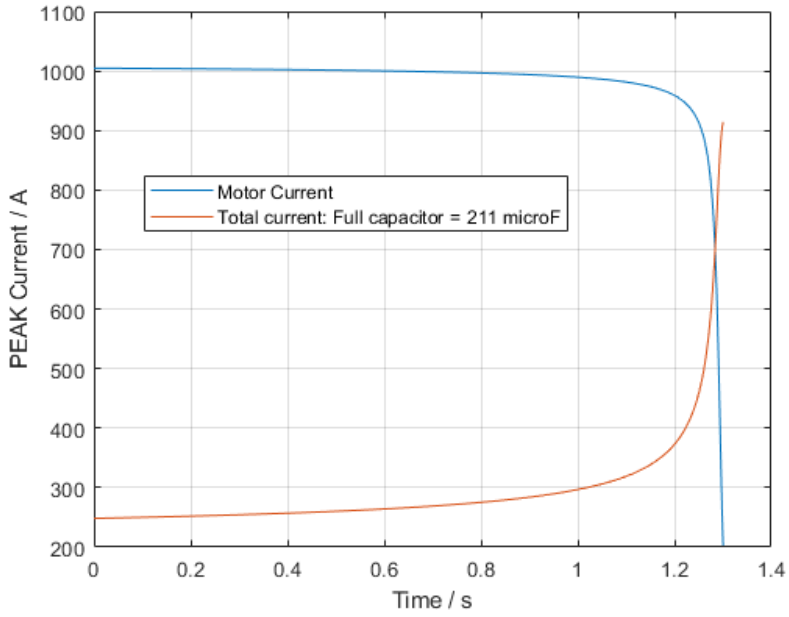

Figure 4.22 Run-up time prediction for 200 kW machine at rated voltage and with no load.

4.4.7 Motor No. 7: 3.75 MW 6900 V Sen 5000 HP Machine

This is a large high-efficiency machine with low starting torque. The starting current can be reduced by 90 % as shown in Fig. 4.23(d) using 343 µF capacitors, with a peak of 1100 A (71 % of the motor starting current) just before capacitor turn off. This would need careful control since it is close the the full load speed. The run-up current is halved if 172 µF capacitors are used, and there is no peak current.

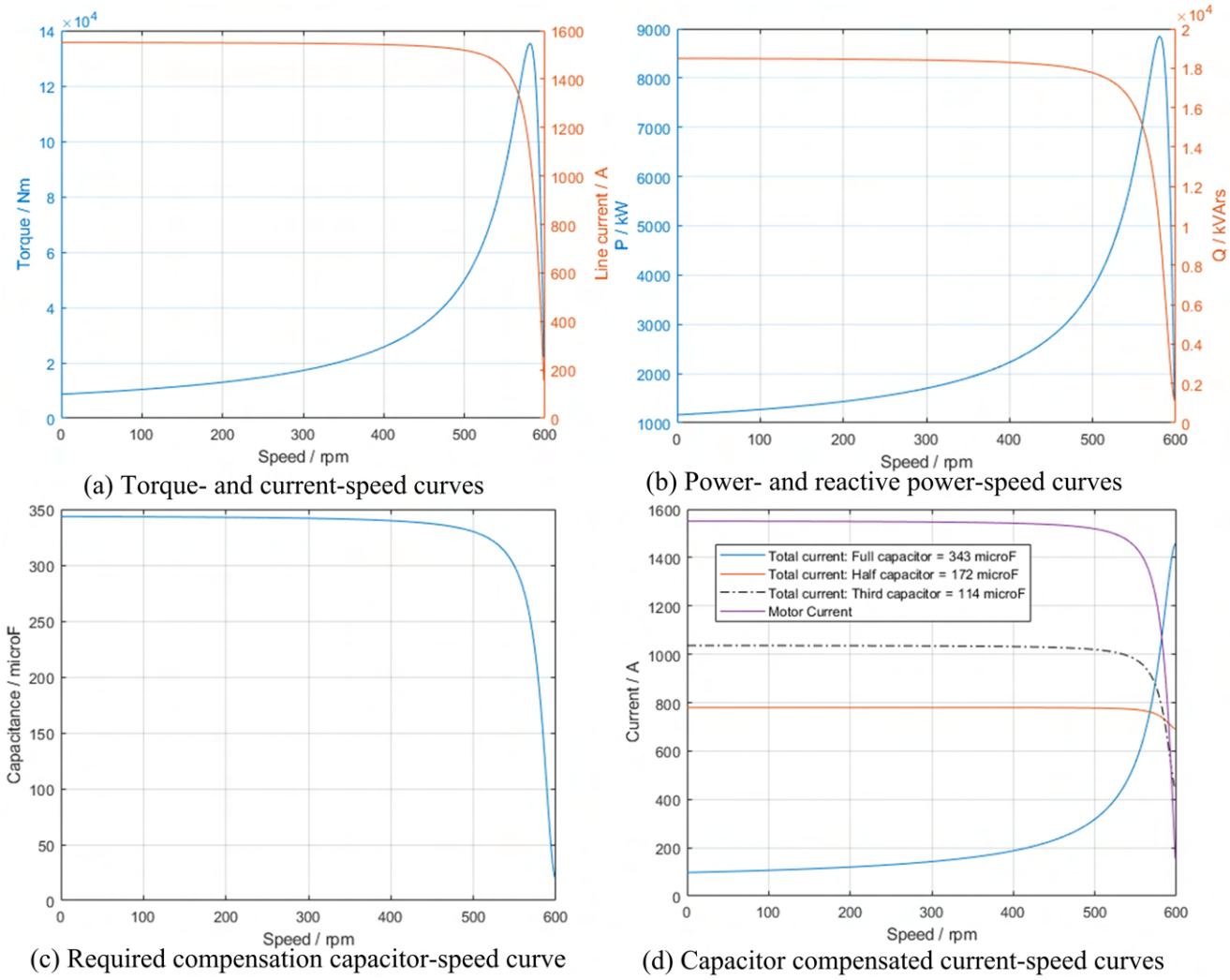

(a) Torque- and current-speed curves

(b) Power- and reactive power-speed curves

(c) Required compensation capacitor-speed curve

(d) Capacitor compensated current-speed curves

Figure 4.23 Comparison of 3.75 MW 6900 V Sen 5000 HP machine capacitor compensation starting.

4.4.7.1 Run-up time at rated voltage and no load

This is a repeat of timed run-up for the 1 MW machine, however, as can be seen in Fig. in Fig. 4.10 the machine does not produce sufficient torque to overcome the load specified in (4.5). Even if this is changed to $K_1 = K_2 = 0$ and $K_3 = 1$ there is still a mid region where the load torque is greater

than the motor torque which would prevent run up. This is illustrated in Fig. 4.24.

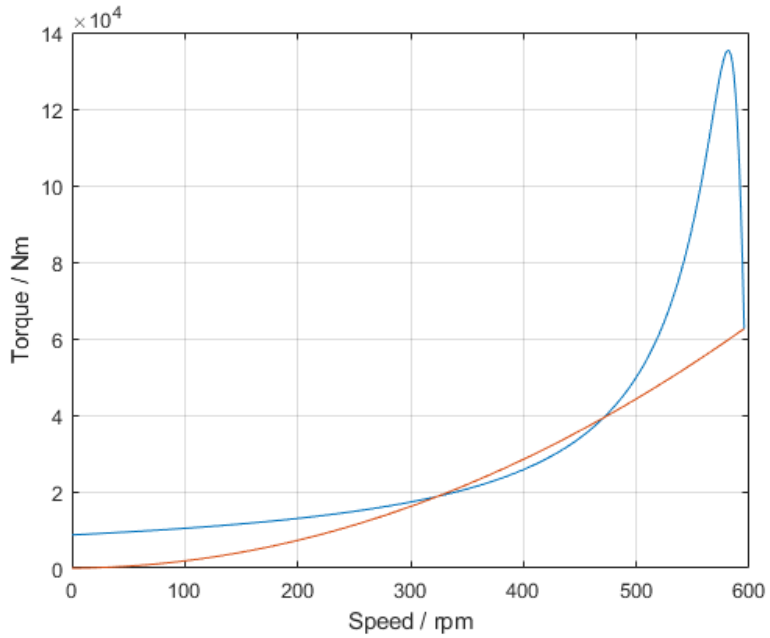

Figure 4.24 Speed-torque curve of 3.75 MW 6900 V Sen 5000 HP machine and load torque with $K_3 = 1$.

The run up has to be conducted with no load however there will be inertia. It is given as 145.47 kgm^2 but the machine will possibly be attached to a pump or fan. To accommodate this then the inertia is doubled so that $J = 145.47 \times 2 = 290.94$ kgm^2. The run-up is shown in Fig. 4.25 and takes approximately 1.1 s.

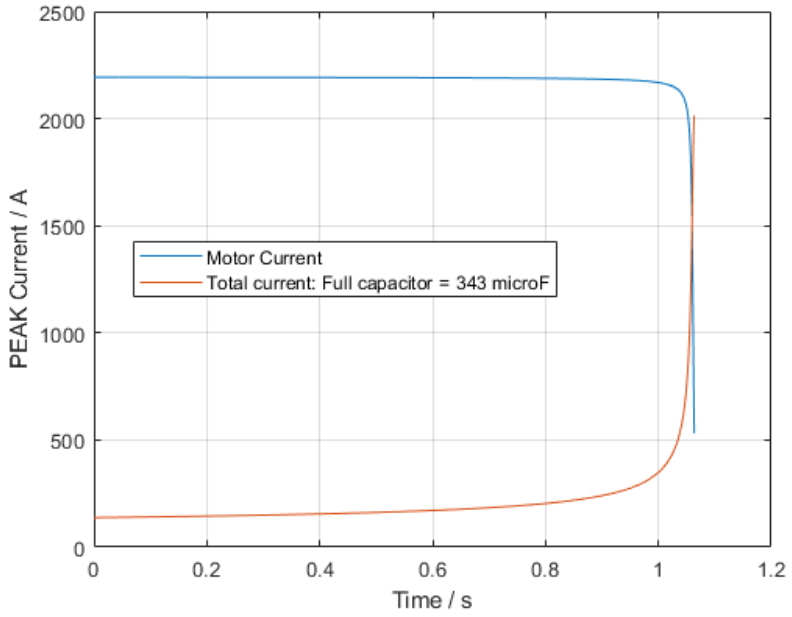

Figure 4.25 Speed-time curve of 3.75 MW 6900 V Sen 5000 HP machine inertia of 290.84 kgm^2 and no load.

4.5 Transient Turn-on and Run-up of Induction Motor with Capacitor Compensation in Simulink Simulations

4.5.1 Initial Model - Motor No. 0

An initial model was used before the seven motor models were settled on. This was reported in [61] and the results are included here for completeness. The equivalent circuit parameters are similar to Motor No. 1 though the machine was run at 380 V giving it a higher power rating. The Simulink model used is shown in [61]. This motor is designated as Motor No. 0. It has a high inertia and load torque so that the run up speed is relatively slow. This model is useful because it studies the

instantaneous power and reactive power during run-up. The run-up speed is shown in Fig. 4.26.

In the simulation of motor, the inrush current peaks at 65.71 A and starts reducing with a run-up time of 5.5 s. Once steady state is reached then the current is 5.8 A as shown in Fig. 4.27. This run-up time varies from one machine to another and is a function of the motor electrical characteristics, the inertia of the motor and its load, and characteristic of the load itself with respect to the grid (a high load with a long run-up time may cause the grid voltage to dip with which is the issue being addressed in this work) [88].

The capacitors are inserted and the inrush current is reduced to 49.01 A that constitutes 25.43 % reduction. The rotational speed characteristics is same as without the capacitors, settling after 5.3 s at 1493 rpm as shown on Fig. 4.28.

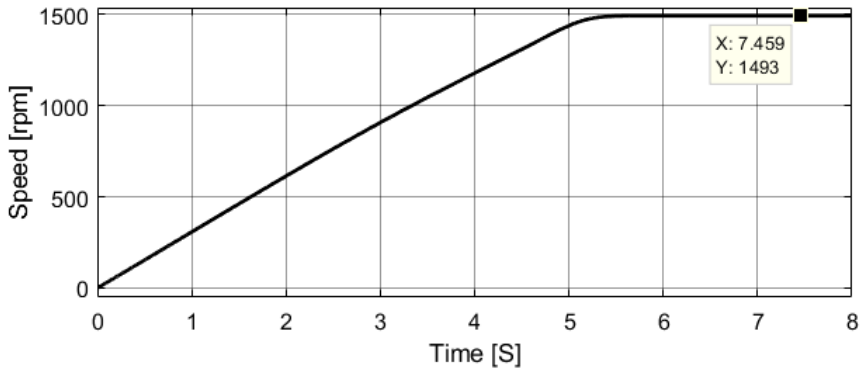

Figure 4.26 Motor No. 0 speed simulation

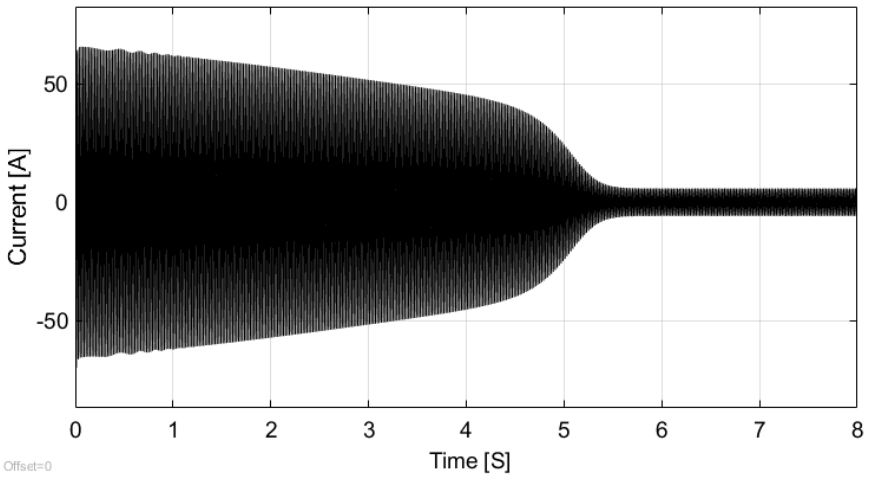

Figure 4.27 Motor No. 1 inrush current

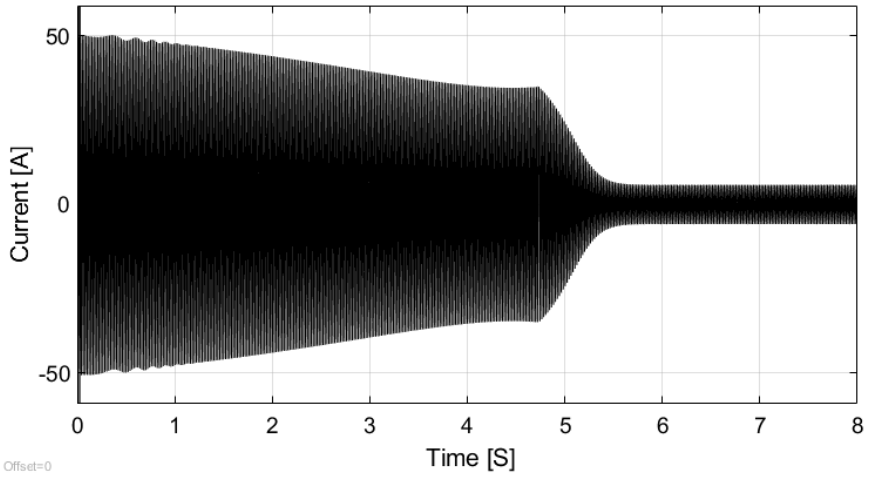

Figure 4.28 Motor No. 1 inrush current with capacitors in circuit.

The power factor is shown on Figure 4.29. This is about 0.75 for most of the run-up. As stated, this machine model is not very inductive when running up to speed. This is illustrated in Fig. 4.32 where there is more active than reactive power being absorbed during run-up. The power factor improves as it approaches full load but then dips because the machine is not heavily loaded with a steady-state speed of 1493 rpm so it becomes more inductive.

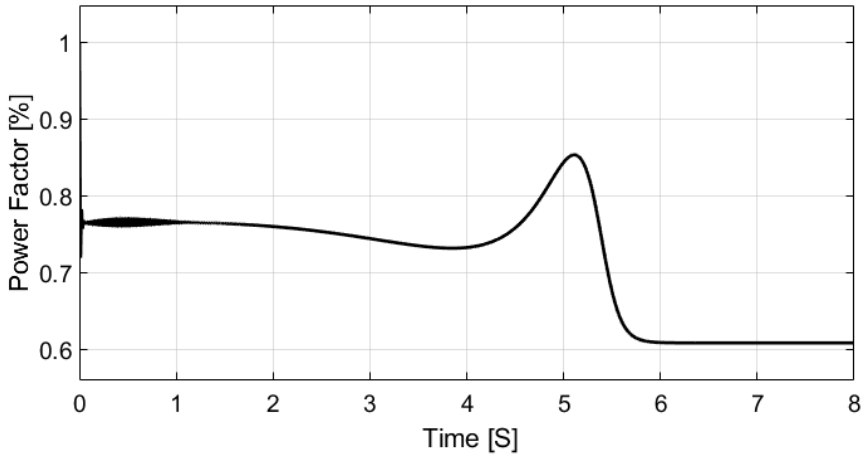

Figure 4.29 Motor No. 1 power factor.

The electromagnetic torque with the motor operating with capacitors at start is shown in Fig. 4.30. This shows the initial transient oscillation that occurs in a motor during starting and then a smooth run-up torque. The motor settles at about 6 Nm at 1493 rpm. This 938 W of mechanical power.

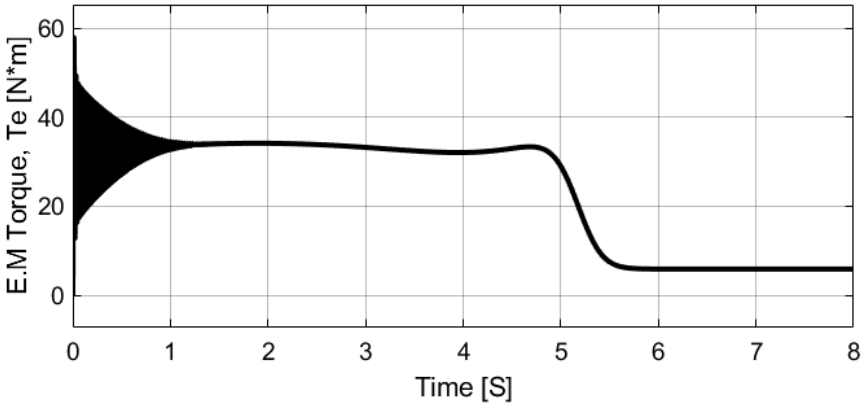

Figure 4.30 Motor No. 1 electromagnetic torque during run-up.

The measured currents with and without capacitors inserted are shown in Fig. 4.31. These illustrate that the current is reduced by about 25 % as mentioned earlier. This is not a substantial

reduction compared to what is possible in larger machines such as Motor Nos. 6 and 7.

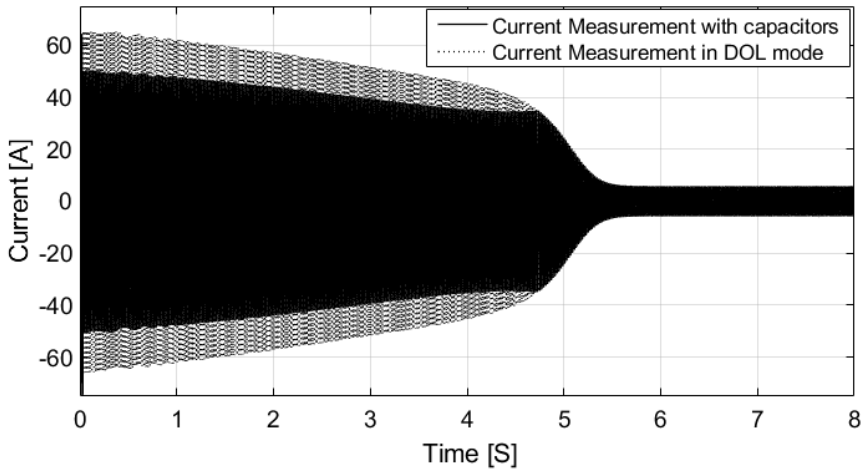

Figure 4.31 Motor No. 1 current simulation comparison.

4.5.1.1 Energy requirement and capacitor calculation for DSTATCOM

As shown in Fig. 4.31 the reduction in current using capacitors for this machine is not substantial. For this sort of smaller machine, where the capacitor compensation does not reduce the starting current by a substantial amount, then a DSTATCOM system as shown in Chapter 2 Fig. 2.11 could be used. As an aside to this work the energy required to start and suitable capacitor calculation can be calculated to compensate for the real energy drawn during starting.

The required power and reactive power is shown in Fig. 4.32. Assume that the mean power drawn is $\frac{(15000+7500)}{2}$ which is an approximate trapezium for the power during run-up, with the time being about 5 s. This gives an energy requirement of $11.25 \times 5 = 56.25$ kJ. The energy stored in a capacitor is $E = \frac{1}{2}CV^2$. For this system the line voltage 380 V. The DC voltage should be more than the peak of the line voltage which is 535 V so assume it is 600 V. Therefore, assuming

that the capacitor does not fall below this level after starting, and does not go over say, 1000 V:

$$C = \frac{2E}{V_{max}^2 - V_{min}^2} = \frac{56.25 \times 10^3}{1000^2 - 600^2} = \frac{56250}{640000} = 88 \text{ mF} \tag{4.6}$$

This is a large capacitor bank which may well require super-capacitors or batteries to realise the energy requirement.

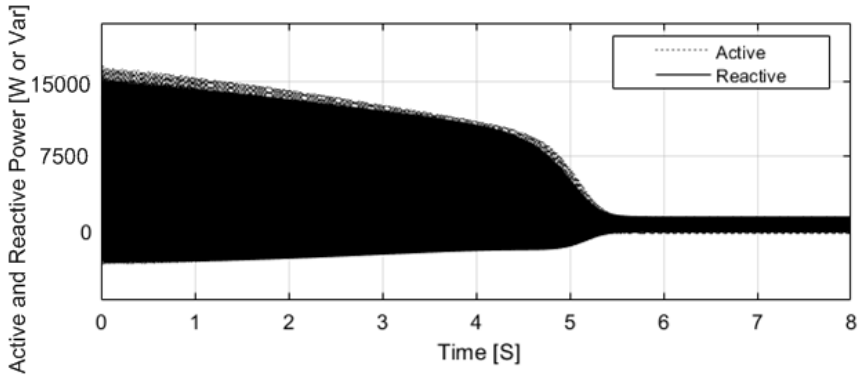

Figure 4.32 Motor No. 1 starting – real and reactive power requirement

4.5.2 Simulations of Motor Nos. 1 and 6

Rather than simulate all the machines then Motor Nos. 1 and 6 were selected. The steady-state simulations for these motors are given in Figs. 4.12 and 4.21. The Simulink model used in these simulations is shown in Fig. 4.33. This was varied depending on the simulation. What can be seen is the induction motor model which has the parameters for the motors input, including the inertia.

The machine is torque controlled and the pink components set this control up. The load torque is set to zero and the no-load speed is controlled by the viscous friction with the load inertia set to a very low level this means that machine will run up to no-load speed with the motor inertia being the main loading.

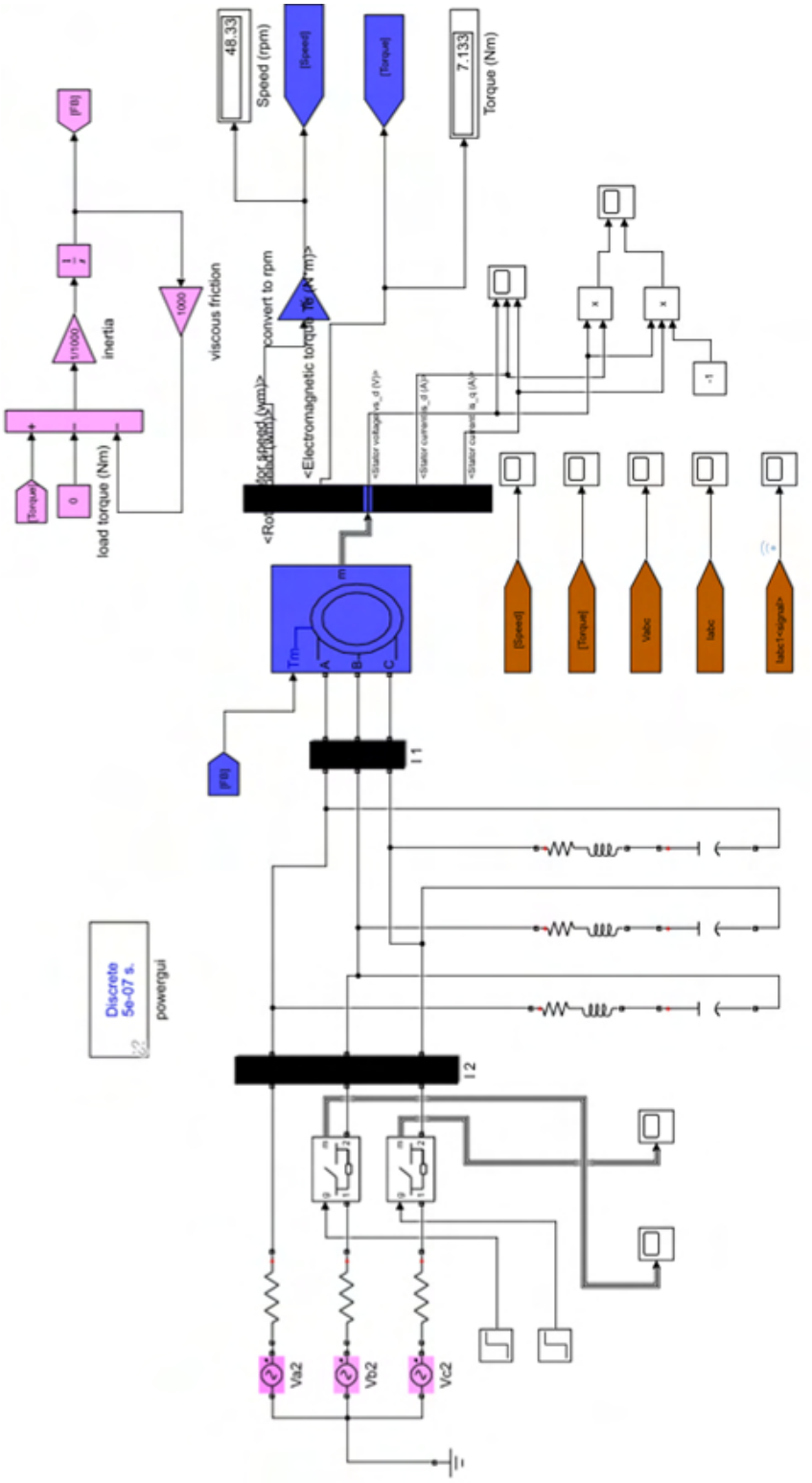

Figure 4.33 Simulink model

In parallel with the motor is a delta-connected capacitor network. In addition to the capacitors, inductors and resistors are connected in series, The reactance is 10 % and the resistance 1 % resistance. The 3-phase supply has small resistors which help stabilize the simulation. This model, for clarity, shows only two relay switches in Phases *b* and *c*. These are controlled by timers. To turn the capacitors off then three would be required - one in series with each capacitor.

At this point only the turn-on is of interest for the motor and capacitors.

4.5.2.1 Motor No. 1

Fig. 4.34 shows the waveforms for Motor 1. These match well with Fig. 4.12. The voltage was set to 100 V line and the simulation runs up close to full load which is after 1.5 s. There is no capacitor turn off for these simulations. Fig. 4.35 examines the first 0.06 ms of the simulation to show the turn-on. This simulation has the capacitors hard-wired in parallel with the motor as shown in Fig. 4.33. The there is grid current when the first two phases are turned on. For the line voltages if can be seen the the red voltage which is $v_b - v_a$ and this is at the zero crossing point of the voltage. During this period $v_c - v_b = v_a - v_c = \frac{v_b + v_a}{2}$. After a further 90° Phase *c* is connected. This is a point where the $v_c - v_b = v_a - v_c = 0$. This is how many small solid-state point-on switches work - they switch on when the voltage across them is zero. It can be noted that even though Phase *c* of the motor is connected to to the Phase *c* point of the capacitor bank there is no current until Phase *c* of the grid is connected because the motor star point and the Phase *c* capacitor point are at the same voltage. There is some transient oscillation of the current. This is due to resonance with the in-line reactance. If this is assumed to be 10% of the resonant frequency,

for 90 μF capacitors, the inductors are 0.113 mH:

$$f = \frac{1}{2\pi\sqrt{LC}} = \frac{1}{2 \times pi \times \sqrt{0.00009 \times 0.0113}} = 157.8 \text{ Hz} \tag{4.7}$$

In the experimental work, 1.1 Ω inductors were used since these were available and different capacitors were used in the testing. This is a 3.2 mH inductance; the resonant frequency is

$$f = \frac{1}{2\pi\sqrt{LC}} = \frac{1}{2 \times pi \times \sqrt{0.00009 \times 0.0032}} = 296.6 \text{ Hz} \tag{4.8}$$

Fig. 4.35 shows that this is the resonant frequency during turn-on of the capacitors.

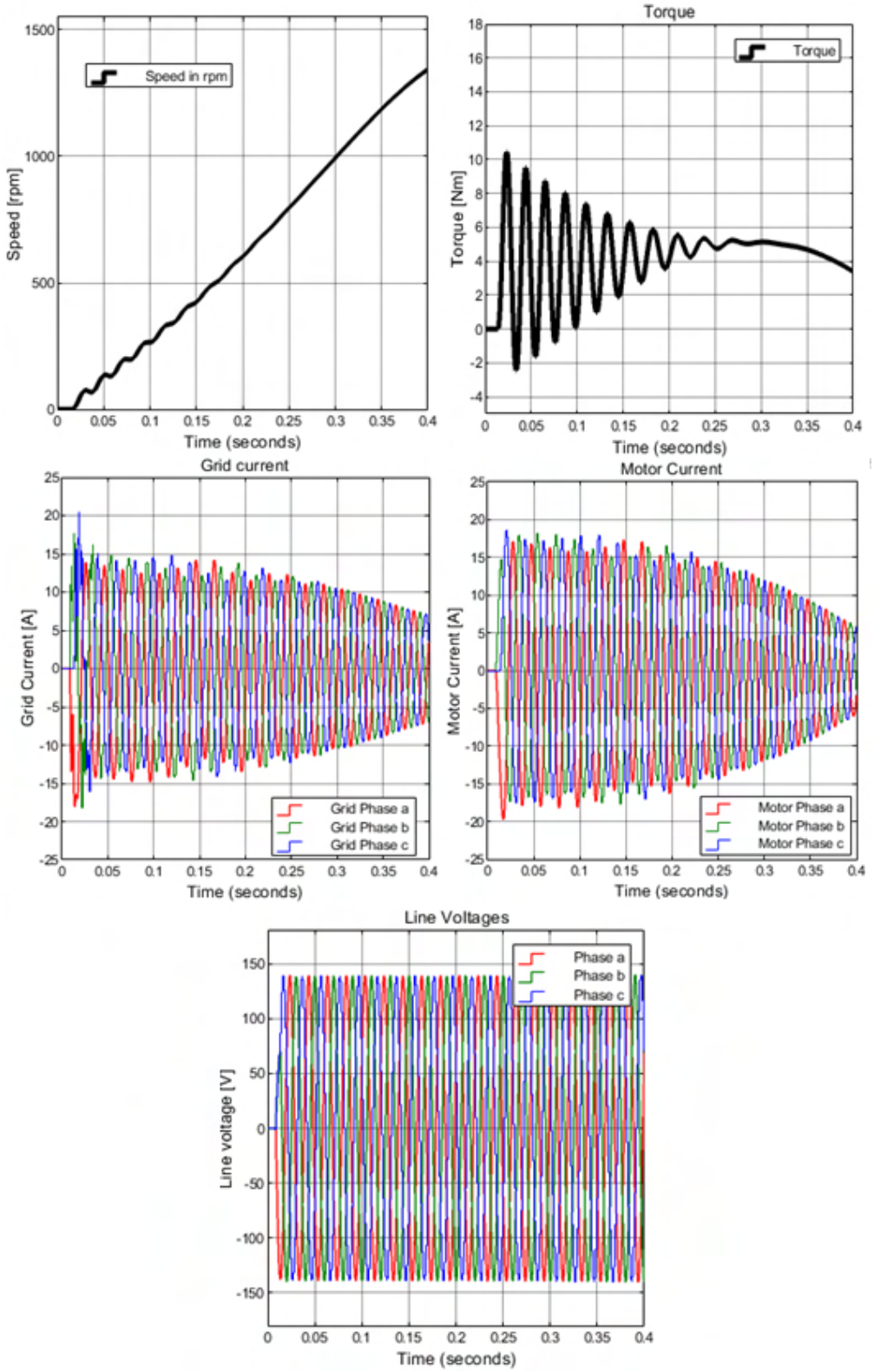

Figure 4.34 Transient simulation of Motor No. 1 with 90 µF capacitors

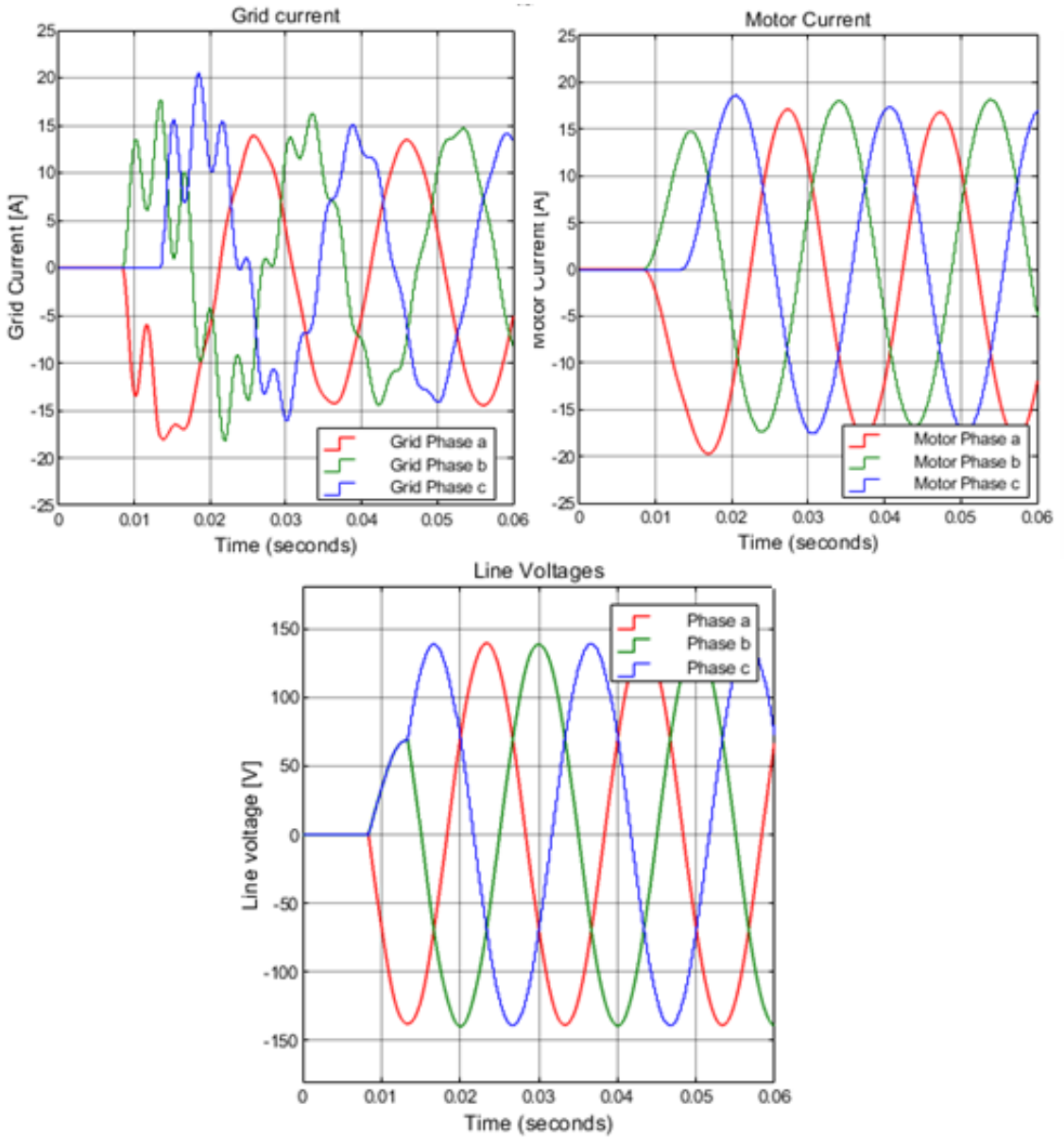

Figure 4.35 Transient simulation of Motor No.1 with 90 μF capacitors - zoomed over 6 ms.

4.5.3 Motor No. 6

Fig. 4.22 shows the run-up time when Motor No. 6 is not loaded for the steady-state per-phase analysis. The simulink model results are shown in Fig. 4.36 and 4.37. The capacitors are 221 μF, the in-line inductors are 46 mH and there is a 0.1 Ω series resistor. In Fig. 4.36 that the run-up current is reduced down to 250 A to 300 A peak when the motor current is 100 A peak. This compares will with the steady-state simulation in Fig. 4.22 and the run-up times match too. This illustrates the effectiveness of the method.

In Fig. 4.37 the first few current cycles are shown for the first 80 mS of the simulation and it shows the issues with turn-on resonance of the capacitance. The peak turn-on grid current is 2000 A and the motor current shows some transient decay components over the first two cycles.

The capacitor turn-off is not modelled in this simulation so that when the motor reaches no load, the grid current is dominated by the capacitor current which is 1000 A peak in steady-state. This is shown in Fig. 4.36. To address this then breakers can be put into the capacitor circuit as shown in Fig. 4.38. There are now two breakers to turn the system on, and three to turn the capacitors off. These are timed to turn off at 1.4 s although other methods of control are possible. For the capacitor network, the capacitance was reduced to 200 μF and the series resistor increased to 2 Ω while the series inductance was maintained at 46 mH. With the change in capacitor and increase in damping resistor the grid current is now reduced to about 400 A peak compared to the motor current during run-up as can be seen in Fig. 4.39. Only the grid current is shown because this, and the capacitor currents, are the only changes. However, the transient capacitor turn-on current is reduced to 1500 A peak which is a reduction of 25 %. This is shown in Fig. 4.40 which can be compared to Fig. 4.37. This illustrates that with fine tuning the turn-on current and transient run-up current can be reduced and controlled.

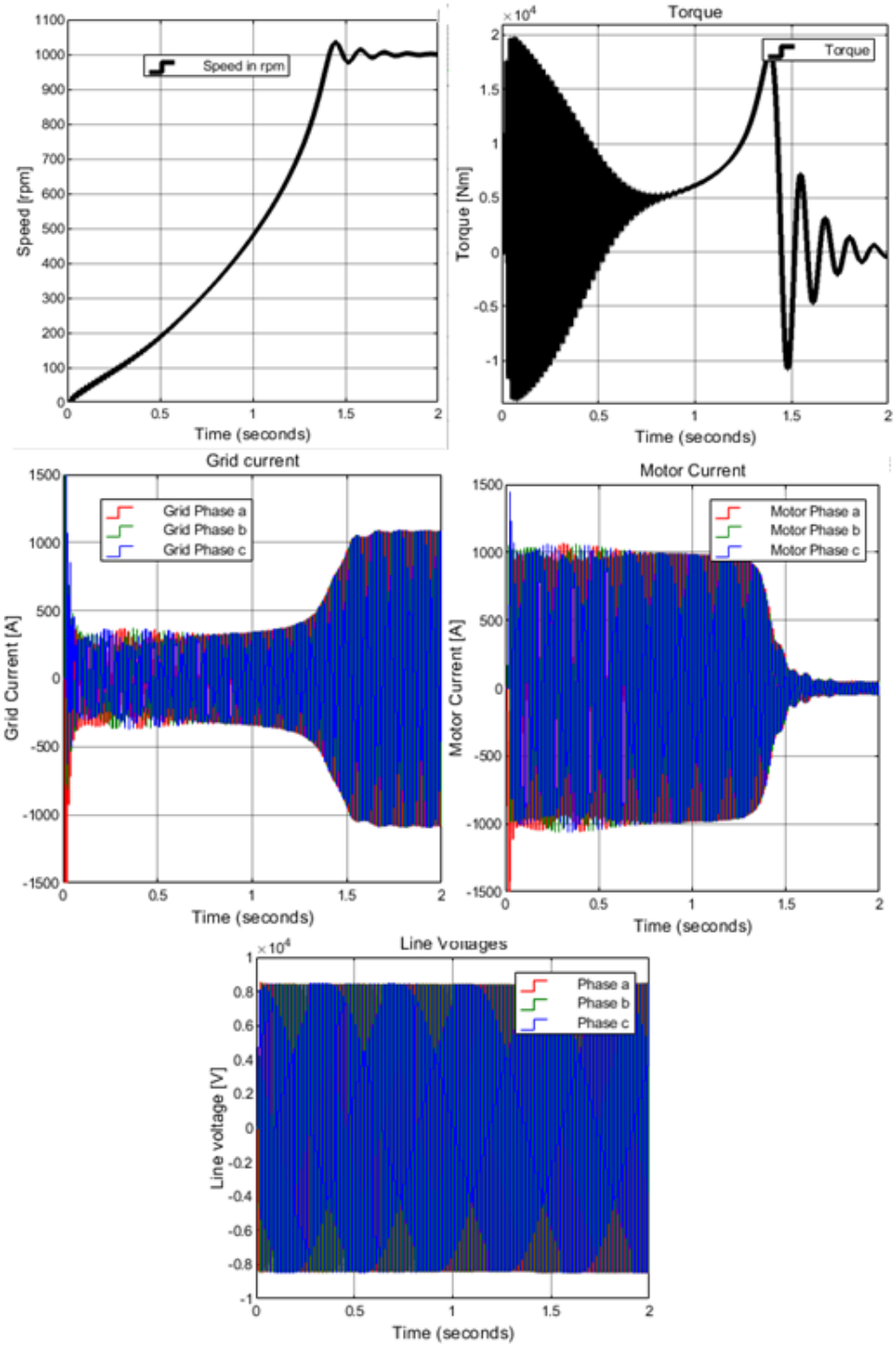

Figure 4.36 Motor No. 6 transient simulation with 221 μF capacitors switching when the line voltages are zero.

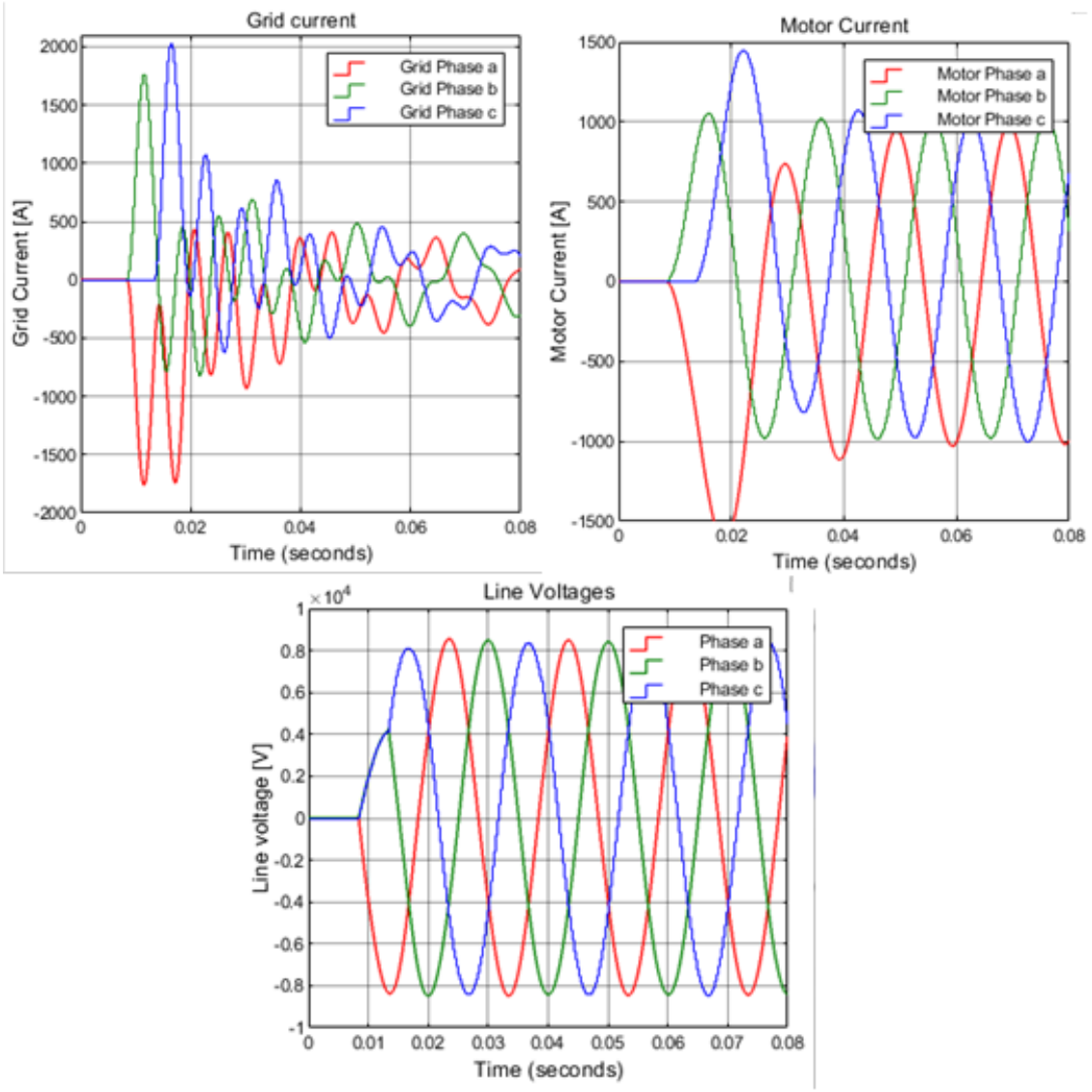

Figure 4.37 Transient simulation of Motor No. 6 with 221 µF capacitors - zoomed over 8 ms.

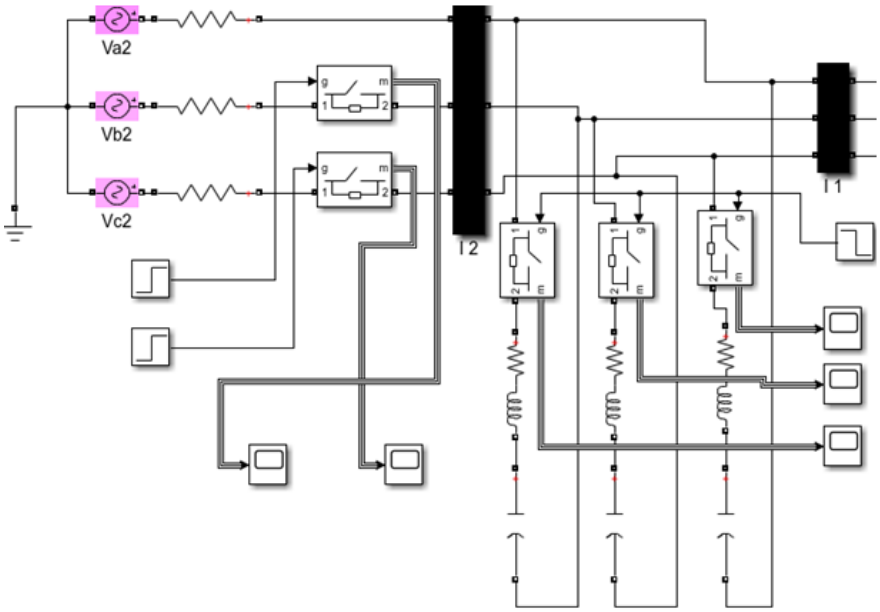

Figure 4.38 Motor No. 6 transient simulation showing supply with turn-on breakers and capacitor turn-off breakers

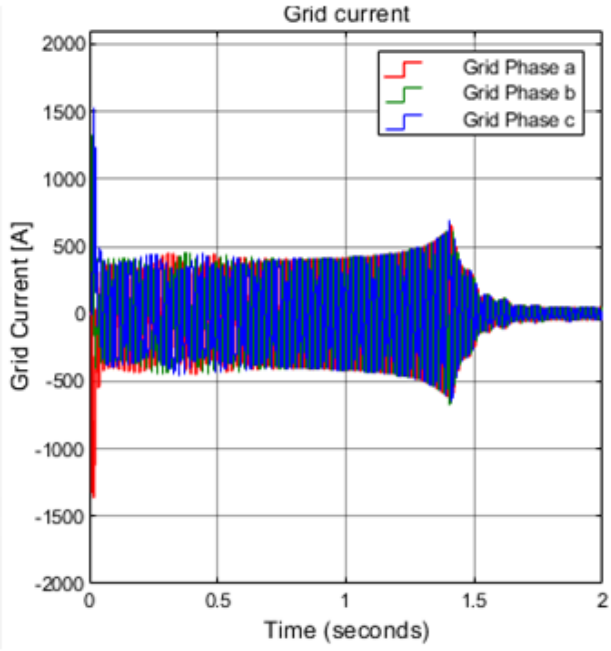

Figure 4.39 Transient simulation of the grid current for Motor No. 6 with 200 μF and series resistor increased to 2 Ω.

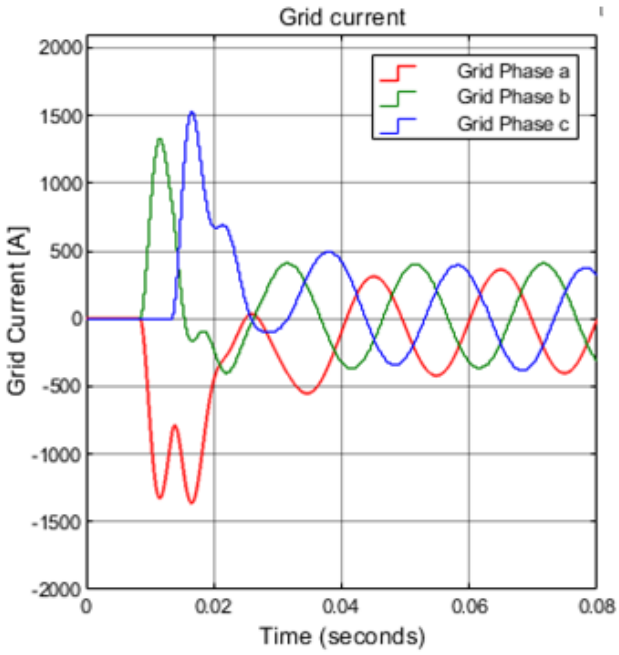

Figure 4.40 Transient simulation of the grid current for Motor No. 6 with 200 µF and series resistor increased to 2 Ω - zoomed to 8 mS.

4.6 Motor No. 1E Simulations

During the experiments it was found that Motor No. 1 was not sufficiently inductive to give meaningful results for capacitor compensation. To address this the 0.2 +j8.75 Ω reactances were added to the machine in series with each phase winding. In the simulations this was an additional 23.6 mH added to the stator leakage reactance so that the machine now has an equivalent circuit that more matched a larger machine with it being more inductive during run-up. The voltage was increased for this machine because it was found that with the added motor inductors, the machine would not run up to speed with a line voltage of 100 V rms, which is 141 V peak. The phase voltage was now set to 100 V peak which gives a line voltage of 173 V peak or 122.5 V rms.

This section gives the steady-state and transient simulations for this modified machine so that they can be compared to the measured in Chapter 6. The machine uses 90 µF compensation capacitors. The steady-state simulation for the motor and grid currents are shown in Fig. 4.41. It takes about 1.5 s to run up to speed and this matches the transient Simulink simulation in Fig. 4.42. It can be seen that there is substantial grid current oscillation during turn-on as illustrated in Fig. 4.42. These graphs are for the first 6 ms of the simulation.

During the experimental work it was found that the machine ran up much slower than the simulations that have low load and use the inertia as the main mechanical load. By simulation experiment it was found that the 5 s run-up time could be achieved by adding a friction torque of 0.625 Nm and this is shown in Fig. 4.44. The machine is old with little maintenance and this seems a reasonable addition to the load profile.

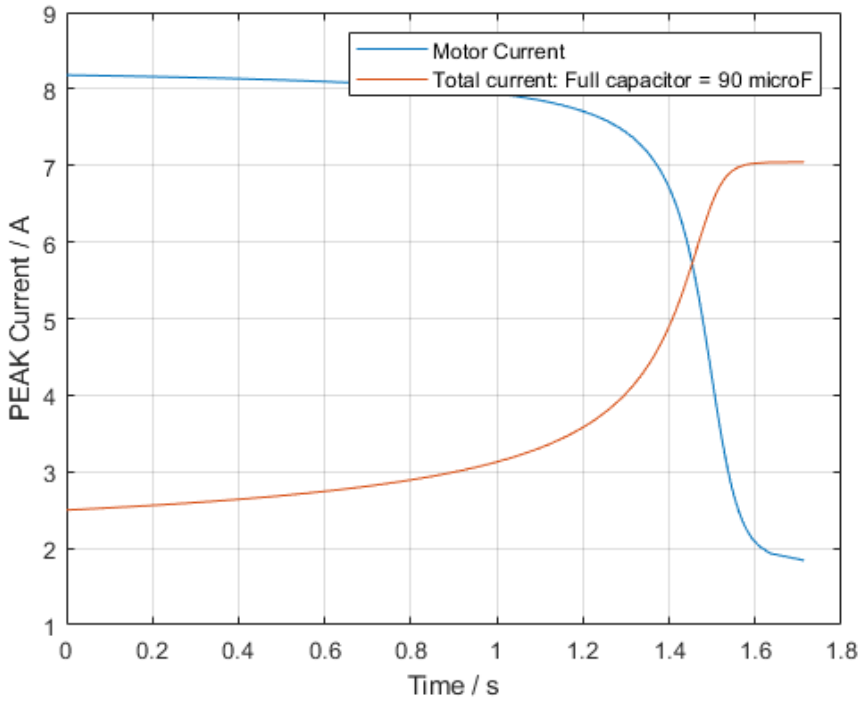

Figure 4.41 Motor No. 1E steady-state simulation with 90 µF capacitors.

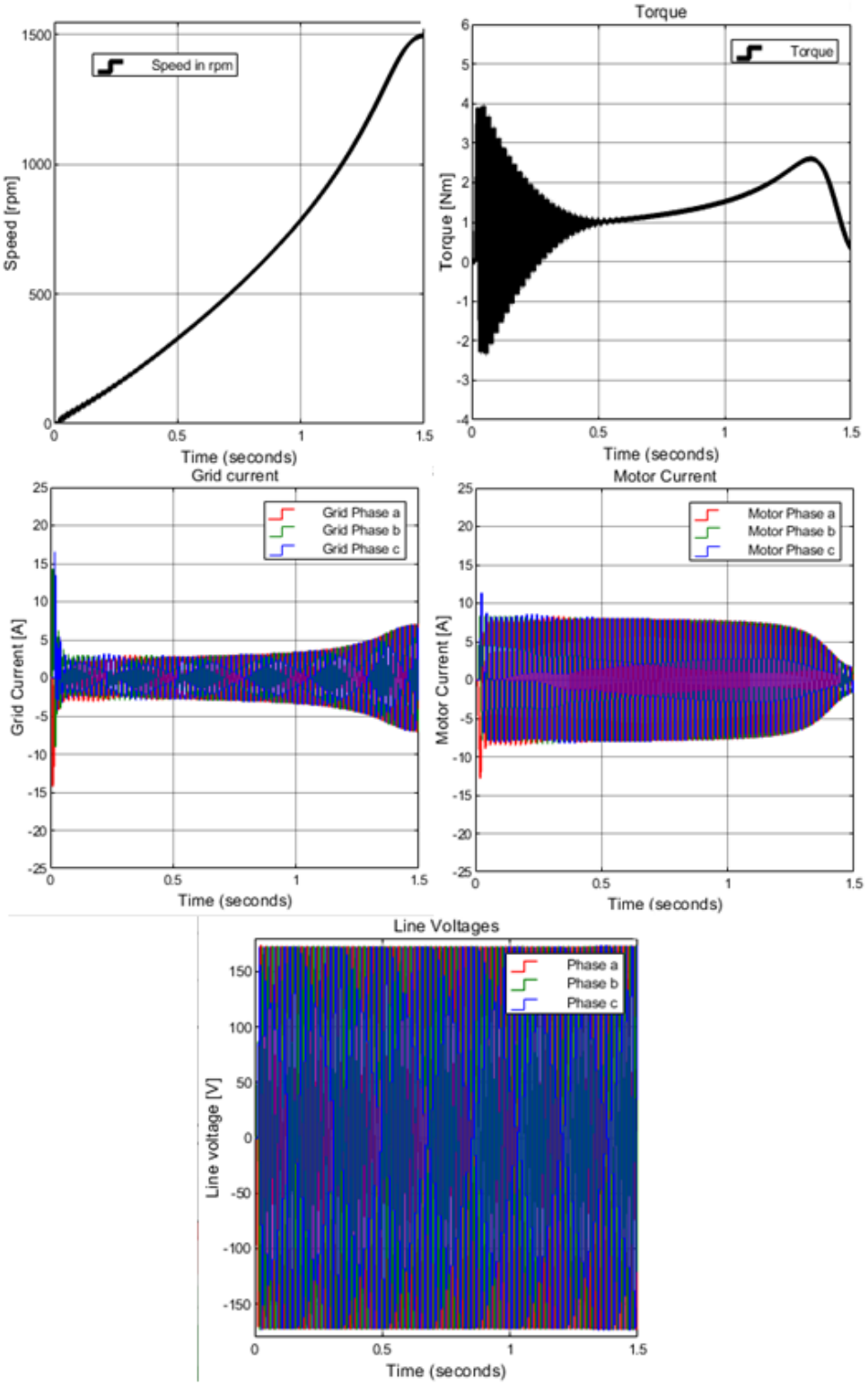

Figure 4.42 Motor 1E transient simulation with 90 µF capacitors switching when the line voltages are zero.

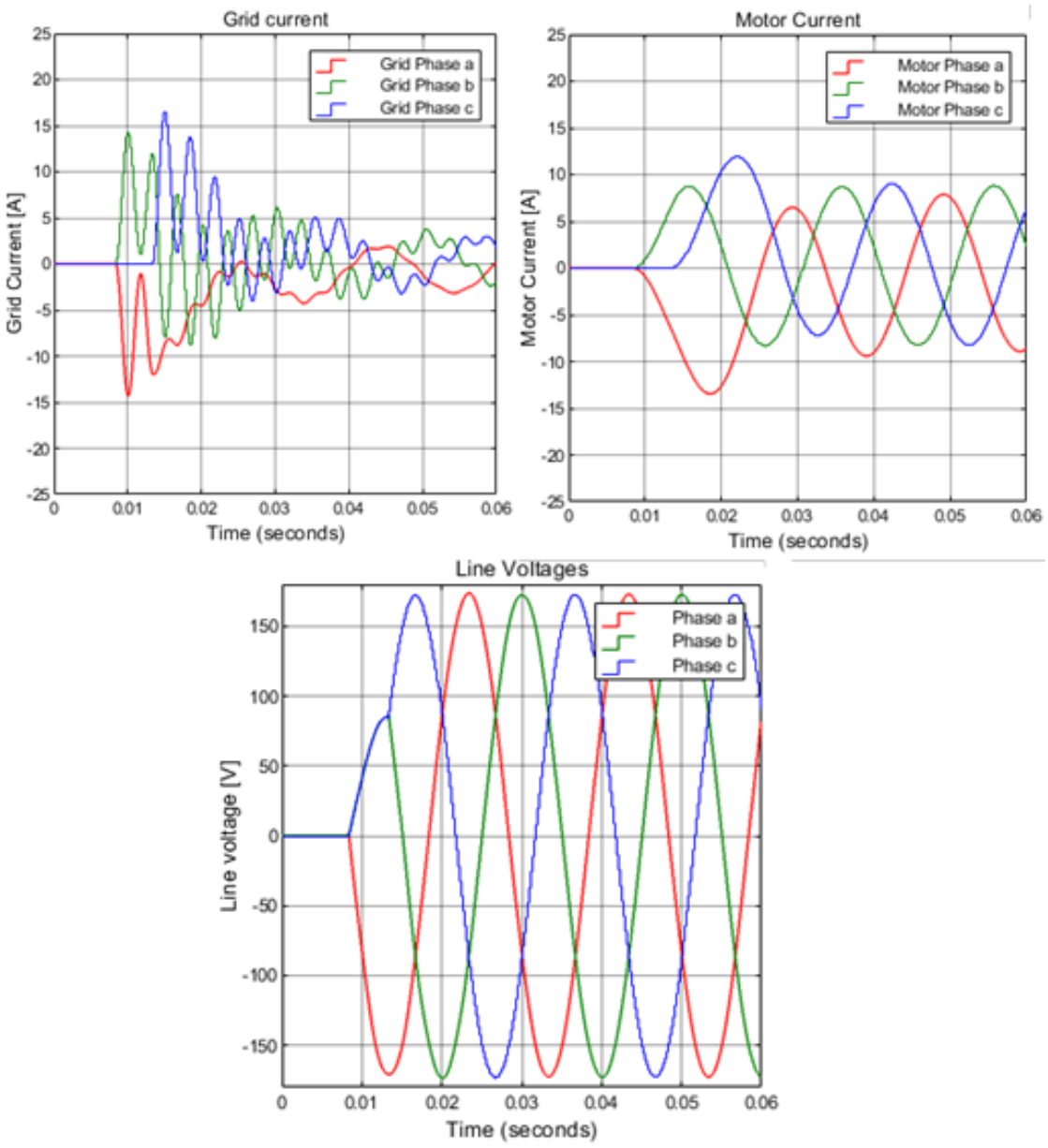

Figure 4.43 Transient simulation of Motor No.1E with 90 μF capacitors switching when the line voltages are zero - zoomed over 6 ms.

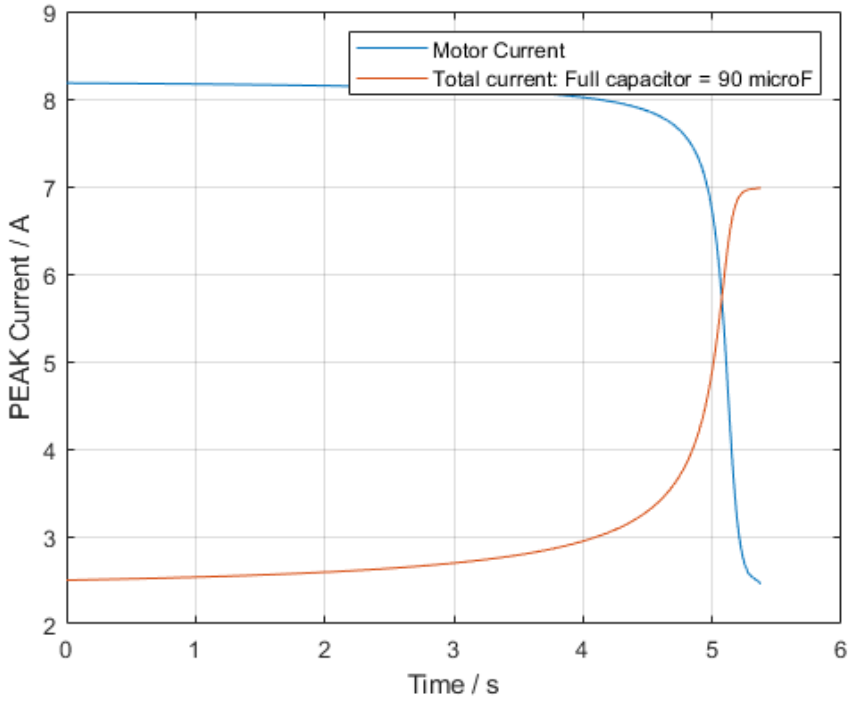

Figure 4.44 Motor No. 1E steady-state simulation with 90 μF capacitors switching and 0.625 Nm of friction added.

4.7 Conclusions

This Chapter has reported on simulations carried out using both per-phase steady-state models developed in Matlab and transient models developed in Simulink. Seven different machine models were used to represent a wide range of 3-phase inductions. The parameters for these were given in Section 4.2. This included P.U. values for direct comparison. For capacitor compensation during start-up to reduce the current substantially, the machine should be very inductive and this is the case as the machines get larger.

In Section 4.3 each motor was assessed using different common starting methods. These were

found to be effective in smaller machines but in larger machines, which have low starting torque, these methods become less appropriate as the machines increase in size.

The main steady-state simulations are given in Section 4.4 which addressed the use of capacitors to reduce the run-up current. It was found that the smaller machines could utilize this method but it was more effective in larger machines where the run-up current could be reduced several fold and where run-up times are longer. This is particularly true for Motor Nos. 4, 5, 6 and 7 when the capacitances used were the values calculated to correct the power factor to unity at start. However there would be a peak in the run-up current close to the full load point where the capacitors should be switched out. A compromise to this is to use a capacitor of half these values. This was found to reduce the starting current by about 50 % with no peak run-up current at capacitor turn-off which would allow more straightforward capacitor switch-out, possibly using a timer.

The transient simulations using Simulink models were reported in Section 4.5. These were for an initial model used in development which was designated Motor No. 0, Motor Nos. 1 and 6, and a modified version of No. 1 which had additional inductance added to the stator, this was designated Motor 1E.

Motor No. 0 had parameters similar to Motor No. 1 and it was found to give reasonable simulation results though this motor was not a good example for using capacitor compensation to reduce the run-up current.

Motor No. 1 did not have a high degree of run-up current reduction using the compensation capacitors and for this reason, when the experimental work was carried out then additional inductors were added to make the motor behave more like a large machine during starting.

It was found that the transient simulations matched the steady-state simulations well. These

used only the motor inertia to run up to speed and the run-up times matched.

The transient turn-on was investigated in Section 4.5 where the motor and capacitors were turned on when the voltages across the breakers were zero. This use of the in-line inductors to prevent capacitor current spikes was investigated. it was found that it is difficult to prevent a large current oscillation in the first turn-on cycle due to the capacitors having zero charge in them. This was also addressed in Chapter 3 in Section 3.3.3. To reduce the transient turn-on current then the motor and capacitors need to be turned-on separately, and to remove it completely the capacitors would have to be pre-charged. However, the transient turn-on can be controlled using the capacitors and their series inductors as shown for Motor No. 6 in Section 4.5.3, so that it is only one cycle of the current.

The next two chapters report on the experimental set-up and the experimental results.

Chapter 5

Experimental Rig

This chapter presents the experimental setup of the hardware and firmware developed to generate experimental results that validate the simulation. Fig. 5.1 illustrates the schematics for the experimental rig. This was slowly developed with different properties of the motor and capacitors investigated. It shows the capacitors with filters and the switches for the capacitors are shown in dashed - these are for turn-off and not critical to the system operation as long as they switch off at an appropriate point in the run-up.

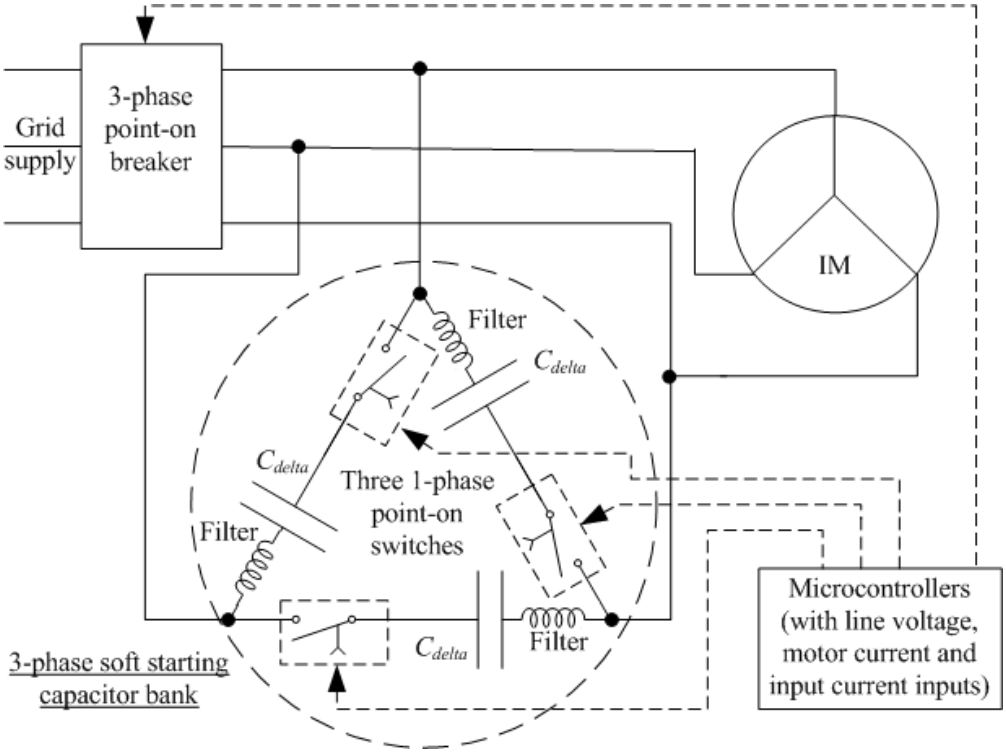

Figure 5.1 Experimental system power circuit.

5.1 Concept Design - Point-On Switching

Power transients in electrical systems are caused by many things. The major source of these transients are switching operations. Some of these are uncontrolled switching of capacitor banks which causes current surges and over voltages. In this work, inrush current caused by switching on and off of induction motors in an electrical network is investigated. The work further proposes a mitigation strategy using PIC18 microcontrollers. The solution is not just is cost effective but also technically efficient.

The zero crossing detector circuit is an important application of the op-amp comparator circuit.

It can also be called as the sine to square wave converter. An input sine wave is given as V_{in} and inverting or non-inverting comparators can be used as a zero-crossing detector. The only change to be brought in is the reference voltage with which the input voltage is to be compared, must be made zero ($V_{ref} = 0$ V). The non-inverting comparator based zero crossing detectors are shown Fig. 5.9

Point-on Switching (PoS), which is often referred to as a Point-on Switching Controller, is a high-speed microprocessor-based relay technique used for the controlled switching of circuit breakers in HVAC systems. The term controlled switching in this context refers to opening or closing a breaker at pre-determined points on the voltage waveform. Generally, such a controller is used for switching of capacitor banks, power transformers, shunt reactors and transmission lines. Point-on switching is an important control mechanism in modern electrical systems, which is used to control high-frequency over-voltage transients and inrush current caused by random switching of equipment within an electrical network. In this work, PoS is used as a control technique to mitigate inrush current as a result of starting or stopping the induction motor within an electrical network. Consequently, the experimental control rig setup is composed of three main parts and these are: current transformer PIC, line voltage sensor and point-on switching controller.

5.2 Detailed Design - Overall Rig

The final hardware is shown in Fig. 5.2. The circuit connection is shown in Fig. 3.23 in Chapter 3. The single-phase point-on switch connected were fitted for separate control of the capacitors as shown in Fig. 3.23. The 3-phase point-on switch allows for separate switching of phases and this was the main breaker used in the point-on switching work with the capacitors and induction motor hard-wired in parallel.

In the Fig. 5.2 there are several capacitors in use as listed in Table 5.3. These are standard AC motor capacitors used to start single phase motors or compensate for a 3-phase system and could be used to form a 50 µF or 90 µF delta connection. These are shown in Fig. 5.3.

Motor No. 1 had inline inductors added to give a more inductive motor when starting. In addition, smaller indicators were needed for capacitor filtering. These are shown in Fig. 5.4.

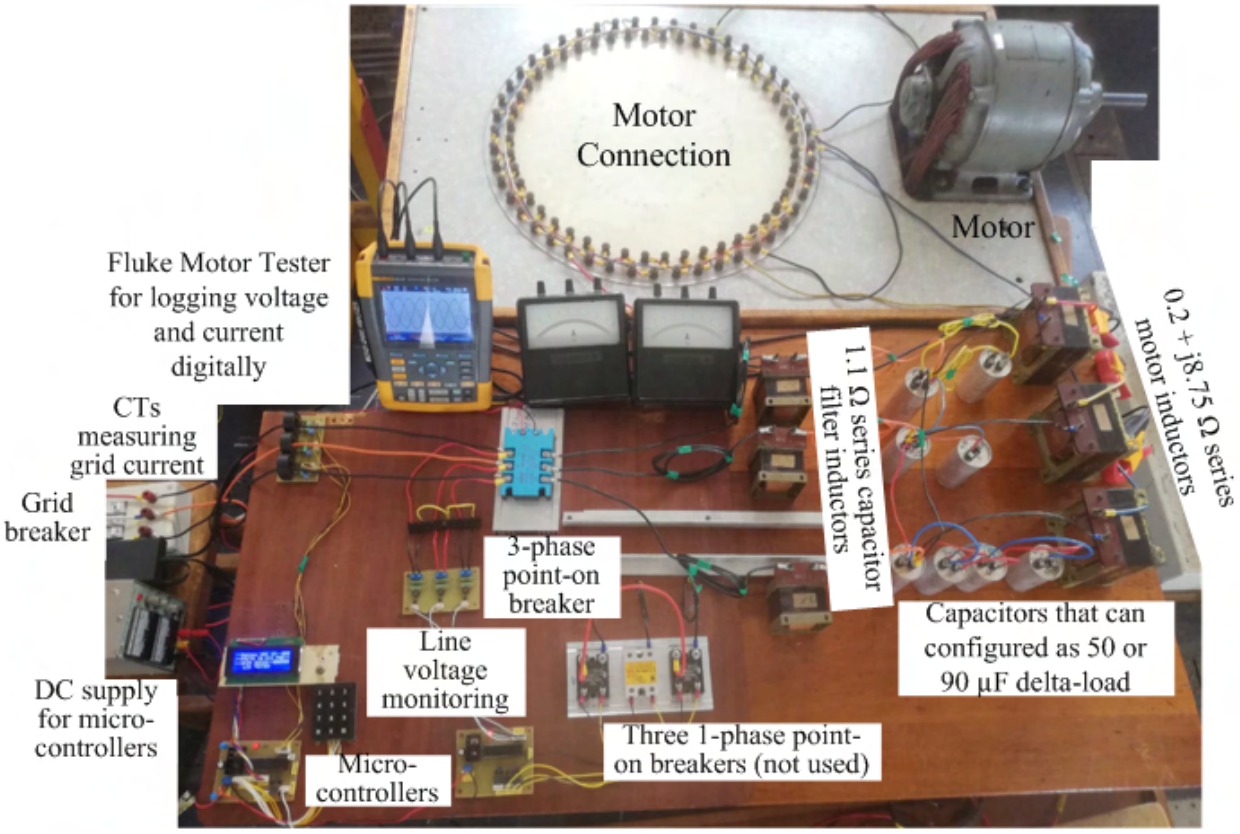

Figure 5.2 Final layout of test rig.

Figure 5.3 Capacitors used.

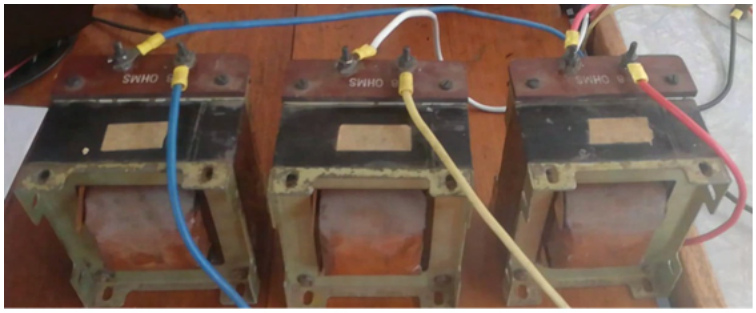

Figure 5.4 Inductors used.

Solid-state breakers were used in the work - one 3-phase breaker and three single-phase breakers as shown in Fig. 5.5. While the control for the 3-phase breaker is only one signal as indicated,

the switches will work in order when there is a zero crossing voltage point, so two phases will close then the next 90° later.

Figure 5.5 Solid state breakers used.

This experimental setup has been achieved by using the PIC MICROCONTROLLER 18F45K22 as illustrated in Fig. 5.7. The block diagram of the PIC18(L)F2X/4XK22 family is illustrated in Fig. 5.6 and www.microchip.com has more details. This family offers the advantages of all PIC18 microcontrollers – which are high computational performance at an economical price – with the addition of high-endurance and flash program memory. On top of these features, the PIC18(L)F2X/4XK22 family introduces design enhancements that make these microcontrollers a

logical choice for many high-performance, power-sensitive applications.

The are three main parts to this experimental switching arrangement, the current sensing (Fig. 5.8), voltage sensing (Fig. 5.9), and the point-on switching control (Fig. 5.10). The list of components are given in Table 5.3. The setup for the implementation of the point-on switching circuit is arranged as shown in Fig. 5.10.

Fig. 5.8 shows the current sensor schematic design used for the rig. The main components used are single-phase current transformers, diodes, resistors and capacitors. Pins J5, J6 and J7 are connectors to current transformers for each single-phase input for a variable voltage of 0-400 Vac. Each single-phase current transformer connects to a bridge rectifier composed of D1, D2, D3 and D4 on Phase *a*, D5, D6, D7 and D8 on Phase *b* and D9, D10, D11 and D12 on Phase *c*. Resistors R1, R2 and R3 are across the bridge rectifier and are 33 Ω for each phase. Resistors R4, R5 and R6 are 1 kΩ. The filtering capacitors C1, C2 and C3 are 1μF each on respective phases. The connector J4 plugs onto the current sensing pin of the PIC microcontroller. Table 5.1 tabulates these components.

Table 5.1 Current sensor component features.

Current Transformer(J5-R6)	Diodes (D1-D12)	Resistors (R1-R3)	Capacitors (C1-C3)
155E 100 A 2500:1	IN4007	33 Ω	1 µF

PIC18(L)F2X/4XK22

FIGURE 1-1: PIC18(L)F2X/4XK22 FAMILY BLOCK DIAGRAM

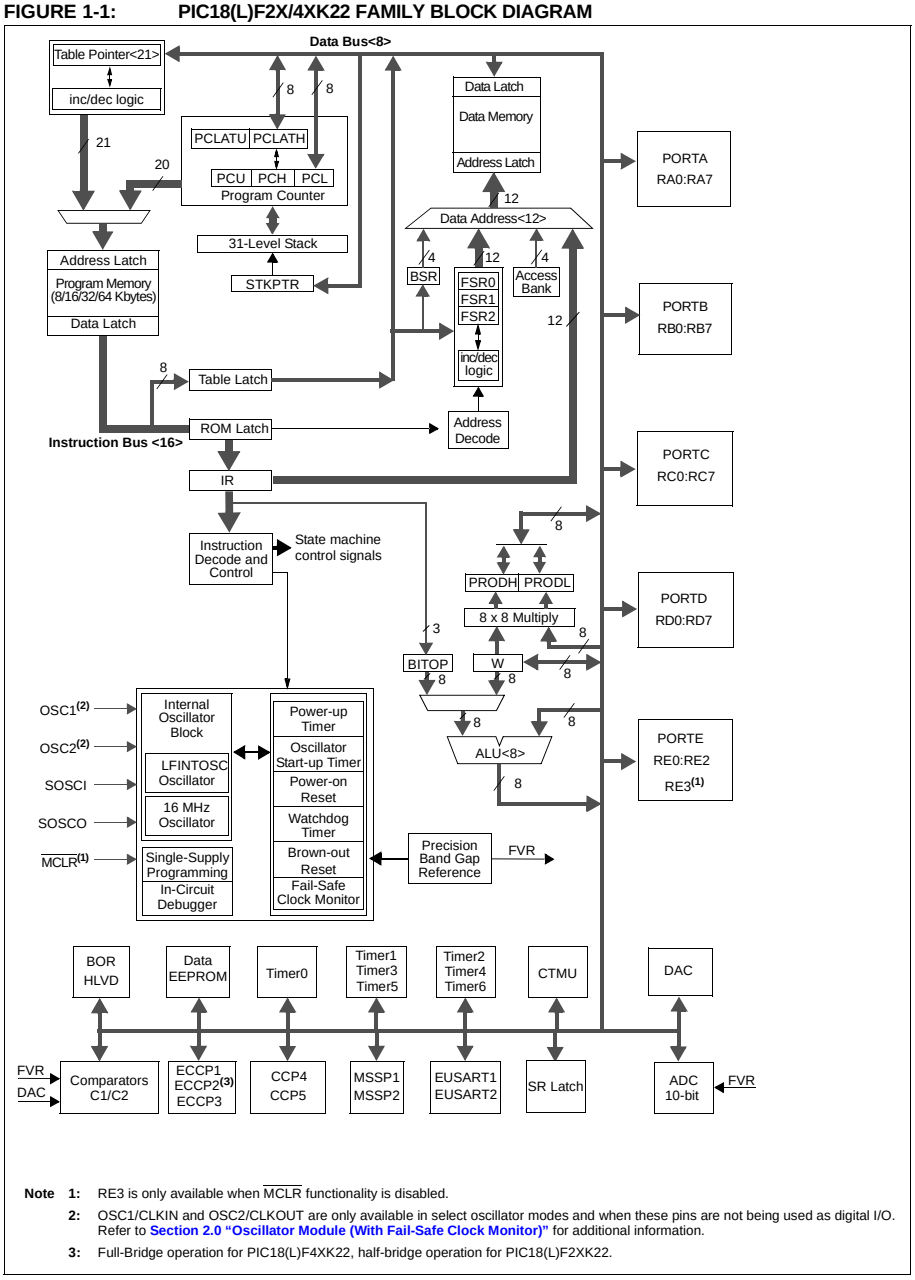

Note 1: RE3 is only available when MCLR functionality is disabled.

2: OSC1/CLKIN and OSC2/CLKOUT are only available in select oscillator modes and when these pins are not being used as digital I/O. Refer to **Section 2.0 "Oscillator Module (With Fail-Safe Clock Monitor)"** for additional information.

3: Full-Bridge operation for PIC18(L)F4XK22, half-bridge operation for PIC18(L)F2XK22.

© 2010-2016 Microchip Technology Inc.

Figure 5.6 PIC18(L)F2X/4XK22 family block diagram.

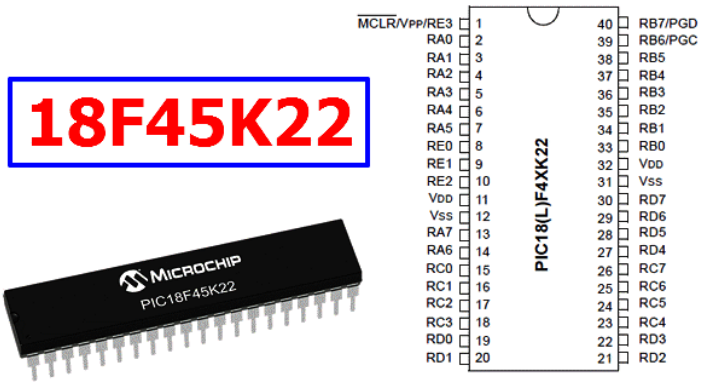

Figure 5.7 PIC 18F45K22 microprocessor.

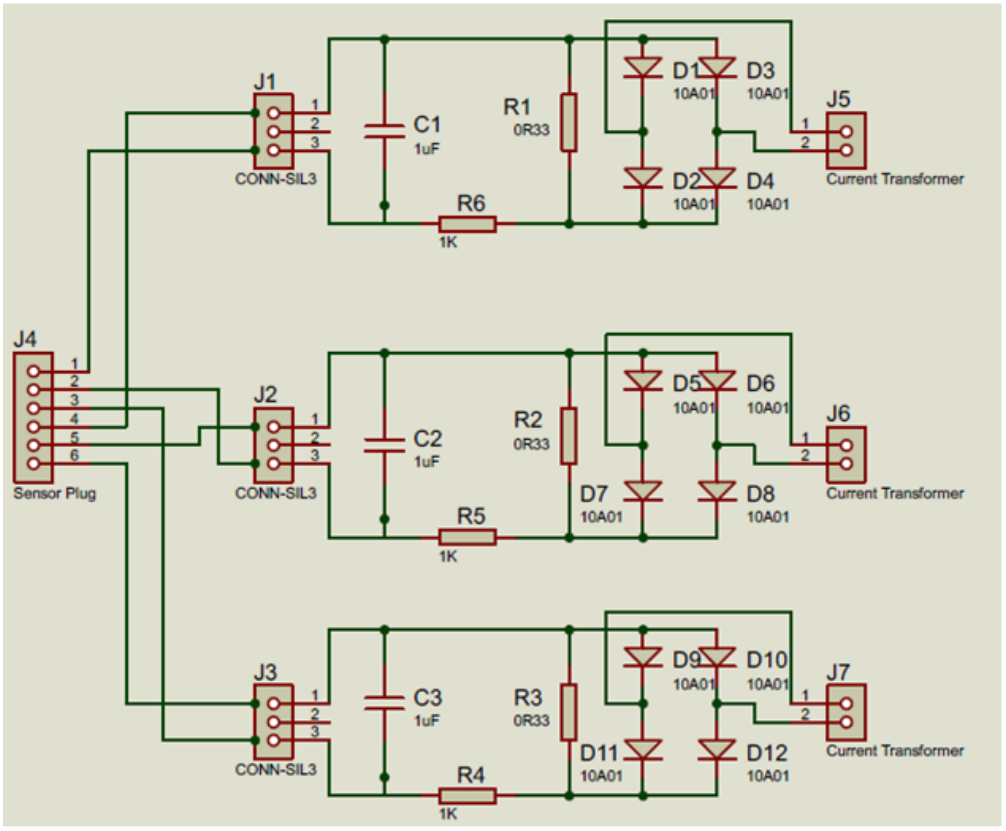

Figure 5.8 Current sensors.

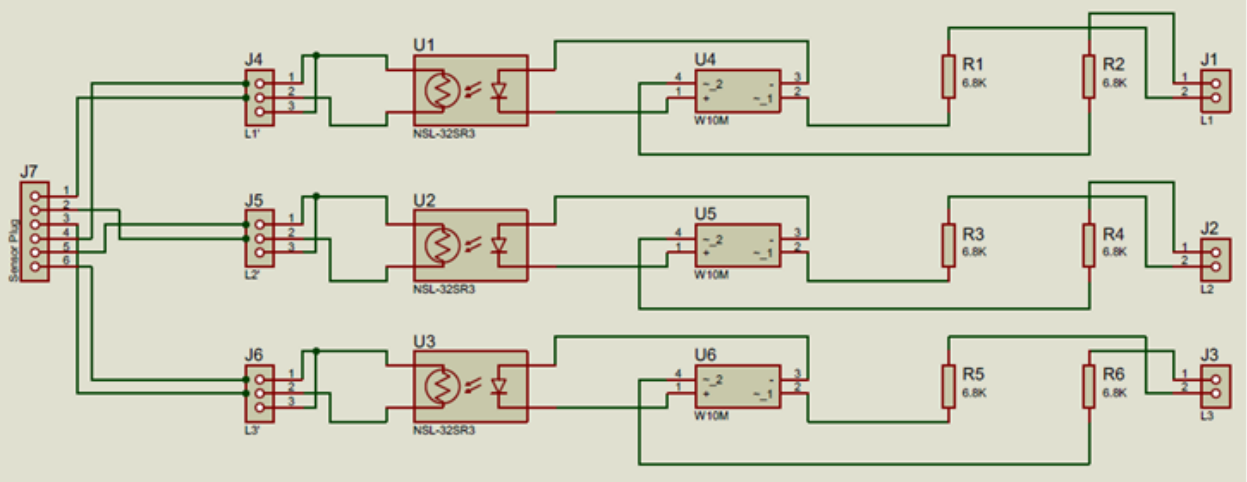

Figure 5.9 Voltage sensors.

Fig. 5.9 illustrates a 3-phase voltage sensor schematic used in this rig. The main components are resisters, a bridge rectifier and an optocoupler on each phase/line. The connectors J1, J2 and J3 are input jumpers for the variable power supply voltage between 0-400 Vac for each phase. The variable input voltage goes through R1 and R2, R3 and R4, and R5 and R6 with resistance values of 6k8 Ω. U4, U5 and U6 are single-phase types of bridge rectifier converting an AC supply voltage and current to DC. The variables U1, U2 and U3 are single-phase optocouplers that ensures protection by isolation of the circuit design whose individual signals are fed into J1. This is an input for the ZCD pin on the microcontroller. A summary of the electrical features of the components used in this figure are tabulated in Table 5.2.

Table 5.2 Voltage sensor component features.

Resistors(R1-R6)	Rectifier (U4-U6)	Optocoupler (U4-U6)
220 Ohms ±10% 1W Through Hole Resistor Axial Moisture Resistant, Pulse Withstanding Ceramic	Peak Reverse Voltage (V_{rrm}): 1000 V Max. RMS Bridge Voltage (V_{rms}): 700 V Max. DC Blocking Voltage (V_{dc}): 1000 V Av. Forward Rectified Current (I_0): 1.5 A Maximum Reverse Current (I_r): 10 µA Forward Volt Drop per Element (V_f): 1.0 V	Input forward current: 60 mA Power Dissipation: 200 mW Collector Current: 50 mA Collector-Emitter Voltage: 35 V Emitter-Collector Voltage: 6 V Rise Time: 18 µs Fall Time: 18 µs

Fig. 5.10 is a schematic diagram showing the PIC point-on switching control unit. The circuit is composed of a PIC18F45K22, 10 kΩ pull up resistors, a 16 MHz internal clock to ensure 50 Hz precision, NPN transistors BC547, Q6-Q10, PNP transistors from Q1-Q5, and BC557 connected to the output control pins for the single-phase solid state relays, J1-J5. It should be noted that pins J4 and J5 are meant for redundancy. The control unit is powered by a 12 Vdc input supply at J6 which is further regulated by U1 to 5 Vdc and filtered by 470, 35 V capacitor C1. The LED signals when circuit is powered on or off. J8 is the PICKIT plug where the firmware is loaded onto the PIC microcontroller.

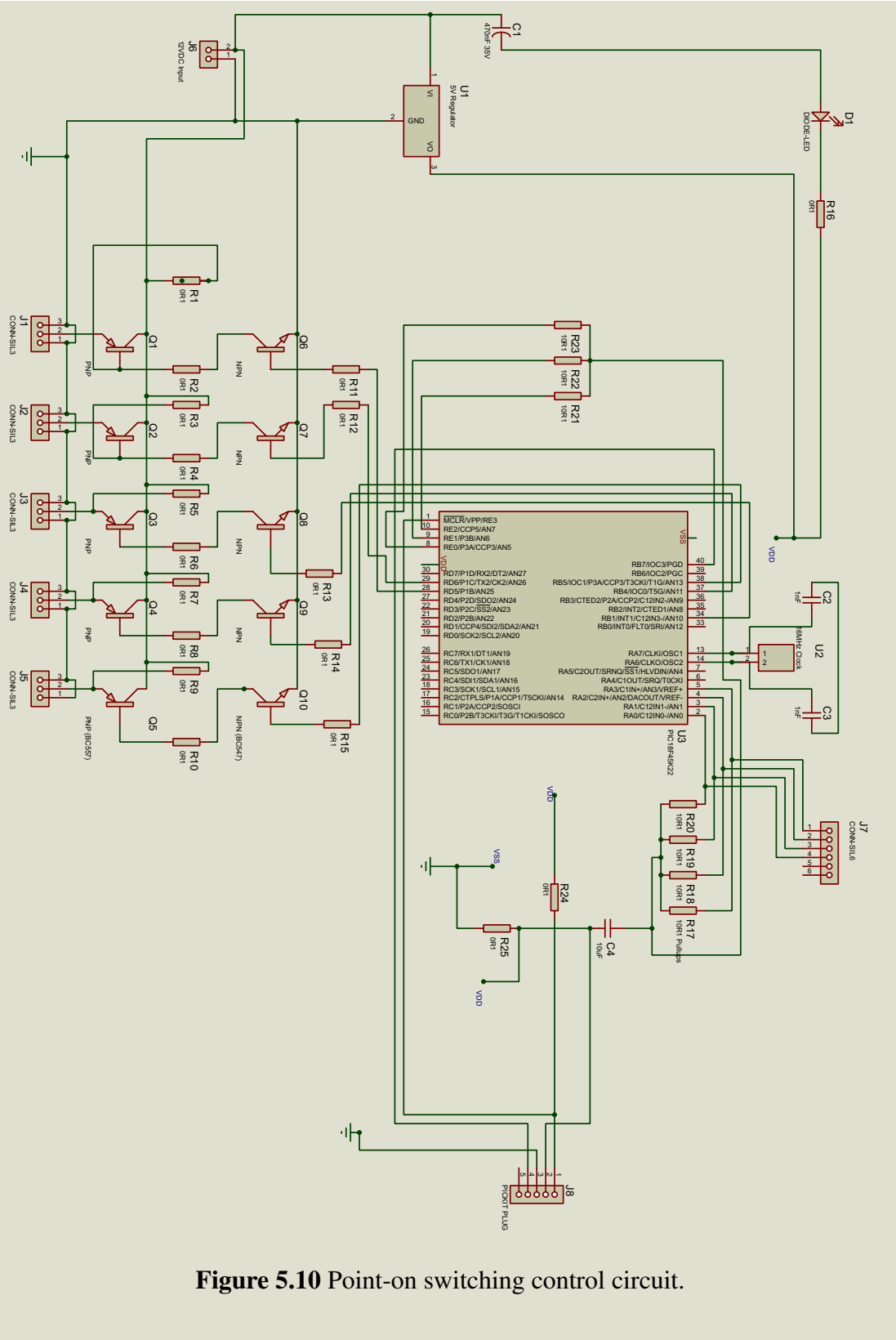

Figure 5.10 Point-on switching control circuit.

The printed circuit boards (PCBs) of all the schematics highlighted above are shown in Fig. 5.11. The first two parts of the PCBs on the right hand side show the voltage and current sensors respectively. While the remaining part on the left hand side represents the PCB for the point-on control part with peripherals to display and keypad input pins as well as input pins from the voltage and current sensor circuits.

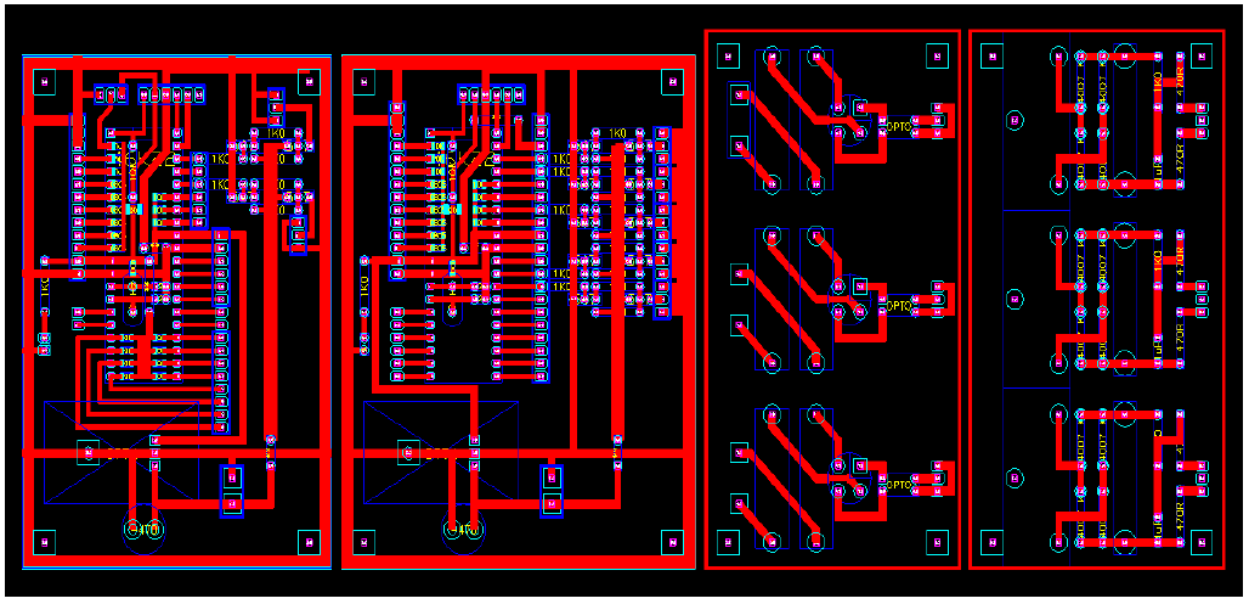

Figure 5.11 Printed circuit boards.

Table 5.3 The used equipment for the point-on-switching circuit and capacitor compensation.

S.N	Name		Number
1	1-phase solid State Relay		3
2	3-phase solid State Relay		1
3	Electric Tesys Pole Contactor		1
4	NPN Transistor		20
5	Bridge Rectifier		5
6	LED Indicator		10
7	PCB LED Indicator		20
8	PIC Microcontroller		2
9	Development board		2
10	USB Cable		2
11	Jumper wires		120
12	Current Sensor		2
13	Photocoupler		8
14	Keypad		1
15	LCD		1
16	Compensation Capacitors	15 µF	1
17		20 µF	2
18		30 µF	3
19		40 µF	2
20		50 µF	2
21	Capacitor	22 pF	3
22	Oscillator	8 MHz	1

5.3 Commissioning and Testing

This section details the commissioning and testing of the designed and developed rig while ensuring the safety operation of the work, especially that this work involved the use of higher voltages and currents. The commissioning involved testing individual subsystems before integrating them to operate as a complete control unit with sensor circuit subsystems including the variable power supply used in the rig. For testing, a Fluke 435 Series II Three-Phase Power Quality and Energy Analyzer was used. This has the following features:

1. Measure all three phases and neutral: With included four flexible current probes.
2. Energy loss calculator: Active and reactive power measurements, unbalance and harmonic power.
3. Power Wave data capture: Capture fast RMS data, show half-cycle and wave forms to characterize electrical system dynamics (generator start-ups, UPS switching etc.)
4. Troubleshoot real-time: Analyze the trends using the cursors and zoom tools.
5. Power inverter efficiency: Simultaneously measure AC output power and DC input power for power electronics systems using optional DC clamp.

Before the rig could be used for taking measurements, the scope was used to test both the voltage and current wave forms for the variable power supply and calibration was done to ensure that good sinusoidal wave forms were obtained from the 3-phase power supply unit. The scope probes were calibrated before the scope was used to take measurements.

This exercise of testing subsystems of the voltage and current into and out of a subsystem was very helpful. It was discovered after integration of subsystems that there was need to have

inductors in-line with capacitor bank. There were larger inductors in-line with the motor to make it more inductive during starting - larger machines are inductive as shown in the motor analysis in this work. Smaller inductors were put in-line with the capacitors as low pass filters. Otherwise a small amount of voltage harmonics gives a lot of harmonic current.

The experimental machine used in this rig is very short pitched which leads to being more resistive and more turns are needed to get the flux. This evidently highlights the importance of commissioning and testing the experimental rig before integration of subsystems and taking meaningful measurements. The detailed analysis of the measurements taken in this work are given and discussed in the next chapter.

Chapter 6

Experimental Results

This Chapter validates the use of capacitor compensation experimentally using Motor Nos. 1 and 1E. Initial running-light and locked-rotor tests were reported in Appendix A and furthered here using compensation capacitor connection. The results investigate the run-up current and its reduction using capacitors and the transient turn on using point-on switches which turn on when the voltage across them is zero.

The use of series inductors with the capacitors is addressed to illustrate the harmonic filtering of low frequency harmonics.

The Chapter first addresses capacitor compensation of Motor No. 1 and the change in grid current during locked rotor and running light tests. This was found not to produce good results so Motor No. 1E was used and found it give better illustration of capacitor compensation with locked rotor.

Transient experiments are then done, first with just parallel 90 μF capacitors and with random

turn-on to show the harmonic capacitor currents and transient turn-on current spikes. Low pass filters were added to the capacitors formed from inductors which are shown to improve the capacitor current.

Finally point-on switching is carried out using the system designed for this project, and these show an improvement in transient current turn-on.

6.1 Initial Motor No. 1 Testing

The initial testing for Motor No. 1 was done at 46 V and 100 V line though here only the 100 V results are reported. Fig. 4.12 gives the simulations and Tables 6.1 to 6.4 give the locked rotor and running light measured currents (using a digital multimeter). The three line currents were measured and the average taken. These are converted to peak currents and the simulation peak currents (I_{Sim}) are given for comparison. It can be seen that the for the locked rotor tests the measured current is a little lower than predicted and the attenuation of current using the capacitors is not as substantial. This is even more noticeable at no load as can be seen in Table 6.4. The capacitors do not appear to be supplying a high current. To address this the waveforms were inspected as shown in Fig. 6.1. While the waveforms look reasonable in (a) and ((b) at locked rotor, it can be seen that there is substantial harmonic content in the line currents when the capacitors are connected and even without the capacitors there appears a degree of low frequency harmonic. At this point there is no filtering using the in-line inductors with the capacitors. It was decided to add inductance to the induction motor so that it is more inductive and more representative of a larger machine.

Table 6.1 Motor No. 1 locked rotor test with and without 50 µF compensation capacitors.

100 V line 50 µF capacitors	I_a	I_b	I_c	I_{mean} rms	I_{mean}**peak**	I_{Sim}**peak**
Motor	11.53	11.66	11.3	11.50	16.26	18.18
Capacitors and motor	11.22	11.39	10.96	11.19	15.83	15.93

Table 6.2 Motor No. 1 locked rotor test with and without 90 µF compensation capacitors.

100 V line 90 µF capacitors	I_a	I_b	I_c	I_{mean} rms	I_{mean}**peak**	I_{Sim}**peak**
Motor	11.18	11.3	11.09	11.19	15.83	18.18
Capacitors and motor	10.45	10.59	10.36	10.47	14.80	14.62

Table 6.3 Motor No. 1 running light test with and without 50 µF compensation capacitors.

100 V line 50 µF capacitors	I_a	I_b	I_c	I_{mean} rms	I_{mean} **peak**	I_{Sim} **peak**
Motor	0.95	1.07	0.79	0.94	1.32	1.75
Capacitors and motor	0.34	0.59	0.5	0.48	0.67	2.75

Table 6.4 Motor No. 1 running light test with and without 90 µF compensation capacitors.

100 V line 90 µF capacitors	I_a	I_b	I_c	I_{mean} rms	I_{mean}**peak**	I_{Sim} **peak**
Motor	0.91	1.03	0.8	0.91	1.29	1.75
Capacitors and motor	0.86	0.95	1.04	0.95	1.34	5.75

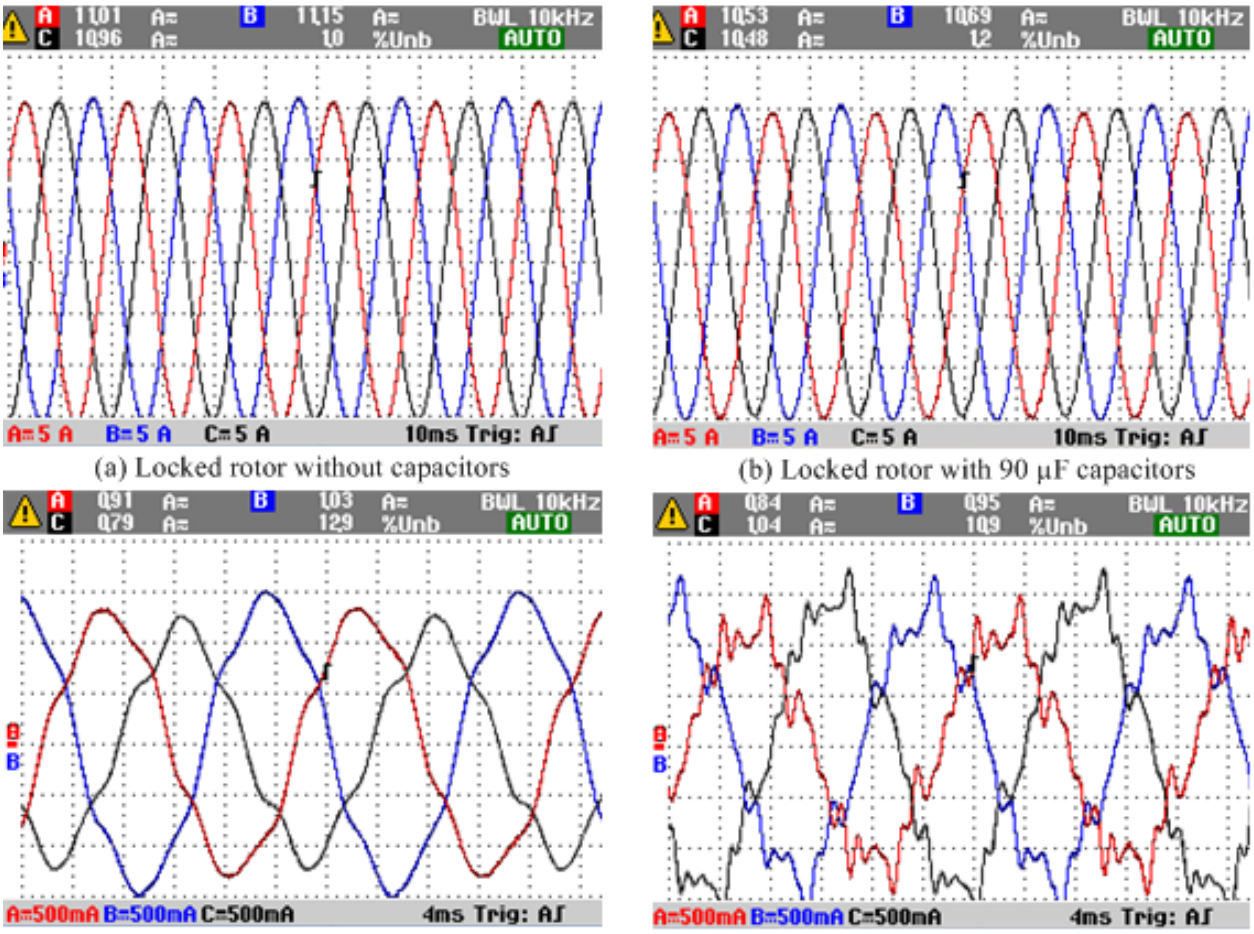

(a) Locked rotor without capacitors

(b) Locked rotor with 90 µF capacitors

(c) Running light test without capacitors

(d) Running light test with 90 µF capacitors

Figure 6.1 Current waveforms for Motor No. 1 at 100 V - currents with and without and 90 µF.

6.2 Motor No. 1E Testing

6.2.1 Running-light and locked-rotor tests

The running-light and locked-rotor tests were repeated with the same capacitor combinations using 50 μF and 90 μF capacitors. Fig. 4.41 shows the steady state simulation at a line voltage of 122.5 V rms with 90 μF capacitors. The locked rotor tests were conducted at a line voltage of 100 V rms but the running light test requires the voltage to be increased to 109 V to reach steady-state. The results in Fig. 4.41 can be ratioed to get the line currents with and without capacitors. It can be seen that the results appear good in terms of correlation between the simulation and measured; however, the measured currents with the capacitors to seem higher. It is worth looking at the locked-rotor current waveform. This is given in Fig. 6.2 for the locked rotor condition with 90 μF capacitors. It can be seen that there is substantial harmonic content. Bear in mind this is still with no inductor filter for the capacitors.

Table 6.5 Motor No. 1E locked rotor test with and without 50 μF compensation capacitors.

100 V line 50 μF capacitors	I_a	I_b	I_c	I_{mean} rms	I_{mean}**peak**	I_{Sim}**peak**
Motor	5.34	5.41	5.45	5.4	7.64	7.02
Capacitors and motor	2.9	2.9	2.9	2.9	4.10	

Table 6.6 Motor No. 1E locked rotor test with and without 90 μF compensation capacitors.

100 V line 90 μF capacitors	I_a	I_b	I_c	I_{mean} rms	I_{mean}**peak**	I_{Sim}**peak**
Motor	5.45	5.65	5.61	5.57	7.88	7.02
Capacitors and motor	2	2.2	2.2	2.13	3.02	2.04

Table 6.7 Motor No. 1 running light test with and without 50 µF compensation capacitors.

109 V line 50 µF capacitors	I_a	I_b	I_c	I_{mean} rms	I_{mean} peak	I_{Sim} peak
Motor	0.98	1.12	0.83	0.98	1.38	1.6
Capacitors and motor	1.9	2	2.3	2.07	2.92	

Table 6.8 Motor No. 1E running light test with and without 90 µF compensation capacitors.

109 V line 90 µF capacitors	I_a	I_b	I_c	I_{mean} rms	I_{mean}peak	I_{Sim} peak
Motor	0.89	0.98	0.89	0.92	1.30	1.60
Capacitors and motor	4.2	4.8		4.85 4.62	6.53	6.23

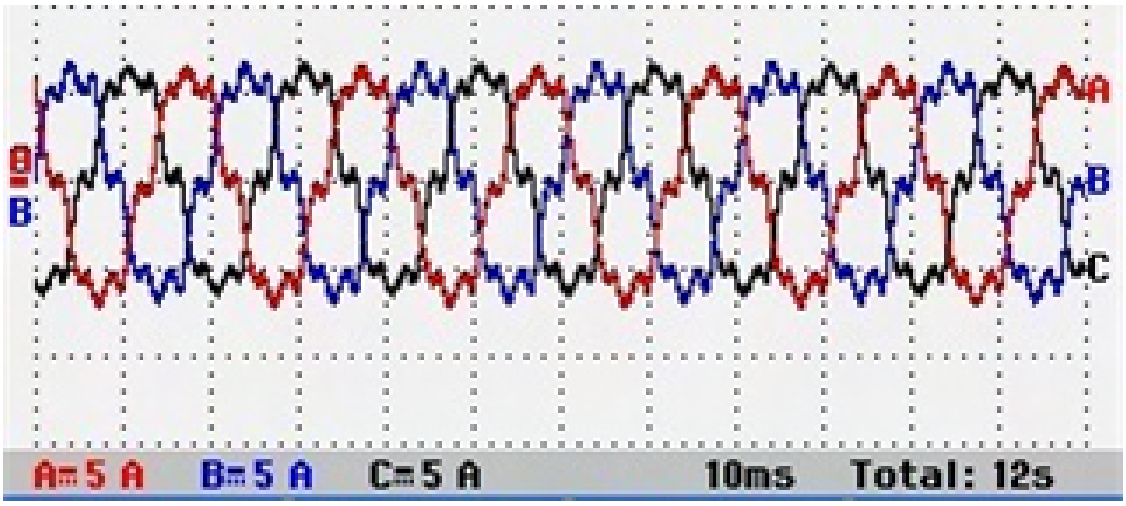

Figure 6.2 Locked-rotor current waveform for Motor No. 1E at 100 V - currents with 90 µF capacitors.

6.2.2 Transient Tests

6.2.2.1 1E with 90 μF capacitors, random 3-phase turn-on and no capacitor filtering

The system voltages are shown in Fig. 6.3. The top graph shows constant voltage over the 2.2 s of the run-up. The second graphs shows a zoom to the start of the run-up. The switching is at a random point and it can be observed that there is some harmonic content. The data could be downloaded and a Fast Fourier Analysis done; however, here a curve fit is done in Matlab with a sine wave and a 3 % 7^{th} harmonic and this fit the waveform well. This means that the harmonic current, with no filtering on the capacitors could be around $3 \times 7 = 21\%$ of the main capacitor current.

For 3 % 7^{th} harmonics then the harmonic voltage is $0.03 \times 170 = 5.1$ V peak for the line voltage. The capacitive harmonic reactance is $1/(2\pi \times 350 \times 0.00009) = 5.05\ \Omega$. The harmonic phase current in the delta-connected capacitors is therefore $5.1/5.05 = 1.01$ A peak. This gives a peak harmonic line current $\sqrt{3} \times 1.01 = 1.74$ A so that the peak-to-peak harmonic current is 3.50 A. The main impedance is $1/(2\pi \times 50 \times 0.00009) = 35.37\ \Omega$. The gives a peak line current of $\sqrt{3} \times 170/35.37 = 8.32$ A. This harmonic will be a maximum. There will be supply inductance that may limit the current harmonics and the voltage may change with loading, i.e., the motor speed.

The transient turn-on current is shown in Fig. 6.4 and this can be compared to Fig. 4.44 for the transient envelope. This has an inertia of 0.12 kg.m^2 and a friction torque of 0.625 Nm. The run-up time is about 5 s. The turn-on current spikes can be observed and these are quite high. Bear in mind that this is random turn-on of all three phases and the capacitors have no filters.

A set of voltages and currents for the grid are shown in Fig. 6.5. For repeatability, each current

measurement was taken twice. The zoomed currents are shown at start, illustrating the transient turn-on, at low speed, which shows harmonic current with about 3 A peak-to-peak, and the steady-state no-load current, which still has considerable harmonics and is trapezoidal in shape. These confirm that there are current spikes during turn-on and that there is substantial harmonic current when there is no capacitor filter. The low-speed current waveforms show harmonics close to that calculated above. The no-load grid current is higher than the low speed current because at no-load, the grid current is dominated by the capacitor current whereas at low speed the induction motor and capacitor currents substantially cancel each other out, hence the dominant harmonic current.

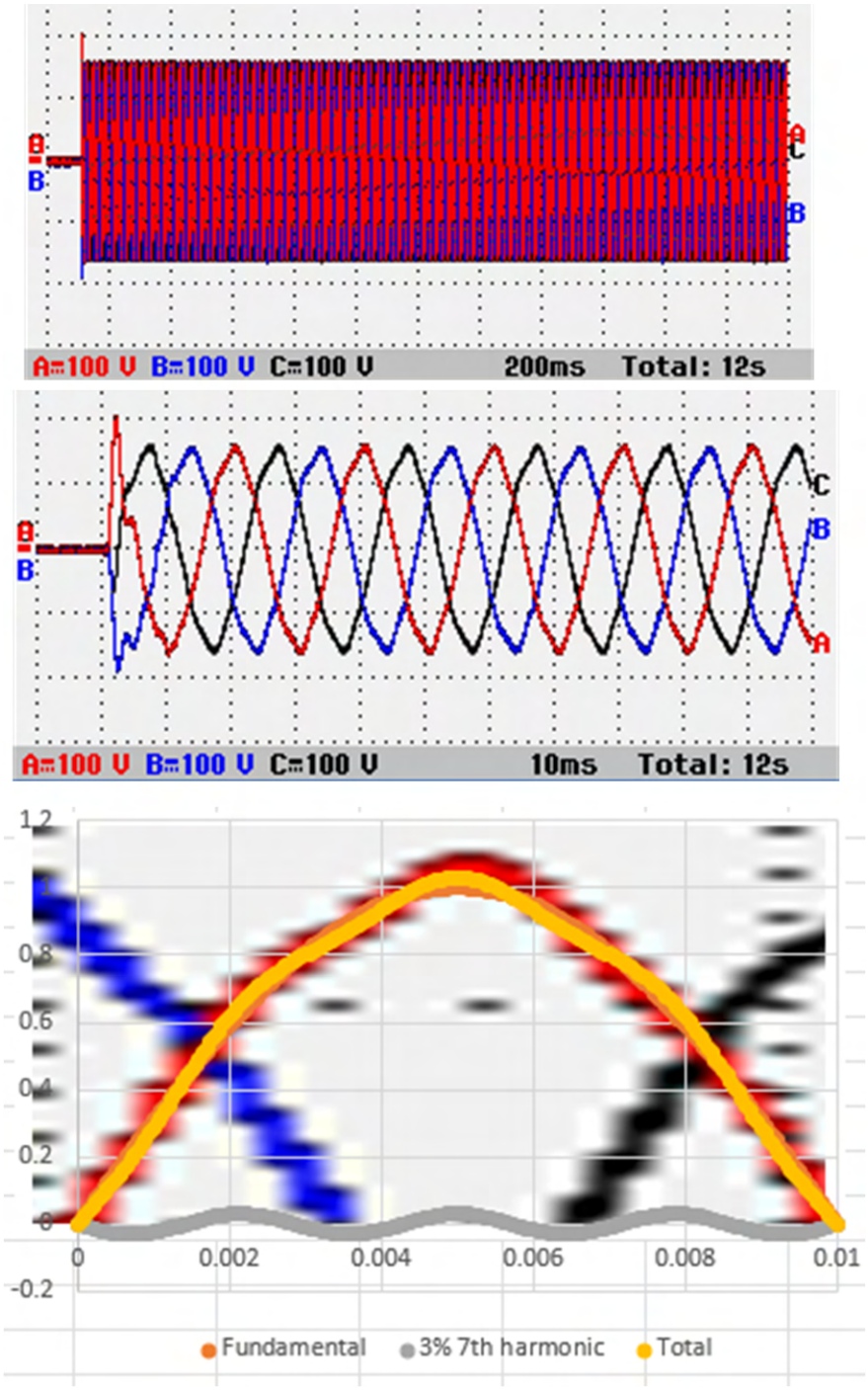

Figure 6.3 Transient system voltage waveforms for Motor No. 1E at 100 V - currents with and 90 µF. Waveforms show about 3 % 7th harmonic as shown in bottom graph. The top and second graphs have 100V/div while the third is in p.u..

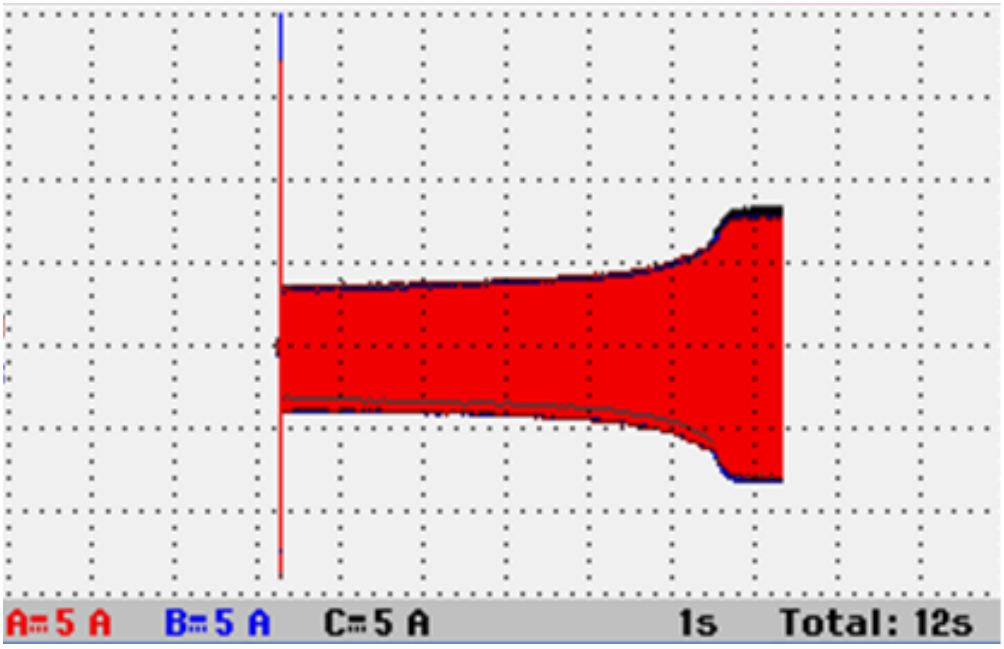

Figure 6.4 Transient system current for Motor No. 1E at 100 V peak for the phase - with 90 µF. The X-axis is 1 s/div and Y-axis is 5A/div.

The motor currents are shown in Fig. 6.6 at across the range of speed as well as zooms at the start and in steady-state. Comparison with Fig. 6.5 shows that the starting current is reduced considerably. The capacitors are not disconnected so the steady-state grid current is higher than the motor current as predicted. Section 4.5.3 shows how to turn capacitors off for Motor No. 6 through simulation. It can be seen in Fig. 6.6 that there are no motor harmonics and the transient turn-on is only about 30 % in the first cycle. Again, each waveform is recorded twice to show consistency.

Fig. 6.7 shows the capacitor voltages and currents. The voltage has some spikes during turn-on and this is to be expected since the capacitor has no filter and is randomly switched across the grid. The currents are the difference between the grid and motor currents and these contain current spikes during turn-on and distortion during operation due to harmonics.

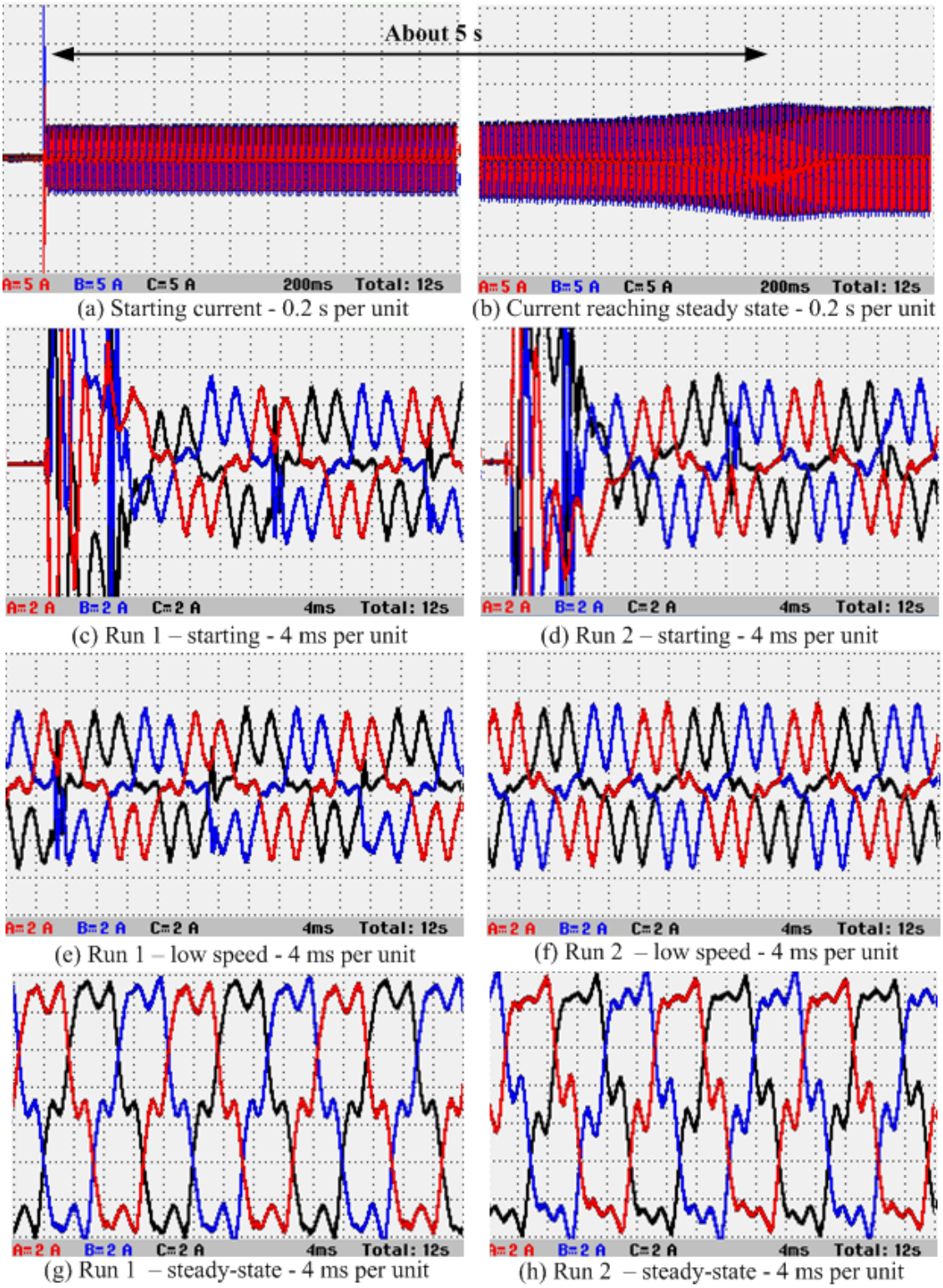

(a) Starting current - 0.2 s per unit

(b) Current reaching steady state - 0.2 s per unit

(c) Run 1 – starting - 4 ms per unit

(d) Run 2 – starting - 4 ms per unit

(e) Run 1 – low speed - 4 ms per unit

(f) Run 2 – low speed - 4 ms per unit

(g) Run 1 – steady-state - 4 ms per unit

(h) Run 2 – steady-state - 4 ms per unit

Figure 6.5 Transient system current for Motor No. 1E at 100 V phase peak - with 90 μF. Y-scales: 5 A/div.

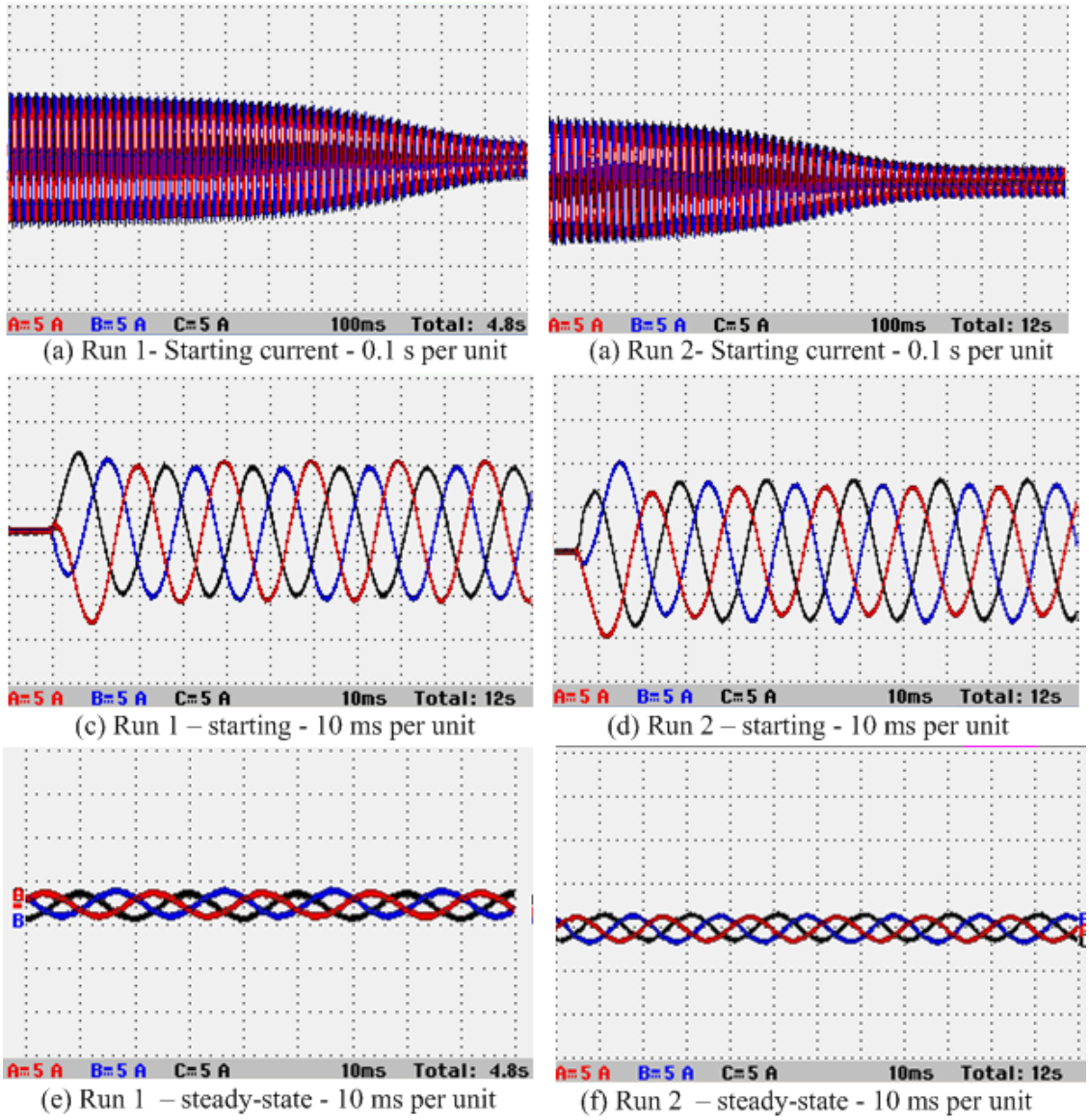

(a) Run 1- Starting current - 0.1 s per unit

(a) Run 2- Starting current - 0.1 s per unit

(c) Run 1 – starting - 10 ms per unit

(d) Run 2 – starting - 10 ms per unit

(e) Run 1 – steady-state - 10 ms per unit

(f) Run 2 – steady-state - 10 ms per unit

Figure 6.6 Transient motor current for Motor No. 1E at 100 V phase peak - with 90 µF. Y-scales: 5 A/div.

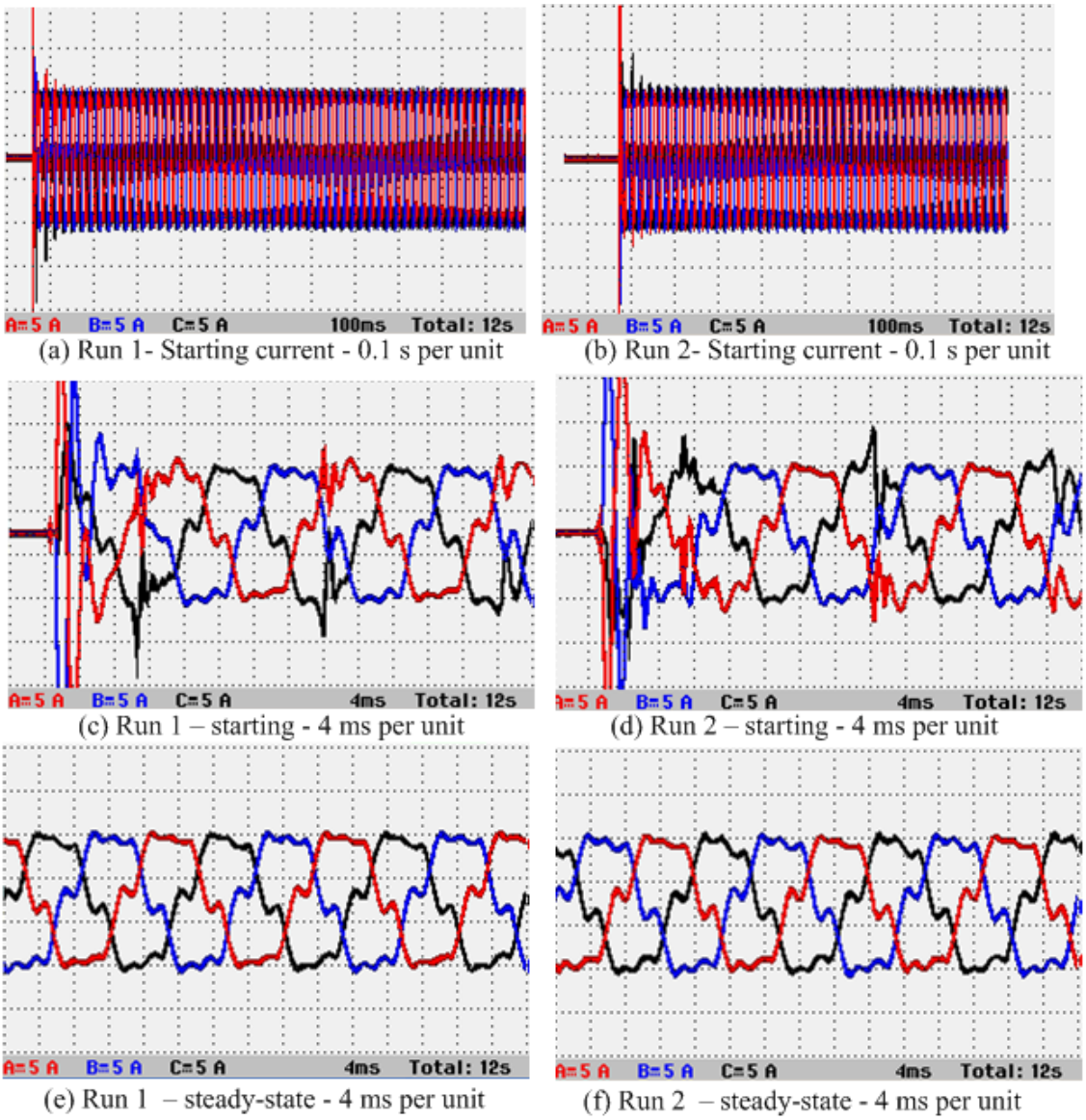

(a) Run 1- Starting current - 0.1 s per unit

(b) Run 2- Starting current - 0.1 s per unit

(c) Run 1 – starting - 4 ms per unit

(d) Run 2 – starting - 4 ms per unit

(e) Run 1 – steady-state - 4 ms per unit

(f) Run 2 – steady-state - 4 ms per unit

Figure 6.7 Transient capacitor current for Motor No. 1E at 100 V phase peak - with 90 μF. Y-scales: 5 A/div.

The capacitor compensation method has been tested in the section on Motor No. 1E and the capacitors have been shown to substantially reduce the run-up current by over 50 %. However, filters appear to be needed on the capacitors which is investigated in the next section.

6.2.2.2 1E with 90 μF capacitors, random 3-phase turn-on but with capacitor filtering

Fig. 6.8 shows the grid current when 1.1 Ω inductive filters are added in series with the 90 μF compensation capacitors. The waveforms show the currents across parts of the run-up period which is still about 5 s. Two different measurements are shown for each waveform. In (c) and (d) if can be seen that the turn-on transient current spikes are attenuated and less sharp. The low speed currents in (e) and (f) have less current harmonic when compared to Fig. 6.5 illustrating the need for filtering. The steady-state currents in (g) and (h) also are not as trapezoidal and have less harmonic.

So far the turn-on has been through a normal breaker that has random turn-on. To try to reduce the transient switch-on voltage and current spikes then point-on switching is addressed in the next section.

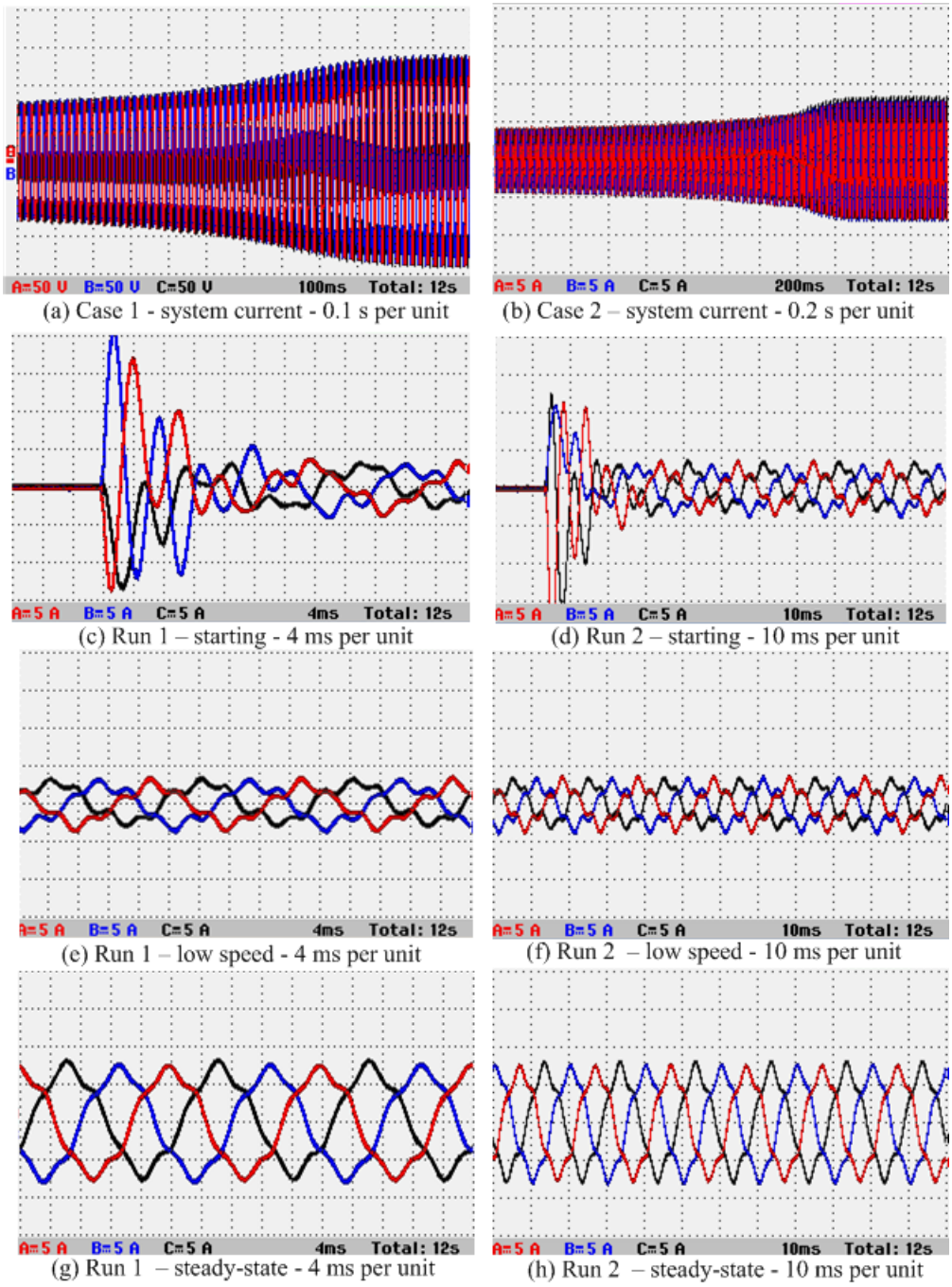

(a) Case 1 - system current - 0.1 s per unit
(b) Case 2 – system current - 0.2 s per unit
(c) Run 1 – starting - 4 ms per unit
(d) Run 2 – starting - 10 ms per unit
(e) Run 1 – low speed - 4 ms per unit
(f) Run 2 – low speed - 10 ms per unit
(g) Run 1 – steady-state - 4 ms per unit
(h) Run 2 – steady-state - 10 ms per unit

Figure 6.8 Transient system current for Motor No. 1E at 100 V phase peak - with 90 μF. Y-scales: top - 5 A/unit, rest - 2 A/unit.

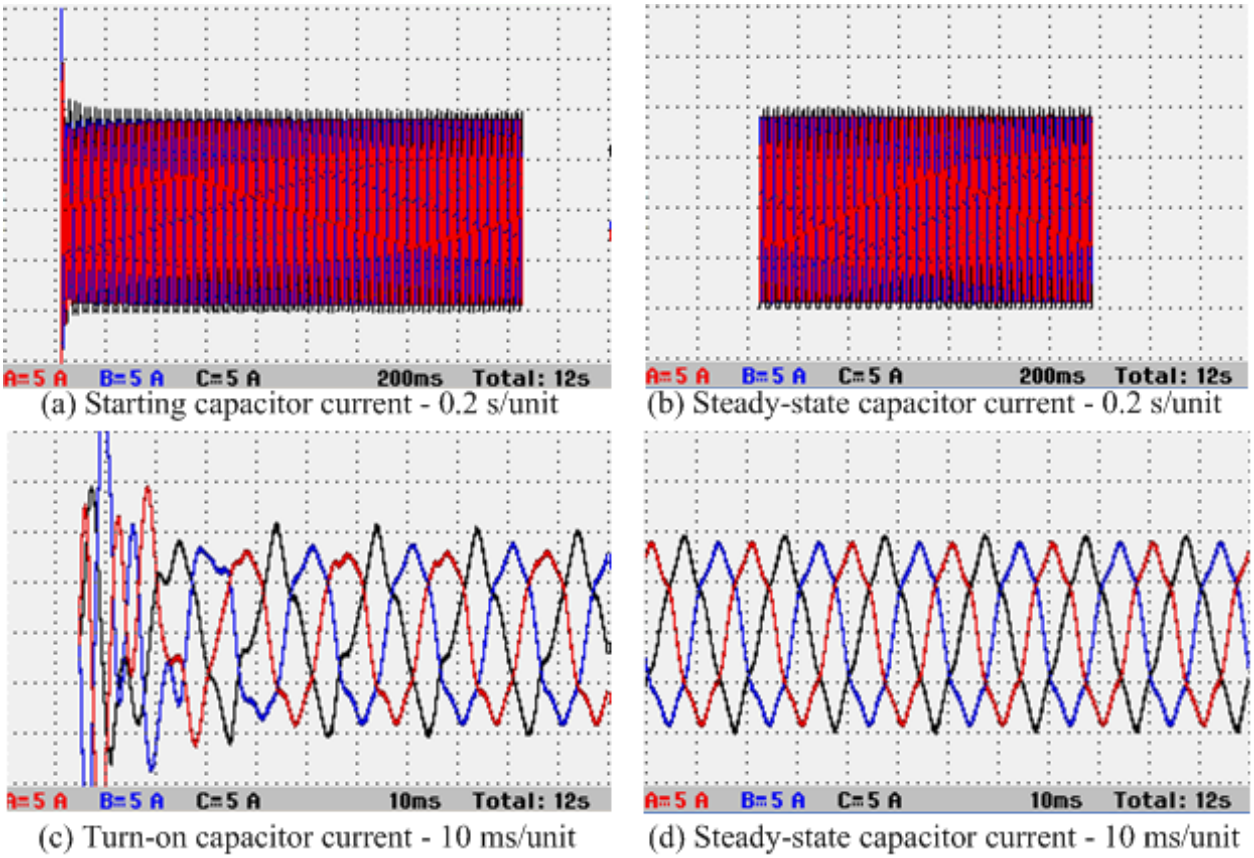

(a) Starting capacitor current - 0.2 s/unit

(b) Steady-state capacitor current - 0.2 s/unit

(c) Turn-on capacitor current - 10 ms/unit

(d) Steady-state capacitor current - 10 ms/unit

Figure 6.9 Transient capacitor current for Motor No. 1E at 100 V phase peak - with 90 µF. Y-scales: top - 5 A/unit, rest - 2 A/unit.

6.3 Point-On Switching

In this section, the effects of point-on switching is investigated. The system was built so that it could be switched on as line voltage across Phases *a* and *b* goes through zero, then 90° later, when the voltage across the Phase *c* breaker is zero. Motor Nos. 1 and 1E are both tested here.

6.3.1 Motor No. 1 Switching

Motor No. 1 is first tested; hence the machine has the series inductors removed and there is no capacitor compensation. Fig. 6.10 shows the line voltages and currents during starting. It can be seen that the Phases *a* and *b* are first connected so that in (a) the blue line and in (b) the black line shows a line voltage that starts at zero as the line voltage goes through the voltage crossing point and turn-on occurs. The other two line voltages are equal and half this since the star point is at the mid point between the two active phases. Then 90° later when Phase *c* is equal to star point, Phase *c* is switched on. The phasor diagram for illustrating this is shown in Fig. 6.11.

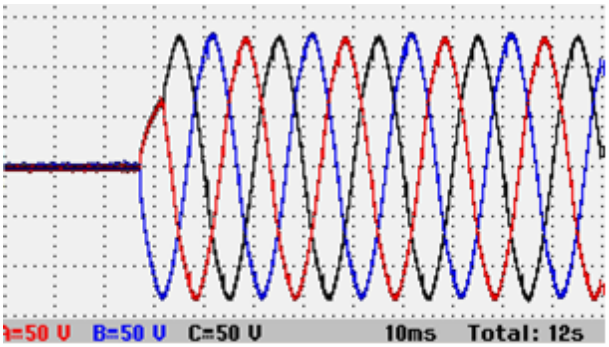

(a) Run 1- Starting voltage - 10 ms per unit

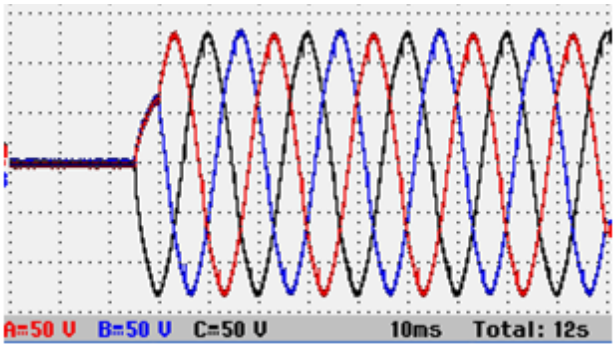

(b) Run 2 - Starting voltage -10 ms per unit

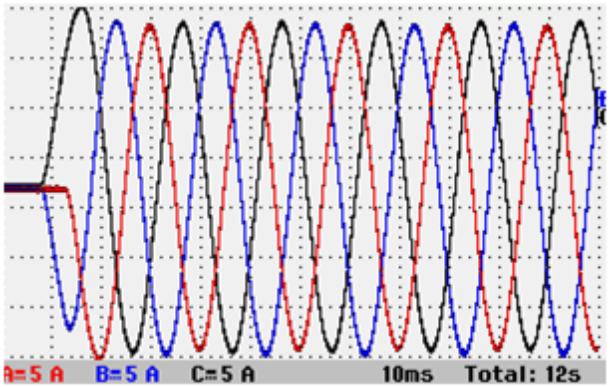

(c) Run 1 – starting current - 10 ms per unit

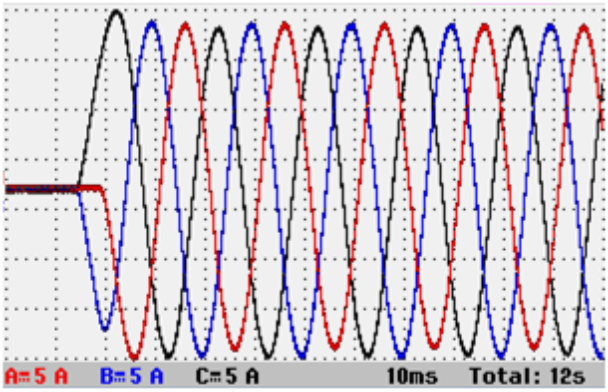

(d) Run 2 – starting current -10 ms per unit

Figure 6.10 Turn-on line voltages and currents for Motor No. 1 at 100 V line rms. Y-scales: top - 50 V/div, bottom - 5 A/div.

The currents in Fig. 6.10(c) and (d) are almost exactly the same as the motor current simulation in Fig. 4.34 apart from the polarity of the currents which may indicate that the line voltages have opposite polarity measurement. This shows the accuracy of the simulation method and that the point-on switching works. Since this is a resistive motor at start the overshoot is not high and this starting method does not offer much improvement over random switch-on. Bear in mind that at this stage only the motor is being switched in.

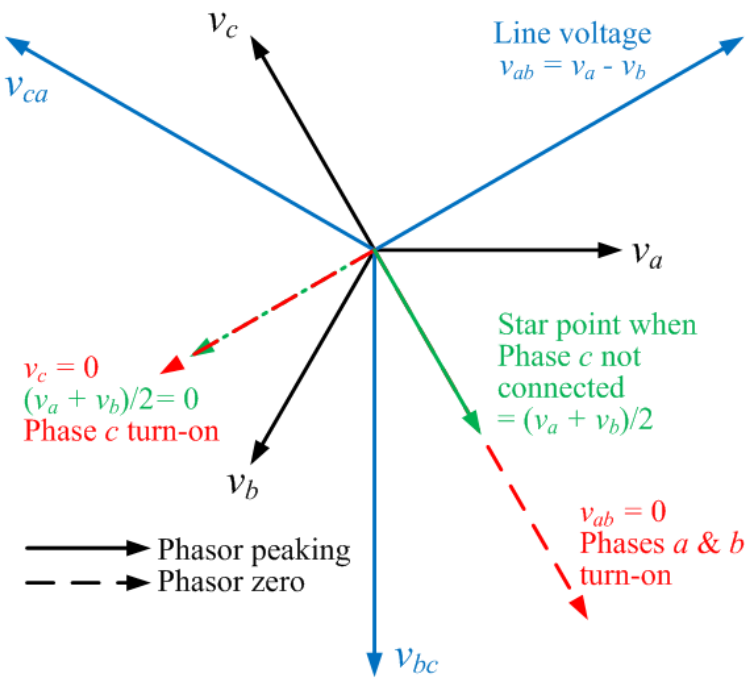

Figure 6.11 Phasor diagram for turn-on sequence.

6.3.2 Motor No. 1E Switching

For Motor No. 1E the voltages and currents are shown in Fig. 6.12. the switch-on occurs at zero line current crossing points and it can be seen in (c) and (d) that the currents are opposite but with the same wave shape between Runs 1 and 2. The current is seen to have about 30 % overshoot in

the first cycle. However, when compared to Fig. 6.6 there appears to be little improvement in the transient motor turn-on current using the zero voltage crossing point method even for this inductive motor. However, the switching methods does give switch-gear protection.

To improve the motor turn-on current a more sophisticated method is demonstrated by simulations in Section 3.3.3. This requires turn-on at a specific point, not just at the zero voltage crossing point.

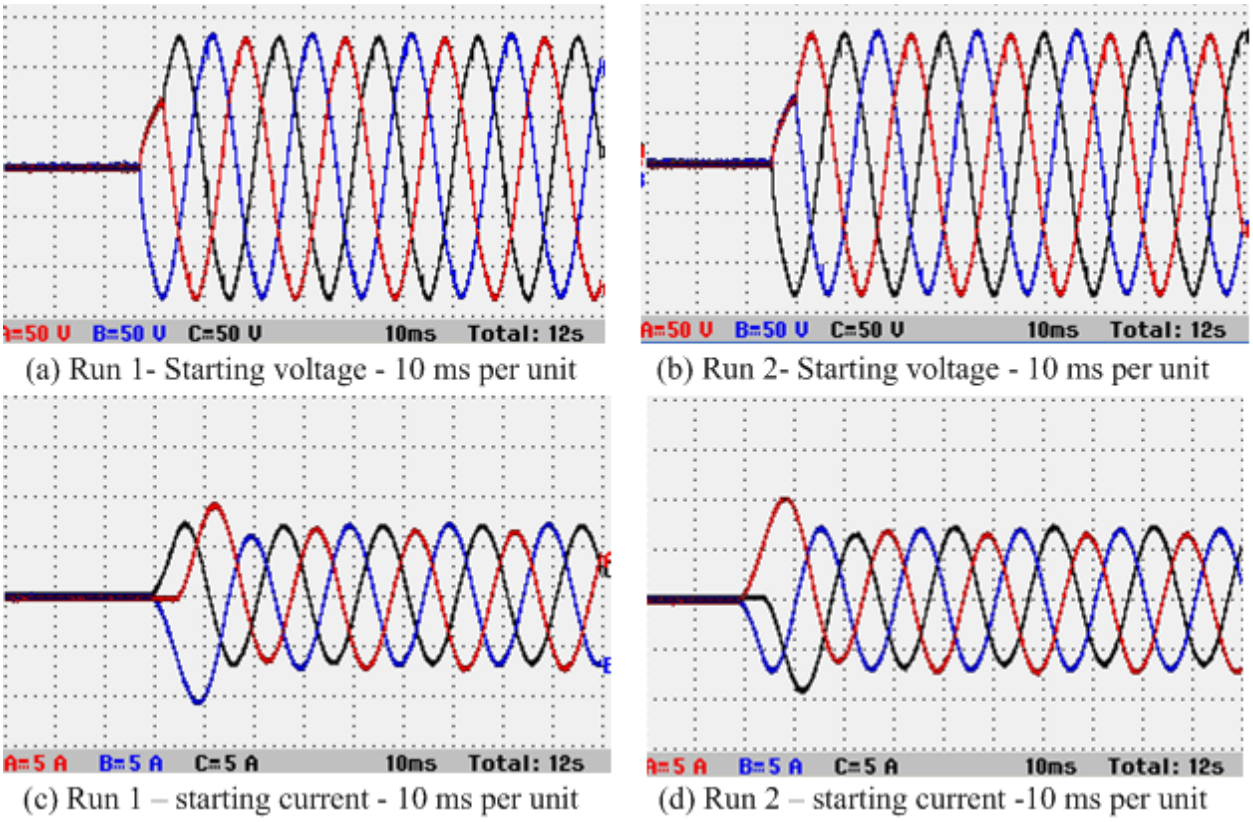

(a) Run 1- Starting voltage - 10 ms per unit

(b) Run 2- Starting voltage - 10 ms per unit

(c) Run 1 – starting current - 10 ms per unit

(d) Run 2 – starting current -10 ms per unit

Figure 6.12 Turn-on line voltages and currents for Motor No. 1E at 100 V line rms. Y-scales: top - 50 V/div, bottom - 5 A/div.

6.3.3 Motor No. 1E Switching with Capacitors and Filters

The motor is now switched on with the delta-connected capacitors connected in parallel. These have the 1.1 Ω inductive filters in series. The measurements are given in Fig. 6.13. It can be seen that the motor currents for Runs 1 and 2 in (c) and (d) are the same and unaffected by the capacitors. There is still transient grid turn-on current. However, for random turn-on shown in Fig. 6.5(c) and (d) the peak of the current spikes are 20 A. With the zero voltage cross point switching as shown in Fig. 6.13(c) and (d) the grid turn-on current spikes appear to be halved to about 10 A (the zoom in (e) and (f) are zoomed to 2A/div so that spike peaks are not quite on the graph). This does present an improvement in capacitor turn-on and also the capacitors can be switched in with zero charge on the capacitor.

6.4 Conclusions

This Chapter has reported on the experimental work carried out to show that the use of capacitor compensation. It has shown that for a large inductive-start motor there is considerable reduction in the start current when using compensation capacitors. However, there needs to be filtering of the capacitors to reduce harmonics. It was shown that using in-line inductors with the capacitors reduced the run-up current considerably. This verified the simulations work.

The use of point-on switching was shown to be possible. This can be used to soft-start the motor and allow connection of the uncharged capacitors when the line voltage is zero. This appears to reduce the capacitor turn-on current spikes. The advantage of this method is to soft-connect equipment.

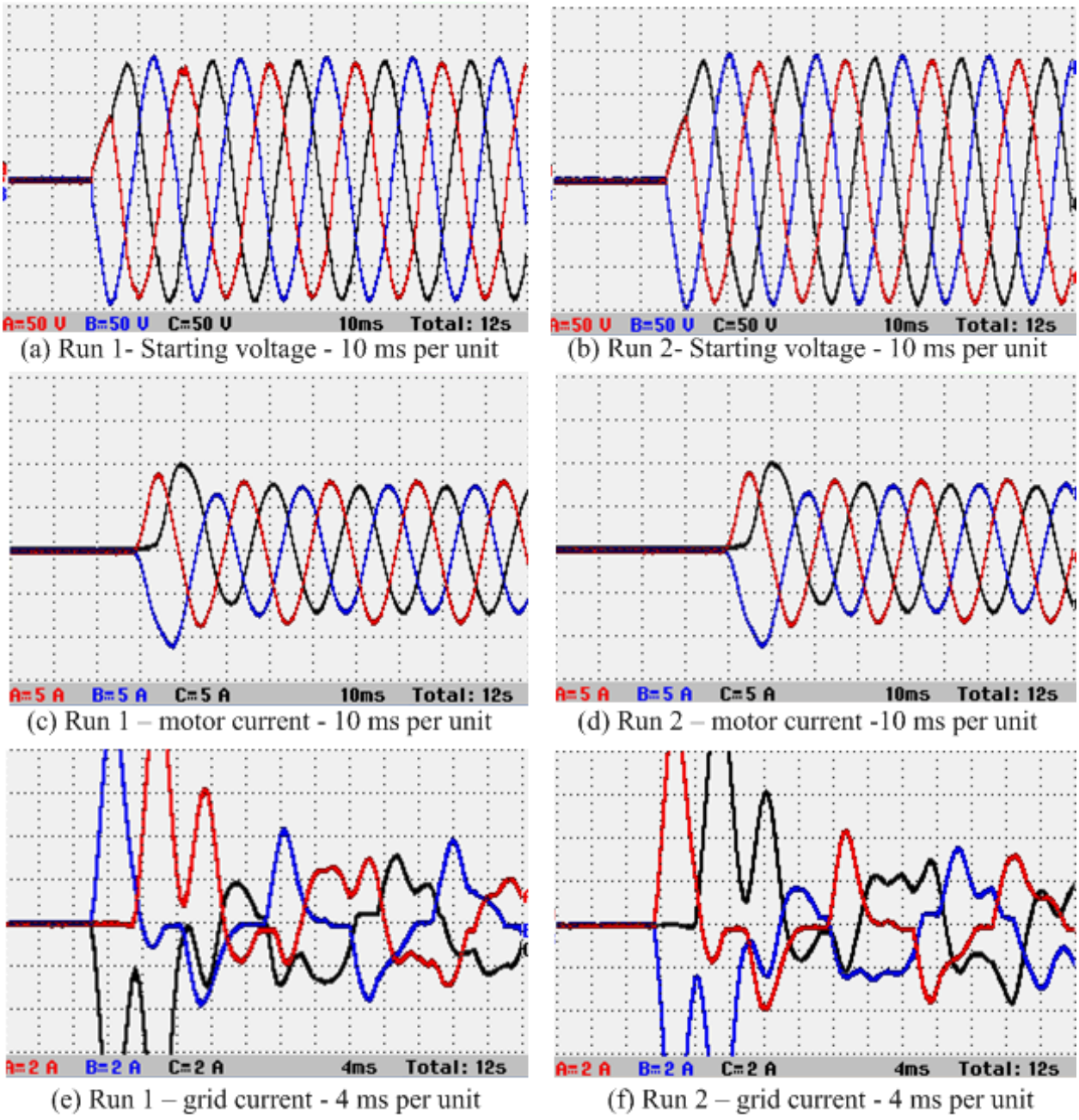

(a) Run 1- Starting voltage - 10 ms per unit

(b) Run 2- Starting voltage - 10 ms per unit

(c) Run 1 – motor current - 10 ms per unit

(d) Run 2 – motor current -10 ms per unit

(e) Run 1 – grid current - 4 ms per unit

(f) Run 2 – grid current - 4 ms per unit

Figure 6.13 Turn-on line voltages and currents for Motor No. 1 at 100 V line rms. Y-scales: top - 50 V/div, middle - 5 A/div, and bottom - 2 A/div.

Chapter 7

Conclusions

By tuning compensation capacitors, it has been possible to reduce the starting current in large 3-phase induction motors as demonstrated in the previous papers [61, 89]. This concept has been expanded and tested both using simulations of real machines and experimentally.

The work has developed analysis for the simulation of the starting of electrical machines and tested them using seven electrical machine equivalent circuits covering a wide range of machines from 1.5 kW up to several MW and with varying pole number. The simulations show that larger machines are more inductive during starting and draw more reactive power. This illustrates the validity of the capacitor compensation method to reduce the starting run-up current. Both steady-state equivalent circuit methods and a transient d-q method were used to simulate the machines and the results match well. It shows that by selection of correct capacitors the methods can be very effective.

The starting current can be split into the transient run up that can be over several seconds, and the transient turn-on which will take one or two cycles of the applied voltage. Point-on switching

was studied using simulation and it was illustrated that the transient inrush-current can be reduced using point-on switching. The experimental work used solid-state breakers that switch on when the voltage is zero across them. While this is not the optimum switching point it will allow soft turn-on and breaker protection, and the work illustrated that point-on power switching is possible.

The switching-in of the capacitors was studied. To go straight to steady-state would require pre-charging. This is not very practical. If the capacitors are not charged, which is good practice, then to obtain soft turn-on then they need to be switched-in when there is zero voltage across them. This will create an exponential delay transient which can be reduced by putting in series line inductances with an inductive reactance of 10 % of the capacitive reactance at the line frequency. These also act as low pass filters.

The experimental work used a small machine but with added line reactance to simulate a much larger machine which would be more inductive. Both capacitor compensation and point-on switching of the motor and capacitors were studied. The effects of voltage harmonics and the use of line reactors with the compensating capacitors to filter low frequency harmonics (5^{th}, 7^{th}, 11^{th}, 13^{th}, etc) was well illustrated.

The experimental work validated the theory and simulations and shows the methods has industrial potential. The methods appear simple and effective. While capacitors are often used for steady-state compensation, indeed this is common practice, the author can find little evidence of their use during starting when the high starting current can cause series problems for soft supplies such as those at the end of a long line or in a small islanded system.

Further current reduction can be obtained by using active power compensation but this will require energy storage and an inverter (Fig 7.1). The aim of this work was to address starting current reduction in a cost-effective manner and this may be expensive for a large machine. As

seen in this study, in large machines it is the reactive power that is mostly drawn during starting - an inverter such as this can supply both reactive and active power and may be more controllable than connecting capacitors. If there are several machines this sort of starter could be used across several machines started in sequence which would be more cost effective. This will be the focus of further work.

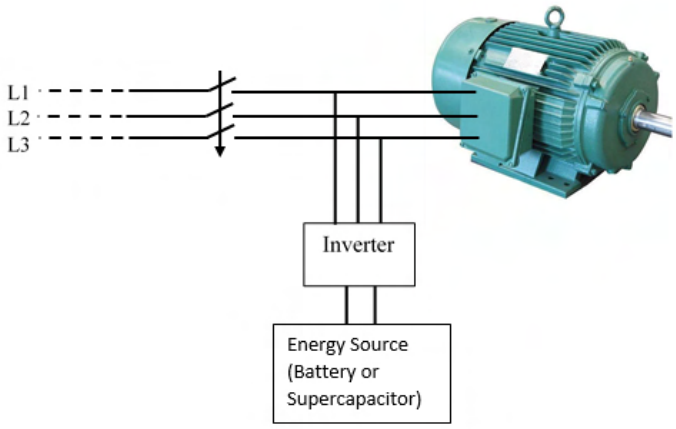

Figure 7.1 Simplified circuit diagram.

Bibliography

[1] Manuel Reta-Hernandez. Section 4.6: Transmission line parameters. In *The Electric Power Engineering Handbook Ed: L. L. Grigsby, 3rd Edition*, pages 4–62 – 4–88. CRC Press, 2018.

[2] Thomas P Smith. Performing detailed power system studies for designing and analyzing electrical distribution systems-power system studies for cement plants. *IEEE Industry Applications Magazine*, 13(4):56–65, 2007.

[3] Erik K Saathoff, Daisy H Green, Rebecca A Agustin, Joseph O'Connell, and Steven B Leeb. Inrush current measurement for transient space characterization and fault detection. *IEEE Transactions on Instrumentation and Measurement*, 70(3520410), 2021.

[4] Stephen Chapman. *Electric Machinery Fundamentals*. Tata McGraw-Hill Education, 2005.

[5] Ewald Fuchs and Mohammad AS Masoum. *Power quality in power systems and electrical machines*. Academic press, 2011.

[6] S. D. Umans. Steady-state, lumped-parameter model for capacitor-run, single-phase induction motors. *IEEE Transactions on Industry Applications*, 32(1), 1996.

[7] S. Leng, R. Ul Haque, N. Perera, A. M. Knight, and J. Salmon. Soft start of induction motors using floating capacitor h-bridge converters. In *7th IET International Conference on Power Electronics, Machines and Drives (PEMD)*, pages 1–6, 2014.

[8] S. Leng, R. Ul Haque, N. Perera, A. M. Knight, and J. Salmon. Soft start and voltage control of induction motors using floating capacitor h-bridge converters. *IEEE Transactions on Industry Applications*, 54(4):3115 – 3123, 2016.

[9] Jonathan Devadason and Paul S. Moses. Analysis of free acceleration and steady state characteristics of line-started induction motors with shunt capacitor compensation. In *IEEE Power and Energy Society General Meeting (PESGM)*, pages 1–5, 2019.

[10] P. K. Sen and L. J. Burleson. Induction motor overvoltage due to power factor improvement capacitor. In *IEEE Industry Applications Society Annual Meeting*, 1989.

[11] C. Locke. Optimal capacitor sizing for induction motors. In *Canadian Conference on Electrical and Computer Engineering. Conference Proceedings*, volume 2, 2000.

[12] H. Rehaoulia and M. Poloujadoff. Transient behavior of the resultant airgap field during run-up of an induction motor. *IEEE Transactions on Energy Conversion*, EC-1(4):92–98, 1986.

[13] H. Banach. Condition for the occurrence of maximum efficiency in induction motors and transformers. In *2018 International Symposium on Electrical Machines (SME)*, pages 1–5, 2018.

[14] JA Fleming. Experimental researches on alternate-current transformers. *Journal of the Institution of Electrical Engineers*, 21(101):594–686, 1892.

[15] Theodore R Specht. Transformer inrush and rectifier transient currents. *IEEE Transactions on Power Apparatus and Systems*, PAS-88(4):269–276, 1969.

[16] R. A. Turner and K. S. Smith. Transformer inrush currents. *IEEE Industry Applications Magazine*, 16(5):14–19, 2010.

[17] Paul CY Ling and Amitava Basak. Investigation of magnetizing inrush current in a single-phase transformer. *IEEE Transactions on Magnetics*, 24(6):3217–3222, 1988.

[18] Robbie F McElveen and Michael K Toney. Starting high-inertia loads. *IEEE Transactions on Industry Applications*, 37(1):137–144, 2001.

[19] James Gover. Transportation electrification: Electric machines in electric drive trains. *IEEE Course*, 2013.

[20] Mihail V Cistelecan, H Baris Cosan, and Mihail Popescu. Part-winding starting improvement of three-phase squirrel-cage induction motor. In *2009 8th International Symposium on Advanced Electromechanical Motion Systems and Electric Drives Joint Symposium*, pages 1–6. IEEE, 2009.

[21] Klaus Uuskoski. Procedure for reducing the starting current of a squirrel-cage motor, and a squirrel-cage motor unit designed for implementing the procedure, 1995. US Patent 5,451,854.

[22] KL Hansen. The rotating magnetic field theory of ac. motors. *Journal of the AIEE*, 44(2):170–178, 1925.

[23] Piotr Wach. Induction machine in electric drives. In *Dynamics and Control of Electrical Drives*, pages 109–280. Springer, 2011.

[24] Paul Ranky and John KL Ho. Introduction and overview of wind turbine design challenges. In *IEEE On-line Course*. IEEE, 2011.

[25] Sakutaro Nonaka and Katsumi Kesamaru. Analysis of voltage-adjustable brushless synchronous generator without exciter. *IEEE Transactions on Industry Applications*, 25(1):126–132, 1989.

[26] L Alberti and G Berardi. Design of a low power synchronous motor for high efficiency applications. In *2018 XIII International Conference on Electrical Machines (ICEM)*, pages 677–682. IEEE, 2018.

[27] Hamid Fekri Azgomi and Javad Poshtan. Induction motor stator fault detection via fuzzy logic. In *2013 21st Iranian Conference on Electrical Engineering (ICEE)*, pages 1–5. IEEE, 2013.

[28] EB Kurtz. Transformer current and power inrushes under load. *Electrical Engineering*, 56(8):989–994, 1937.

[29] CD Hayward. Prolonged inrush currents with parallel transformers affect differential relaying. *Electrical Engineering*, 60(12):1096–1101, 1941.

[30] M Akherraz. Inrush current and speed regulation of induction motor drives. In *6th Mediterranean Electrotechnical Conference*, pages 1285–1288, 1991.

[31] Babak Badrzadeh. High power variable speed drives: Performance issues, application guide, and network studies, Part 2. *IEEE Course*, 2010.

[32] M Jamali, M Mirzaie, and S Asghar-Gholamian. Calculation and analysis of transformer inrush current based on parameters of transformer and operating conditions. *Elektronika ir Elektrotechnika*, 109(3):17–20, 2011.

[33] Rares Popescu, Gabriel Botez, Catalin Mihai, and Dan Stoia. A comparative study of transformers losses with eco-design requirements. In *2017 International Conference on Optimization of Electrical and Electronic Equipment (OPTIM) and 2017 Intl Aegean Conference on Electrical Machines and Power Electronics (ACEMP)*, pages 25–30. IEEE, 2017.

[34] K Pillay, Mutasim Nour, KH Yang, DN Datu Harun, and LK Haw. Assessment and comparison of conventional motor starters and modern power electronic drives for induction motor

starting characteristics. In *IEEE Symposium on Industrial Electronics and Applications*, volume 2, pages 584–589, 2009.

[35] HH Goh, MS Looi, and BC Kok. Comparison between direct-on-line, star-delta and auto-transformer induction motor starting method in terms of power quality. In *Proceedings of the international multiconference of engineers and computer scientists*, volume 2, pages 18–20, 2009.

[36] Adel A Shaltout. Analysis of torsional torques in starting of large squirrel cage induction motors. *IEEE Transactions on Energy Conversion*, 9(1):135–142, 1994.

[37] PSCAD Software. https://www.pscad.com/.

[38] Mohammad Hassan Abderrazzaq, Mohamad Samih Hussin, and Khalil Alhayek. The effect of high frequency, high voltage supply on the growth of electrical trees on cross linked polyethlyne insulation of power cables. In *2013 IEEE International Conference on Solid Dielectrics (ICSD)*, pages 812–815. IEEE, 2013.

[39] Viv Cohen. Induction motors-protection and starting. *Elektron Journal - South African Institute of Electrical Engineers*, 12:5–10, 1995.

[40] F. J. T. E. Ferreira, B. Ge, E. C. Quispe, and A. T. De Almeida. Star- and delta-connected windings tolerance to voltage unbalance in induction motors. In *2014 International Conference on Electrical Machines (ICEM)*, pages 2045–2054, 2014.

[41] John Larabee, Brian Pellegrino, and Benjamin Flick. Induction motor starting methods and issues. In *IEEE Industry Applications Society 52nd Annual Petroleum and Chemical Industry Conference*, pages 217–222, 2005.

[42] Frank M Bruce, Richard J Graefe, Arthur Lutz, and Michael D Panlener. Reduced-voltage starting of squirrel-cage induction motors. *IEEE Transactions on Industry Applications*, IA-20(1):46–55, 1984.

[43] MG Say. *Alternating Current machines*. Longman scientific and Technical, 1983.

[44] Junichi Fukushima, Yoshihisa Uriu, Keita Katayama, Hiroyuki Iki, and Yoshihide Kado. Optimal capacitor sizing for induction motors. In *44th International Universities Power Engineering Conference (UPEC)*, 2009.

[45] Kevin Lee, Scott K Becker, and Kevin J Schmidt. Method and compensation modulator for dynamically controlling induction machine regenerating energy flow and direct current bus voltage for an adjustable frequency drive system, 2004. US Patent 6,768,284.

[46] PL Alger. Performance calculations for part-winding starting of 3-phase motors [includes discussion]. *Transactions of the American Institute of Electrical Engineers. Part III: Power Apparatus and Systems*, 75(3):1535–1543, 1956.

[47] Langlang Gumilar, Dezetty Monika, Mokhammad Sholeh, and Stieven Netanel Rumokoy. Transient in electrical power system under large induction motor starting condition. In *2nd International Conference on Cybernetics and Intelligent System (ICORIS)*, 2020.

[48] Michael J. Russell. The impact of mains impedance on power quality. In *Power Quality 2000 (Boston, MA)*, 2000.

[49] Bhim Singh, A. Adya, A.P. Mittal, J.R.P. Gupta, and B.N. Singh. Application of DSTATCOM for mitigation of voltage sag for motor loads in isolated distribution systems. In *IEEE International Symposium on Industrial Electronics*, 2006.

[50] Robert Ferdinand and Antonello Monti. Export transformer switching transient mitigation in hvdc connected offshore wind farms. *IEEE Transactions on Power Delivery*, 35(1), 2020.

[51] Andreas Ebner. Transient transformer inrush currents due to closing time-and residual flux measurement-deviations if controlled switching is used. *ETH Zurich, High Voltage Laboratory, Zurich, Switzerland*, 2007.

[52] Pradeep J.Kotak and Alka Thakur. Comparative analysis of point on wave switching technique & prefluxing technique to mitigate in-rush current in three phase power transformer. *International Journal of Scientific & Engineering Research*, 5(11):831–836, November 2014.

[53] Guy Olivier, I Mougharbel, and G Dobson-Mack. Minimal transient switching of capacitors. *IEEE Transactions on Power Delivery*, 8(4):1988–1994, 1993.

[54] J. A. Jardini, R. P. Casolari, G. Y. Saiki, M. Masuda, L. C. Magrini, and R. M. Jacobsen. Point-on-wave controller developed for circuit breaker switching. In *IEEE/PES Transmission and Distribution Conference and Exposition*, 2008.

[55] KSIM Series Single Phase AC Output. https://img.waimaoniu.net/2064/2064-202106160921234659.pdf [Accessed: 25/11/2021].

[56] Celduc Solid State Relay SC869110. https://docs.rs-online.com/a175/0900766b800af969.pdf [Accessed: 25/11/2021].

[57] R. Oliveira and P. Bokoro. Application of point-on wave switching technique for the generation of slow-front overvoltages. In *Southern Africa universities Power Engineering Conference (SAUPEC)*, 2008.

[58] Solid State Relay. https://www.electronics-tutorials.ws/power/solid-state-relay.html [Accessed: 25/11/2021].

[59] Powertech Labs. Point On Wave Switching. https://powertechlabs.com/point-on-wave-switching/ [Accessed: 25/11/2021].

[60] Electrical Concepts. Point on Wave Switch / Controller, 2017. https://electricalbaba.com/point-on-wave-switch-controller/ [Accessed: 25/11/2021].

[61] M Habyarimana and DG Dorrell. Methods to reduce the starting current of an induction motor. In *2017 IEEE International Conference on Power, Control, Signals and Instrumentation Engineering (ICPCSI)*, pages 34–38. IEEE, 2017.

[62] LA Finzi and WH Mutschler. The inrush of magnetizing current in single-phase transformers. *Transactions of the American Institute of Electrical Engineers*, 70(2):1436–1438, 1951.

[63] Pouya Amiri and Mahdi Akhbari. Transient current limiter for suppressing transformer inrush, motor starting and fault currents in power system. *IET Electric Power Applications*, 11(3):423–433, 2017.

[64] Werner Deleroi, Johan B Woudstra, and Azza A Fahim. Analysis and application of three-phase induction motor voltage controller with improved transient performance. *IEEE Transactions on Industry Applications*, 25(2):280–286, 1989.

[65] Milad Falahi, Karen L Butler-Purry, and Mehrdad Ehsani. Induction motor starting in islanded microgrids. *IEEE Transactions on Smart Grid*, 4(3):1323–1331, 2013.

[66] Laszlo Gyugyi, John Rosa, and Eric J Stacey. Static reactive power generating apparatus, 1977. US Patent 4,001,670.

[67] D. G. Dorrell, P. J. Holik, P. Lombard, H.-J. Thougaard, and F. Jensen. Multisliced finite-element model for induction machines incorporating interbar current. *IEEE Transactions on Industry Application*, 45(1):131–141, 2009.

[68] D. G. Dorrell, P. J. Holik, and C. B. Rasmussen. Analysis and effects of inter-bar current on a long skewed-rotor induction motor for pump applications. *IEEE Transactions on Magnetics*, 43(6):2534–2536, June 2007.

[69] Hany M. Jabr and Narayan C. Kar. Starting performance of saturated induction motors. In *IEEE Power Engineering Society General Meeting*, July 2007.

[70] Eemeli Molsa, Seppo E. Saarakkala, Marko Hinkkanen, Antero Arkkio, and Mikko Routimo. A dynamic model for saturated induction machines with closed rotor slots and deep bars. *IEEE Transactions on Energy Conversion*, 35(1):157–165, 2020.

[71] Masahiro Ikeda and Takashi Hiyama. Simulation studies of the transients of squirrel-cage induction motors. *IEEE Transactions on Energy Conversion*, 22(2):233–239, 2007.

[72] N. Erdogan, H. Henao, and R. Grisel. The analysis of saturation effects on transient behavior of induction machine direct starting. In *2004 IEEE International Symposium on Industrial Electronics*, volume 2, pages 975–979 vol. 2, 2004.

[73] Fanqing Meng, Dong Wang, Zhixin Liu, and Wu Su. Fast circuit-field coupling analysis for skewed induction motor. *IEEE Transactions on Industrial Electronics*, 68(6):5088–5099, 2021.

[74] Jaehong Kim, Jinseok Hong, and Kwanghee Nam. A current distortion compensation scheme for four-switch inverters. *IEEE Transactions on Power Electronics*, 24(4):1032–1040, 2009.

[75] John R Linders. Effects of power supply variations on ac motor characteristics. *IEEE Transactions on Industry Applications*, IA-8(4):383–400, 1972.

[76] V. E. Wagner, J. C. Balda, D. C. Griffith, A. McEachern, T. M. Barnes, D. P. Hartmann, D. J. Phileggi, A. E. Emannuel, W. F. Horton, W. E. Reid, R. J. Ferraro, and W.T. Jewell. Effects of harmonics on equipment. *IEEE Transactions on Power Delivery*, 8(2):672–680, 1993.

[77] R Barnes. Harmonics in power systems. *IEE Power Engineering Journal*, 3(1):11–15, 1989.

[78] A. Castanheira R. Dudley and M. Sharp. section 3.7: Reactors. In *The Electric Power Engineering Handbook Ed: L. L. Grigsby, 3rd Edition*, pages 3–95. CRC Press, 2018.

[79] YHA Rahim. Excitation of isolated three-phase induction generator by a single capacitor. *IEE Proceedings B (Electric Power Applications)*, 140(1):44–50, 1993.

[80] Austin H. Bonnett, Helmuth Glatt, and Steve Hauck. Effect of power deviations on squirrel-cage induction motors: Addressing the impact of voltage and frequency variations. *IEEE Industry Applications Magazine*, 22(6):39–47, 2016.

[81] How to Read a Positive Displacement Pump Curve. https://www.csidesigns.com/blog/articles/how-to-read-a-positive-displacement-pump-curve.

[82] Cephas Mutize and Rong-Jie Wang. Performance comparison of an induction machine and line-start pm motor for cooling fan applications. In *21st Southern African Universities Power Engineering Conference (SAUPEC)*, pages 122–126, 01 2013.

[83] Hirofumi Akagi, Yoshihira Kanazawa, Koetsu Fujita, and Akira Nabae. Generalized theory of the instantaneous reactive power and its application. *The Transactions of the Institute of Electrical Engineers of Japan. B*, 103(7):483–490, 1983.

[84] Fang Zheng Peng and Jih-Sheng Lai. Generalized instantaneous reactive power theory for three-phase power systems. *IEEE Transactions on Instrumentation and Measurement*, 45(1):293 – 297, 1996.

[85] T. M. Blooming and D. J. Carnovale. Application of IEEE Std 519-1992 Harmonic Limits. https://www.mathworks.com/help/mcb/ref/inductionmotor.html.

[86] Valiadis Hellenic Motors. https://www.valiadis.gr/.

[87] P. C. Sen. *Principles of Electric Machines and Power Electronics*. Wiley, 1989.

[88] Michael J Melfi and Stephen D Umans. Squirrel-cage induction motors: Understanding starting transients. *IEEE Industry Applications Magazine*, 18(6):28–36, 2012.

[89] M. Habyarimana R. Musumpuka and D. G. Dorrell. Mitigating in-rush currents for induction motor loads. In *IEEE Southern Power Electronics Conference (SPEC-2021)*, pages 1–6. IEEE, 2021.

Appendix A

Laboratory Motor Specification and Equivalent Circuit Parameters

This appendix gives the technical details of the test motor together with the results of running-light and locked-rotor tests to ascertain the equivalent circuit parameters. Because the machine is an experimental machine (it is shown to have a very short pitched winding) and rated at 60 Hz on the nameplate with no indication of star or delta connection, a running light test is finally done to address the correct voltage level - this was done when it has 4 poles and is star-connected. This confirms that a line voltage, when connected in star, of between 200 V and 220 V is an appropriate full voltage for the machine.

A.1 Motor Technical Details

The machine tested is a 50 Hz, 4-pole, 1.5 kW, 3-phase induction motor. The nameplate shown on Figure A.3. The machine has 48 slots and is double layer wound. Basic calculations can be done. The synchronous speed is given by:

$$N = \frac{120f}{p} = \frac{120 \times 50}{4} = 1500 \text{ rpm} \tag{A.1}$$

and the full pitch coils span is

$$\text{Coil span(full pitch)} = \frac{48}{4} = 12 \text{ slots} \tag{A.2}$$

This is configured in a 4-pole connection, and the coils in each pole are connected in series. The poles are also in series. Fig. A.1 shows the the winding arrangement and this illustrates that the winding has two coil sides per slot so there are 96 terminals. The pitch of each coil is 7 slots. Fig. A.2) shows the top view of the motor table and winding connections. This pitch allows the machine to be connected as a 4-pole lap winding (short pitching of 7/12), 6-pole fractional slot winding (short pitching of 7/8) or 8-pole lap winding (over pitching of 7/6).

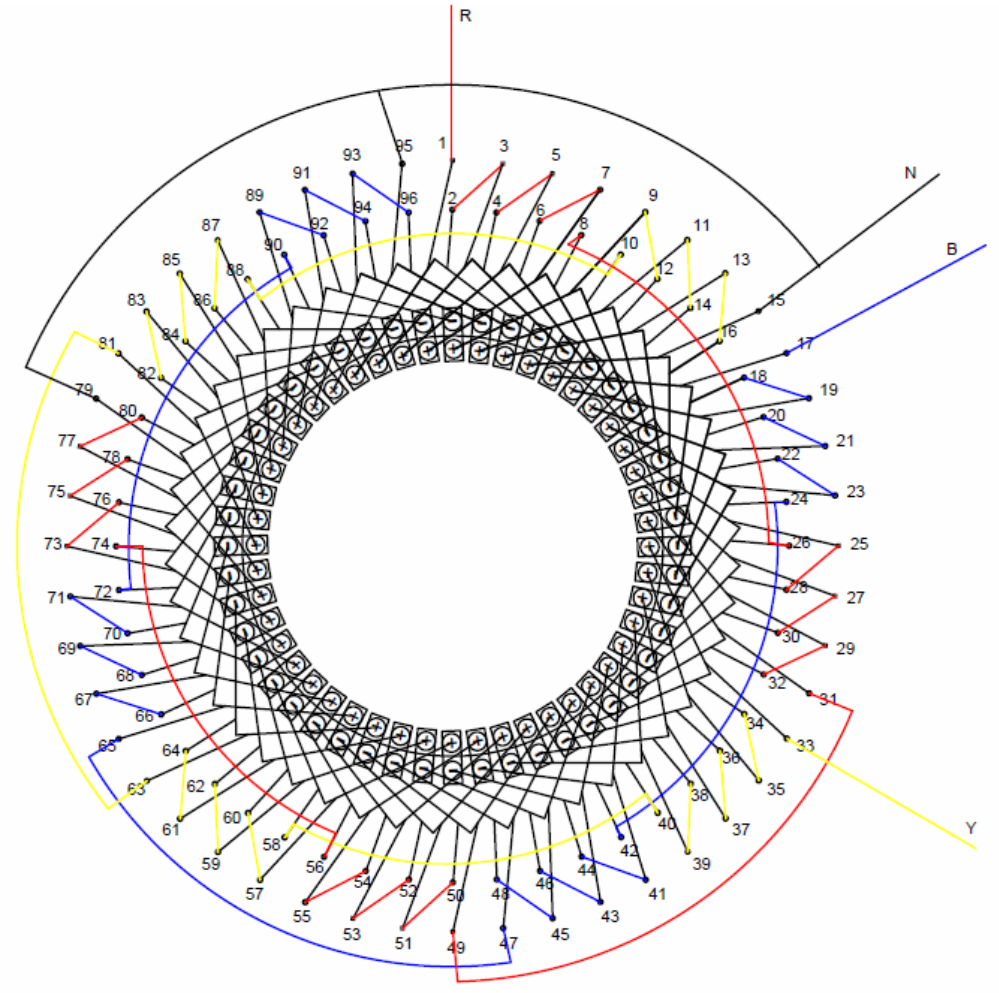

Figure A.1 Stator connection diagram.

There are two nameplates on the machine but one is for 2-phase operation. The 3-phase nameplate shows that is is a Westinghouse machine operating at 60 Hz (Fig. A.3). However, here it is operating at 50 Hz which may require an adjustment in the line voltage.

For 60 Hz the machine could be delta connection. However, later simulations seem to suggest this is for a star connection and that the voltages are line voltages. Normally they are quoted as line but this is an experimental machine. The ratings are stated as:

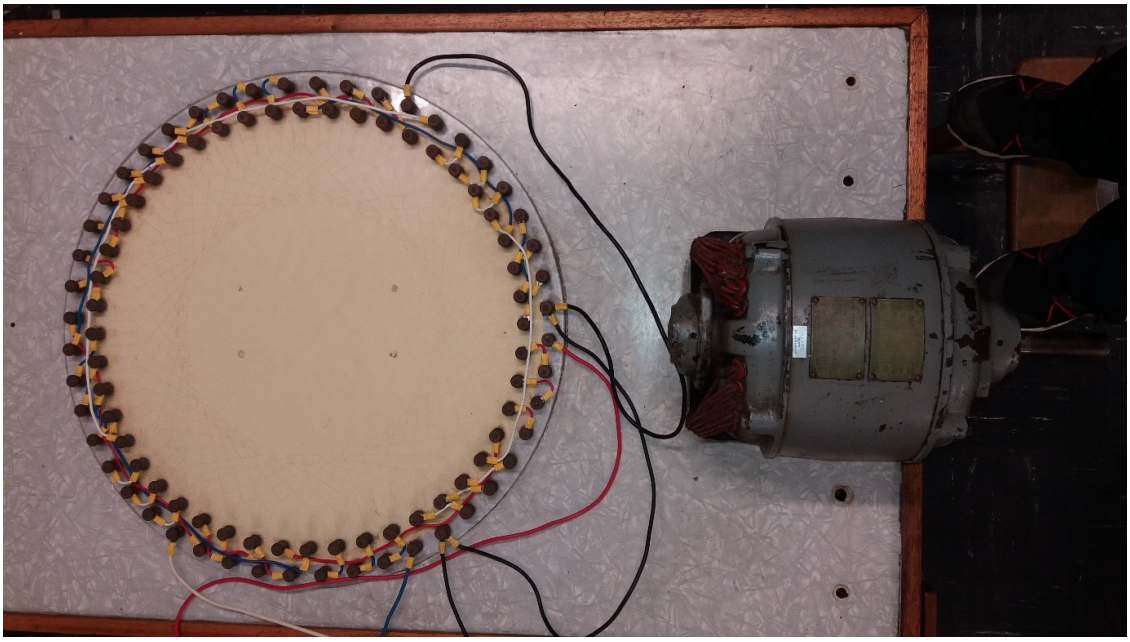

Figure A.2 Stator connection layout.

Power: 2 HP (1.5 kW) / 2 HP / 1 HP

Voltage (line): 220 V / 220 V / 180 V

Current (line): 5.8 A / 5.9 A / 4.6 A

Rated speed (at 60 Hz): 1725 rpm / 1135 rpm / 865 rpm

Clearly these are the ratings for the 4-, 6-, and 8-pole windings. Converting to approximate values for a star-connect 50 Hz arrangement will give approximately the same results because of the high resistance of the circuit. The 2-phase nameplate gives the 4-pole power as 2 HP again, with the voltage as 180 V (which will be across a phase), current as 6.8 A and speed at 1725 rpm again.

The full load speed will be $1500 - 75 = 1425$ rpm assuming the same drop in speed from synchronous speed, although this is very approximate. The wiring connection plan is given in Table A.1.

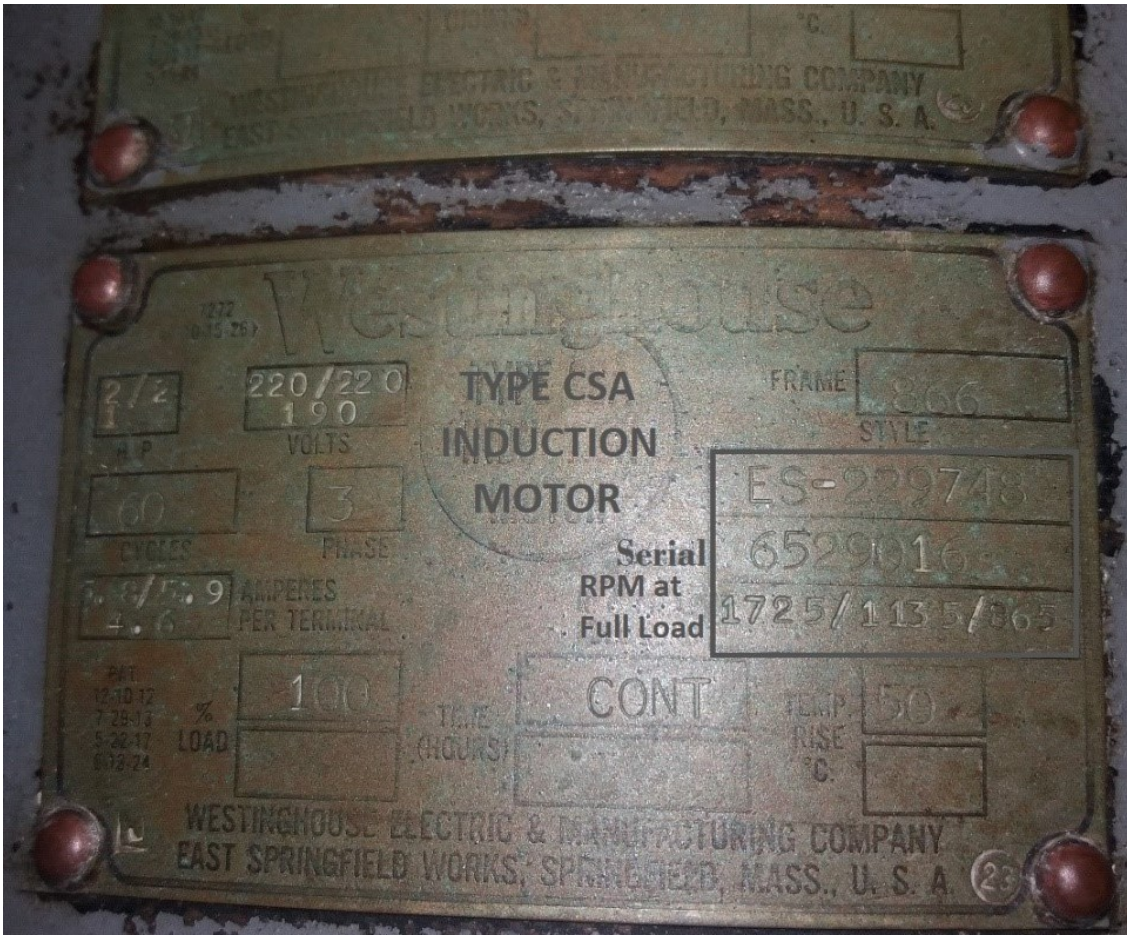

Figure A.3 Three phase Induction Motor name plate.

Table A.1 Coil connections

Coil inter-connection (series)		
Phase A	**Phase B**	**Phase C**
1 (Input terminal point)	**17 (Input terminal point)**	**33 (Input terminal point)**
2-3	18-19	4-35
4-5	20-21	36-37
6-7	22-23	38-39
8-26	24-42	40-58
25-28	41-44	57-60
27-30	43-46	59-62
29-32	45-48	61-64
31-49	47-65	63-81
50-51	66-67	82-83
52-53	68-69	84-85
54-55	70-71	86-87
56-74	72-90	88-10
73-76	89-92	9-12
75-78	91-94	11-14
77-80	93-96	13-16
79 (Neutral point)	**95 (Neutral point)**	**15 (Neutral point)**

A.2 Running-Light and Locked-Rotor Tests

The machine was star connected and the input power measured using two wattmeters as shown in Fig. A.4. The machine was then tested with the machine running light and then at reduced voltage with the rotor locked. The total power flowing into the circuit is $P_{in} = P_1 + P_2$ and the total volt-amps is $S_{in} = \sqrt{3} V_{Line} I_{Line}$.

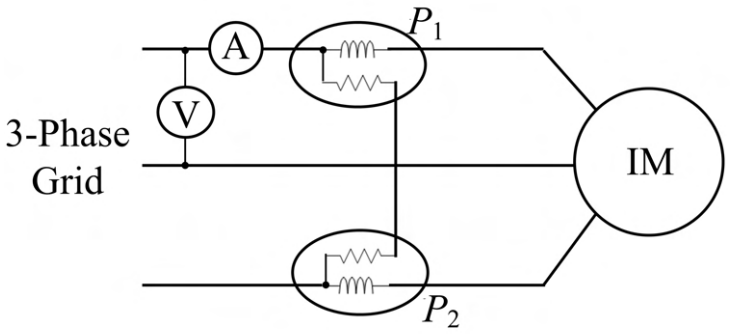

Figure A.4 Two single-phase wattmeters.

A.2.1 Running-Light Test

The test was conducted with the motor running at no load. The results in Table A.2. The scaling factors 2 and 5 for P_1 and P_2 are simply the wattmeter scalings factors. While the full equivalent circuit is shown in Fig. 3.1(a), the simplified circuit is shown in Fig. A.5. The test was done as slightly reduced voltage. The speed should be close to 1500 rpm but because of the reduced voltage and the fact that the full load speed is approximately 1425 rpm, which is 5 % and quite high, then the no load speed is 1484 rpm.

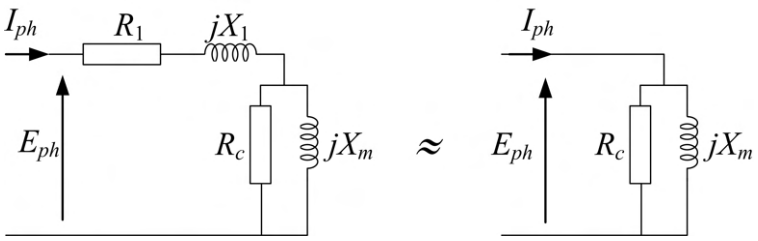

Figure A.5 Running light approximate circuit.

Table A.2 Measured no load values from the test

Measured	**Symbol**	**Value**
Line to line voltage	V_{L-L}	220 V
Line current	I_L	2.7 A
Rotor speed	rpm	1484 rpm
Supply frequency	f_s	50 Hz
Stator resistance	R_1	2.13 Ω
3-phase power with two Wattmeters	P_1	$90 \times 2 = 180$ W
	P_2	$83 \times 5 = 415$ W
	P_{in}	595 W

The core loss can be calculated from the input power and applied voltage so that

$$R_c = \frac{V_{ph}^2}{P_{ph}} = \frac{(220/\sqrt{3})^2}{595/3} = 81.34 \ \ \Omega \tag{A.3}$$

The reactive power per phase is

$$Q_{ph} = \sqrt{\left(V_{ph}I_{ph}\right)^2 - P_{ph}^2} = \sqrt{(220/\sqrt{3} \times 2.7)^2 - (595/3)^2} = 279.78 \ \ \text{VAr} \tag{A.4}$$

So that the magnetizing reactance can be calculated as

$$X_m = \frac{V_{ph}^2}{Q_{ph}} = \frac{(220/\sqrt{3})^2}{279.7783} = 57.66 \ \ \Omega \tag{A.5}$$

with the magnetizing inductance being $57.66/(2\pi \times 50) = 183$ mH.

A.2.2 Locked-Rotor Test

The locked rotor test is obtained at reduced voltage with the rotor locked. This is to avoid over-current. The full equivalent circuit is shown in Fig. 3.1(b) since it the starting approximate circuit. The results are given in Table A.3. The same scaling factors for the wattmeters are used for P_1 and P_2. The stator resistance R_1 is simply measured using a ohmmeter.

Table A.3 Locked Rotor Test Results

Measured	**Unit**	**Value**
Line to line voltage	V_L	46 V
Line current	I_L	5.8 A
Supply frequency	f_s	50 Hz
Stator resistance	R_1	2.1293 Ω
3-phase power with two wattmeters	P_1	$45 \times 2 = 90$ W
	P_2	$52 \times 5 = 260$ W
	P_{in}	350 W

The circuit is now series rather than parallel so that the sum of the input resistances is

$$R_1 + R_2^{/} = R_{bl} = \frac{P_{ph}}{I_1^2} = \frac{350}{3 \times 5.8^2} = 3.47 \ \ \Omega \tag{A.6}$$

and the stator Resistance is calculate by measuring the voltage and current between two phases when star connected and disconnected from the supply:

$$R_1 = \frac{1}{2} \times \frac{24.7}{5.8} = 2.13 \ \ \Omega \tag{A.7}$$

giving

$$R_2^{/} = 3.47 - 2.13 = 1.34 \ \ \Omega \tag{A.8}$$

The reactive power

$$Q_{ph} = \sqrt{\left(V_{ph} I_{ph}\right)^2 - P_{ph}^2} = \sqrt{(46/\sqrt{3} \times 5.8)^2 - (350/3)^2} = 100.58 \ \ \text{VAr} \tag{A.9}$$

The reactance is then

$$X_1 + X_2^{/} = \frac{Q_{in}}{I_1^2} = \frac{100.38}{5.8^2} = 2.99 \ \ \Omega \tag{A.10}$$

If using the full equivalent circuit in Fig. 3.1(a) is is usual to split X_1 and $X_2^{/}$ equally so that $X_1 = X_2^{/}$ since it is not possible split them using these simple tests.

The values for X_m, R_c, R_1, $R_2^{/}$ and $X_1 + X_2^{/}$ can be used in Table 4.2.

A.2.3 Running-light Test Over Voltage Range

Since the motor has a 60 Hz rating on the nameplate and it is unclear if it is star or delta connected then the motor was run light in star and the voltage varied. Table A.4 shows the individual measured line voltages and currents. The mean was taken and plotted in Fig. A.6. The machine appears to be properly rated at between 200 V an 220 V where the current starts to become nonlinear as it saturates. When induction motors are loaded as a motor they demagnetize due to the voltage from across R_1 and X_1. The current wave-forms were also checked as illustrated in Fig. A.7. These show some distortion, probably due to saturation and the short-pitched winding.

Table A.4 Locked Rotor Test Results

$V_{13}[V]$	V_{21} [V]	V_{32} [V]	$V_{Line-mean}[V]$	$I_1[A]$	I_2 [A]	I_3 [A]	$I_{Line-mean}[A]$
160.50	147.80	150.30	152.87	1.44	1.44	1.44	1.44
175.50	178.80	176.30	176.87	1.78	1.96	1.64	1.79
200.30	198.60	200.80	199.90	2.19	2.40	2.09	2.23
220.10	218.30	220.60	219.67	2.69	2.85	2.51	2.68
252.30	250.00	252.20	251.50	3.68	3.77	3.39	3.61
302.30	300.10	302.20	301.53	6.02	6.06	5.63	5.90
332.90	332.90	332.90	332.90	7.80	7.84	7.51	7.72
350.20	347.00	347.50	348.23	9.19	9.19	8.73	9.04

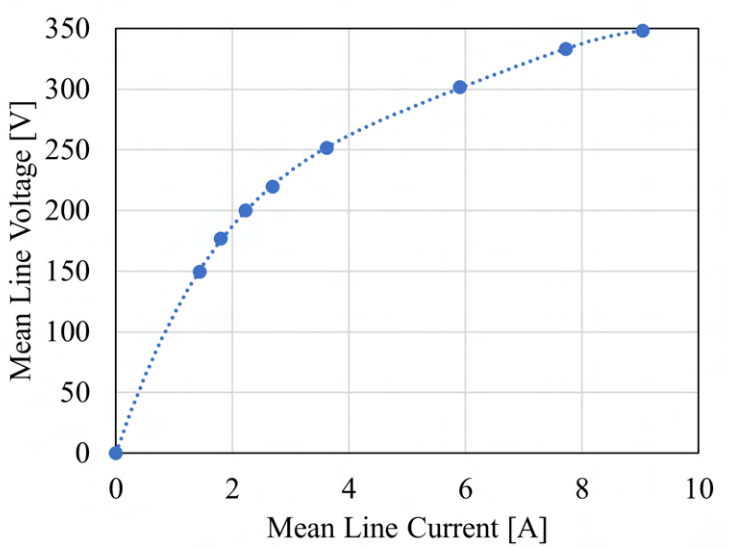

Figure A.6 Running light test - variation of current with voltage.

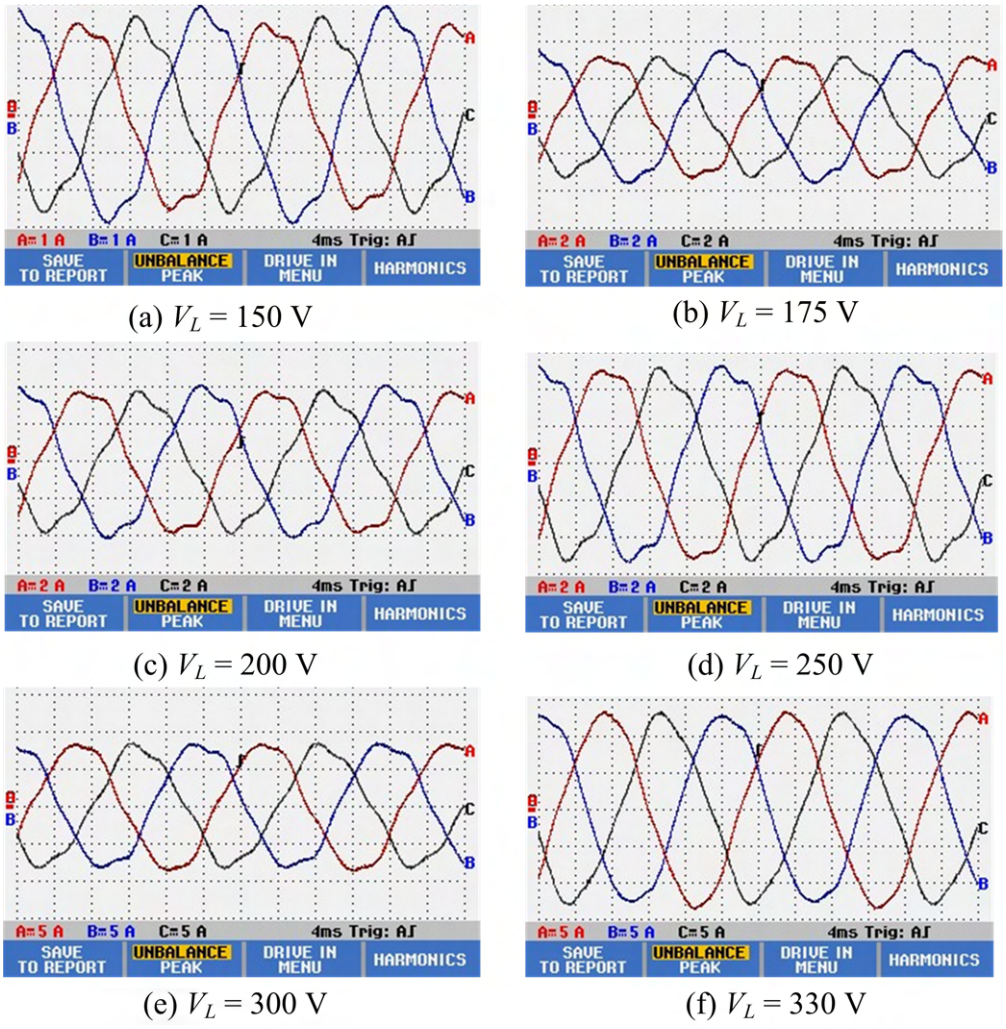

(a) $V_L = 150$ V (b) $V_L = 175$ V

(c) $V_L = 200$ V (d) $V_L = 250$ V

(e) $V_L = 300$ V (f) $V_L = 330$ V

Figure A.7 Running light test current waveforms.

Appendix B

Matlab Code for Comparing Starting Methods

```
clear

% PROGRAM TO CALCULATE EFFECTS OF DIFFERENT STARTING METHODS FOR INDUCTION
% MOTOR – 2021

% MOTOR PARAMETERS FOR 7 MOTORS USED

%Motordata = [P f vline Rc Xm R1 R2 X12 Prated]

Motordata(1:9,1) = [4, 50, 220, 81, 58, 2.13, 1.33, 2.99, 1500];
Motordata(1:9,2) = [4, 50, 400, 1568.2, 115.2, 1.325, 3.87, 8.44, 1500];
Motordata(1:9,3) = [4, 60, 440, 900, 110, 1.2, 1.56, 6, 3750];
Motordata(1:9,4) = [4, 50, 400, 178.1, 5.13, 0.059, 0.013, 0.48, 45000];
Motordata(1:9,5) = [2, 50, 3300, 1333, 118, 0.79, 0.57, 5.75, 200000];
Motordata(1:9,6) = [6, 50, 6000, 900.0, 102.5, 0.97, 0.24, 4.78, 1000000];
Motordata(1:9,7) = [12, 60, 6900, 600.0, 46.0, 0.083, 0.080, 2.60, 3750000];

% Set motor number to analyze
n=1;

%put into motor parameters
P=Motordata(1,n);
fs=Motordata(2,n);
Vline=Motordata(3,n);
```

```
Rc=Motordata(4,n);
Xm=Motordata(5,n);
R1=Motordata(6,n);
R2=Motordata(7,n);
X12=Motordata(8,n);
Prated=Motordata(9,n);

%Split X1 and X2 equally
X1r=X12/2;
X2r=X12/2;
CCp=150/1000000;

% frequency in rad/s
ws=2*pi*fs;

%phase voltage
Vph=Vline/(3^0.5);

%impedance of Rc and XM
Zm=Rc*i*Xm/(Rc+i*Xm);

%nagnetizing current
Im=Vph/(Zm);

%set count to zero
n=0;

%step slip from 1 to 0.0025 in decriments of 0.0025
for s=1:-0.0025:0.0025

%increament count for index
n=n+1;

if s==0;

    %slip should not be zero but in case it is set to zero
    I2=0;
    I22=0;
    T(n)=0;
    T1(n)=0;
else

    %impedance of rotor
    Z2r=((R2/s)+i*X2r);

    %impedance of rotro in parallel with magnetizing impedance
    Zrin=Zm*Z2r/(Zm+Z2r);

    %total impedance including stator resistance and reactance
    Zin=Zrin+R1+i*X1r;
```

```
I2=Vph/(R1+(R2/s)+i*X12);

%Star-delta works at slip greater than 0.33. It is assumed the motor is
%normally delta connected
if s>=0.33

    %when reconnected as star the voltage is decreased by sqrt(3)
    Vphdelta=Vph/sqrt(3);

    %when reconnected as start the impedance increase by 3
    R2delta=R2*3;
    Zindelta=Zin*3;
else

    %When below s=0.33 the motor is connected as normal
    Vphdelta=Vph;
    R2delta=R2;
    Zindelta=Zin;
end

%when s>=0.6 the autotranformer supplies 60 % voltage
if s>=0.6
    Vphauto=Vph*0.6;
    %transformer ratio
    Xt=1/0.6;

%when s<0.6 and >=0.25 the autotranformer supplies 75 % voltage
elseif s>=0.25
    Vphauto=Vph/1.5;
    %transformer ratio
    Xt=1.5;
%when s<0.25 normal operation
else
    Vphauto=Vph;
    Xt=1;
end

%in-line resistance or reactance switched in at s=1 and slowly
%decreased until s=0
sres=(s-0.1)/0.9;

%set the resistance or reactance to zero when s<0.1
if sres<0
    sres=0;
end

%set external in-line resistance (sqrt(3)-1)*|input impedance|*scaling
%factor sres
Rex=(sqrt(3)-1)*abs(Zin)*sres;
Zinres=Zin+Rex;
```

```
    %set external in-line reactance (sqrt(3)-1)*|input impedance|*scaling
    %factor sres
    Xex=(sqrt(3)-1)*abs(Zin)*sres;
    ZinXes=Zin+i*Xex;

    %calculate input current
    I22=Vph/Zin;
    %calculate rotor current using current divider
    I2r=I22*Zm/(Zm+Z2r);

    %calculate torque
    T(n)=3*P*((abs(I2r))^2)*R2/(2*s*ws);

    %calculate input current and rotor current for star-delta starting
    I22delta=Vph/(Zindelta);
    I2rdelta=I22delta*Zm/(Zm+Z2r);

    %calculate input current and rotor current for autotransformer starting
    I22auto=Vphauto/(Zin);
    I2rauto=I22auto*Zm/(Zm+Z2r);
    %tranform input motor current to input autotransfomer current
    I22auto=I22auto/Xt;

    %calculate input current and rotor current for resistance starting
    I22res=Vph/(Zinres);
    I2rres=I22res*Zm/(Zm+Z2r);

    %calculate input current and rotor current for reactance starting
    I22Xes=Vph/(ZinXes);
    I2rXes=I22Xes*Zm/(Zm+Z2r);

    %calcuate torques for different methods
    Tdelta(n)=3*P*((abs(I2rdelta))^2)*R2delta/(2*s*ws);
    Tres(n)=3*P*((abs(I2rres))^2)*R2/(2*s*ws);
    TXes(n)=3*P*((abs(I2rXes))^2)*R2/(2*s*ws);
    Tauto(n)=3*P*((abs(I2rauto))^2)*R2/(2*s*ws);
end

%calcuate absolute values of input currents
Iin(n)=abs(I22);
Iindelta(n)=abs(I22delta);
Iinres(n)=abs(I22res);
IinXes(n)=abs(I22Xes);
Iinauto(n)=abs(I22auto);

%calculate input power and reactive powers
Pin(n)=3*real(Vph*(I22))/1000;
Qin(n)=-3*imag(Vph*(I22))/1000;
Pindelta(n)=3*real(Vph*(I22delta))/1000;
```

```
Qindelta(n)=-3*imag(Vph*(I22delta))/1000;
Pinres(n)=3*real(Vph*(I22res))/1000;
Qinres(n)=-3*imag(Vph*(I22res))/1000;
Pinauto(n)=3*real(Vph*(I22auto))/1000;
Qinauto(n)=-3*imag(Vph*(I22auto))/1000;
PinXes(n)=3*real(Vph*(I22Xes))/1000;
QinXes(n)=-3*imag(Vph*(I22Xes))/1000;

%calculate speeds
Speed(n)=2*60*fs*(1-s)/P;

end

%set a count value based on previous slip iteration loop
ns=n+1;

%set flag for point of full load
kpos=0

%go back from s=0.0025 to find full load point
for s=0.0025:0.0025:1

    %decrement count
    ns=ns-1;

    %calcuate motor output power
    Pmot=T(ns)*Speed(ns)*2*pi/60;

    %find point were motor power is higher than rated or full power
    if (Pmot>Prated)

        %if condition met check flag to see if this is first time met
        if kpos==0

            %set full load torque, speed, current, power, reactive
            %power, and slip
            Tload=T(ns);
            SpeedL=Speed(ns);
            CurrentL=Iin(ns);
            PowerL=Pin(ns);
            QL=Qin(ns);
            sl=s;

            %set flag to full load point found
            kpos=1
        end
    end
end

%calculate a cubic function load with speed^2 coefficent = 0.85, speed
```

```
%coefficent is 0.1 and constant term is 0.05
TL1=Tload/20;
TL2=Tload*0.1;
TL3=Tload*0.85;

%set count to zero
n=0;

%calculate typical load across slip range
for s=1:-0.0025:0.0025;
    n=n+1;
TL(n)=TL1+TL2*(1-s+s1)+TL3*(1-s+s1)^2;
end

%plot torques
p=plot(Speed,T,Speed,Tdelta,Speed,Tauto,Speed,Tres,Speed,TXes,Speed,TL,
SpeedL,Tload,"*");
 p(1).LineWidth = 2;
 p(2).LineWidth = 0.5;
 p(3).LineWidth = 1;
 p(4).LineWidth = 1;
 p(5).LineWidth = 1;
 p(6).LineWidth = 1;
 p(7).MarkerEdgeColor =[0.25, 0.25, 0.25];
 p(7).MarkerSize = 12;
 lgd = legend('DOL','Star-Delta','AutoTx','High Res','Phase Angle Control',
 'Load Torque','Full Load Torque');
grid on;
xlabel('Speed / rpm');
ylabel('Torque / Nm');

%plot currents
input('Press RETURN for Current/speed curve');
p=plot(Speed,Iin,Speed,Iindelta,Speed,Iinauto,Speed,Iinres,Speed,IinXes,
SpeedL,CurrentL,"*");
 p(1).LineWidth = 0.5;
 p(2).LineWidth = 1;
 p(3).LineWidth = 1;
 p(4).LineWidth = 1;
 p(5).LineWidth = 1;
 p(6).MarkerEdgeColor =[0.25, 0.25, 0.25];
 p(6).MarkerSize = 12;
  lgd = legend('DOL Current','Star-Delta','AutoTx','High Res',
  'Phase Angle Control','Full load current');
xlabel('Speed / rpm');
ylabel('Line current / A');
grid on;

%plot powers
input('Press RETURN for P/speed curve');
```

```
p=plot(Speed,Pin,Speed,Pindelta,Speed,Pinauto,Speed,Pinres,Speed,PinXes,SpeedL,
PowerL,"*");
 p(1).LineWidth = 0.5;
 p(2).LineWidth = 2;
 p(3).LineWidth = 1;
 p(4).LineWidth = 1;
 p(5).LineWidth = 1;
 p(6).MarkerEdgeColor =[0.25, 0.25, 0.25];
 p(6).MarkerSize = 12;
 lgd = legend('DOL Current','Star-Delta','AutoTx','High Res',
 'Phase Angle Control','Full load Pin');
grid on;
xlabel('Speed / rpm');
ylabel('P / kW');

%plot reactive powers;
input('Press RETURN for Q/speed curve');
%yyaxis right
p=plot(Speed,Qin,Speed,Qindelta,Speed,Qinauto,Speed,Qinres,Speed,QinXes,
SpeedL,QL,"*");
 p(1).LineWidth = 0.5;
 p(2).LineWidth = 2;
 p(3).LineWidth = 1;
 p(4).LineWidth = 1;
 p(5).LineWidth = 1;
 p(6).MarkerEdgeColor =[0.25, 0.25, 0.25];
 p(6).MarkerSize = 12;
 lgd = legend('DOL Current','Star-Delta','AutoTx','High Res',
 'Phase Angle Control','Full load Qin');
xlabel('Speed / rpm');
ylabel('Q / kVArs');
grid on;
```

Appendix C

Matlab Code for Comparing Capacitor Compensation for Different Machines

```
clear

%  PROGRAM TO CALCULATE EFFECTS OF CAPACITORS ON STARTING FOR INDUCTION
% MOTOR 2021

%  MOTOR PARAMETERS FOR 7 MOTORS USED

%Motordata = [P f vline Rc Xm R1 R2 X12 Prated

Motordata(1:9,1) = [4, 50, 220, 81, 58, 2.13, 1.33, 2.99, 1500];
Motordata(1:9,2) = [4, 50, 400, 1568.2, 115.2, 1.325, 3.87, 8.44, 1500];
Motordata(1:9,3) = [4, 60, 440, 900, 110, 1.2, 1.56, 6, 3750];
Motordata(1:9,4) = [4, 50, 400, 178.1, 5.13, 0.059, 0.013, 0.48, 45000];
Motordata(1:9,5) = [2, 50, 3300, 1333, 118, 0.79, 0.57, 5.75, 200000];
Motordata(1:9,6) = [6, 50, 6000, 900.0, 102.5, 0.97, 0.24, 4.78, 1000000];
Motordata(1:9,7) = [12, 60, 6900, 600.0, 46.0, 0.083, 0.080, 2.60, 3750000];

%set motor number to analize
n=7;

%put into motor calculation parameters
P=Motordata(1,n);
fs=Motordata(2,n);
Vline=Motordata(3,n);
Rc=Motordata(4,n);
```

```
Xm=Motordata(5,n);
R1=Motordata(6,n);
R2=Motordata(7,n);
X12=Motordata(8,n);

%split X1 and X2 equally
X1r=X12/2;
X2r=X12/2;

%freq in rad/sec
ws=2*pi*fs;

%phase voltage
Vph=Vline/(3^0.5);

%impedance of paralle combination of Rc and Xm
Zm=Rc*i*Xm/(Rc+i*Xm);

%magnetizing current
Im=Vph/(Zm);

%set count to zero
n=0;

%step slip from 1 to 0.0025 in decreaments of 0.0025
for s=1:-0.0025:0.0025;

    %increment count for index
    n=n+1;

    if s==0;

        %slip should not be zero but in case it is set to zero
        I2=0;
        I22=0;
        T(n)=0;
        T1(n)=0;
    else

        %impedance of rotor
        Z2r=((R2/s)+i*X2r);

        %impedance of rotor and magnetizing impedances
        Zrin=Zm*Z2r/(Zm+Z2r);

        %total input impedance
        Zin=Zrin+R1+i*X1r;
        %current using starting approximaate circuit
        I2=Vph/(R1+(R2/s)+i*X12);
```

```
    %input current from correct per-phase equivalent circuit
    I22=Vph/Zin;

    %rotor current from current divider
    I2r=I22*Zm/(Zm+Z2r);

    %torque using rotor current and R2/
    T(n)=3*P*((abs(I2r))^2)*R2/(2*s*ws);

end

%calculate input current, power factor, input power and reactive power
Iin(n)=abs(I22);
PF(n)=-real(I22)/Iin(n)*imag(I22)/abs(imag(I22));
Pin(n)=3*real(Vph*(I22))/1000;
Qin(n)=-3*imag(Vph*(I22))/1000;

%calculate required capacitive reactance to correct current to unity PF
Xcc=3*Vline^2/(Qin(n)*1000);

%calculate initial capacito required at s = 1
if n==1
    CapM=1/(Xcc*2*3.1415*fs);
end

%calculate capacitance across whole slip range, convert to mircoF
Cap1=1/(Xcc*2*3.1415*fs);
Cap(n)=Cap1*1000000;

%calculate speed
Speed(n)=2*60*fs*(1-s)/P;

%calculate efficiency
Eff(n)=T(n)*2*(1-s)*ws*100/(P*Pin(n));

%calculate capacitor current using capacitor at start
Icap1=i*Vline*2*pi*fs*CapM*sqrt(3);

%calculate total input current magnitude
Itot1(n)=abs(I22+Icap1);

%calculate PF
PF1(n)=-real(I22+Icap1)/Itot1(n)*imag(I22+Icap1)/abs(imag(I22+Icap1));

%calculate capacitor current using half value of capacitor at start
Icap2=i*Vline*2*pi*fs*CapM/2*sqrt(3);
Itot2(n)=abs(I22+Icap2);
PF2(n)=-real(I22+Icap2)/Itot2(n)*imag(I22+Icap2)/abs(imag(I22+Icap2));

%calculate capacitor current using third value of capacitor at start
```

```
    Icap3=i*Vline*2*pi*fs*CapM/3*sqrt(3);
    Itot3(n)=abs(I22+Icap3);
    PF3(n)=-real(I22+Icap3)/Itot3(n)*imag(I22+Icap3)/abs(imag(I22+Icap3));

end
%plot torque and speed together
yyaxis left
plot(Speed,T);
grid on;
xlabel('Speed / rpm');
ylabel('Torque / Nm');
yyaxis right
plot(Speed,Iin);
ylabel('Line current / A');
grid on;

%plot power and reactive power together
input('Press RETURN for PQ/speed curve');
yyaxis left
plot(Speed,Pin);
grid on;
xlabel('Speed / rpm');
ylabel('P / kW');
yyaxis right
plot(Speed,Qin);
ylabel('Q / kVArs');
grid on;

%plot required capacitance across speed range
input('Press RETURN for required capacitor/speed curve');
plot(Speed,Cap);
xlabel('Speed / rpm');
ylabel('Capacitance / microF');
grid on;

%plot currents for different capacitor compensation and motor current
input('Press RETURN for Improved current/speed curve');
plot(Speed,Itot1,Speed,Itot2,Speed,Itot3,'k-.',Speed,Iin);
grid on;
xlabel('Speed / rpm');
ylabel('Current / A');

%legend includes capacitor values
Fullcap1= strcat('Total current: Full capacitor ={ }',
num2str(int16(CapM*1000000)),' microF');
Fullcap2= strcat('Total current: Half capacitor ={ }',
num2str(int16(CapM*1000000/2)),' microF');
Fullcap3= strcat('Total current: Third capacitor ={ }',
num2str(int16(CapM*1000000/3)),' microF');
lgd = legend(Fullcap1,Fullcap2,Fullcap3,'Motor Current');
```

Appendix D

Published Papers

D.1 IEEE International Conference on Power, Control, Signals and Instrumentation Engineering (ICPCSI-2017)

Methods to Reduce the Starting Current of an Induction Motor

M. Habyarimana and D. G. Dorrell
University of KwaZulu-Natal
School of Engineering
Howard College Campus
Durban, 4041, South Africa
E-mail: 213573647@stu.ukzn.ac.za and dorrelld@ukzn.ac.za

***Abstract*— An inrush current is produced when an electric load is turned on. For an induction motor this current can reach 5-10 times the full-load current. This transient current can cause issues in large machines attached to weak grid connections. To protect the grid connection this paper explores ways that the starting current can be reduced. Standard starting techniques are reviewed then the starting energy and reactive power requirements are examined by way of example. These illustrate that to some degree the starting current can be reduced with a tuned capacitor bank; however, for better reduction then an energy storage unit is used, such as a battery or a storage capacitor, and this is accessed through a PWM inverter for charging and discharging.**

***Keywords*— Induction motor, starting, efficiency.**

I. INTRODUCTION

The inrush current, also called input surge current or switch-on surge, occurs when an electrical device is first turned on. AC or DC electric motors and transformers may draw several times their normal full-load current when first energized as the machine starts and runs up to speed. High torque is required when an electric motor is first switched on and accelerated [1]. High and unbalanced starting current causes start oscillation and can harm the shaft, gears, belt, etc. The starting current can be large in high power systems. If the motor is connected to a weak power system, the sudden high current can cause a temporary voltage drop, not only at the motor terminals, but the entire power bus feeding the starting motor. In this paper we will examine the induction motor starting current. The starting current of the induction motor is given by [2].

$$I = \frac{\text{(Rated HP) (Code Letter Factor)} \times 100}{\sqrt{3} \times V} \qquad (1)$$

and generally, it is 5 to 10 times the full load current.

II. STARTING CURRENT REDUCTION

A. Direct Online

There are several methods for starting an induction motor: direct-on-line (DOL) starting, star-delta starting, auto-transformer starting, and reactor or resistor starting [3]; other starting techniques are also used, often with the aim of reducing the inrush currents while maintaining the starting torque.

This paper is funded by the eThekwini ED-TEA programme and supported by Eskom EPPEI Centre of excellence in HVDC and FACTS.

978-1-5386-0814-2/17/$31.00 ©2017 IEEE

DOL starting is the main way of starting an machine without reducing the supply voltage to the motor. The starting current in a DOL start is in the range of 5 to 8 times than the motor full load current rating [4], while the transient starting torque oscillation can produce torque peaks that are up to 3 times higher than the rated torque. A typical transient torque is shown in Fig. 2. This generates mechanical stress on the machine which can affect service life [5]. DOL starting is often using in applications below 25 kW and when the starting load is relatively light [3].

B. Star-delta starter

The voltage per phase supplied to each winding is reduced by $1/\sqrt{3}$ when the windings are connected in star. For a delta connected machine (DOL start), if the phase current in each stator winding is V_s/Z_s, where the voltage across a phase winding is the line voltage V_s and input impedance of a phase winding is Z_s at standstill, the line current to the motor is $I_{st(delta)} = \sqrt{3} \times V_s/Z_s$. If the machine is star connected then the applied winding voltage is reduced by $\sqrt{3}$ while the line current is now equal to the phase current so that $I_{st(star)} = (1/\sqrt{3}) \times V_s/Z_s$. Hence, the starting current using a star-delta starter is 1/3 of the starting current during a DOL. This also reduces the starting torque by 3. However, the star-delta starter has some disadvantages [6]:

- Low starting torque
- Six terminal motor required
- It requires two sets of cables from starter to motor
- The starting torque is reduced by 3 and heavy stresses and transients are produced when switching from star to delta connections during un-up
- Star-delta starter will not be able to start a motor with a high starting torque

C. Autotransformer

For the autotransformer starting method, the torque is reduced as the square of the applied voltage: taps on the autotransformer allow for a variable selection of the starting current and torque and gives more flexibility than the star-delta starter [4]. When the machine is connected to lower voltage taps then the starting current and toque are reduced. If machine is left connected at this lower tap setting then the machine will operate at a higher slip and slightly lower speed at steady state which will increase the machine current and reduce the efficiency.

Reference [4] conducted an experimental study in order to compare DOL, star-delta and autotransformer starting methods for small motors of less than 3 HP. The results are shown in Table I. These are also applicable to large machines although there will be differences in supply requirements in terms of p.u. current, power and reactive power demands, and the p.u. torque performance.

TABLE I. DOL, STAR-DELTA AND AUTOTRANSFORMER STARTING METHODS COMPARISON [4]

Criteria	Direct-On- Line	Star Delta	Autotransformer
Inrush Current	High	Low	Low
Voltage Sags	Severe > 0.5 p.u.	Less Severe < 0.2 p.u.	Less Severe < 0.2 p.u.
Harmonics	Less (THD < 1%)	Less (THD < 1%)	Severe during starting (THD = 18.9%)
Transients	Severe	Less Severe	Severe

The major drawback of the autotransformer is the cost; the circuit for the transformer and switching is quite complex therefore much more expensive [7].

D. Reactor or resistor starting

From the torque equation, the three phase induction motor has the starting torque roughly relative to the square of the connected voltage, the torque given by [8]:

$$T = K_1 E_2 I_2 \cos\phi_2 \tag{2}$$

If X_2 is the standstill rotor reactance and R_2 the rotor resistance per phase then

$$Z_2 = \sqrt{R_2^2 + X_2^2} \tag{3}$$

Which is the rotor impedance at standstill so that

$$I_2 = \frac{E_2}{Z_2} = \frac{E_2}{\sqrt{R_2^2 + X_2^2}} \text{ and } \cos\phi_2 = \frac{R_2}{\sqrt{R_2^2 + X_2^2}} \tag{4}$$

Therefore, starting torque can be given as

$$T_{st} = K_1 E_2 \frac{E_2}{\sqrt{R_2^2 + X_2^2}} \times \frac{R_2}{\sqrt{R_2^2 + X_2^2}} = \frac{K_1 E_2^2 R_2}{R_2^2 + X_2^2} \tag{5}$$

The constant $k_1 = \frac{3p}{\omega_o}$ where p is the pole-pair number and ω_s is the supply frequency in rad/s, so that

$$T_{st} = \frac{3p}{\omega_s} \frac{E_2^2 R_2}{R_2^2 + X_2^2} \tag{6}$$

The condition to have a maximum starting torque is that, in the first instance, if the supply voltage V is constant, E_2 and ϕ_2 must be kept constant. Hence

$$T_{st} = k_2 \frac{R_2}{R_2^2 + X_2^2} \tag{7}$$

where $k_2 = \frac{3p}{\omega_s} E_2^2$

Continuing on from this, the maximum starting torque is then obtained when the standstill rotor reactance and the resistance are equal; i.e

$$R_2^2 + X_2^2 = 2R_2^2 \tag{8}$$

The starting torque is a function of the voltage squared. This means, if the applied voltage is 50 % of the rated value, the starting torque will be only 25 % of its normal voltage value. This method (resistor starting method) is generally used for smooth starting of small induction motors. It is not recommended to use this type of starting method with high starting torque requirements.

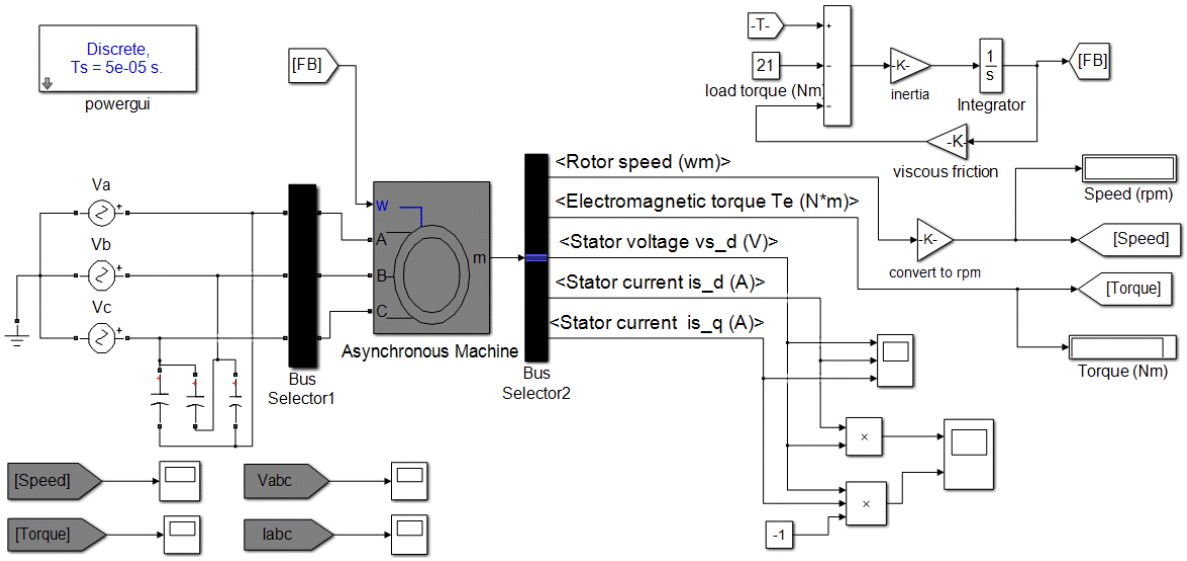

Fig. 1. Simulink model used.

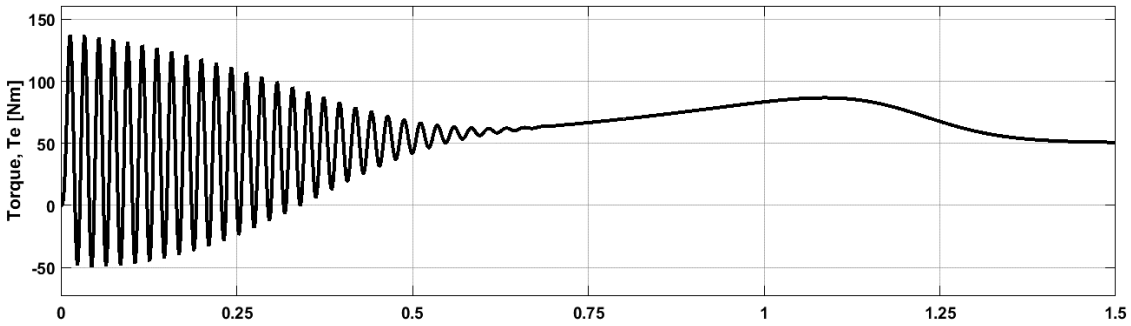

Fig. 2. Induction motor starting on DOL; torque waveform.

E. Soft starter

The control of the current flow and the voltage applied to the motor is achieved by means of electrical soft starters which use solid state devices. They are normally connected in series with the motor, or else inside the delta loop of a delta connected motor, and the voltage applied to each winding can be controlled. Typically, the voltage is controlled by thyristors [9] using phase angle control where the phase turn-on is delayed by the thyristor; this is relatively old technology. The technique of the voltage ramp has been proposed to reduce the starting current for preventing motor speed ripple and reducing the starting current.

As an alternative, a three-phase induction motor can also be started from a single-phase inverter as illustrated in [10]. The inverter is connected across two phases of a delta connected machine and the third phase is connected to the inverter via a capacitor to give a phase shifted third voltage point. This is only suitable for a small machine.

The benefit of a soft starter is to provide less stress due to smooth acceleration and pulsating torque. Compared to direct starting, this method reduces the line current during the transient start. When compared to using a full 3-phase PWM inverter, a thyristor soft starter is not able to control the speed, thus unsuitable for applications requiring speed control. Soft starters are classified among five types of equipment generating that generate harmonics. This are: switched mode power supplies, fluorescent lighting ballasts, variable speed DC drives, uninterruptible power supplies and magnetic-cored devices. Soft starters inject harmonic currents into the system which can disrupt other processes [11].

F. Discussion

For a star-delta starter, the three windings are brought out separately via six wires, and the motor starts at reduced voltage in star formation, then switches to delta connection (full line voltage) when the speed has built up. They are cheap since the starter can be formed from contactors and a time delay. They can solve many problems although the inrush current is not eliminated completely. Older motors sometimes have built-in starting arrangements, such as wound rotor machines where a starter resistor is switched in to the rotor circuit (using slip-rings) [13] but these are now obsolete.

III. Energy and Reactive Power Requirement

In this research the starting behavior of squirrel cage induction motors is investigated in order assess their requirements. Fig. 1 shows the SIMULINK model used to assess the motor performance. A 5 HP machine was used and the simulation for the starting torque is shown in Fig. 2. To compensate for the reactive power during starting then a parallel capacitor bank can be used with the motor, either star of delta connected. The capacitances can be calculated for the starting transient and disconnected when the machine has run up to speed. This will help reduce the starting current. When the machine reaches steady-state the capacitors will be over compensating for the current and thus should be disconnected. To improve the running power factor then a different set of capacitors can be used since less reactive power is required. This method will not reduce the starting torque. When a further reduction in starting current is required then an energy storage device can be used to supply the extra power required to start the machine; the inertia in the system means there is stored energy to be put into the system.

The amount of energy required in the device can be calculated by an integration of the additional power during the starting transient. To realize this type of device then a battery or supercapacitor is used on the DC side of a PWM inverter and the inverter AC side is connected in parallel with the motor. This will supply both power and reactive power to the system. To measure the instantaneous power and reactive power then the 3-phase voltages and currents can be resolved into a synchronously rotating d-q axes set so that

$$\begin{bmatrix} v_d \\ v_q \end{bmatrix} = \begin{bmatrix} \cos(\omega t) & \cos\left(\omega t + \frac{2\pi}{3}\right) & \cos\left(\omega t - \frac{2\pi}{3}\right) \\ \sin(\omega t) & \sin\left(\omega t + \frac{2\pi}{3}\right) & \sin\left(\omega t - \frac{2\pi}{3}\right) \end{bmatrix} \begin{bmatrix} v_a \\ v_b \\ v_c \end{bmatrix}$$

$$v_a = \hat{V}_{ph}\cos(\omega t + \theta); \quad v_b = \hat{V}_{ph}\cos\left(\omega t - \frac{2\pi}{3} + \theta\right); \quad (9)$$

$$v_c = \hat{V}_{ph}\cos\left(\omega t + \frac{2\pi}{3} + \theta\right)$$

A similar set exists for the currents. If for the voltage set $\theta = 0$ then the synchronous rotating d-q voltages reduce to only v_d, and $v_q = 0$. The instantaneous power and reactive power are then

$$p(t) = v_d i_d + v_q i_q = v_d i_d$$
$$q(t) = v_q i_d - v_d i_q = -v_d i_q \quad (10)$$

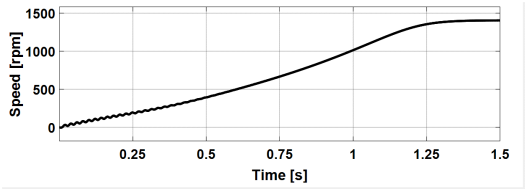

Fig. 3. Induction motor starting using DOL speed waveform.

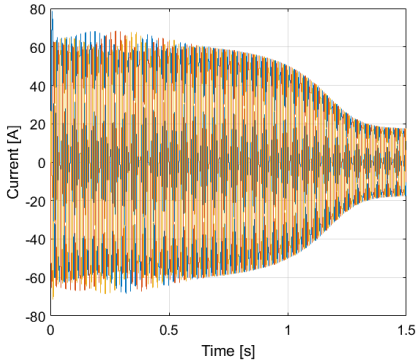

Fig. 4. Transient start current for the machine (all three phases).

The instantaneous power in the system is

$$p(t) = v_d i_d\big|_{v_q=0} = v_a i_a + v_b i_b + v_c i_c = \left(\frac{3}{2} v_a i_a\right)\Big|_{t=0} \quad (11)$$

if phase *a* is maximum at $t = 0$ and there is unity power factor. If there is unity power factor so that there is only v_d and i_d then

$$p = \int_0^{1/f} v_d i_d dt = \hat{v}_d \hat{i}_d = 3\,\mathrm{Re}\left[\overline{V}_{ph} \overline{I}_{ph}\right]$$
$$v_d = \sqrt{3} V_{ph} \quad i_d = \sqrt{3} I_{ph} \quad (12)$$

IV. Simulation Results

For the simulation work, a 5 HP motor was model was utilized. The machine was a 60 Hz, 1800 rpm, 440 V induction motor; though for this simulation 50 Hz was used. The equivalent circuit parameters are: $R_1 = 1.5\ \Omega$, $R_2' = 1.2\ \Omega$, $X_1+X_2' = 6\ \Omega$, $R_C = 900\ \Omega$ and $X_m = 110\ \Omega$ with full load current of about 7 A. The leakage reactances were equally split for the simulation. The inertia was adjusted to give a reasonable starting time. Fig. 3 shows the speed obtained when the motor is connected on DOL. The speed is steady after 1.25 s.

Fig. 4 shows the 3-phase currents during the start. Fig. 5 shows i_d and i_q during the start. This illustrates that high i_q required during the start period. The torque is also shown earlier in Fig. 2 which is typical for this size of machine. The real and reactive power drawn (Fig. 6) shows that the reactive power demand during starting is higher than the real power demand. When steady state is reached the reactive power requirement falls back and the power factor improves. These waveforms are obtained from the synchronous d and q axis equations in (10). One point is that the Simulink modules work with the *d* and *q* values for the voltages and current being the peak values of the *abc* phase values. The difference has been left here to illustrate that when converting to d-q and using synchronous components, the scaling should be carefully considered. Therefore, according to (10) the Simulink power and reactive power using the module d-q values needs to be scaled by 3/2 in accordance to (11).

A basic requirement could be to reduce the reactive power during starting using a connected capacitor bank. In Fig. 4, it can be seen the starting current is about 42 Arms. There is about 30 kVAr at start (scaled from 20 kVAr as explained above) of reactive power and 20 kW of real power. This corresponds, at 440 V line start, to 26.2 A for the in-phase current for the phase (real power requirement) and 39.4 A for the quadrature component of the phase current. The phase current at start is then 47.3 A. These are rms values; the peak start phase current is then 67 A and this is illustrated in Fig. 4. Approximately 30 kVAr is required so that the capacitor value (for star-connected bank) to compensate for the reactive start current (Fig. 6) at start is

$$X_c = \frac{3V_{ph}^2}{Q_{start}} = \frac{3\times 254^2}{35000} = 5.525\ \Omega$$
$$C = \frac{1}{2\pi 50 \times X_c} = 576\ \mu\mathrm{F};\quad I_c = \frac{254}{5.525} = 45.9\ \mathrm{A} \quad (13)$$

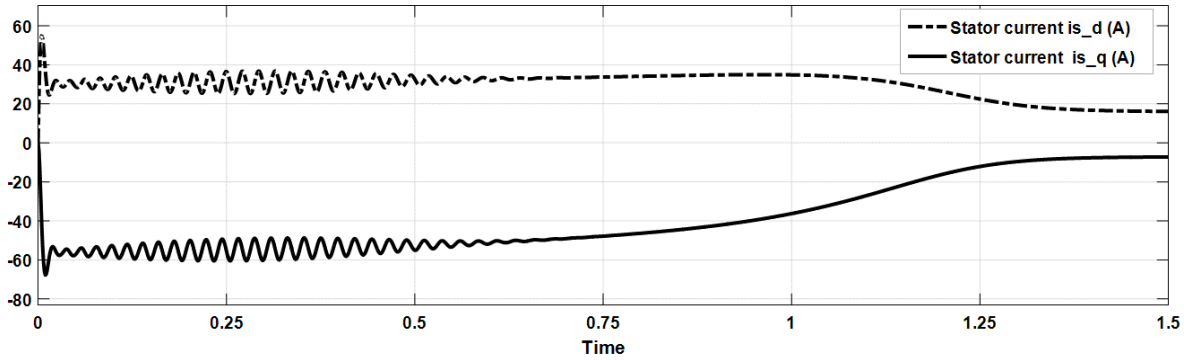

Fig. 5. Induction motor starting on DOL; torque waveform.

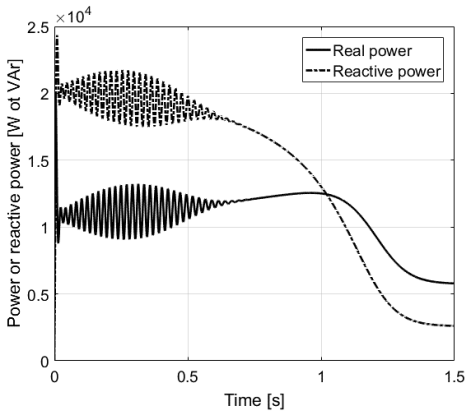

Fig. 6. Induction motor starting – real and reactive power requirement (these need to be scaled up by 3/2 as discussed in the text).

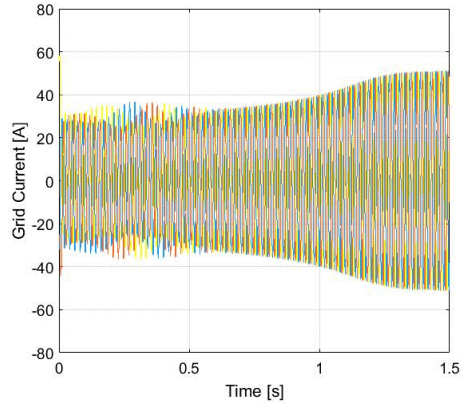

Fig. 7. Transient grid current with 493 μF capacitor compensation (all three phases).

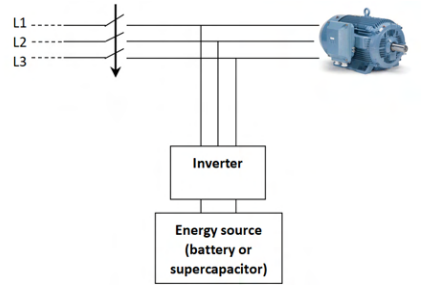

Fig. 8. The simple circuit diagram.

Fig. 7 gives the transient grid current with this compensation. The starting current should be about 26 Arms, which is about 37 A peak and the starting current in Fig. 7 is close to this. It can be seen that when steady-state is reached then the system is over compensated and the capacitors should be switched out. This illustrates that the starting current is more than halved using capacitor compensation at start. To further reduce the starting current then an active energy input must be used to reduce the input power as well as in the input reactive power (Fig. 8).

To compensate for the real energy, we require an energy source that can provide the energy under the starting curve for the real power in Fig. 6. If we assume this to be about 15 kW (remembering to scale by 3/2) for 1.5 s then this is

$$E_{start} = 1500 \times 1.5 = 22500 \text{ J} = 6.25\text{W-hours}$$

which is quite low. However, for large machines this will be far more substantial and this will be the focus of further work.

V. CONCLUSION

This paper reports some initial investigations into the starting mechanism of an induction motor by examining the starting characteristics in terms of its instantaneous power and reactive power. By tuning compensation capacitors, it is possible to reduce the current by maybe 50 %. This is for a small 5 HP machine and different machines will be investigated and tested. Further current reduction can be obtained by using active power compensation but this will require energy storage and an inverter (Fig. 8); however, it will be more controllable. This will also be the focus of further work.

VI. REFERENCES

[1] J. Larabee, B. Pellegrino, and B. Flick, "Induction motor starting methods and issues," *IEEE Industry Applications Society 52nd Annual Petroleum and Chemical Industry Conference*, 2005, pp. 217-222.

[2] S. Pandey, S. Bahadure, K. Kanakgiri, and N. Singh, "Two-phase soft start control of three-phase induction motor," *IEEE 6th International Conference on Power Systems (ICPS)*, 2016, pp. 1-6.

[3] V. Cohen, "Induction motors-protection and starting," *Elektron Journal-South African Institute of Electrical Engineers*, vol. 12, pp. 5-10, 1995.

[4] H. Goh, M. Looi, and B. Kok, "Comparison between direct-on-line, Star-Delta and auto-transformer induction motor starting method in terms of power quality," *Proceedings of the International MultiConference of Engineers and Computer Scientists*, 2009, pp. 18-20.

[5] M. H. Abderrazzaq, M. S. Hussin, and K. Alhayek, "The effect of high frequency, high voltage supply on the growth of electrical trees on cross linked polyethlyne insulation of power cables," *IEEE International Conference on Solid Dielectrics (ICSD)*, 2013, pp. 812-815.

[6] K. Pillay, M. Nour, K. Yang, D. D. Harun, and L. Haw, "Assessment and comparison of conventional motor starters and modern power electronic drives for induction motor starting characteristics," *IEEE Symp. Industrial Electronics & Appl., (ISIEA),* 2009, pp. 584-589.

[7] T. Orosz, Á. Sleisz, and Z. Á. Tamus, "Metaheuristic Optimization Preliminary Design Process of Core-Form Autotransformers," *IEEE Transactions on Magnetics*, vol. 52, pp. 1-10, 2016.

[8] A. A. Shaltout, "Analysis of torsional torques in starting of large squirrel cage induction motors," *IEEE Trans. on Energy Conv.*, vol. 9, pp. 135-142, 1994.

[9] J. A. Antonino-Daviu, J. Corral-Hernandez, E. Resina-Munoz, and V. Climente-Alarcon, "A study of the harmonics introduced by soft-starters in the induction motor starting current using continuous time-frequency transforms," *IEEE 13th International Conference on Industrial Informatics (INDIN)*, 2015, pp. 777-781.

[10] C. Bumroongphuck, V. Thanyaphirak, and V. Kinnares, "Soft starting method for single-phase PWM AC chopper fed three-phase induction motor," *International Conference on Electrical Machines and Systems (ICEMS),* 2013, pp. 1991-1995.

[11] P. Zhang, Y. Du, T. G. Habetler, and B. Lu, "Improving thermal recovery time for soft-starter-connected AC motors with intermittent periodic duty cycles," *IEEE Trans. on Industry Appl.*, vol. 46, pp. 1927-1935, 2010.

[12] A. P. Sloan, *My Years With General Motors*. Ed. By John Mcdonald With Catharine Stevens: Doubleday, 1963.

D.2 IEEE Southern Power Electronics Conference (SPEC-2021)

Mitigating In-rush Currents for Induction Motor Loads

Mathew Habyarimana and Remmy Musumpuka
Discipline of Electrical, Electronic and Computer Engineering
University of Kwazulu-Natal
Durban, 4041, South Africa.
hmatayoh@gmail.com
remmy.musumpuka@gmail.com

D. G. Dorrell
School of Electrical
and Information Engineering
University of the Witwatersrand
Johannesburg, South Africa
david.dorrell@wits.ac.za

***Abstract*—Power loads can have high starting. These can be a serious source of concern in weak grids. This problem is envisaged to be exacerbated by the rollout of smart microgrids. When a high power induction motor is turned on, its inrush current drawn can be more than ten times the full-load current. This transient current can cause problems in weak grid connections. The increased current is due to both power required to start the load and the increased reactive power demand during the starting process. To protect the grid connection as well as the load, energy storage units can be used to compensate for the increased power requirement. A more pragmatic approach is to reduce the reactive power requirement using tuned compensation capacitors in order to reduce the inrush current. The aim of this work is to address the selection, calculation and switching of the capacitor bank for reactive power compensation. This first requires the study of the reactive power drawn by an induction motor during starting. The capacitances are calculated and switched on to compensate the starting transient and disconnected when the machine has run up to speed using a point-on switching approach that reduces the switching transient.**

***Index Terms*—Point-on-Switching, Capacitor compensation, Inrush Current, Induction Motor.**

I. Introduction

In power systems, the inrush current, also called the input surge current or switch-on surge, of a large load can cause problems related to excessive current drawn. It has the potential to damage the system apparatus as well as the system network in weak grids. It can trip protection relays unnecessarily thereby causing voltage drops that impair the function of other equipment connected to the same system.

Inrush current is basically defined as the maximum instantaneous input current drawn by an electrical device when first turned on [1], [2]. Induction motors (IMs) switched-mode power supplies, transformers and incandescent lamps are devices that exhibit high inrush current. When there are large electro-magnetic devices then there will be a surge during switch on to establish the magnetic field. Induction motors have the transient start-up period as well as magnetization if it is direct on-line connected. During the run-up to steady-state the machine can draw between five and ten times the rated current.

If the inrush current is left unaddressed for a large load, the inrush current can cause voltage busbars to fall out of regulation. In more serious cases this results in the system exceeding the current carrying capability of the system resulting in overloading and system tripping.

Three-phase IMs are the main industrial workhorse that consume both active and reactive power [3], [4]. IMs are inductive loads that can produce a power quality problem as well as high inductive load producing power quality issues in electrical systems. In industry, capacitor banks are often used to correct poor power factor in plants.

At the time of starting of a line-connected IM, the induced voltage in the rotor is maximum because slip is maximum (s = 1). At this stage the rotor impedance is low, therefore the rotor current becomes large and the high current in the rotor reflects into the stator due to transformer action. This results in a large starting current in the stator at low power factor. Depending on the motor size and design, the value of starting torque may be low. This is particularly true for a large high-efficiency machine. This may negate the use of a high resistance or star-delta starter to restrict the starting current. These reduce the starting current but also the starting torque.

This work focuses on reducing the inrush current in induction motors by way of capacitor compensation during the starting cycle. In smaller IMs it is possible to use an inverter to reduce the starting current since it becomes a variable speed drive. However in larger IMs this will not be cost effective. If they are driving pumps and fans then variable speed is not required. During the starting cycle in large IMs, most current is for reactive power absorption and thus it is possible to compensate for this by generating reactive power using capacitors. This work will illustrate this.

During the starting of an induction motor there are also pulsating torques and unbalanced currents. Such performance is undesirable for electrical supply, mechanical gearing systems and the electrical protection unit of the machine. If the motor is connected to a weak power system, the sudden high current can cause a temporary voltage drop, not only at the motor terminals, but the entire power bus feeding the starting motor

The authors acknowledge the Eskom EPPEI Specialization Center on HVDC and FACTS, University of KwaZulu-Natal, South Africa for providing research facilities and funding for this work.

[5]. The work outlines the use of point-on switching to reduce this transient.

The induction motor is analogous to the transformer - it is formed from electrical circuits linked by a magnetic circuit. According to [6] the induction motor behaves as a transformer but with the secondary windings shorted until the rotor begins to move when an electro-mechanical energy conversion component in the rotor circuit (represented by $(1-s)/s \times R_2^{/}$) comes into play. The length of the starting transient is less if the mechanical load on the motor is reduced but most mechanical systems have a degree of inertia. For high-power motors, the winding arrangement might be changed during start-up to reduce the inrush current - this is called start-delta starting.

In this work, a model is developed that reduces inrush current in large IMs using capacitors. In many locations the grid is weak, such as in islanded microgrids and locations remote from the main grid.

II. Steady-State Power and Reactive Power

The total power P and total reactive power Q in a 3-phase AC system can be given by

$$P = \sum_{ph=1}^{3} \Re\left\{\overline{E}_{ph}\overline{I}_{ph}^{*}\right\} \tag{1}$$

and

$$Q = \sum_{ph=1}^{3} \Im\left\{\overline{E}_{ph}\overline{I}_{ph}^{*}\right\} \tag{2}$$

where ph is the phase number, $\overline{E}_{ph}$ is the phase voltage phasor and $\overline{I}_{ph}$ is the phase current phasor. These are rms values.

The induction motor is a three wire system so that the fourth neutral line is not available for obtaining the the phase voltages. The "two wattmeter" method can be used to measure the total power where

$$P = \sum_{ph=1}^{3} \Re\left\{\left(\overline{E}_1 - \overline{E}_2\right)\overline{I}_2^{*} + \left(\overline{E}_3 - \overline{E}_2\right)\overline{I}_2^{*}\right\} \tag{3}$$

this is a well know relationship and will work for an unbalanced 3-phase system.

Less well know is that two wattmeters can be used to measure the reactive power too. However this is for a balanced system. For this it is assumed that

$$\overline{I}_1 = \frac{j}{\sqrt{3}}\left(\overline{I}_2 - \overline{I}_3\right) \tag{4}$$

The total reactive power is obtained by considering the reactive power in the a-phase and multiplying by three

$$\begin{aligned} Q =& 3\Im\left\{\overline{E}_1\overline{I}_1^{*}\right\} = 3\Im\left\{\frac{j}{\sqrt{3}}\overline{E}_1\left(\overline{I}_2^{*} - \overline{I}_3^{*}\right)\right\} \\ =& \Re\left\{\frac{1}{\sqrt{3}}\overline{E}_1\left(\overline{I}_2^{*} - \overline{I}_3^{*}\right)\right\} = \sqrt{3}\Re\left\{\overline{E}_1\overline{I}_2^{*} - \overline{E}_1\overline{I}_3^{*}\right\} \end{aligned} \tag{5}$$

Again, the reactive power can be obtained using two wattmeters.

In a modern 3-phase power analyser the power factor and reactive power is electronically calculated but the connections often require the two wattmeter connection.

III. Instantaneous Power and Reactive Power

Real and reactive power flow are associated with averaged values over a cycle in a sinusoidal AC system. However, during the transient starting sequence is it convenient to give instantaneous power and reactive power. Since reactive power is associated with the cycling of energy in an AC system then for instantaneous reactive power to have meaning then the transient starting cycle is assumed to be much longer than the supply period.

A. Park's Transformation

A 3-phase system can be converted to a 2-phase system using Park's Transformation (abc-to-dq0). This allows the forwards, backwards and zero order components to be accounted for. However, there will be no zero order currents going into an induction motor because the machine is either delta-connected or star-connected with now earth on the start point. The 2-axis reference frame is either static or rotating. In this work it is assumed to be static $\alpha-\beta$ axes where α corresponds with the a-axis of the 3-phase system. This is illustrated in Fig. 1.

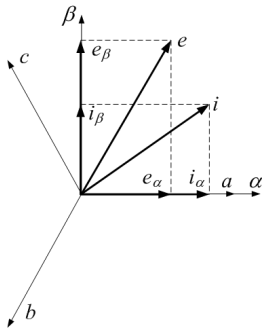

Fig. 1. $\alpha-\beta$ transformation.

The transformations from 3-phases to 2-phases for the voltages and currents are

$$\begin{bmatrix} e_\alpha \\ e_\beta \end{bmatrix} = \sqrt{\frac{2}{3}}\begin{bmatrix} 1 & -\frac{1}{2} & -\frac{1}{2} \\ 0 & \frac{\sqrt{3}}{2} & -\frac{\sqrt{3}}{2} \end{bmatrix}\begin{bmatrix} e_a \\ e_b \\ e_c \end{bmatrix} \tag{6}$$

and

$$\begin{bmatrix} i_\alpha \\ i_\beta \end{bmatrix} = \sqrt{\frac{2}{3}}\begin{bmatrix} 1 & -\frac{1}{2} & -\frac{1}{2} \\ 0 & \frac{\sqrt{3}}{2} & -\frac{\sqrt{3}}{2} \end{bmatrix}\begin{bmatrix} i_a \\ i_b \\ i_c \end{bmatrix} \tag{7}$$

With voltages e_α, e_β and currents i_α, i_β instantaneous voltages. These can be vectorized so that

$$\overline{e} = e_\alpha + je_\beta \tag{8}$$

and

$$\overline{i} = i_\alpha + ji_\beta \tag{9}$$

B. Instantaneous power

The instantaneous power p of a three-phase circuit is represented generally by

$$p = e_a i_a + e_b i_b + e_c i_c \tag{10}$$

In $\alpha - \beta$ coordinates, p is expressed as:

$$p = e_\alpha i_\alpha + e_\beta i_\beta \tag{11}$$

Moving from 3-phase to a 2-phase system means that the power in one phase of the two phase system is 3/2 times that in one phase of the 3-phase system. Using (6) and (7) then for the α phase

$$e_\alpha = \sqrt{\frac{2}{3}}\left(e_a - \frac{1}{2}e_b - \frac{1}{2}e_c\right) \tag{12}$$

and

$$i_\alpha = \sqrt{\frac{2}{3}}\left(i_a - \frac{1}{2}i_b - \frac{1}{2}i_c\right) \tag{13}$$

To verify this balances then assume the a-phase voltage is peaking and the power factor is unity. If the system is a balanced 3-phase system then:

$$e_b = e_c = -0.5\hat{e}_a \text{ and } i_b = i_c = -0.5\hat{i}_a$$

so that working through from (12) gives

$$\hat{e}_\alpha = \sqrt{\frac{2}{3}}\left(\hat{e}_a + \frac{1}{4}\hat{e}_a + \frac{1}{4}\hat{e}_a\right) = \sqrt{\frac{3}{2}}\hat{e}_a \tag{14}$$

and

$$\hat{i}_\alpha = \sqrt{\frac{2}{3}}\left(\hat{i}_a + \frac{1}{4}\hat{i}_a + \frac{1}{4}\hat{i}_a\right) = \sqrt{\frac{3}{2}}\hat{i}_a \tag{15}$$

So the peak instantaneous power in the α phase is

$$\hat{e}_\alpha \hat{i}_\alpha = \frac{3}{2}\hat{e}_a \hat{i}_a \tag{16}$$

which validates the Park's Transform and gives the correct ratio between the peak power in the a-phase and α-phase.

It is worth looking at how the power instantaneously. Assuming that the 3-phase set is sinusoidal and balanced then (10) can be rewritten as

$$\begin{aligned} p =& \hat{e}\hat{i}\sin^2(\omega t) + \hat{e}\hat{i}\sin^2(\omega t - 120°) \\ &+ \hat{e}\hat{i}\sin^2(\omega t + 120°) \\ =& \frac{3\hat{e}\hat{i}}{2}\left((1 + \cos(2\omega t)\right) \\ &+ \cos(2\omega t + 120°) + \cos(2\omega t - 120°)) = \frac{3\hat{e}\hat{i}}{2} \end{aligned} \tag{17}$$

This illustrates that the power is constant.

C. Instantaneous reactive power

Reactive power is related to circulating cycling energy so instantaneous reactive power is difficult to assess. However, in $\alpha - \beta$ coordinates the reactive power can be assessed using

$$q = e_\alpha i_\beta - e_\beta i_\alpha \tag{18}$$

which can be rewritten as

$$q = \begin{bmatrix} e_\alpha & -e_\beta \end{bmatrix} \begin{bmatrix} i_\beta \\ i_\alpha \end{bmatrix} \tag{19}$$

From (6)

$$\begin{aligned} &\begin{bmatrix} e_\alpha & -e_\beta \end{bmatrix} \\ =&\sqrt{\frac{2}{3}}\begin{bmatrix} e_a - 0.5(e_b + e_c) & 0.866(e_b - e_c) \end{bmatrix} \\ =&\sqrt{\frac{2}{3}}\begin{bmatrix} 0.5(e_{ab} - e_{ca}) & -0.866 e_{bc}) \end{bmatrix} \end{aligned} \tag{20}$$

where e_{ab}, e_{bc} and e_{ca} are the instantaneous line voltages.

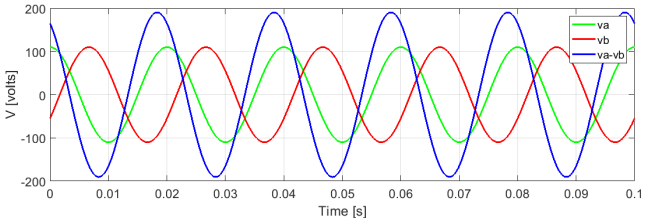

Fig. 2. Voltages e_a, e_b and e_a-e_b waveforms.

It can be seen in Fig. 2 that the line voltage e_{ab} leads phase voltage e_a by 30 From (7)

$$\begin{aligned} \begin{bmatrix} i_\beta \\ i_\alpha \end{bmatrix} &= \sqrt{\frac{2}{3}}\begin{bmatrix} 0.866(i_b - i_c) \\ i_a - 0.5(i_b + i_c) \end{bmatrix} \\ &= \sqrt{\frac{2}{3}}\begin{bmatrix} 0.866(i_b - i_c) \\ -1.5(i_b + i_c) \end{bmatrix} \end{aligned} \tag{21}$$

What can be seen from (20) and (21) is that the instantaneous reactive power can be obtained from the measurement of the line voltages and currents in phases b and c. By measurements of the voltages and currents instantaneously it is possible to compensate for reactive power. A block diagram is shown in Fig. 3 as put forward in [7]. How this is realised is the focus of this study.

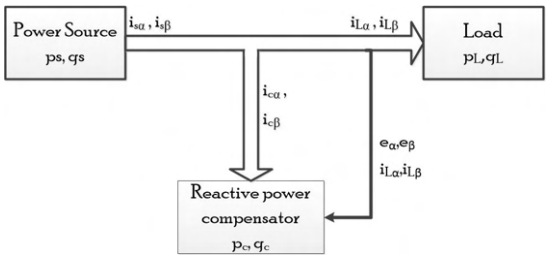

Fig. 3. The reactive power compensator.

Further detailing of instantaneous reactive power flow is given by [7] in terms of instantaneous power. This is further backed up by [8].

IV. Steady State Analysis and simulations

In this section the equivalent circuit is studied to assess the effect of capacitor compensation. This can be used to calculate the correct size of the capacitor.

A. Equivalent circuits

The standard per-phase equivalent circuit for a 3-phase induction motor is given in Fig. 4(a). X_m and R_c are the magnetizing reactance and core loss resistance and these are, for a well designed machine, much greater then at stator resistance R_1, the stator leakage reactance X_1, the referred rotor leakage reactance $X_1^{/}$ and the referred rotor resistance $R_1^{/}$. The slip s is given by

$$s = \frac{\omega_s - \omega_r}{\omega_s} \tag{22}$$

where ω_s is the synchronous speed and ω_r is the motor speed. The effective rotor resistance $\frac{R_2^{/}}{s}$ is the sum of the rotor resistance and the electro-mechanical energy conversion component in the circuit so that

$$\frac{R_2^{/}}{s} = R_2^{/} + \frac{(1-s)\,R_2^{/}}{s} \tag{23}$$

The rotor loss is then $3|I_r|^2 R_2^{/}$ and the mechanical power is

$$\frac{3\,(1-s)\,|I_r|^2 R_2^{/}}{s}. \tag{24}$$

Using (24) and 22), the torque is then

$$\begin{aligned} T_{mech} =& \frac{P_{mech}}{\omega_r} = \frac{3\,(1-s)\,|I_r|^2 R_2^{/}}{s} \times \frac{1}{\omega_r} \\ =& \frac{3\,(1-s)\,|I_r|^2 R_2^{/}}{s} \times \frac{1}{(1-s)\,\omega_s} = \frac{3|I_r|^2 R_2^{/}}{s\omega_s} \end{aligned} \tag{25}$$

and

$$I_r = I_{in} \frac{Z_m \left(\frac{R_2^{/}}{s} + jX_2^{/} \right)}{Z_m + \left(\frac{R_2^{/}}{s} + jX_2^{/} \right)} \tag{26}$$

where

$$Z_m = \frac{jX_m R_c}{R_c + jX_m} \tag{27}$$

With a knowledge of the equivalent circuit parameters, the torque/speed and current/speed steady-state curves can easily be obtained. The steady-state power and reactive power can also be obtained. As stated earlier, the magnetizing components of the equivalent circuit which form Z_m are much higher than the other components of the equivalent so that they can be ignored when s is close to 1 in Fig. 4(a) which gives the approximate circuit in Fig. 4(b). At what point this ceases to be valid depends on the ratio of X/R of the circuit. If it is high, i.e., very inductive, the speed will have increased to close to the synchronous speed before the resistive part begins to have an affect. This means that the starting current will be almost constant through the run-up of the motor. This is very much a function of the motor though they generally become more inductive as the size increases. This will be addressed in the simulations. The simplified circuit in Fig. 4(b) can be put into parallel in order to calculate the capacitance of the compensating capacitors. For the circuit in Fig. 4(c) with $s = 1$:

$$R_1 + R_2^{/} + j\left(X_1 + X_2^{/}\right) = \frac{jR_{st}X_{st}}{R_{st} + jX_{st}} \tag{28}$$

giving

$$R_{st} = \frac{1}{\left(R_1 + R_2^{/}\right)} \left(\left(R_1 + R_2^{/}\right)^2 + \left(X_1 + X_2^{/}\right)^2 \right) \tag{29}$$

$$X_{st} = \frac{1}{\left(X_1 + X_2^{/}\right)} \left(\left(R_1 + R_2^{/}\right)^2 + \left(X_1 + X_2^{/}\right)^2 \right) \tag{30}$$

To get resonance, when I_{in} will be wholly real, then in Fig. 4(c)

$$X_{cap} = Xst \tag{31}$$

These are easily calculated.

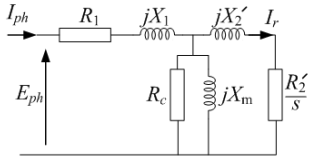

(a) Full per-phase equivalent circuit

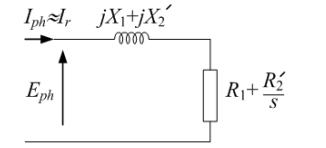

(b) Simplified circuit during starting

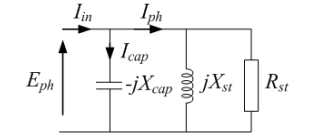

(c) Parallel simplified circuit for capacitor calculation

Fig. 4. Equivalent circuits.

B. Machine parameters

Two machines are studied here to address the calculations. The first is a small 4 pole 1.5 kW 346 V laboratory machine and the second is a larger 2-pole 200 kW 3300 V commercial machine from Valiadas (KHV355-2 - available at https://www.valiadis.gr/?viewp=1632). The parameters are given in Table I. The ratio X/R is the reaction/resistance at start and it can be seen that the larger machine is far more inductive at start than the smaller machine.

TABLE I
MOTOR PARAMETERS (VALUES IN OHMS)

Machine	X_m	R_c	R_1	$R_2^{/}$	$X_1 + X_2^{/}$	X/R
1.5 kW	58	81	2.13	1.34	2.99	0.86 p.u.
200 kW	118	1333	0.79	0.57	5.75	4.2 p.u.

C. Capacitor calculation

Table II shows the calculations for X_{st} and the capacitance when in star and delta; X_{st} assumes star connection. One advantage to connecting in delta is that it reduces the capacitance required. These capacitances are are not unreasonable values and lie within the ranges of common power factor correction capacitors. For larger machines series/parallel combinations would be required to meet the voltage and current requirements. In Table II, the no-load power factor correction capacitors $C_{NL-delta}$ are calculated. For this, the reactive power required is assumed to be for X_m so that $X_{NL-delta} = X_m$. These are smaller capacitors. Power factor correction at full load would require capacitors somewhere between the two values.

TABLE II
CAPACITOR COMPENSATION CALCULATIONS AT 50 HZ - VALUES IN µF

Machine	X_{st} **(Ω - star)**	C_{star}	C_{delta}	$C_{NL-delta}$
1.5 kW	7.01	454	151	18.4
200 kW	6.08	524	175	9

D. Steady-state simulations of 1.5 kW and 200 kW machine

As a contrast, two machines are studied here - the 1.5 kW 4-pole machine and the 200 kW 2-pole machine given in Section IV-B. The simulations were run at the rated line voltage and the slip was stepped from 1 down to 0.0025 in steps of -0.0025. The results are given in Figs. 5 and 6. In (a), the torques and line currents (rms) are given and it can be seen that in the 200 kW machine, the line current is more constant through the slip range because it is more inductive. The torque/speed characteristic is also more "peaky" with a lower p.u. starting torque. In (b) the power and reactive power are given. This is interesting, it can be seen that the power is always greater than the reactive power in the 1.5 kW motor showing the equivalent circuit is more resistive - this means that the 200 kW machine is more susceptible to power factor improvement during starting using capacitor compensation. The 200 kW machine also draws a more constant reactive power over the starting cycle. To emphasize this, in (c) the per-phase capacitance for a delta-connected network is calculated to correct the motor current to unity during starting. It can be seen in the 1.5 kW machine the reactive power is continuously changing whereas it is more constant in the 200 kW machine so that in smaller machines, the choice of compensating capacitors is a compromise. To illustrate this, in (d) the input currents are given for different values of compensation capacitance. The largest is C_{delta} as calculated for the machines in Table II, and then $C_{delta}/2$ and $C_{delta}/3$. It can be seen that the 1.5 kW has its current improved by about

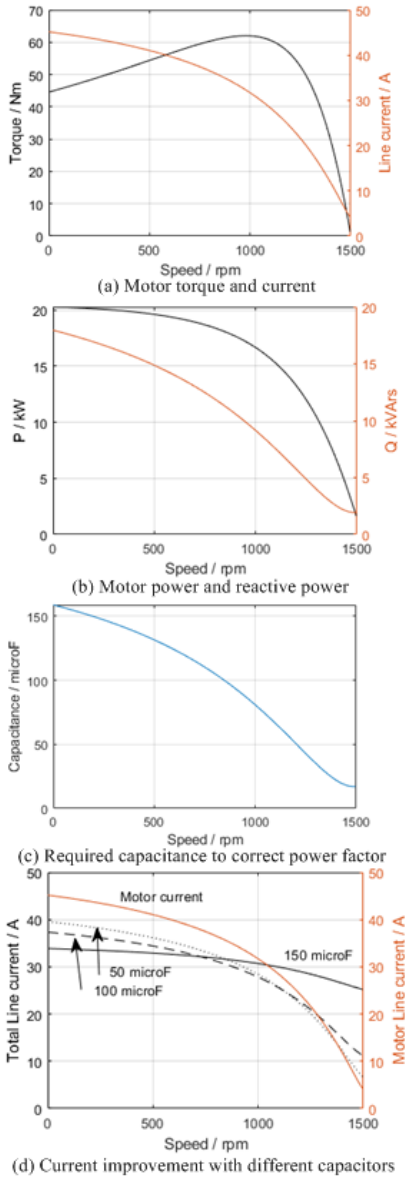

Fig. 5. Steady-state simulations of 1.5 kW machine.

25 % and using 150 µF does not improve the performance when $s < 0.3$. In fact 50 µappears to give better overall performance. The point of switch-off of the capacitors would be when the input current exceeds motor current. The 200 kW machine results shows that the machine can be improved with the full 175 µF at starting. This gives a starting current of 13 % of the motor current. However, this will increase to a peak at 225 A and there may be issues with leading power factor. 100 µF gives a starting current that is 50 % of starting motor current and this remains so across most of the slip profile. This is an improved level of starting across the whole starting transient.

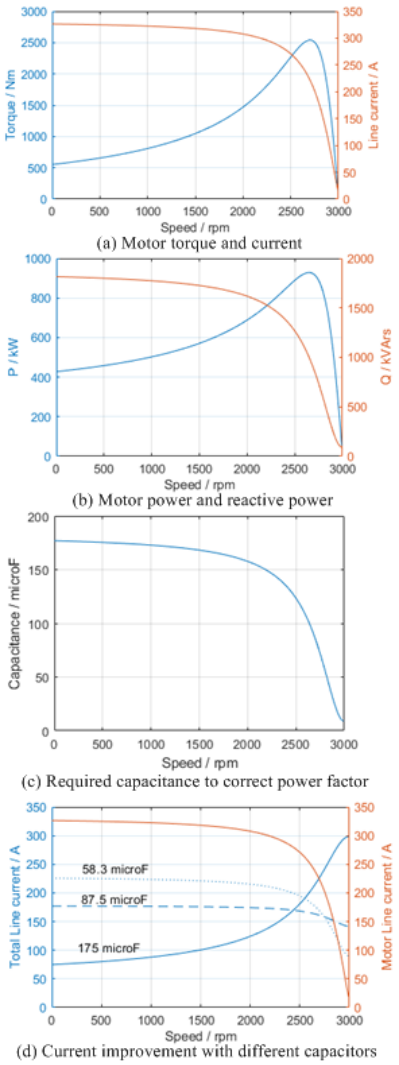

Fig. 6. Steady-state simulations of 200 kW machine.

V. System layout and Experimental Results

A. System under development

A system is being developed that allows soft switching of the machine and the capacitor bank. Modern point-on switching coupled with a microprocessor and measurement of voltages and currents will realise such a system. A diagram is shown in Fig. 8 and this is current work. This has been partially developed to allow the capacitor starting to be tested in terms of the run-up current rather than the point-on switching.

B. Preliminary results

The simulation work was validated for the 1.5 kW machine with DOL starting. The motor starts with the 66.3 A peak (46 A rms); the designed compensating system reduces it to 47.8 A peak (33.8 A rms) which constitutes 27.9 % reduction in current. This is with 40 µF capacitors which is similar to the

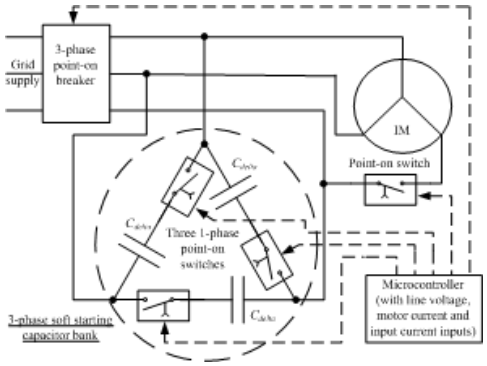

Fig. 7. Soft switching for starting machine and capacitor bank.

Fig. 8. Starting currents of 1.5 kW machine.

results in Fig. 5(d). The no-load current is measured at 6.1 A peak (4.31 A rms).

VI. Conclusions and Future Work

By tuning compensation capacitors, it was shown in [9] to be possible to reduce the starting current by 50% in a 5 HP 3-phase induction motor. This has been further developed here to illustrate that compromise values of capacitor can improve the operation of the machines; contrasting 1.5 kW and 200 kW machine simulations were carried out. This was explained. The 1.5 kW model was validated experimentally. Further work will be to develop the soft starter and validate it on an effective large machine by adding inductance to the 1.5 kW machine so that it appears more inductive during starting.

References

[1] T. P. Smith, "Performing detailed power system studies for designing and analyzing electrical distribution systems-power system studies for cement plants," *IEEE Ind. Appl. Mag.*, vol. 13, no. 4, pp. 56–65, 2007.
[2] E. K. Saathoff, D. H. Green, R. A. Agustin, J. O'Connell, and S. B. Leeb, "Inrush current measurement for transient space characterization and fault detection," *IEEE Trans. on Instr. and Meas.*, 2021.
[3] S. Chapman, *Electric machinery fundamentals*. Tata McGraw-Hill, 2005.
[4] E. Fuchs and M. A. Masoum, *Power quality in power systems and electrical machines*. Academic press, 2011.
[5] H. Rehaoulia and M. Poloujadoff, "Transient behavior of the resultant airgap field during run-up of an induction motor," *IEEE Transactions on Energy Conversion*, no. 4, pp. 92–98, 1986.
[6] H. Banach, "Condition for the occurrence of maximum efficiency in induction motors and transformers," in *2018 International Symposium on Electrical Machines (SME)*, 2018, pp. 1–5.
[7] H. Akagi, Y. Kanazawa, K. Fujita, and A. Nabae, "Generalized theory of the instantaneous reactive power and its application," *Trans. of the Inst, of Elect, Eng. of Japan. B*, vol. 103, no. 7, pp. 483–490, 1983.
[8] M. Z. Peng and J.-S. Lai, "Generalized instantaneous reactive power theory for three-phase power systems," *IEEE Transactions on Instrumentation and Measurement*, vol. 45, no. 1, pp. 293 – 297, 1996.
[9] M. Habyarimana and D. Dorrell, "Methods to reduce the starting current of an induction motor," in *IEEE Int. Conf. on Power, Control, Signals and Instr. Eng. (ICPCSI)*. IEEE, 2017, pp. 34–38.

D.3 Journal Paper Submitted to Energies

Paper submitted to *Energies* for consideration - only first page included due to space constraints (twenty-six pages in length). It is based on steady-state analysis and experimental validation chapters.

MDPI

Article

Reduction of Starting Current in Large Induction Motors

Mathew Habyarimana [1], David George Dorrell [2,*] and Remmy Musumpuka [3]

[1] Discipline of Electrical, Electronic and Computer Engineering, University of Kwazulu-Natal, Durban 4041, South Africa; adeniyi.onaolapo@gmail.com
[2] School of Electrical and Information Engineering, University of the Witwatersrand, Johannesburg 4041, South Africa; david.dorrell@wits.ac.za
[3] R&D Division, Icarus Avionics (Pty), Durban, South Africa; remmy.musumpuka@gmail.com
* Correspondence: david.dorrell@wits.ac.za; Tel.: +27-(0)11-7177244

Abstract: Large induction motors can have a high inrush and run-up current during starting, often five to ten times the full load current. In weak supplies this can cause a problem with system stability with the voltage dipping below acceptable levels, and in islanded systems, the capacity pulled below its maximum. There are several different starting methods possible but often only suitable for smaller machines. One method not investigated is the use of parallel capacitor compensation during the starting because large induction motors are very inductive during the starting sequence so that supplying reactive power may be more effective than supplying energy. This paper addresses this by investigating several different induction motors, assessing their compensation requirements, and testing the methods via simulations and experiments.

Keywords: Induction motors, starting, inrush current, power system

Citation: Habyarimana, M.; Dorrell, D.G.; Musumpuka, R. Reduction of Starting Current in Large Induction Motors. *Energies* **2022**, *1*, 0. https://doi.org/

Received:
Accepted:
Published:

Publisher's Note: MDPI stays neutral with regard to jurisdictional claims in published maps and institutional affiliations.

Copyright: © 2022 by the authors. Submitted to *Energies* for possible open access publication under the terms and conditions of the Creative Commons Attri- bution (CC BY) license (https://creativecommons.org/licenses/by/4.0/).

1. Introduction

In power systems, the inrush current, also called the input surge current or switch-on surge, of a large load can cause problems related to excessive current drawn. It has the potential to damage system apparatus as well as destabilizing the system network in weak grids. It can trip protection relays unnecessarily thereby causing voltage drops that impair the function of other equipment connected to the same system.

Inrush current can be defined as the maximum instantaneous input current drawn by an electrical device when first turned on [1,2]. Induction motors (IMs) switched-mode power supplies, and transformers and are devices that exhibit high inrush current. When there are large electro-magnetic devices then there will be a surge during switch on to establish the magnetic field. Induction motors have the transient start-up period as well as magnetization if it is direct on-line connected. During the run-up to steady-state the machine can draw between five and ten times the rated current.

If the inrush current is left unaddressed for a large load,it can cause voltage busbars to fall out of regulation. In more serious cases this results in the system exceeding the current carrying capability of the system and possibly leading to overloading and system tripping.

Three-phase IMs consume both active and reactive power [3,4]. They can produce power quality problems due to high inductive loading. In industry, capacitor banks are often used to correct poor power factor in plants.

When starting a line-connected IM, the induced voltage in the rotor is maximum because slip is maximum ($s = 1$). At this stage the rotor impedance is low, therefore the rotor current becomes large and the high current in the rotor reflects into the stator due to transformer action. This results in a large starting current in the stator at low power factor. Depending on the motor size and design, the value of starting torque may be low. This is particularly true for a large high-efficiency machine. This may negate the use of a high resistance or star-delta starter to restrict the starting current. These reduce the starting current but also the starting torque.